NASA CR-114503

Available to the Public

THE DEVELOPMENT OF AN AUGMENTOR
WING JET STOL RESEARCH
AIRPLANE (MODIFIED C-8A)

Volume I—Summary

By R. H. Ashleman and H. Skavdahl

August 1972

D6-40720-1

THE DEVELOPMENT OF AN AUGMENTOR WING JET STOL RESEARCH AIRPLANE (MODIFIED C-8A)

Volume I—Summary

By R. H. Ashleman and H. Skavdahl

August 1972

D6-40720-1
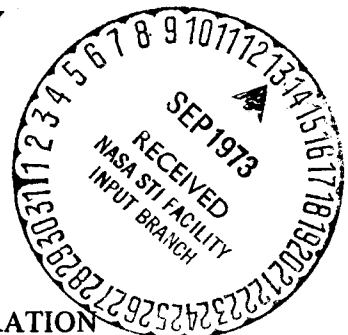
CONTENTS

CONTENTS—Concluded

SUMMARY

The Boeing Company was awarded contract NAS2-6025 on July 6, 1970 to design, fabricate, and install modifications to the de Havilland C-8A airplane (exclusive of the engine, nacelle, and contents) which would convert it to an augmentor wing jet STOL research aircraft. The contract further specified that ground and flight testing be conducted to verify airworthiness.

In parallel with the above contract, the Canadian Department of Industry, Trade and Commerce contracted wwith de Havilland Aircraft of Canada, Ltd. to provide the new propulsion system (excluding the bypass air ducts) consisting of new Rolls-Royce split-flow Spey engines and their podded installation. The mixed-flow Spey engine was modified to the split-flow version (MK 801-SF) with two adjacent fan air offtakes by Rolls-Royce (Canada).

The primary purpose of the augmentor wing jet STOL modification program is to provide NASA and the Canadian Government with an experimental research airplane which may be used as an in-flight demonstrator of the augmentor wing concept and its applicability to commercial STOL airplanes.

To achieve an airplane which could operate within the STOL regime and be representative of a commercial transport, it was necessary to increase the wing loading for the maximum landing weight from the 41.4 lb/sq ft of the basic Buffalo to 49.6 lb/sq ft on the modified airplane. This provides a maximum design lift coefficient capability of over 5.0 at thrust settings for 60- to 65-kt landing speeds.

Since the major purpose of the airplane is to explore the takeoff, approach, and landing regimes of flight and there was little requirement for high-speed cruise, the modification was designed with fixed slats and landing gear. Similarly, the augmentor flaps were not designed to fair into the wing at flaps up. Their deflection is variable in flight from 5.6° to 73°. Cruise nozzles were not provided to divert the fan air used in the augmentor flap.

The split-flow Spey MK 801-SF engine was chosen for the propulsion system since its major hardware components were available and it provided sufficient fan air at the correct pressure ratio for the augmentor flaps.

The modifications of the Spey engine, propulsion system, and airframe were completed in January 1972 with ground tests starting January 25, 1972. These were followed by taxi and flight tests, which were essentially completed May 18, 1972. On the last flight, the starter on the left-hand

engine malfunctioned during an in-flight start, which resulted in the loss of the lower cowling of the left engine and subsequent damage to the airplane. Repairs were made, a brief check flight was conducted, and the airplane delivered to NASA on July 31, 1972.

During the flight test program the flight range was investigated from a minimum airspeed of 50 KEAS to the design dive speed of 180 KEAS. Flap placards were reached at flaps 65° (90 KEAS) and flaps 30° (120 KEAS). Approaches to stall were made at three primary flap settings: up, 30°, and 65°. The full ranges of flap setting, conical nozzle deflection, and power setting were evaluated.

Angles of attack from -3° to 24° were investigated. Variations in load factor from 0.3 to 1.8 g were obtained during pushover/pull-up maneuvers. Sideslip angles of 15° were tested and bank angles exceeding 45° were flown. The flight envelope was sufficiently explored to clear the airplane for the augmentor wing research flight test program.

Since the original objectives of the Modified C-8A program were to prove the augmentor wing concept with respect to aerodynamics, performance, and handling qualities and to contribute to the development of jet STOL transport design and operating criteria, it is recommended that NASA extend the flight test program into the following areas:

● Conduct a test program exploring the STOL flight regime in further depth. Particular emphasis should be placed on landing maneuvers, including the following specific items:

Steep approach flare techniques related to simulator findings.

Evaluation and, possibly, measurement of ground effects.

Simulation of engine failure at critical conditions.

Caution is urged in approaching flight conditions having low margins. Give particular attention to the type of longitudinal stability augmentation needed on the airplane.

● Conduct a flight test investigation to determine accurate performance characteristics including a ground test to measure static thrust. With accurate data in hand, conduct an analysis of airplane performance. Static thrust data, flaps on and off, will allow identification of static augmentation. Tuft studies of suspected areas of poor flow during both flight and static tests will allow qualitative assessment of drag sources and will guide corrective action to improve performance. This work is recommended as essential to the proof of the augmentor wing concept.

- Install a powered elevator system on the airplane to permit full and safe exploration of the airplane's high lift and STOL operation capabilities.

- Use the variable-gain SAS to find the optimum lateral-directional handling qualities and reduce the "snaking" tendency, then modify the fixed-gain SAS to this configuration.

INTRODUCTION

Early in 1970, the National Aeronautics and Space Administration issued a request for proposal to modify a de Havilland C-8A airplane to an augmentor wing jet flap STOL configuration. Based on its response to the request for proposal, The Boeing Company was awarded contract NAS2-6025 on July 6, 1970 to design, fabricate, and install modifications to the airplane (exclusive of the engine, nacelle, and contents) which would convert it to a jet-powered augmentor wing configuration. The contract further specified that ground and flight testing be conducted to verify airworthiness.

As the program progressed, the contract was altered to include the following significant items:

- Lateral and directional stability augmentation system

- Installation of a pulse code modulation (PCM) data system provided by NASA

- An improved braking system

- Fuel system modification to reduce roll moment of inertia at lower gross weights

- Pilot escape provisions

- Modification to the longitudinal control system to reduce stick forces

In parallel with the above contract, the Canadian Department of Industry, Trade and Commerce contracted with de Havilland Aircraft of Canada, Ltd. to provide the new propulsion system (excluding the bypass air ducts) consisting of new split-flow Spey engines and their podded installation.

The program was based on original research of an augmentor wing concept by de Havilland of Canada. Because of the attractive characteristics of this concept for application to STOL airplanes, the Ames Research Center of NASA and the Defence Research Board of Canada contracted with de Havilland to supply an augmentor wing model for a series of large-scale wind tunnel tests in their 40- by 80-ft tunnel. These tests began in 1965 with the basic purpose of investigating an augmentor wing configuration which could be applied to a STOL transport airplane. Results from these tests provided the wind tunnel data used in the modified design of the airplane.

The airframe modification program and associated development, ground, and flight tests are summarized in this volume. Results of the contractor's flight testing are presented in detail in volume II of this report, reference 1. The schedule and significant milestones of the program are summarized in figure 1.
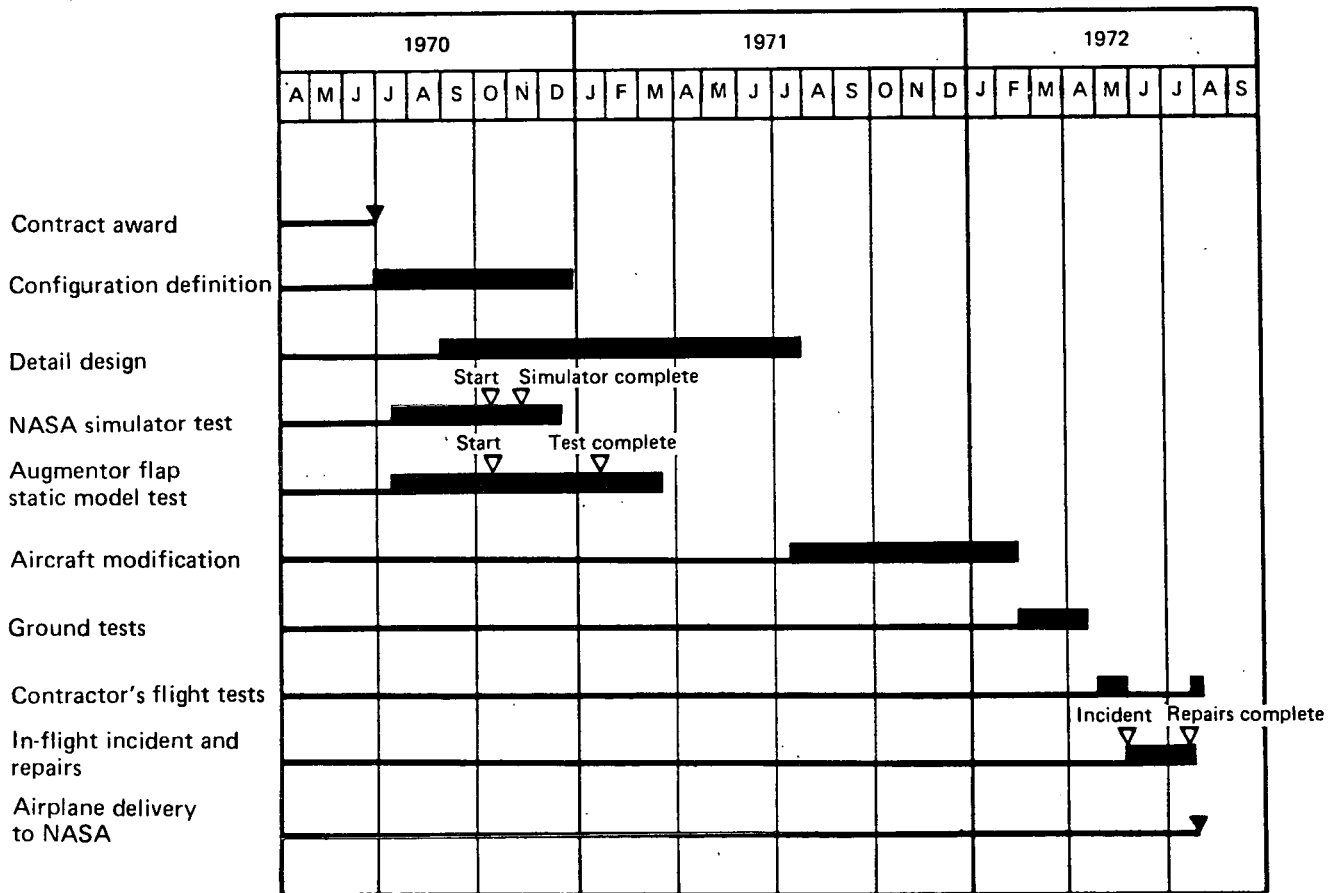
FIGURE 1.—SCHEDULE AND MILESTONES

ABBREVIATIONS AND SYMBOLS

A_E nozzle exit area, in.^{2}

AR   flap augmentation ratio = flaps-on thrust/flaps-off thrust

$A\!R$ aspect ratio = span^2/reference area

AWJSRA   Augmentor Wing Jet STOL Research Aircraft

BLC   boundary layer control

b_H, b_V, b_W span of horizontal tail, vertical tail, and wing, respectively, ft

$\bar{C}_a, \bar{C}_e, \bar{C}_H, \bar{C}_r,$ average chord length of aileron, elevator, horizontal tail, rudder, spoiler, vertical
$\bar{C}_{sp}, \bar{C}_V, \bar{C}_W$ tail, and wing, respectively, in.

C_g gross thrust coefficient = measured thrust/ideal thrust

C_j isentropic thrust coefficient = cold thrust/qS_W

C_L airplane lift coefficient = lift/qS_W (positive up)

C_ℓ rolling moment coefficient = rolling moment/$qS_W b_W$

C_n yawing moment coefficient = yawing moment/$qS_W b_W$ (positive nose right)

C_V nozzle velocity coefficient = measured velocity/isentropic velocity

CG   center of gravity

ECS   environmental control system

EGT   exhaust gas temperature

F_g gross thrust where F_{g_P} is the hot thrust from the primary exhaust, F_{g_A} is the cold thrust from the upper and lower augmentor nozzles, $F_{g_{AB}}$ is the cold thrust from the aileron blowing nozzles, $F_{g_{BB}}$ is the cold thrust from the body blowing nozzles, and F_{g_R} is the resultant thrust

F_N	net thrust, lb
$F/P_{T_1}\sqrt{T_1}$	corrected engine fuel flow where P_{T_1} is the inlet total pressure in pounds/inch^2 and T_1 is the inlet total temperature in degrees Kelvin
F_S	stick force, lb (positive for pull)
F_W	wheel force, lb (positive for right wheel)
FSAA	Flight Simulator for Advanced Aircraft
FTE	flight test equipment
GPM	gallons per minute
g	acceleration due to gravity, ft/sec^2
h_N	sum of lower and upper augmentor nozzle gaps (fig. 6)
IAS	indicated airspeed, kt
i_T, i_W	horizontal tail and wing incidence angles relative to the fuselage, deg
I_{XX}	airplane rolling moment of inertia, slug-ft^2
kVA	kilovolt-amperes
ℓ_T	augmentor flap distance from the most forward part of the Coanda flap portion perpendicular to the intake door (fig. 6)
ℓ'_Z	augmentor flap distance from nozzle exit measured parallel to the geometric nozzle centerline to the part on the Coanda flap nearest the geometric nozzle centerline (fig. 6)
LP	low pressure
MAC	wing mean aerodynamic chord, 12.4 ft
N_H, N_L	high- and low-pressure engine shaft speed, RPM

$N_H/\sqrt{T_1}, N_L/\sqrt{T_1}$ corrected high- and low-pressure shaft speed, where T_1 is the total inlet temperature in degrees Kelvin

n, n_z normal load factor, g

OEW   operating empty weight including pilot, copilot, trapped fuel, engine oil, and deliverable flight test equipment, lb

P_{AMB} ambient pressure, psi

P_T total pressure, psi

P_S static pressure, psi

PCM   data acquisition system termed "pulse code modulation"

PCU   power control unit

PR   nozzle pressure ratio

q freestream dynamic pressure

S_H, S_{LE}, S_V, S_W reference area of the horizontal tail, leading edge slat, vertical tail, and wing, respectively

SAS   stability augmentation system

T   total temperature, degrees Kelvin

T/W   total airplane thrust to airplane weight ratio

t/c   airfoil thickness nondimensionalized by its chord

t_{30} time to reach 30° bank angle

V_{app} approach velocity in equivalent airspeed, kt

V_D design dive speed, kt

V_F	flap placard airspeed, kt
V_{MO}	maximum operating airspeed, kt
V_e	equivalent airspeed (KEAS), kt
V_2	takeoff climb speed with an engine out, kt
$\bar{V}_H, \bar{V}_V$	horizontal and vertical tail volume coefficients = (tail reference area)·length between tail and wing 1/4 MACs)/$S_W b_W$
W	airplane gross weight, lb
X_E	primary gross thrust, lb
X_S	column position, in. (positive aft)
Z	augmentor flap distance measured perpendicular from the nozzle flow line to the Coanda flap
α, α_F	fuselage angle of attack as measured on the nose boom, deg (positive leading edge up)
β	sideslip, deg (positive nose left)
γ	flightpath angle, deg (positive up)
δ	pressure ratio = absolute pressure/sea level absolute pressure
δ_a	aileron deflection, deg (positive trailing edge down)
δ_C	column deflection, deg (positive aft)
δ_{CH}	augmentor choke deflection, deg (positive up)
δ_e	elevator deflection, deg (positive trailing edge down)
δ_F	flap deflection, deg (positive trailing edge down)

δ_{slat} leading edge slat deflection, deg

δ_{SP} spoiler deflection, deg (positive trailing edge up)

δ_r rudder deflection, deg (positive trailing edge left)

δ_w wheel deflection, deg (positive right)

$\dot{\delta}_w$ wheel deflection rate, deg/sec

η station along wing span divided by total span

θ pitch attitude, deg

$\dot{\theta}$ pitch rate, deg/sec

$\ddot{\theta}$ pitch acceleration, deg/sec^2

θ_e flap diffuser angle, deg (fig. 6)

θ_i intake door angle, deg (fig. 6)

Λ wing sweep angle, deg

λ wing taper ratio

ν hot thrust nozzle angle measured relative to the fuselage datum, deg (positive down)

τ_R roll mode time constant

ϕ bank angle, deg

$\dot{\phi}$ roll rate, deg/sec

$\ddot{\phi}$ roll acceleration, deg/sec^2

ψ yaw angle, deg

$\dot{\psi}$ yaw rate, deg/sec

$\ddot{\psi}$ yaw acceleration, deg/sec^2

SUBSCRIPTS

B	engine station at bypass air outlet
E	engine station at exhaust nozzle outlet
LE,TE	leading edge and trailing edge
LH, RH	left-hand and right-hand locations as viewed from the pilot's station looking forward
1	engine station at inlet
2	engine station at low-pressure compressor delivery
2.5	engine station at bypass duct reference station
3	engine station at high-pressure compressor delivery
4	engine station at high-pressure turbine entry
6	engine station at low-pressure turbine exit (upstream of colander)
8	engine station at exhaust nozzle hinge plate

12

OBJECTIVES AND DESIGN CONSTRAINTS

The primary purpose of the jet STOL augmentor wing program is to provide NASA and the Canadian Government with an experimental STOL research airplane which may be used for in-flight studies of the augmentor wing concept and its applicability to commercial STOL airplanes.

The airplane will be used for the following purposes:

- To determine the aerodynamic, performance, and handling qualities of a jet-powered STOL aircraft which incorporates the augmentor wing concept

- To contribute to the development of criteria for design and operation of jet STOL transport airplanes

- To provide a jet STOL transport airplane for STOL systems research and development

To achieve an airplane which could operate within the STOL regime at a wing loading more representative of a commercial transport, it was necessary to increase the wing loading for the maximum landing weight from the 41.4 lb/sq ft of the basic Buffalo to 49.6 lb/sq ft on the modified airplane. This provides a maximum lift coefficient capability of over 5.0 at thrust settings for 60- to 65-kt landing speeds.

The achievement of the increased wing loading and high lift coefficients provided the major restraints to the airplane modification. These restraints resulted in a reduction in wing aspect ratio and a reduction in the chordwise length of the augmentor flap as compared to the configuration tested in the phase IV wind tunnel tests discussed in reference 2. The design gross takeoff weight was also increased to 45 000 lb with an associated maximum landing weight of 43 000 lb. The design rate of sink was 12.0 ft/sec at the maximum landing weight.

Since the primary purpose of the airplane is to explore the takeoff, approach, and landing regimes of flight and there was little requirement for high-speed cruise, the modification was designed with fixed slats and landing gear. Similarly, the augmentor flaps were not designed to fair into the wing at flaps up. Their deflection is variable in flight from 5.6° to 73°. Cruise nozzles were not provided to divert the fan air used in the augmentor flap.

The split-flow Spey MK 801-SF engine was chosen for the propulsion system since its major hardware components were available and it provided sufficient fan air at the correct pressure ratio

for the augmentor flaps. Its one disadvantage is relatively high noise level because it was initially designed without noise constraints and is a relatively low bypass ratio engine (0.65). Methods to reduce the community sideline noise were investigated early in the program. It was concluded that some noise reductions could be achieved by lining of the inlet, fan duct, and nozzle vanes, but the hot jet noise prevented reducing the noise significantly. The decision was made to include only peripheral lining in the inlet and fan duct, thereby achieving a small reduction in community noise levels within reasonable costs and with no change in the program schedule.

DESCRIPTION OF AIRPLANE AND MODIFICATIONS

GENERAL FEATURES

The Augmentor Wing Jet STOL Research Airplane (AWJSRA) presented in figures 2 through 5 is a 45 000-lb, 50-psf wing loading, turbofan-powered airplane designed for research in the STOL terminal flight regime (takeoff, climb out, approach, landing, low-speed flight and handling qualities). It is intentionally rugged and possesses many adjustable or easily modified components which enhance its role in providing answers to a new style of flight with a new concept for developing high wing lift.

The most significant feature of the airplane is its augmentor flap that extends over approximately 70% of the exposed wing span. This is a bi-surface flap that uses engine low-pressure bypass air to provide lift and thrust augmentation. Engine bypass air is ducted to a two-dimensional nozzle that exhausts the entire flap span between the bi-surface elements (see fig. 6). Additional lift benefits are derived by drooping the ailerons when the flaps are deflected. Ailerons are blown to provide boundary layer control to avoid separation and to provide some direct-reaction lateral control from the aileron system. The effect is that of a full span flap (exposed span). Additional air is used to control the boundary layer on the wing center section across the fuselage. All of the engine low-pressure bypass air is collected and distributed for these three uses.

Since the bypass (cool fan air) is collected and used in this fashion, the engine must operate in a split-flow mode in which the hot turbine gases are indeed separate from the bypass fan air. This special feature is furnished in the Rolls-Royce Spey MK 801-SF (split flow) engine. Control and use of the fan air is straightforward in that it is deflected downward by both the flaps and ailerons when the landing approach configuration is needed and the desired amount of airflow is adjusted by the engine throttle setting. However, the hot gas thrust must be cancelled or used in some other helpful manner or aircraft descent is not possible. This condition is resolved by adapting the Pegasus (Harrier-type installation) nozzle to collect and control the hot turbine gases. Hot gases are thus vectored downward from the flightpath by the controllable nozzle. Two such nozzles are used per engine and are vectorable with pilot controls from thrusting almost directly aft to downward and slightly forward. The takeoff setting is in the most aft vector orientation.

The airplane may be operated by a pilot alone or with a copilot. It has fully powered lateral and directional control systems and a spring tab longitudinal control system. A lateral directional stability augmentation system (SAS) is provided to improve the airplane handling characteristics below 100 kt. In addition, a variable lateral directional SAS mode is provided to permit studying the effects of variations in handling characteristics during terminal flight trajectory evaluation.

Maximum gross weight = 45 000 lb
V_{MO} (flaps up)   = 160 kt

Aspect ratio   7.2
Wing area   865.0 ft^2
Span   78.75 ft
Flap semispan   23.0 ft

Nose boom

Augmentor choke
(lift dump)

Augmentor flaps
deflect to 73°

Augmentor choke
(lateral control and
(lift dump)

LE slats

Spoiler (lateral control)

BLC aileron

33

335

25% MAC

78 ft-9 in.

32 ft-0 in.

28 ft-8 in.

5°

30 ft-6 in.

Pegasus nozzles

Rolls-Royce
Spey MK 801-SF

27 ft-10 in.

77 ft-4 in.
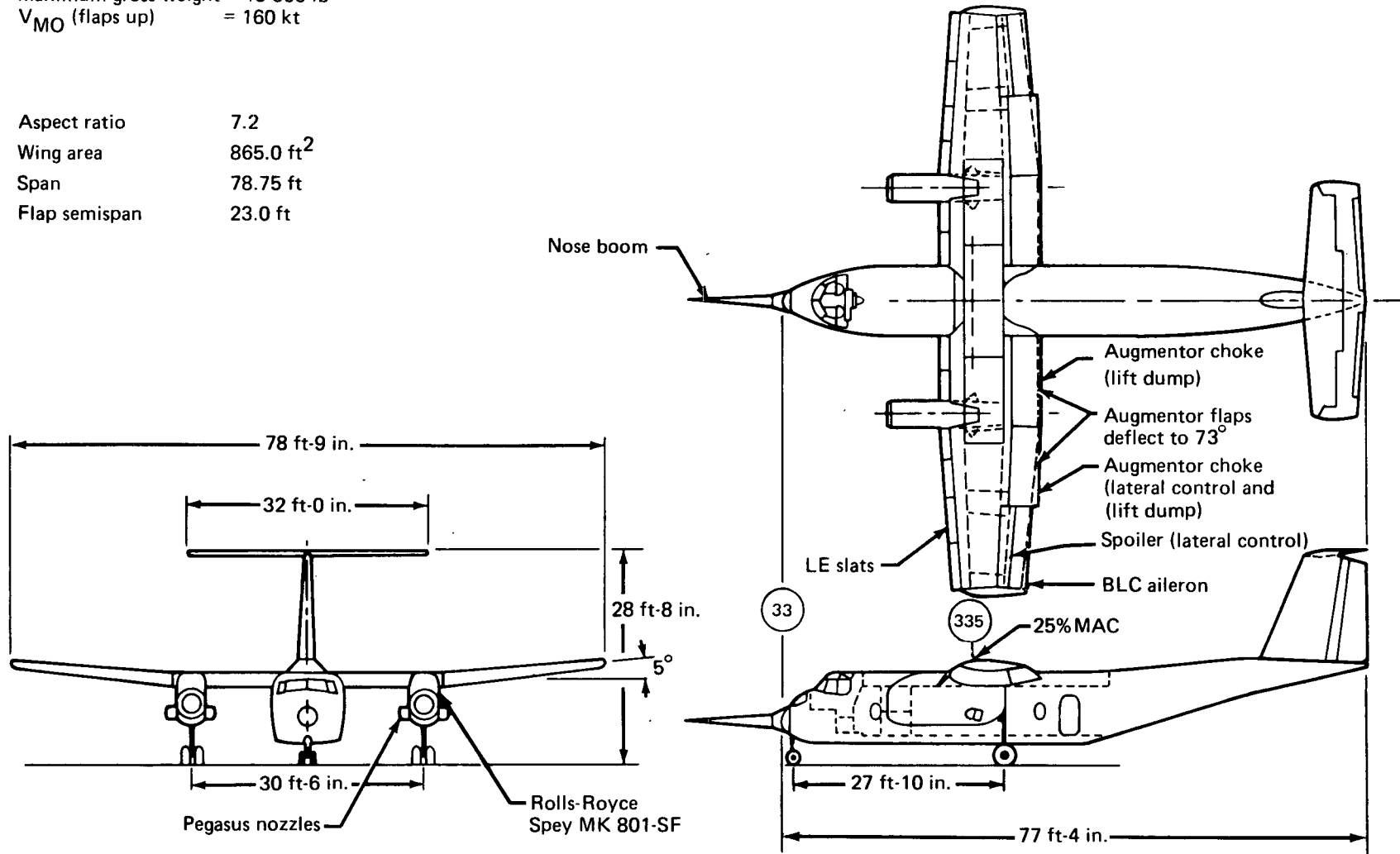
FIGURE 2.—THREE-VIEW DRAWING OF MODIFIED C-8A

FIGURE 3.—THREE-QUARTER FRONT VIEW OF MODIFIED C-8A

17
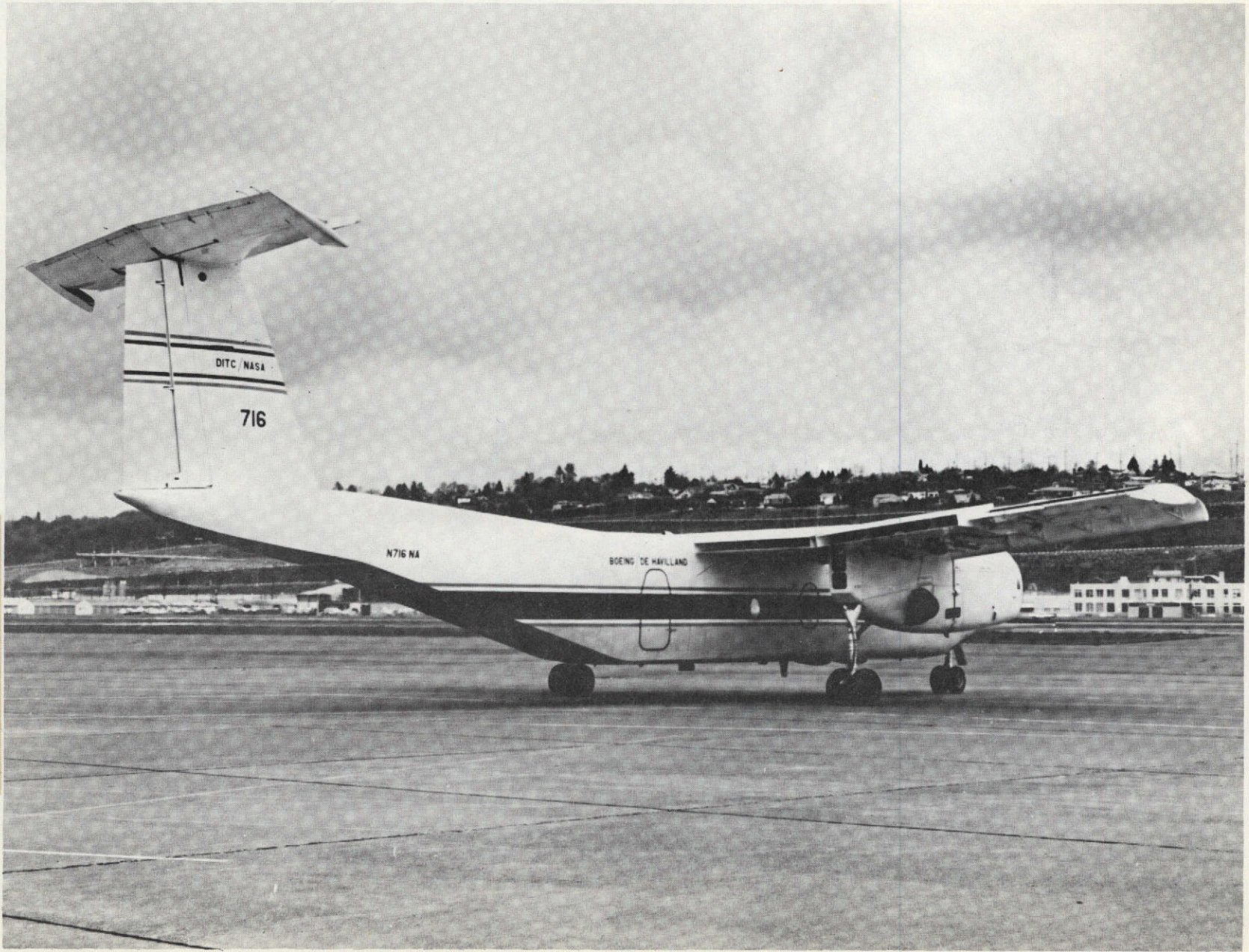
FIGURE 4.—THREE-QUARTER REAR VIEW OF MODIFIED C-8A

WING

S_W = 865 ft^2
b_W = 78.75 ft
$\bar{c}_{W_{REF}}$ = 149 in.
C_{root} = 149 in.
C_{tip} = 94 in.
$\mathcal{R}$ = 7.2
$\Lambda_{0.25}$ ≈ 0°
t/c ≈ 16%
i_W = 2.5°
λ_{eff} = 0.80

HORIZONTAL TAIL

S_H = 233 ft^2
b_H = 32 ft
$\bar{c}_H$ = 88 in.

$\mathcal{R}$ = 4.4
$\Lambda_{0.25}$ = 3°
t/c ≈ 12%
$\bar{V}_H$ = 1.0
λ = 0.75
i_T = +1°

VERTICAL TAIL

S_V = 152 ft^2
b_V = 13.6 ft
$\bar{c}_V$ = 137 in.

$\mathcal{R}$ = 1.22
$\Lambda_{0.25}$ = 17°
t/c ≈ 14%
$\bar{V}_V$ = 0.097
λ = 0.57

AUGMENTOR FLAPS

. Avg chord = 29% C_W
(LE coanda to TE/
wing chord)

. Span: 12% (side of body) $\leqslant \eta \leqslant$ 71%

. 5.6° (up) $\leqslant \delta_F \leqslant$ 73°

θ_e = 4.75°
ℓ_T/h_N = 15

ELEVATOR

. Avg chord = 35%

. Full span

. -25° $\leqslant \delta_e \leqslant$ +15°

. Two 83% semispan tabs
(7% tail cord)

. $S\bar{c}_e$ = 209 ft^3

RUDDER

. Avg chord = 40%

. Double-hinged rudder (hinge
line at 60% and 80% chord)

. Full span

. -25° $\leqslant \delta_r \leqslant$ +25°

. Aft rudder segment deflects
an additional 25° at 1:1 gearing

. $S\bar{c}_{r \, (total)}$ = 272 ft^3

BLC AILERON

. Avg chord = 22.5% C_W
. Span: 71% $\leqslant \eta \leqslant$ 100%
. -16.5° $\leqslant \delta_a \leqslant$ 64°

. Half-span geared tab
(4% wing chord)

. $S\bar{c}_a$ = 46 ft^3/surface

SPOILER

. Avg chord = 14% C_W
. Hinge line at 62% C_W
. 0° $\leqslant \delta_{SP} \leqslant$ 50°

. $S\bar{c}_{SP}$ = 17 ft^3/surface

SLAT

. Chord = 20.7 in.
. δ_{SLAT} = 60°
. Gap = 2.35% C_W
. $\dfrac{\Delta S_{LE}}{S_W}$ = 0.124

AUGMENTOR CHOKE

. Avg chord = 9% C_W
. Full-span on all flap panels
(0% $\leqslant \delta_{CH} \leqslant$ 65%)

FIGURE 5.—AIRPLANE GEOMETRY
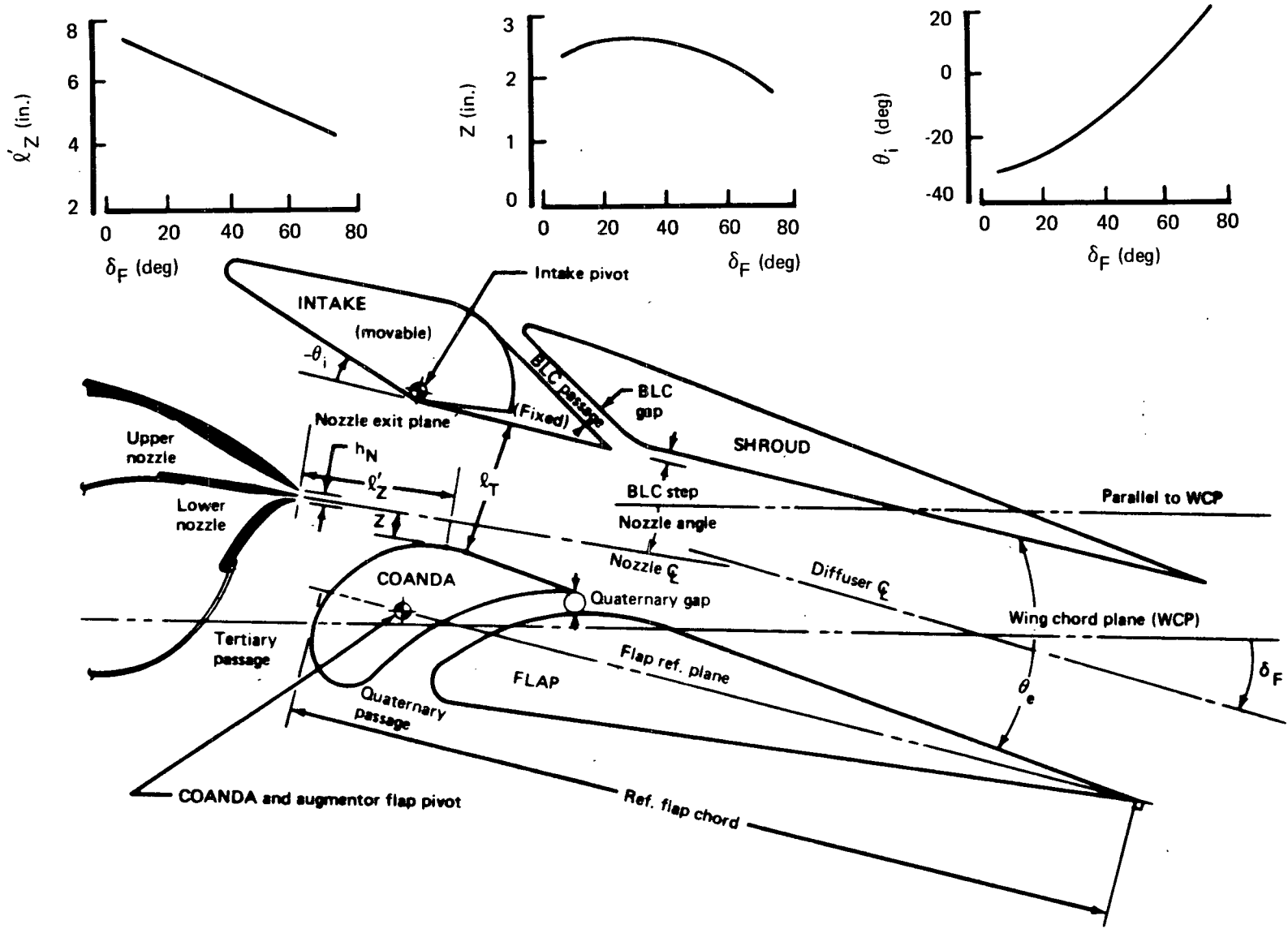
FIGURE 6.—AUGMENTOR FLAP CROSS SECTION

Lateral control is provided through ailerons, spoilers, and augmentor chokes. The latter modulate the performance of the outboard flap to produce a control mode unique to the augmentor configuration. Available rolling moment coefficients are approximately twice those of conventional jet transports.

A PCM flight test instrumentation system is provided with 100 channels for data collection to measure pressures, temperatures, control surface positions, flight conditions, etc.

The design incorporates many simplifications because the airplane is to be used in exploring only the low-speed end of the jet STOL flight spectrum. The landing gear and leading edge slats are fixed in the extended position. The flaps are deflectable but maintain their fixed high-lift bi-surface configuration at all times. Control surface supports and actuation are left exposed for reasons of simplicity and economy. Existing control system components such as SAS, actuator, lateral control mixing, and feel sensing are adapted from existing Boeing production hardware to gain the advantage of their reliability and previous development experience. Many structural and system safety features have been incorporated and are discussed in "Safety Features."

EXTENT OF MODIFICATION

The original C-8A airplane received the following modifications to derive the AWJSRA:

- New augmentor flaps, blown ailerons, spoilers, supporting structure, and actuation replace all original structure aft of the rear spar.

- A new hydraulic power and distribution system is provided to actuate all of the above.

- Wing span is reduced from 96 to 78.75 ft.

- Fixed constant-section leading edge slat segments are attached forward of the existing wing contour.

- The T-64 turboprop engines were replaced with Rolls-Royce Spey MK 801-SF engines, and the nacelles were modified to accommodate the new installation. Vectorable Pegasus nozzles were installed.

- A crossover air-distribution duct system supplies air to the augmentor flaps, ailerons, and fuselage blowing nozzles.

21

- The landing gear is fixed in the down position.

- A nose boom is installed for instrumentation.

- Cockpit side windows can be jettisoned for emergency egress or rescue.

- The pilot and copilot's seats incorporate shock attenuation struts for crash landing protection.

- Lateral-directional stability augmentation is provided and a variable stability mode is added for handling investigations.

- The original C-8A main wheels and brakes are replaced by 727 nose wheel and brake assemblies.

- The elevator gear tab ratio and torsion spring are changed to reduce stick forces.

- The rudder dual-acting hydraulic system automatically reverts to single-acting mode above 100 kt for structural safety.

- A PCM data acquisition system is installed for research use.

- A constant speed drive is installed to drive the original C-8A generators.

DESCRIPTION OF MODIFICATIONS AND FEATURES

Augmentor Flaps

Augmentor flaps are installed in four segments of about 12-ft span and are mounted from two external support beams per segment (see fig. 7). The beams are of built-up construction and are attached externally to the front and rear spars. The design permits change of only the end fittings in the event that research evaluation of varying the flap/nozzle relative geometry is desirable. The flap aerodynamic cross section is constant, as depicted in figures 6 and 7. Each flap segment is composed of five major elements, Coanda surface, flap, shroud, inlet, and the augmentor choke control.

The Coanda surface turns the high-velocity air from the augmentor nozzle to align its flow as nearly as possible to the centerline of the diffuser and mixing chamber formed by the upper and lower inner surface. The high-velocity (sonic) air from the nozzle does not contact the
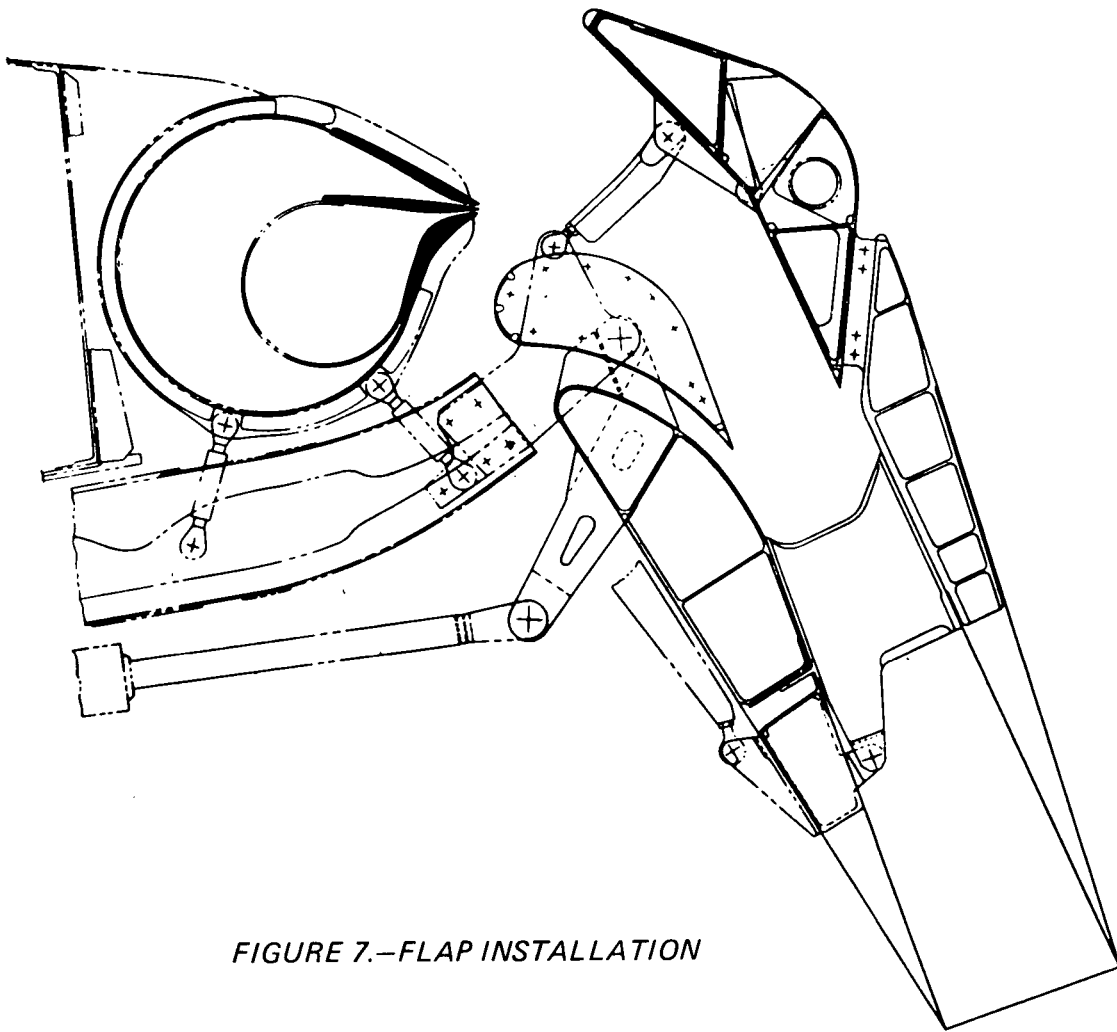
FIGURE 7.—FLAP INSTALLATION

Coanda directly in this turning process, since secondary airflow (airflow that is induced by the augmentation action) passes between the nozzle jet and the Coanda surface. This feature minimizes losses that might occur from scrubbing, but it does require accurate placement of the Coanda surface relative to the nozzle exit to obtain good augmentation performance. This requirement resulted in the design of relatively rigid flap structure to minimize spanwise and chordwise deflections. The structural design accommodates minor adjustment of the nozzle relative to the Coanda. Larger geometry changes can be easily incorporated by replacing fittings or links. The nozzle duct and nozzle are supported from the flap beams so that external loading deflects the flaps and nozzles nearly the same amount and does not disturb critical geometry.

Flap and shroud members utilize multispar construction to minimize spanwise deflection and maintain the desired geometry tolerances.

Controllable augmentor choke surfaces are incorporated to provide lift dump for landing run out, and those on the outboard flaps provide a portion of the lateral control during flight. These choke surfaces incorporate some aerodynamic balance.

The inlet door and its aft element are supported from the shroud element. The door is hinged and a slave link from the door to the end fitting on the flap beam provides the desired angle program as the flaps are actuated. The intake door angle (θ_i), shown in figure 6, varies from -30° at flaps up to +21° when the flaps are fully deflected.

End plates are used for structural members and to close off the end of each flap segment to prevent augmentation losses at the end gaps.

The upper slot between the inlet and the shroud is provided for some BLC or wake control behind this inlet to reduce flow separation. The lower slot between the Coanda and the flap element admits additional secondary airflow to the mixing region and also provides a production break that would permit repositioning of the Coanda surface relative to the other elements if testing results indicate the need.

The entire augmentor flap rotates about simple pivots and maintains its bi-surface geometry at all times. The left- and right-hand surfaces are bussed across the fuselage by a 5-in.-diameter torque tube. Inboard and outboard flap segments are bussed by interconnecting links.

Each flap segment is positioned to the desired angle by a hydraulic actuator attached to each of the two flap beams. One actuator is powered by hydraulic system A and the other by system B. Either actuator can support the aerodynamic loading. A schematic of the flap drive mechanical system is given in figure 8.
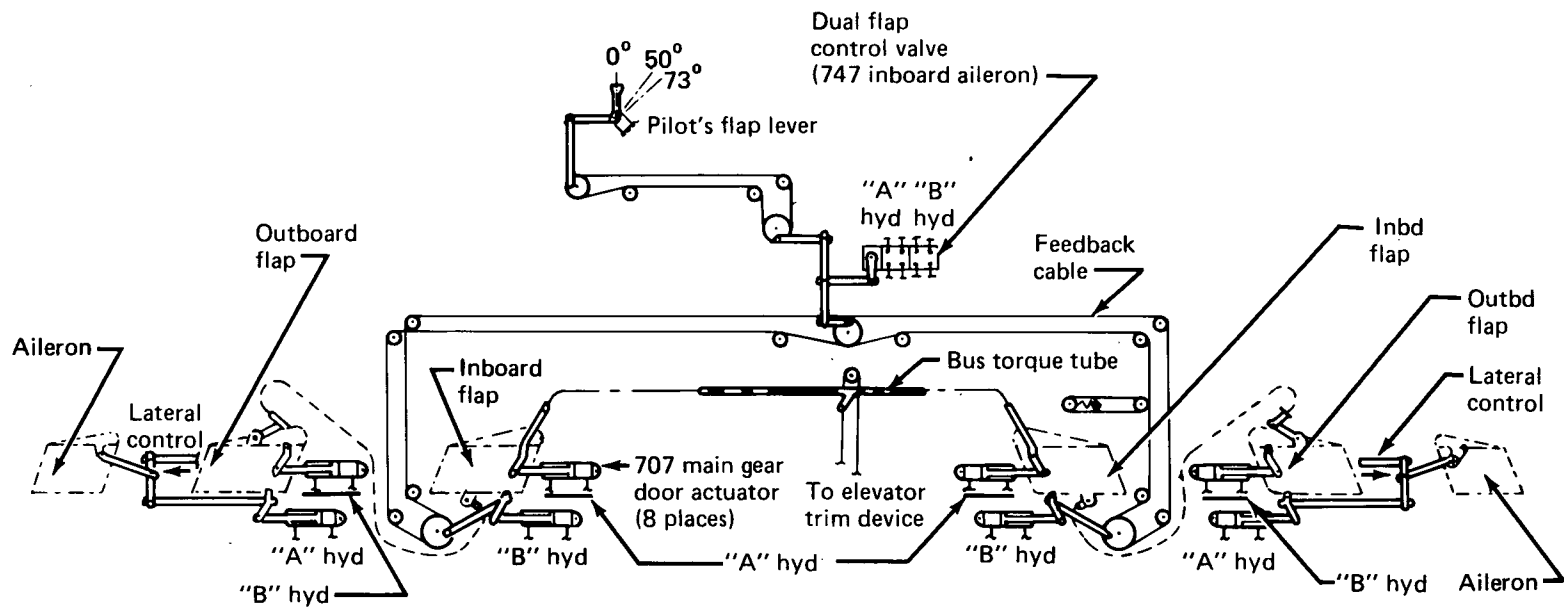
FIGURE 8.—FLAP DRIVE MECHANICAL SYSTEM

Blown Aileron High-Lift System

The blown aileron high-lift system uses drooped, constant-aerodynamic-section ailerons with blowing over the leading edges to maintain flow attachment. Aileron droop is actuated by a torque tube and idler link system deriving its motion and driving torque from hookup with the outer end of the outboard flap. The nominal droop schedule provides 30° maximum droop when the flaps are deflected 30°. Droop angle remains constant at this value for greater flap deflection. This nominal value can be adjusted to 45° for evaluation. Aileron differential motion up and down occurs about the droop angle.

Air for blowing the aileron is manifolded from the outer duct of the augmentor nozzle. This air supply originates from the engine on the opposite wing. Individual flared blowing nozzle tubes carry the air from the spanwise manifold that lies forward of the aileron near the rear spar aft to the point of exhaust onto the aileron. This manifold-nozzle tube assembly, shown in figure 9, is a welded 6061 aluminum alloy structure.

Air Supply, Distribution, and Augmentor Nozzle

The air supply, distribution, and augmentor nozzle arrangement is shown in figure 10. The entire bypass fan air source is collected by a specially installed shroud on the MK 801-SF engine and is available at the two 13-in.-diameter offtakes shown in figure 18. Approximately 36% of the air goes through one offtake and is conducted aft through the nacelle to a T duct structure that feeds the inner augmentor nozzle duct. This is the sole use of this air.

Approximately 64% of the air goes through the other offtake and is conducted spanwise through the leading edge and across the body to feed the outer augmentor nozzle duct and the aileron. The air supply for the body blowing along the theoretical wing leading edge carry-through on the fuselage is also tapped from this routing.

The unequal distribution of air from one engine to the flap section on each side of the airplane, and the fact that the boundary-layer control (BLC) air for the aileron comes from the engine on the opposite wing, provides compensation for the initial rolling moment associated with single-engine failure. Large rolling moment is developed by the working engine's hot gas efflux since the nozzles are directed predominantly downward during approach. Roll compensation effects are shown in figure 11.

A fundamental design approach was to avoid routing ducting within the wing box. This saved the present integral fuel tank system for fuel and avoided the installation of cargo compartment fuel
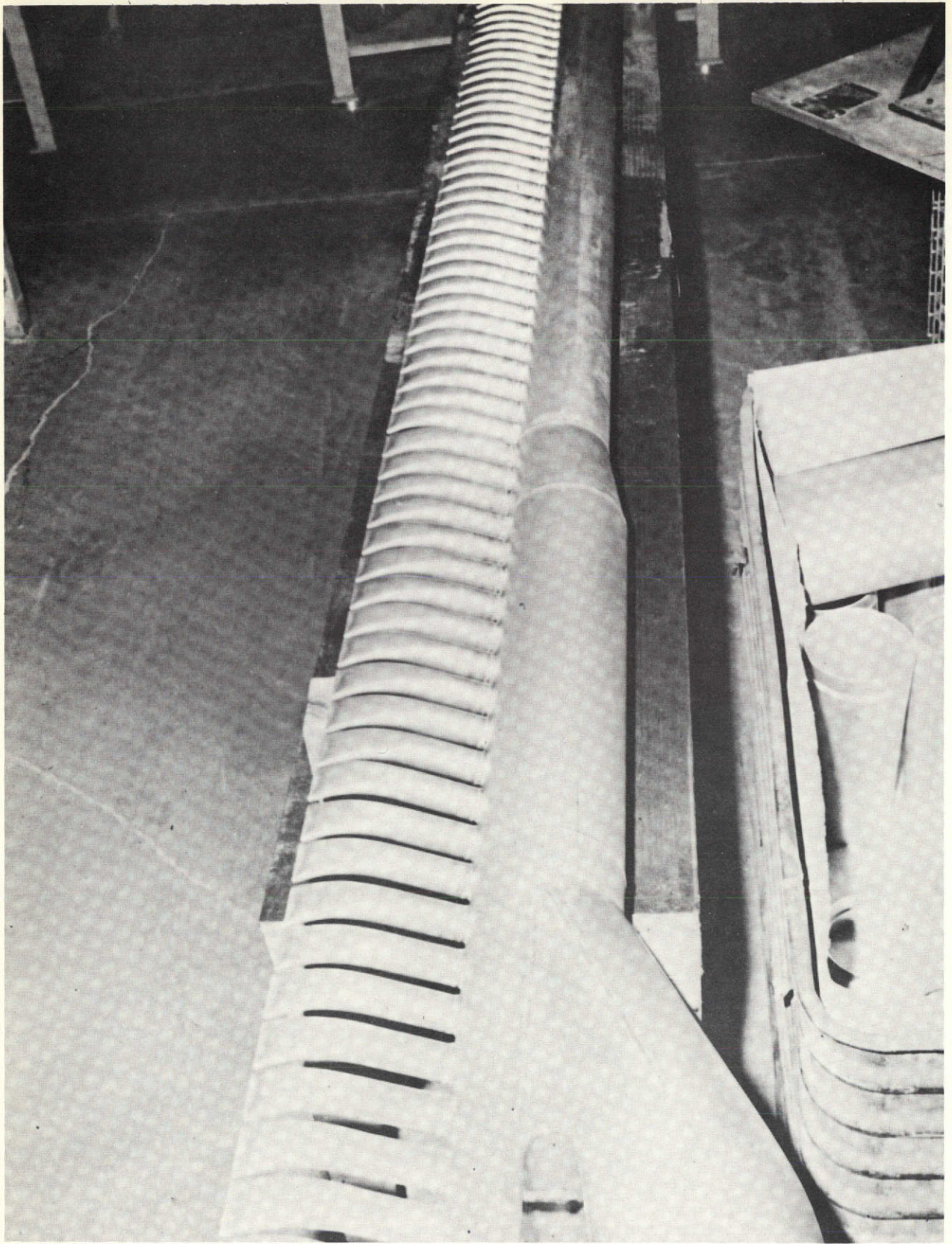
FIGURE 9.—AILERON DUCT AND BLOWING TUBES

Outer

Inner

Wing chord plane

Ducting system
- Fuselage crossover
- Independent system per engine
- No valves
- Duct-within-a-duct

Aileron

Spoiler

Augmentor
flaps

Inner
duct

Spey MK 801-SF
fan flow
(eng. 1)

Outer
duct

Body
BLC

Fuselage
crossover duct

Spey MK 801-SF
fan flow
(eng. 2)

Aileron
BLC
duct

FIGURE 10.—AIR DISTRIBUTION SYSTEM
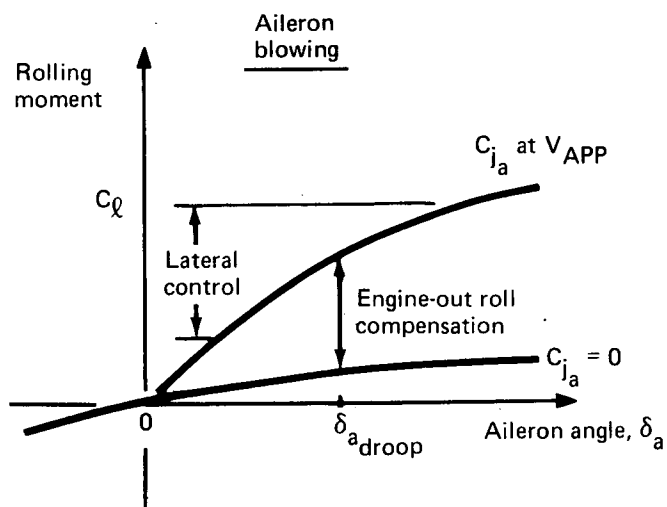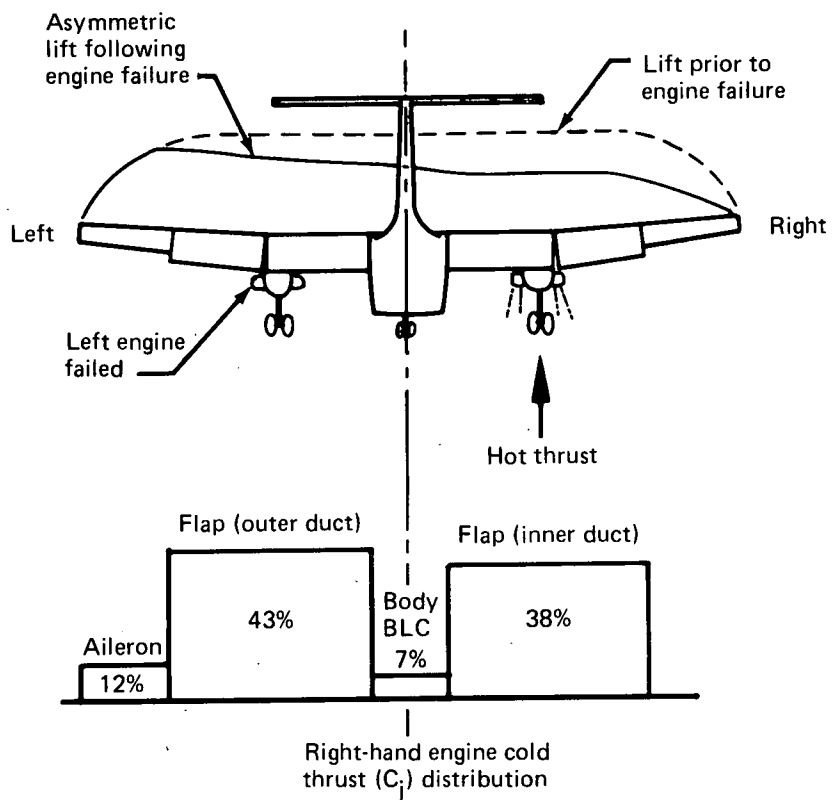
FIGURE 11.—LATERAL CONTROL INFLUENCE ON BLOWING DISTRIBUTION

tanks which would be appreciably more hazardous in a crash landing. Also, the avoidance of penetrating the wing box saved much rework to primary structure.

Supply ducts carrying the larger airflow requirement are 14 in. in diameter. All ducting from the engine to the augmentor T is corrosion-resistant steel and performs a fire containment function in the event of an engine burn-through.

The augmentor nozzle duct along the trailing edge is welded 5456 aluminum alloy. This alloy was selected because of its weldability, fracture toughness, and resistance to crack propagation. Critical loading on the augmentor nozzle ducting is derived from thermal stresses and the fact that the duct does possess considerable spanwise rigidi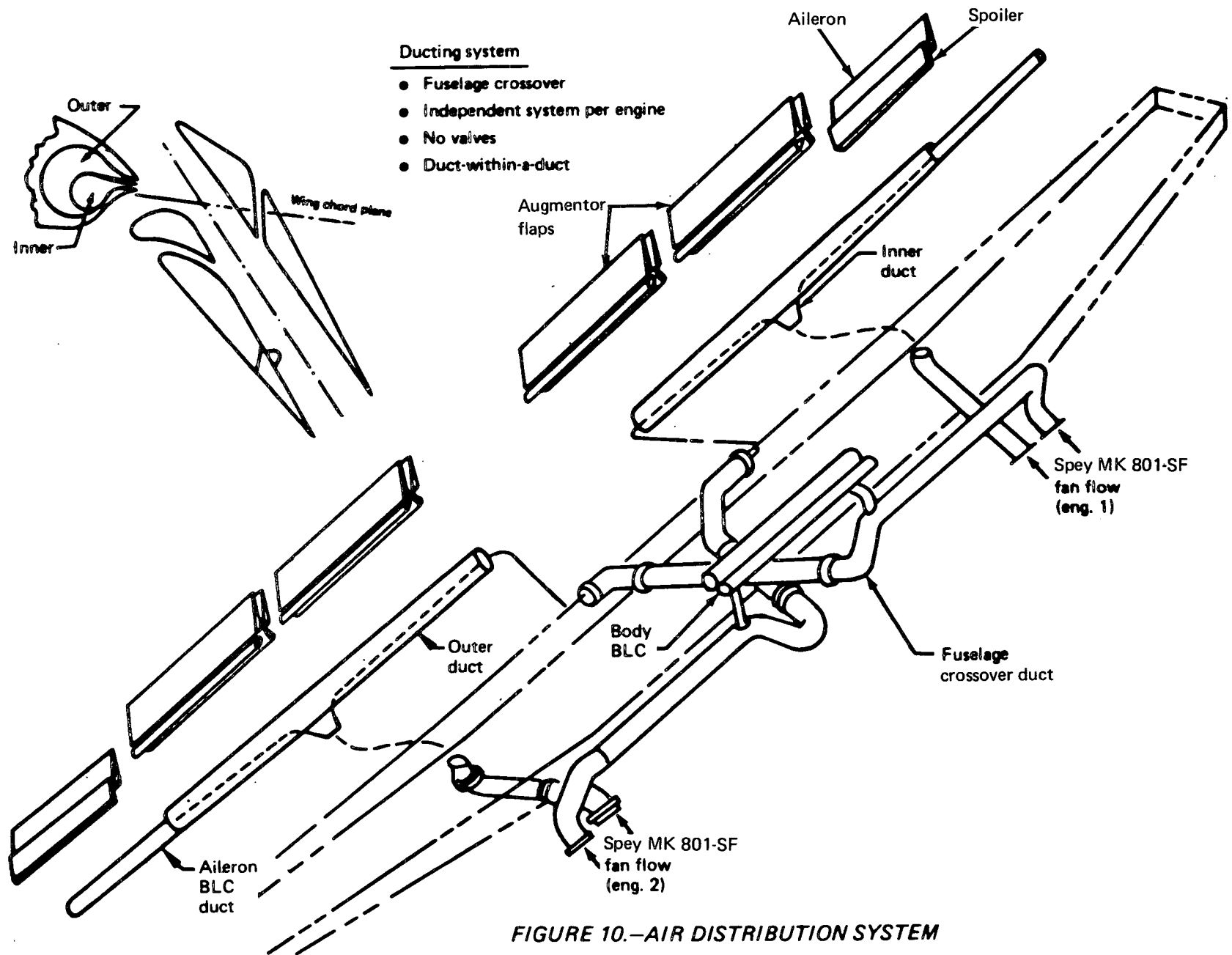ty. A nonrigid duct would be preferred; however, for this one-of-a-kind design, a material and design approach was taken that utilized the best of available knowledge and experience.

The duct-within-a-duct configuration was chosen to feed the dual nozzle arrangement since a fundamentally round pressure vessel is the most efficient design and because it is rather isotropic in local rigidity and is less likely to result in a crack-prone configuration. For example, the rigidity of a bent or welded-up corner in a square duct would be greater spanwise along the corner than for adjacent duct sheet in a chordwise direction, and the corner would tend to open up toward roundness under pressure load. The present configuration also fits the space available and allows a reasonable amount of room for cable runs, hydraulic lines, electrical runs, and control components.

Flexible connectors are used in the distribution runs to accommodate thermal and structural deflections. Tension connectors are required because of limitations in external loading of the engine shroud 13-in. air offtakes. Therefore, three connectors are necessary for every run to permit duct elongations to occur between fixed-geometry end points. The connector details are shown in figure 12. The center tie bolt is surrounded with three tension cables that are loaded only if a bolt has failed. This redundancy is necessary to prevent joint failure, which would change the bypass air nozzle area and result in engine surge and, very likely, failure.

Secondary load path (3 locations)
Primary load path
Support struts
Streamlining cone
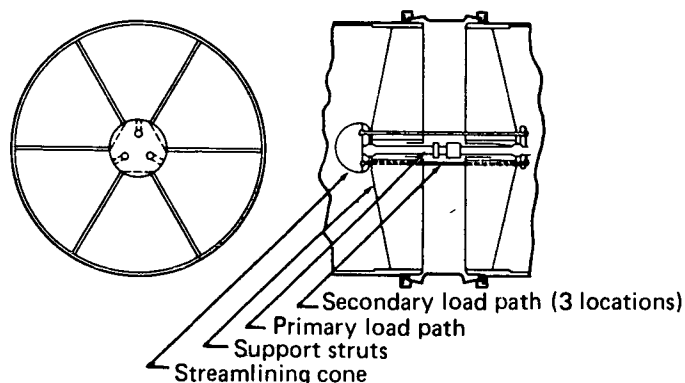
FIGURE 12.—SCHEMATIC DIAGRAM OF FLEXIBLE CONNECTOR SUPPORT SYSTEM

The augmentor nozzle, which is attached to the nozzle duct, is made of three major nozzle elements (see fig. 7) which provide dimensional stability to nozzle area and flow geometry. It is important to note that all bypass air openings—the augmentor nozzle, the aileron nozzle, and body blowing nozzle—are indeed part of the propulsion system as well as important components in providing the intended aerodynamic features.

To permit matching the nozzle to the engine, the augmentor nozzle gaps are made adjustable with shims inserted between the turning vanes and the central nozzle element. The elements composing the nozzle are all bolted together with bolts at 2-in. intervals which pass through each of the turning vanes. See "Safety Features" for a discussion of the safety provisions in the event of one or more bolt failures.

Each engine can operate independently of the other with this nozzle and distribution system. There are no valves in the system. This approach to design is very simple and avoids the problem of transients while opening or closing valves and is certainly reliable since it is a passive configuration.

Intended flow Mach numbers for the ducting have been designed to be less than 0.25. There are a few local excursions above this value, but the losses have proven acceptable. Flow conditions are depicted on figure 13. All ducting turns use a radius of one duct diameter to keep losses to a minimum. The alternative using turning vanes is heavy and more complicated.
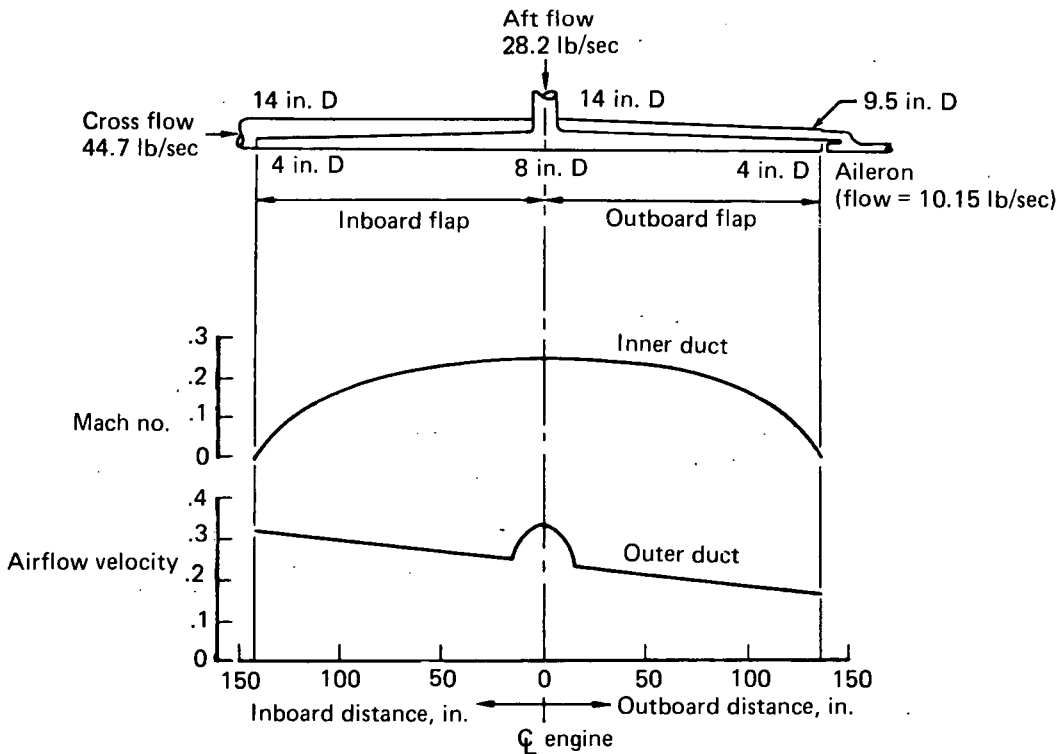
FIGURE 13.—AUGMENTOR NOZZLE DUCT AIRFLOW VELOCITY

Leading Edge Slats

Leading edge slats are installed forward of the existing wing leading edge contour, as shown in figure 14, and are mounted on beam supports that are adjustable or easily modified in the event that repositioning is desired. The spanwise dimension of slat segments is selected to achieve local loads that are acceptable to the available attachment structure on the wing and to control the amount of lost lift (hence rolling moment) that results if a segment fails. Slats have structural interties to stabilize sideloads. The ends are tied to the fuselage and to the nacelle structure.

Slats are of conventional sheet metal construction, front and rear spars with ribs. A constant aerodynamic section is used.

(a) INBOARD

(b) OUTBOARD
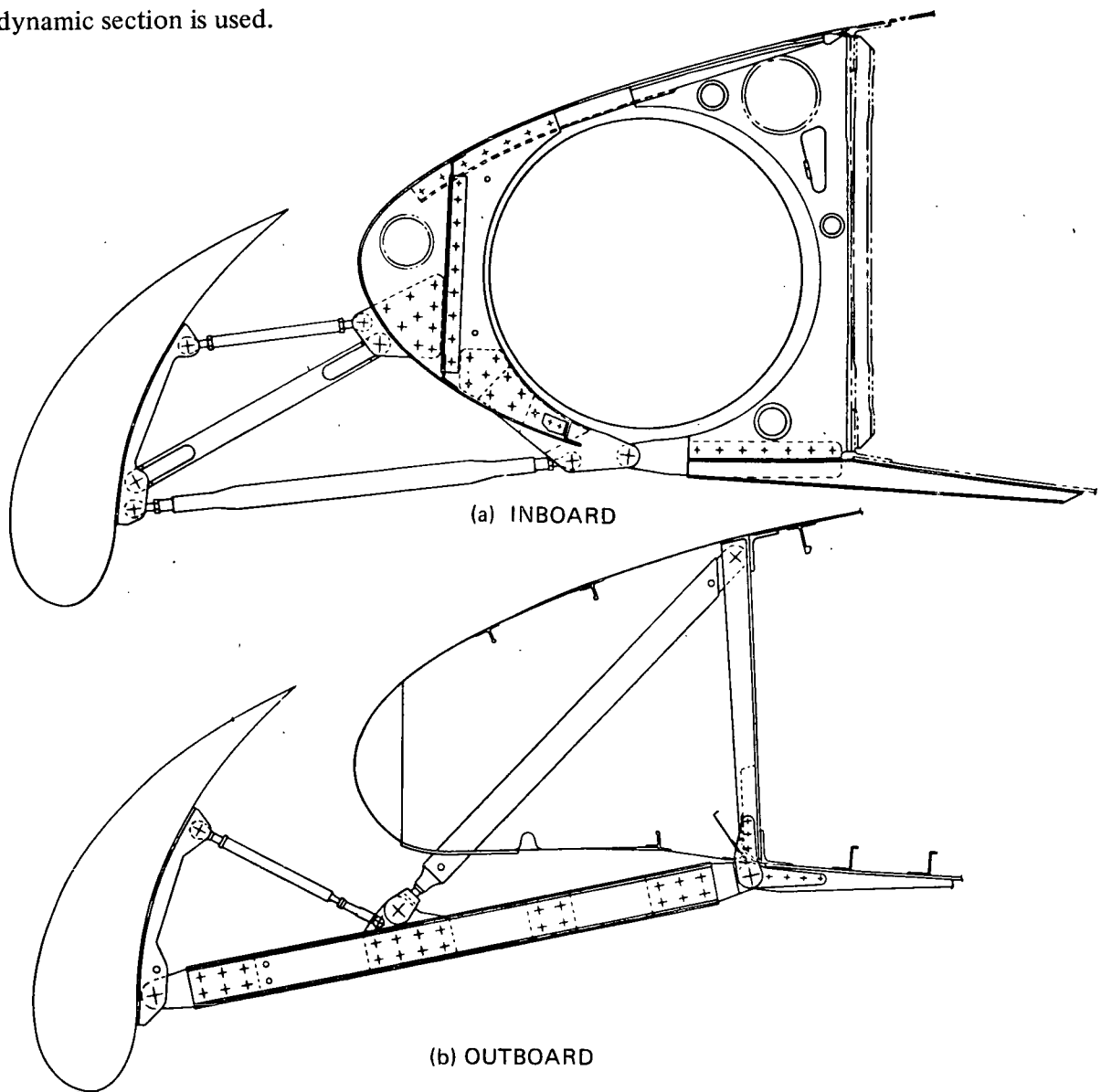
FIGURE 14.—SLAT CROSS SECTION

32

Propulsion Installation

The split-flow MK 801-SF modified Spey engine is used and installed in a nacelle assembly that was engineered, integrated, and manufactured by the de Havilland Company of Canada.

Existing firewall attachments and structure are used for supporting a new engine mount. A new rear mount support is provided on the front spar. The nacelle structural provisions for landing gear loads remain unchanged from the original C-8A. Nacelle structural arrangement is shown in figure 15. The nacelle is attached to the wing box using existing fastener holes, and the mating parts of the nacelle that match this attachment remained undisturbed during the modification. A good fit was attained.

Figure 16 portrays the air supply distribution ducting in the nacelle. The outboard bypass offtake is the one that supplies air to the opposite wing. Use of the outboard offtake for this distribution furnishes enough room and nacelle volume to achieve the desired liberal turn radius in the supply line in matching its routing through the wing leading edge.

The nacelle is divided into three fire protection/detection zones: zone 1 is the area immediately surrounding the compressor section, zone 2 is the area surrounding the hot section, and zone 3 includes the remainder of the nacelle volume through which augmentor air, fuel line, hydraulic lines, controls, and electrical services are routed. Zone 1 is provided fire detection and suppression service; zone 2 and a portion of zone 3 are provided detection only.

To meet the basic requirement of low cost, the engine has been developed by modifying an existing fan engine, separating the cold bypass flow and feeding it into ducts to "blow" the augmentor flaps. The Rolls-Royce Spey engine was chosen because of the relatively high pressure bypass airflow (maximum 39 psia at 80 lb/sec) which leads to a duct size which can be accommodated within the existing wing contour.

The engine, illustrated in figures 17 and 18, is the MK 801-SF which is a hybrid Spey engine modified from an MK 511-8 (Grumman Gulfstream II) by addition of an MK 512 (BAC .1-11 series 500) LP compressor, and MK 555-15 (Fokker Fellowship) HP external gear box. The 512 compressor is chosen because it has titanium stage 1 and 5 rotor blades with midspan snubbers, which make it very tolerant of intake flow distortions and variations from the normal outlet pressure ratio. The 555-15 wheelcase is used to enable use of the original C-8A CSD and alternator and to accommodate two high-capacity hydraulic pumps.

The new bypass duct (or shroud) mounts eight LP dump valves. These are AVON MK 101 compressor bleed valves and are provided to prevent LP compressor surge at low speeds.

33
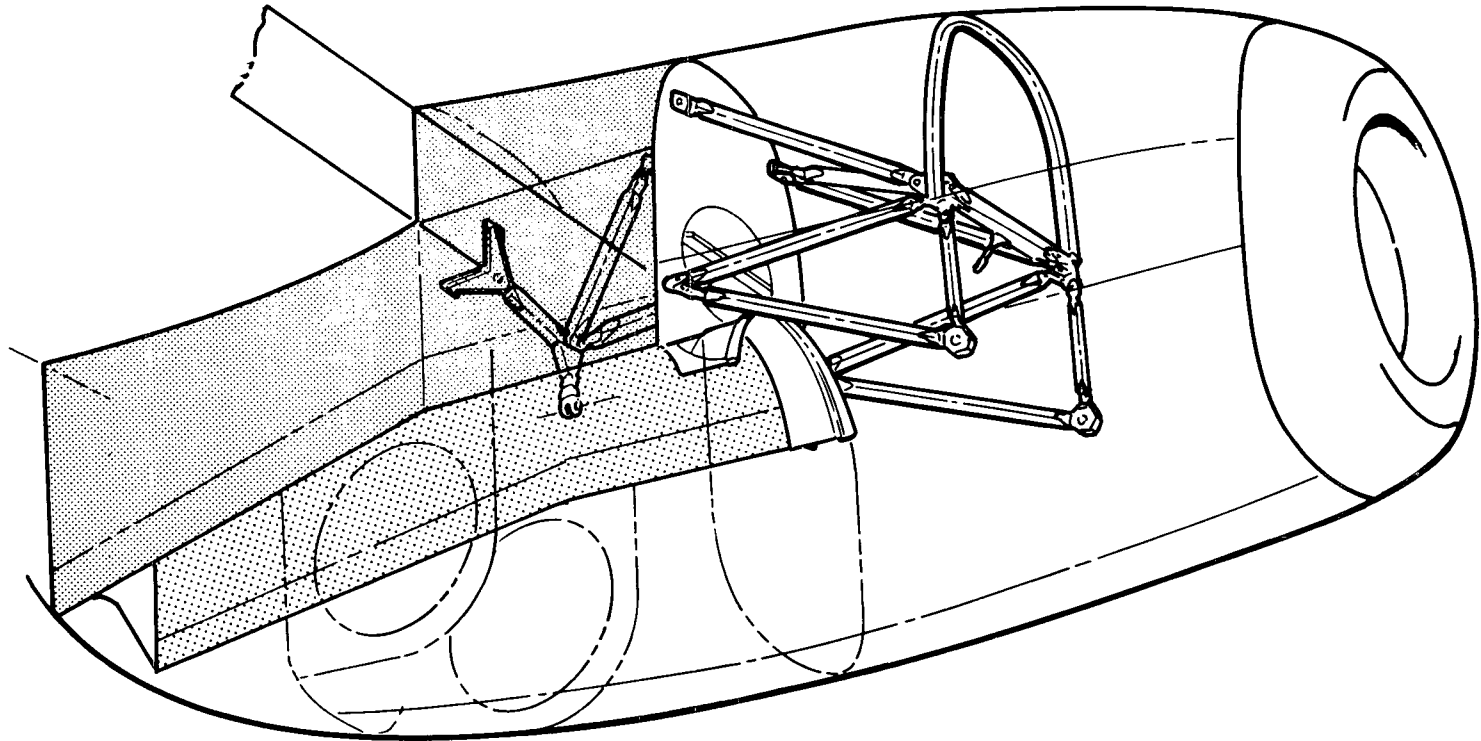
FIGURE 15.—ARRANGEMENT OF NACELLE STRUCTURE AND ENGINE MOUNTS

Sta -13.0 nac
Sta 0.0 nac
Sta 197.0 fus
Sta 44.195 nac
Sta 86.0 nac
Sta 188.22 nac

Bypass air cross duct

Conical nozzles

Boeing/de Havilland interface

20.0 centers

₵ nacelle

Bypass air rear duct

Sta 111.55 nac

Rolls Royce/deHavilland interface

Rear mount assy

Boeing/de Havilland interface

Main engine mount

6°

₵ engine

Engine mount trunnion

Engine access doors

Firewall

Firewall

Firewall shroud, engine mounted

Airbleed exit engine bypass

Nozzle actuator

FIGURE 16.—NACELLE INSTALLATION

35

LP compressor—Spey MK 512

New rear mount

New rear bypass duct

Colander plate

Conical nozzle

Pegasus MK 5 nozzle system

New transition system

Avon MK 101 LP dump valves

Spey MK 555-15 wheelcase

Basic engine—Spey MK 511-8

FIGURE 17.—DERIVATION OF MK 801-SF COMPONENTS

FIGURE 18.—SPEY MK 801-SF ENGINE FOR MODIFIED C-8A AIRPLANE

The standard exhaust unit is replaced by a new mechanical steel transition section. To this transition is bolted the colander plate retainer and the Pegasus trouser piece.

The colander plate, a steel plate with 400 one-inch-diameter holes, is interposed between the engine and the final nozzle to allow the abrupt change in area between the basic engine and the larger trouser piece without the danger of unsteady flows upsetting the engine operation. Thus, a shorter diffuser section is achieved between the engine and the jet pipe so that the two components can be closely coupled, and permits the Spey engine to operate very close to its original design running line.

The hot gas nozzle vectoring system is derived from Pegasus 5 components; the trouser piece has a new front flange welded to it to enable fastening it rigidly to the mounting ring. Nozzles are rotatable from 6° below horizontal to 14° forward of vertical. This angle range can be shifted in increments of 12° by rotating the bolt pattern of the nozzle bearings.

The nozzle airmotor drive system provides nozzle rotation rates as high as full travel in less than 1 second.

Pegasus nozzle pilot controls consist of two overhead levers adapted from the original C-8A propeller pitch control installation. These are operable from either the pilot or copilot's stations.

Lateral Control

Lateral control is provided by ailerons, spoilers, and an augmentor choke control on the outboard flaps. The concept is shown in figures 19 and 20. Pilot control signals are transmitted by the instrumented control wheel and body cable system to a centrally located dual hydraulic 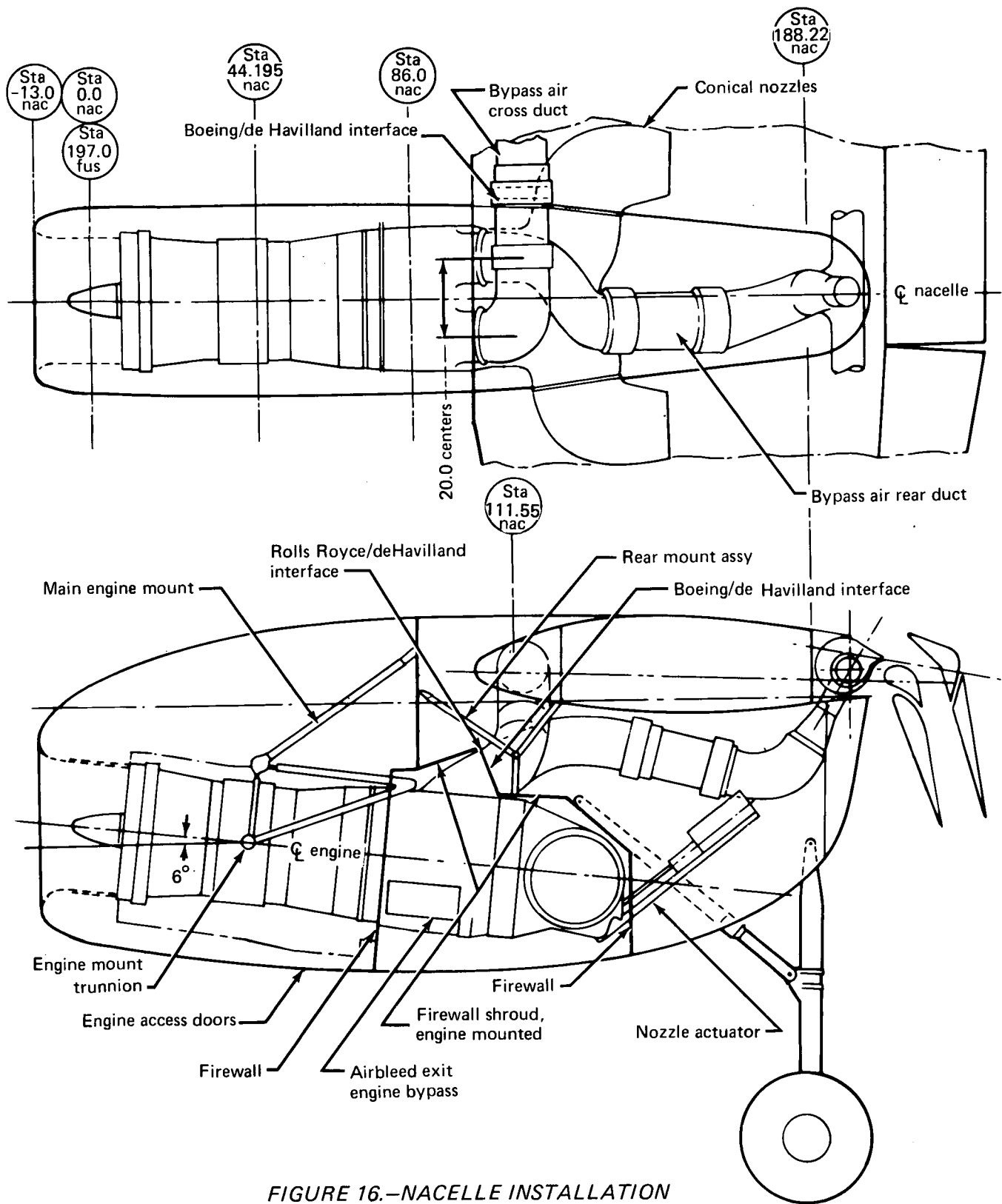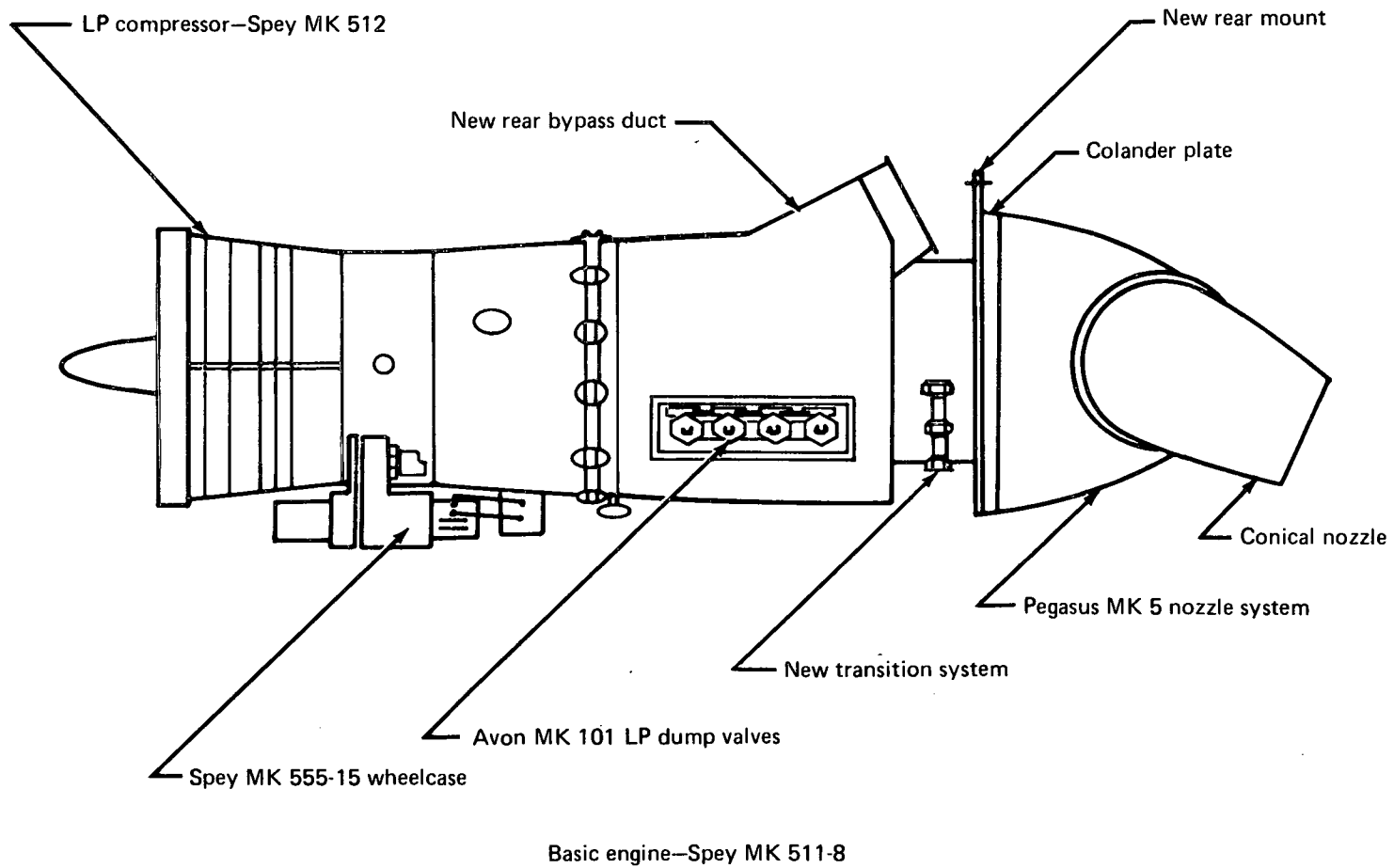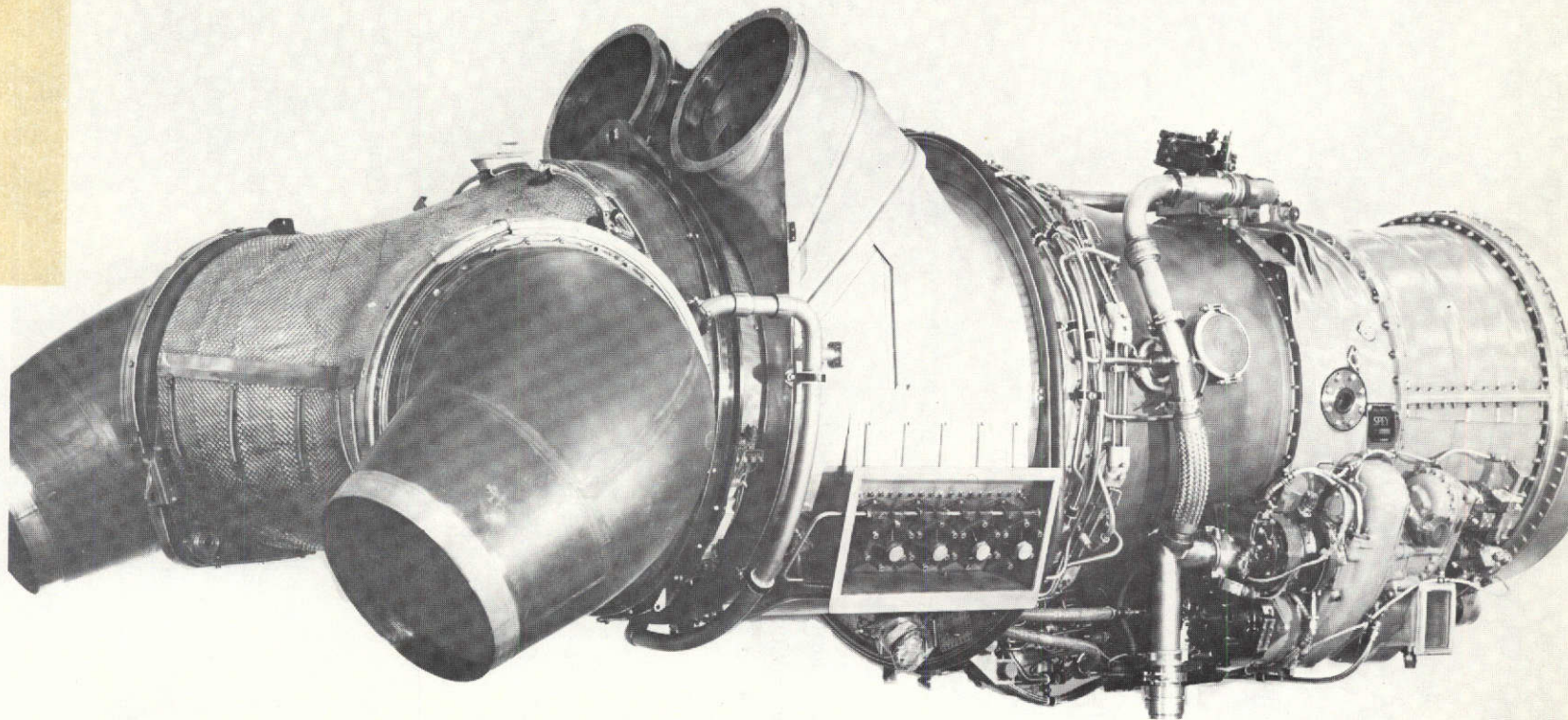lateral control servo actuator. This actuator powers the ailerons and signals the spoiler control valves and augmentor choke control valves through the wing cable system. Lateral feel, centering, and electrically actuated trim are provided by a unit mounted adjacent to the lateral control actuator.

Stability augmentation of limited authority is summed in series with the pilot's input to the lateral control actuator. Shearouts and spring pogos are provided for the spoiler, augmentor chokes, and ailerons to prevent total loss of lateral control due to jamming. The shearouts provide two alternatives: aileron-only control or the combination of spoilers and augmentor chokes. Manual reversion for aileron control is available, although the wheel forces are large since the radiused aileron leading edge that is provided to give the proper blowing geometry at all aileron angles affords no aerodynamic balance.

Spoiler

Aileron

Tab

Augmentor chokes

Outboard
lateral control
and lift dump

Inboard
lift dump
only

$\delta_{SP} = 50°$

SPOILER

BLC
duct

AILERON

Droop angle

Lateral control ±17°

Outer
duct

Inner
duct

Wing chord plane

FLAP DEFLECTION, δ_F

AUGMENTOR
CHOKE

$\delta_{CH} = 55\%$ closed
for lateral control

$\delta_{CH} = 65\%$ closed
for lift dump
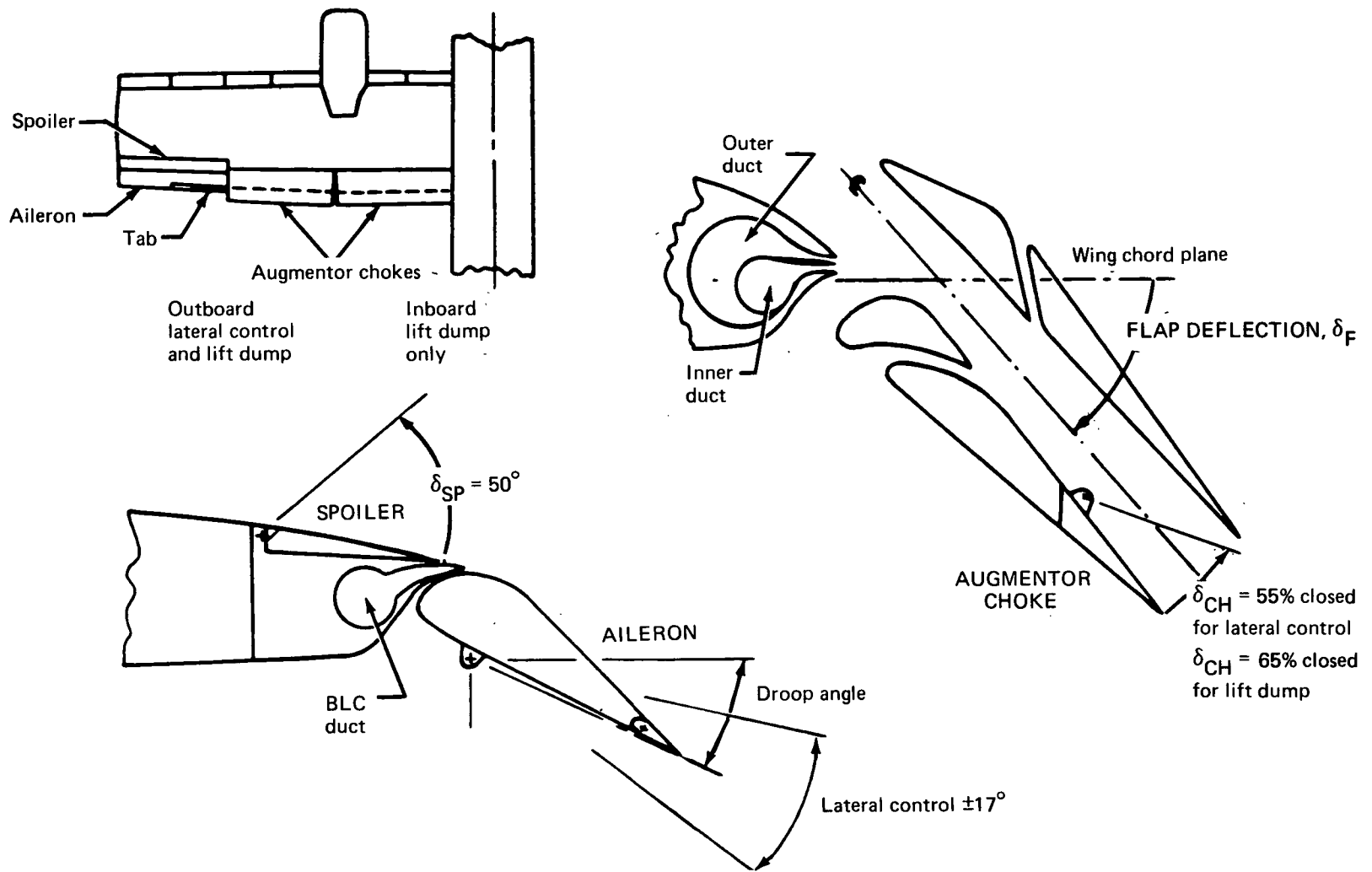
FIGURE 19.—AUGMENTOR FLAP AND LATERAL CONTROL GEOMETRY

Lateral control input to aileron

Shear outs

POGO (spring link)

Programmer

Torque shaft

707 spoiler actuator

POGO (spring link)

747 feel centering and trim unit

727 dual lateral actuator

Hydraulic system "A"

Programmer

707 spoiler control valve

Aileron control and droop mixer

Hyd system "B"

707 spoiler control valve

SAS actuator

Droop input to aileron

Sol. valve

Hyd sys "B"

Augmentor choke

Hyd sys "A"

Pilot   Copilot

$\delta_W = \pm 75°$

Geared tab

737 ground spoiler actuator

707 spoiler actuator

Lift dump sol. valve

Inboard augmentor choke

Body cable run

SPOILER

$\delta = 50°$

AILERON

$\delta_{LAT} = \pm 17°$

$\delta_{DROOP} = -33°$
$-45°$ optl

Mass balance

OUTBOARD AUGMENTOR CHOKE

$\delta = +55\%$ (lateral)

$\delta = +65\%$ (lift dump)

INBOARD AUGMENTOR CHOKE

$\delta = +65\%$ (lift dump)

Note: Electric trim at rate of $\delta_W = \pm 4.2$ deg/sec
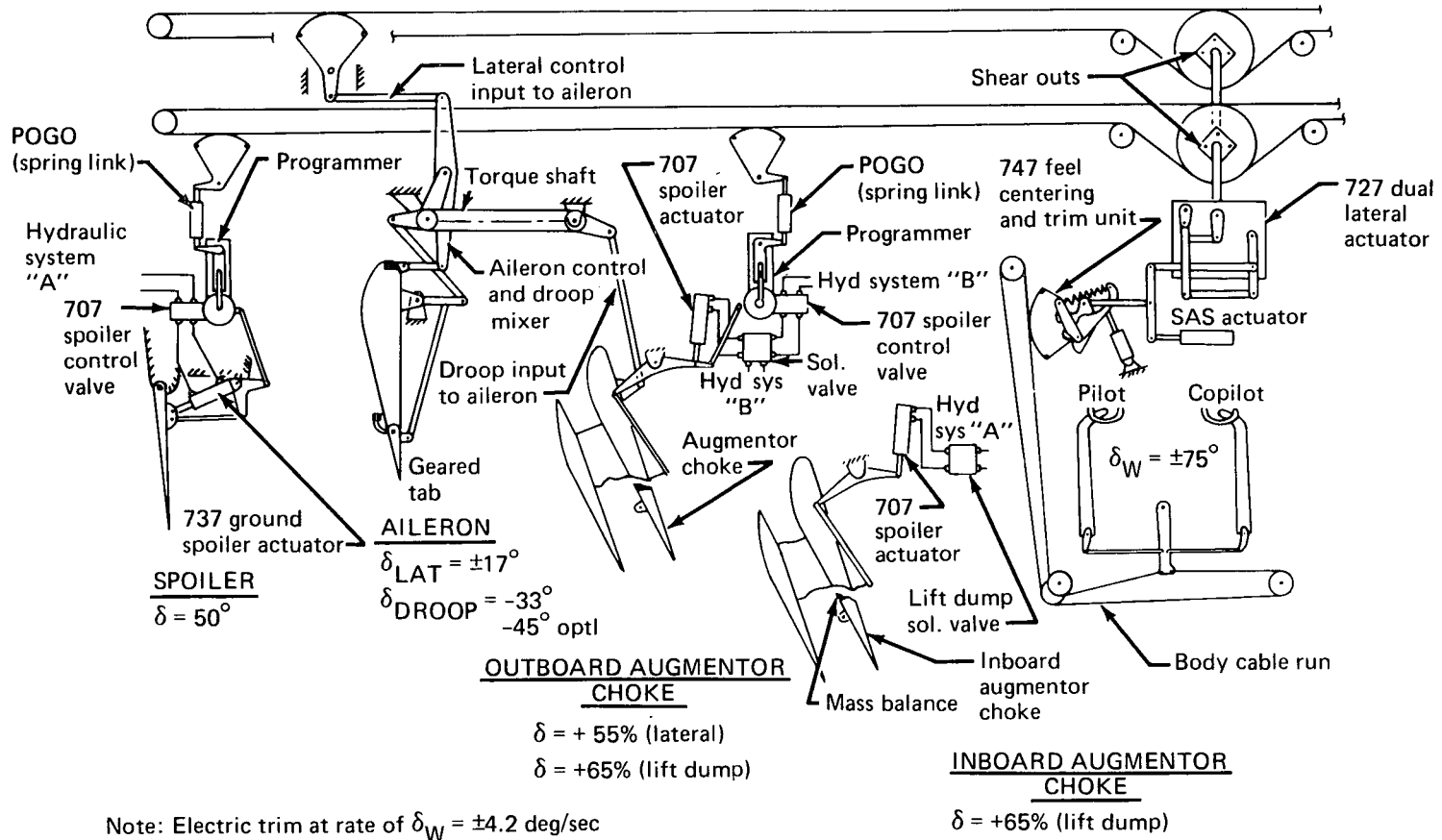
FIGURE 20.—LATERAL CONTROL SYSTEM

Simulator tests revealed that lateral control sensitivity (roll acceleration per unit wheel input) should be high for satisfactory pilot ratings. The lateral control system was improved to increase control sensitivity by these steps:

- Revised spoiler programming with minimum delay in motion with initial wheel input and full spoiler deflection at two-thirds wheel

- Modified spoiler actuators and control linkages to decrease backlash and hysteresis.

- Provision of "quickening" by electrical feed forward of wheel position through the lateral SAS to effectively double the system gearing about neutral wheel.

A balance tab is provided over the inboard half of the aileron to reduce the hinge moment. The outboard half has a geometrically similar fixed tab that is deflected upward on both ailerons. It is set at 16° upward deflection on the delivered airplane. This tab is provided to limit the amount of aileron upfloat in the event that the droop intertie with the flap should fail. The upfloat should be related to drooped aileron settings for which a failed interconnect causes rolling moment because the good side is still effective.

Low-speed lateral control rolling moment coefficient capability is high to meet the roll response requirements (see fig. 21). It is apparent that approximately one-third of the total rolling moment capability is derived from each of the three systems. The fuel system is designed to supply from the outer wing tanks initially so that rolling inertia values reduce quite rapidly.

Longitudinal Control

Longitudinal control is essentially the same as provided in the original C-8A. A minor modification has been made to the spring tab gear ratio and to the centering spring stiffness to reduce stick forces. The longitudinal control is entirely manual, and the RH elevator possesses the spring tab for force reduction. The LH elevator incorporates a trim tab installation. The stabilizer setting remains unchanged from the basic C-8A at 1° nose-up incidence relative to the fuselage angle-of-attack reference line.

Lateral-Directional Stability Augmentation (SAS)

Lateral-directional stability augmentation (SAS) is provided to improve handling qualities in the STOL flight regime. It operates at speeds below 100 kt and is automatically disengaged above this speed by a q-sensing switch. Two basic modes are used, normal SAS and variable SAS.

Note: $\delta_F = 75°$, $V_{APP} = 60$ kt, $C_{j_{total}} = 0.49$, $\alpha_W = 2.5°$
Landing approach condition

Choke

Spoiler

Ailerons

Total

C_ℓ

C_n

Total

Ailerons + spoiler

Ailerons only

Ailerons only

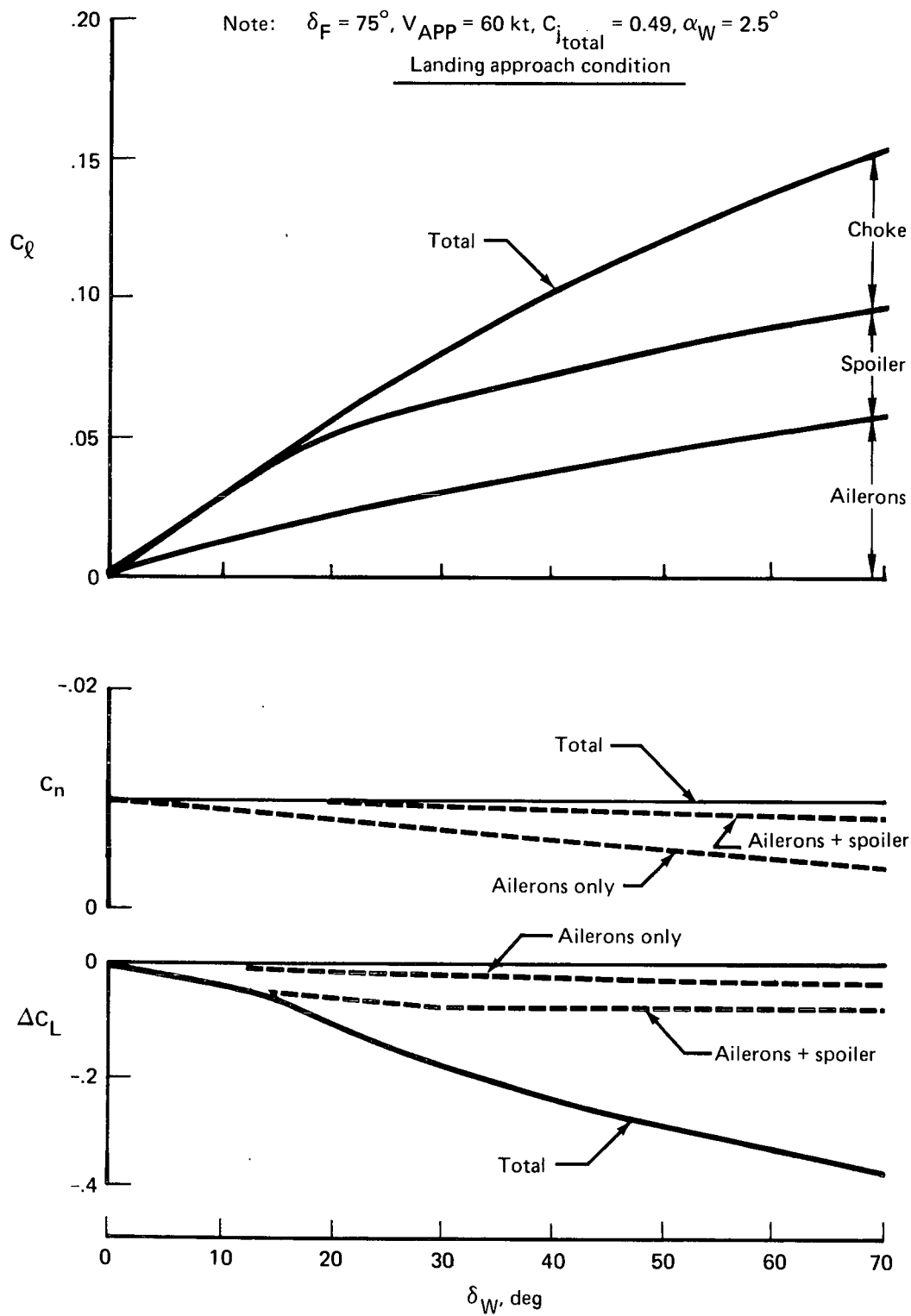Ailerons + spoiler

Δc_L

Total

δ_W, deg

FIGURE 21.—LATERAL CONTROL EFFECTIVENESS

The normal SAS mode improves qualities through:

- Roll mode augmentation
- Spiral mode augmentation
- Turn coordination
- Dutch roll damping

Control wheel position information is used in the lateral axis to improve linearity of roll response to wheel inputs. Automatic gain switching with flap position is provided for more uniform response over the operating envelope.

The variable SAS mode permits selection of a wide range of lateral-directional characteristics by gain and sense control of the following:

- Roll rate to aileron feedback
- Yaw rate to aileron feedback
- Sideslip to aileron feedback
- Yaw rate to rudder feedback
- Roll rate to rudder feedback
- Roll attitude to rudder feedback
- Aileron to rudder crossfeed

The SAS is nonredundant, with authority limited to a safe value. Automatic transfer ability is provided to ensure continuous electrical power supply following the loss of one electrical system. Total system isolation is maintained between the lateral and directional axes for the normal mode. All signal computation for the variable stability mode is done in one computer, so that no axis isolation exists in this mode.

Two control panels are provided for mode and gain control. In addition, a quick-disconnect switch is provided on the pilot's and copilot's control wheels for completely disconnecting the SAS system. The basic system implementation is shown in figure 22.

Hydraulic System

The C-8A hydraulic system has been modified to provide two independent, equal-capacity, 3000-psi systems. The brake and nose gear steering systems remain unchanged except for rerouting of plumbing in the centerbody section and on the wing. The rudder system is modified only to include a q shutoff valve in one leg of the dual actuation to reduce the amount of rudder authority above 100 kt. This is done for structural load constraint. Equipment and plumbing installation for

ROLL AXIS COMPUTER

(New)

Flaps

Demod

SAS servo

Lateral PCU

Mixer

Pot.

Wheel posn

$F > 40$

Easy on

$\dfrac{10}{(5S+1)}$

Eng sync

TV   SV

Spoilers   Ailerons
chokes

RG

Roll rate

Demod

$\dfrac{K}{(.1S+1)}$

Sys test

Lateral controls

Sys test

Yaw rate gyro

Demod

$\dfrac{.87}{(.1S+1)}$

SA

+ 28V eng

Airspeed < 100 kt

A/P cables

VSS and SAS disconnect

Yaw rate

ISOL amp

To engage sys test, auto disengage logic

Test interlock and servo shutoff gain change

Pilot's control wheel

Copilot's control wheel

VARIABLE STABILITY COMPUTER

Gain   Filter

Invert amp

Gain   Filter

Roll Sum

Variable roll axis normal

On

Stability yaw axis normal

Invert

Gain   Filter

Off

Reverse polarity

Reverse polarity

Vane

Sideslip

Gain   Filter

ISOL   Invert

From ISOL and invert amps to filter amps

Oleo sw

Airspeed > 100 kt sw

Flaps $> 45°$ sw (2)

Pot

Ail posn

Gain   Filter

ISOL   Invert

Yaw Sum

Stability augmentation

Yaw/roll damper off

Warning light

Gain   Filter

ISOL   Invert

Test   Roll
RR ○ YR

Yaw SAS off

On/off lights

Gain   Filter

ISOL   Invert

Test   Off Engage
TC ○ YR
Yaw

Roll SAS off

YAW AXIS COMPUTER

Oleo sw

To engage sys test, auto disengage logic

Test interlock auto servo shutoff gain chg

Airspeed > 100 kt sw (2)

Flaps $> 45°$ sw

(New)

VG

Roll attitude

Demod

Sys test

$\dfrac{.21S}{(.1S+1)^2}$

Rate taking filter

Easy on

Flaps $> 40°$

Demod

SAS servo

LVDT MOD

Rudder PCU

(Existing)

Rudder

Sys test

TV   SV

A/P cables

Sys test

Yaw rate gyro

Demod

.24

$\dfrac{2.72S}{(2.7S+1)\cdot(.27S+1)}$

Band pass filter

VSS

$\dfrac{10}{(5S+1)}$

SA

Eng sync

Yaw rate

ISOL amp

SAS
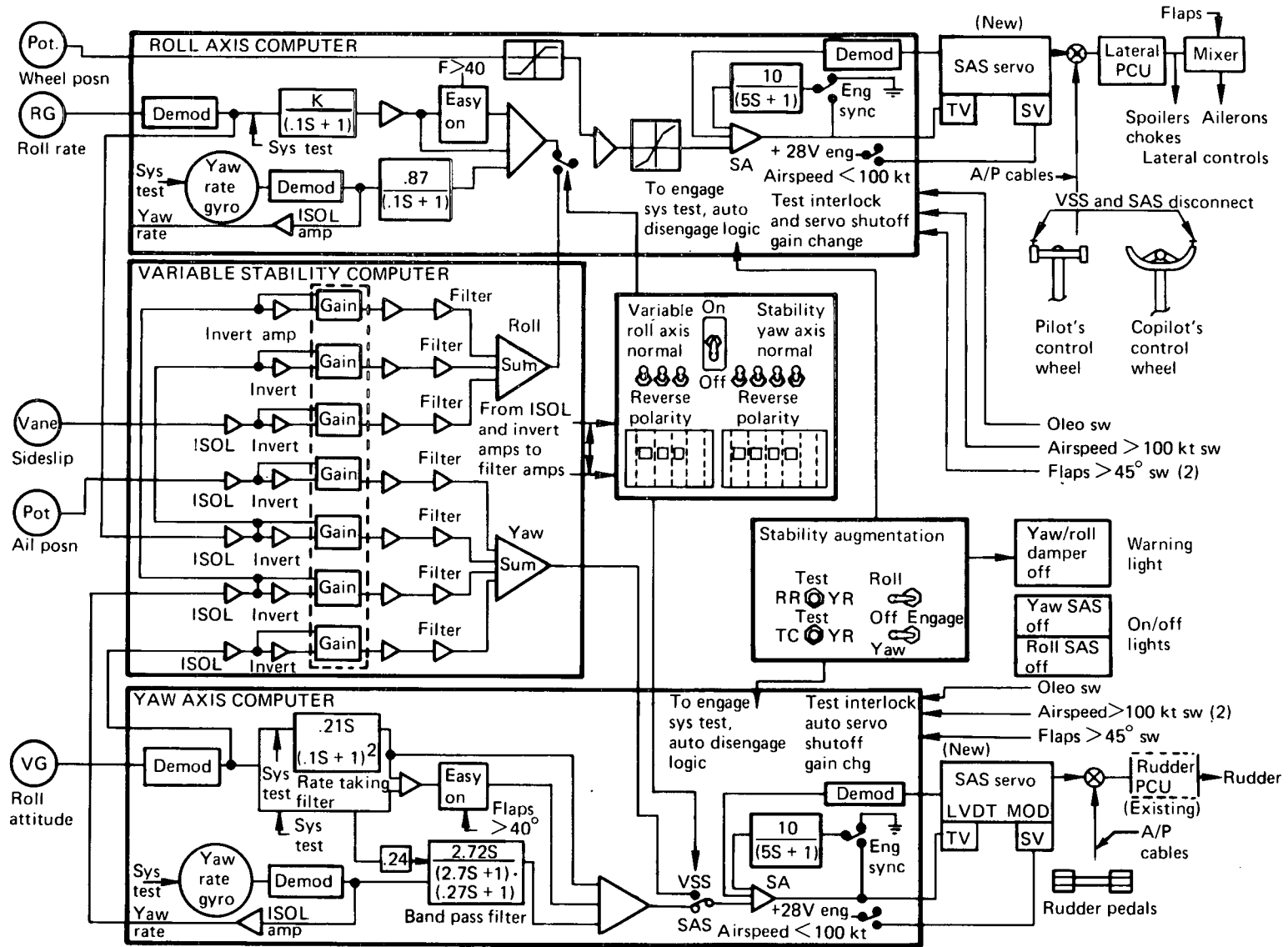
+28V eng

Airspeed < 100 kt

Rudder pedals

FIGURE 22.—STABILITY AUGMENTATION SYSTEM

the wing control surfaces (ailerons, spoilers, flaps, augmentor choke) and the power systems are entirely new. The original C-8A hydraulic system had insufficient capacity to accommodate the new requirements, particularly rapid flap retraction for configuration cleanup and go-around in the event of engine failure shortly after takeoff. Furthermore, hydraulic actuation of the flaps through cylinders located at each flap beam was preferred to a central actuation with mechanical drive along the rear spar because of a lack of installation space after providing for the large-diameter augmentor nozzle duct.

The power system capacity is 12 gpm from each of four engine-mounted, positive-displacement pumps. The independent systems, A and B, have two pumps per system, one mounted on each engine for engine-out redundancy. Pressure is regulated to the flaps and augmentor choke system to provide blowback capability to prevent exceeding design hinge moments. This feature is particularly desirable because of the limited design data base. All actuators were selected from model usage on existing Boeing transport aircraft. This resulted in actuator sizing considerably over required capacity, but does provide extra rigidity.

Main Landing Gear Wheels and Brakes

Main landing gear wheels and brakes have been changed to use 727 nose wheels and brakes. This modification was made to accommodate the heavier gross weight of this configuration and also to furnish the greater braking capacity needed because of the absence of thrust reversal. The airplane is not equipped with an antiskid system.

Electrical System

The airplane is equipped with two General Electric model 2CM351D2 engine-driven, 120/200-volt, 3-phase, 400-cycle (nominal) alternating current, brushless generators, wye connected with grounded neutral. Each generator is rated at 15 kVA when self-ventilated under ground conditions and 20 kVA when ventilated in flight. Voltage output is regulated to within ±2.5% of nominal. The associated control panels provide protection against overvoltage, undervoltage, bus fault, underfrequency, and feeder faults. The airplane is also equipped with three 28-volt, 200-ampere transformer-rectifier units (TRU).

In addition, the airplane is provided with a 36-ampere-hour, 24-volt battery which is maintained in charged condition by floating on the left-hand direct current bus.

Data Acquisition System

The test data recording system is installed in a rack in the main cabin. The existing rack was modified to accommodate cabin height restrictions caused by added ducting. The complete data

system, exclusive of sensing devices and cockpit controls and indicators, is mounted in the laterally centered rack, allowing passage and access on either side. It is attached to existing cargo tiedown fittings, and electrical connecting cables have sufficient length to permit the rack to be relocated longitudinally to change the airplane center of gravity.

The basic system is a model DAS-5600 data acquisition system manufactured by Gulton Industries of Albuquerque, New Mexico. It is capable of recording 72 analog measurement signals and 28 digital signals at 100 samples per second per measurement at an accuracy of 0.1%. The recorder is a MARS 1000 tape recorder manufactured by Astro-Science Corporation, South El Monte, California. It accepts a 4600-ft reel of 1-in. tape which is driven at 15 in. per second, allowing 1 hour of recording time. A data record is started by closing the record switch on the pilot's panel, the copilot's panel, or the control panel on the instrumentation rack. When the switch is opened an automatic zero-calibrate cycle is recorded, after which the recorder turns off. A Gulton time code generator furnishes time code to the recorders and to displays in the cockpit and at the instrumentation rack.

Additional recording capability is provided by a CEC model 5-114 18-channel oscillograph installed on the instrumentation rack. The total recording capability is 118 channels, of which 100 are PCM and 18 are oscillographic. At the time of airplane delivery all channels are in use except for 10 on the oscillograph.

Airplane Weight Breakdown

After delivery of the airplane for modification, a number of items were removed prior to installation of the new parts. The weights of the removed items are tabulated in table I.

TABLE I.—ITEMIZED WEIGHT OF AIRPLANE REMOVALS

Item	Weight, lb
Nacelle and contents	6 787
Wing	1 439
Flight controls	215
Electrical	141
Bleed system	37
Anti-ice	175
Hydraulics	185
Instruments	20
Furnishings	239
Ramp door floor	75
Cargo equipment	337
Radio equipment	64
Emergency equipment	43
NASA equipment	1 381
Total removals	**11 138**

Table II presents the itemized weights for both the de Havilland and Boeing additions to the airplane. The weights of the majority of the items (85%) are based on actual weighing data; the remaining 15% are based on calculated data. A summary of the airplane weight is given in table III.

TABLE II.—ITEMIZED WEIGHT OF AIRPLANE ADDITIONS

Item	Weight, lb
I. DHC additions	
Inlet	132
Upper cowl	193
Lower cowl	486
Aft fairing	38
Fixed structure	570
Engine mount	274
Firewall	45
Systems	412
Nozzle actuation	163
Spey and Pegasus installation	7044
Total DHC additions	9357
II. Boeing additions	
Flaps	1604
Ailerons	262
Spoilers	63
Leading edge	800
TE shroud	169
Flap supports	500
Aileron supports	50
Wingtips	15
Hydraulics	825
Electrical and electronics	250
Instruments and flight deck	75
Flight controls	400
ECS	30
Fuel system	-175
Augmentor duct system	1800
Nose boom	115
Main gear modifications	250
Fuselage modifications	50
Paint	150
Total Boeing additions	7233

TABLE III.—WEIGHT SUMMARY MODIFIED C-8A
DELIVERY CONFIGURATION

Item	Weight, lb
Baseline empty weight	25 255
Removals	-11 138
"Stripped" configuration	14 117
DHC additions	+9 357
Boeing additions	+7 233
Pilot and copilot	+ 400
Trapped fuel	+ 110
Engine oil	+ 28
OEW	31 245
Deliverable flight test equipment	+1 320
OEW + FTE	32 565
Fuel	+12 435
Maximum design gross weight (STOL operation)	45 000

Although the maximum gross weight when used for STOL operation is 45 000 lb, the airplane was cleared for a maximum gross weight of 48 000 lb for conventional operation where the rate of sink at touchdown would be considerably less than the design value of 12 ft/sec.

SAFETY FEATURES

Some of the basic design features of the augmentor wing modification keyed directly to safety are reviewed in the following paragraphs. The primary consideration has been to design the aircraft such that the pilot can maintain control in the event of any single equipment failure.

The internal ducting system for the augmentor air provides for a minimum of roll asymmetry with loss of an engine. During the landing approach, which is most crucial for an engine loss condition, each engine is supplying vectored thrust through the Pegasus nozzles and fan air to the augmentor flaps; 36% to the flaps directly behind the engine, and the remaining 64% to the body blowing and to the flaps and the aileron on the opposite wing.

Due to this airflow split, loss of an engine results in an asymmetrical loss in aerodynamic lift, the lift on the side with the failed engine being larger, thus introducing a rolling moment to counter the rolling moment due to the vectored hot thrust of the operating engine. The remaining unbalanced rolling moment is controllable using the lateral control system. The Ames Flight Simulator for Advanced Aircraft was used extensively to verify that the aircraft was controllable with an engine failure and to develop and optimize piloting techniques to minimize exposure of the aircraft to areas of marginal performance capability.

The lateral and directional flight controls operate in the irreversible hydraulic-boost mode. The ailerons, rudder, and flaps have dual hydraulic actuators on separate systems; loss of either of the two hydraulic systems would still allow satisfactory control. The augmentor choke and spoilers have single actuators but are connected to separate systems. Loss of all hydraulic power leaves the controls in the mechanical backup mode.

Lateral control is achieved through three separate inputs: ailerons, spoilers, and the outboard flap augmentor chokes. Each unit contributes roughly a third of the available rolling moment authority. Failure of any one to operate correctly leaves sufficient control reserve for all normal flight conditions, including takeoff and landing.

The lateral and directional control systems utilize existing flight-proven hardware, much of it from various models of Boeing transport aircraft. Most of the units, such as hydraulic actuators, are used unmodified. Others, such as control quadrants and position feedback sensors, are modified to fit the particular function. The lateral control system, for instance, used a 747 feel and centering unit, a 727 dual hydraulic lateral actuator, several 707 spoiler control valves and spoiler actuators, and a 737 ground spoiler actuator.

The original manual longitudinal control system, a single cable system, is retained although it has been modified to reduce the stick forces to improve the handling qualities. In the event of a cable failure, the elevator trim tab can be utilized to provide approximately 50% of the original elevator control authority, which provides a measure of longitudinal control system redundancy. The stabilizer incidence is ground adjustable, which increased the airplane's research versatility and increased safety in the event that a single stabilizer incidence setting is not adequate over the entire flight envelope.

A lift dump feature, composed of flap elements that close the augmentor channel, is utilized to spoil the lift and thrust of the augmentor after touchdown to reduce landing roll. To prevent inadvertent actuation of the lift dump during flight, the operating signal must be conditioned by an arming switch, a retarded throttle, and a switch on the landing gear that senses deflection.

Fixed landing gear, fixed leading edge slats, and noncollapsible augmentor flaps are used on the airplane to reduce structural complexity.

Redundant hydraulic systems are used, each driven by two pumps, one on each engine. Either system, operating on only one pump, can operate the critical flight control surfaces, including the actuation of the flaps. If a complete hydraulic failure should occur, the flaps will blow back to the "up" position, and the ailerons are operable by direct mechanical backup.

The flaps are hydraulically actuated, each flap segment having two actuators, one powered by each hydraulic system. In addition, the flap segments are interconnected by mechanical links to ensure in-phase operation. The actuation system has been designed to allow the flaps to blow back in the event that excessive loads are encountered.

It has been recognized from the start of the program that safe operation of the AWJSRA, and other powered lift aircraft, are in large part dependent on proper functioning and reliable operation of the propulsion system. Two Rolls-Royce Spey MK 801-SF engines, which are derived from a Spey MK 511 engine case, mated with a Spey MK 512 compressor, MK 555 HP external gearbox, and Aron MK 101 LP dump valves, are used in the aircraft. These components have been proven to be very reliable in commercial service. To these basic components a Pegasus 5 engine nozzle trouser piece, with new conical nozzles, is added to allow the hot thrust to be vectored. A colander plate, a steel plate with 400 one-inch-diameter holes, is placed between the basic engine and the Pegasus trouser piece to provide matching between the engine turbine exit and the larger Pegasus trouser piece entrance. A new fan air bypass duct and new rear transition section complete the basic engine. The engine accessories, such as the constant speed drive units and electrical generators, are standard parts modified as necessary to fit the engine and meet the operating requirements of the aircraft systems. Even though the basic engine components and accessories have a rated time between

overhauls much greater than 200 hours, the engine was developed as a prototype and has completed a 50-hour cyclic pass-off test on the manufacturer's test bed before being approved for 200 hours initial life.

The engine originally used Pegasus 5 vane nozzles, but early engine tests showed a tendency for fatigue cracks to develop in these nozzles. Although Pegasus nozzles are considered flight qualified, they have been replaced with new conical nozzles to achieve longer life. The conical nozzles were not used in the 50-hour pass-off test, but they are considered flightworthy and have completed 25 hours of combined ground and flight testing.

The engine nozzle control system utilized unmodified actuation components from the Hawker Siddeley, Kestrel, and Harrier aircraft. Inputs to the actuator are provided through the modified C-8A propeller cockpit controls. The nozzle actuators were new with all improvements gained from the Harrier program incorporated at the time of manufacture. The actuator consists of two air motors driven by engine high-pressure bleed air driving an epicyclic differential; either air motor having adequate torque to drive the system in the event of the failure of the other air motor. The nozzle control system is entirely pneumatic/mechanical and requires no electrical or hydraulic power. Shearout sections are provided in the mechanical transmission path between the nozzles of each engine to allow movement of the remaining operable nozzle if the nozzle bearing should seize.

The unique feature of the airplane propulsion system is the air distribution system, which transports the engine bypass air from the engine to the wing slot nozzles, fuselage blowing nozzles, and aileron blowing nozzles. The entire system has been conservatively designed with low hoop stresses. System thermal stresses have been identified and reflected in the design. Stresses on the critical duct elements, such as the rear duct T-joint, were monitored during the contractor's test program. The measured stresses are discussed in the "Ground Tests" and "Flight Tests" sections. Two dual-opposed pressure gages are on the control panel to allow the pilot to detect a failed duct and take corrective action. Dual load paths are used in the system wherever possible, e.g., any two adjacent bolts can fail within a group of ten on the wing slot nozzle without overloading the adjacent bolts, and every other bolt can fail without impairing the nozzle integrity. The flexible couplings in the duct system transmit only tension loads and have a dual load path feature; in the event of the center tie bolt failure, the load is carried by a simple cable system. The ducts are sized for an airflow velocity of Mach 0.25 with only local excursions up to Mach 0.30 to minimize duct turbulence (and losses) and resultant possible duct fatigue. Duct turns are generous, and no turning vanes are required except at the T-duct.

Three simulator tests were conducted during the modification program. The objectives set forth for the simulator program were as follows:

- Provide design requirements and design confirmation data in time to impact the modified design.

- Provide information on the airplane's predicted flight characteristics, with particular emphasis on STOL-mode handling qualities, transitions, and engine-out control.

- Familiarize the project pilots with the airplane's operating characteristics and develop procedures for the early flight test program.

The first simulator tests were conducted early in the program (October-November 1970) and prior to design freeze. Three pilots, one each from NASA, Boeing, and de Havilland of Canada, accumulated 47-1/2 hours of "flying" time. Literally hundreds of STOL approaches at 60 kt were "flown." All three of the foregoing objectives were realized, but major emphasis was placed on obtaining design data.

The second simulator test was conducted in May 1971. One portion of the test period was devoted to evaluating updated airplane characteristics, revised lateral control sensitivity, and improved cockpit controls for engine-out go-around. Another part (13-1/2 hours of "flying" time) was devoted to longitudinal control improvements, including reduced stick forces.

The third simulation test took place in late January and early February 1972, just before the ground and flight test program. The purpose of these tests was to familiarize the project pilots with the airplane's operating characteristics, particularly system failures, and to determine specific operational procedures for the initial flight tests.

SIMULATION DESCRIPTION

The piloted simulator tests were performed on the NASA-Ames Flight Simulator for Advanced Aircraft (FSAA) (ref. 3). The large rotational and translational displacement capability (±50 ft for lateral motion) of this advanced simulator provided for realistic motion cues. The cockpit flight deck was equipped with instruments and overhead control levers matching the Modified C-8A. Realistic pilot column, wheel, and pedal control forces and gearing were generated by the control force-feel analog computer system. A color television display provided the pilot with a 46°

horizontal and 36° vertical view of the three-dimensional scale model landscape. The landscape model included an airport with a conventional runway and a 1500-ft STOL runway. An aircraft engine noise generator was used to give proper aural cues.

The simulation system was operated through a large-capacity digital computer, which processed the mathematical model of the airplane. Analog computers and special interface systems were used to tie the digital computer to the simulator. Figure 23 presents a schematic diagram of the FSAA simulation system. Further explanation of the augmentor wing simulation may be found in reference 4.

DATA BASE

The aerodynamic data for the Modified C-8A were extrapolated and interpolated from the results of a large-scale augmentor wing model tested for NASA in the Ames 40- by 80-ft wind tunnel and from the original DHC-5 Buffalo itself. Jet flap theory and linear superposition techniques were used in the data buildup. Downwash was computed using a "horseshoe" vortex model factored to match the limited wind tunnel data. Lateral-directional data were a combination of wind tunnel data and theoretical jet-flap expressions. Horizontal and vertical tail contributions were calculated separately using "force-times-arm" techniques. Propulsion system properties for the simulator came from Rolls-Royce Spey 801-SF estimated engine characteristics. Control systems, flight instruments, and cockpit controls and the airplane's mass and inertial properties all came from latest design information for each simulator test.

The simulation mathematical model (ref. 5) had several unique features. The engine characteristics had to be separated into vectored hot thrust (primary flow), inlet mass flow (ram drag and inlet moments), and cold thrust (augmentor and aileron blowing). The cold thrust was converted to isentropic nozzle blowing coefficient and distributed along the span of the wing according to the independent, dual air ducting system. The wing aerodynamics were also separated into spanwise segments for the purpose of calculating rolling and yawing moments due to asymmetric blowing. Lateral control characteristics were described as a function of blowing coefficient as well as surface deflection. All control surfaces were described separately to permit simulation of system malfunctions, including hydraulic power supply failures.

SIMULATOR TEST RESULTS

Results from the simulator tests, including design data and predicted flight characteristics, have been published in references 6, 7, 8 and 9. The effect of simulator tests on airplane hardware and operation is summarized below for seven key areas of design.
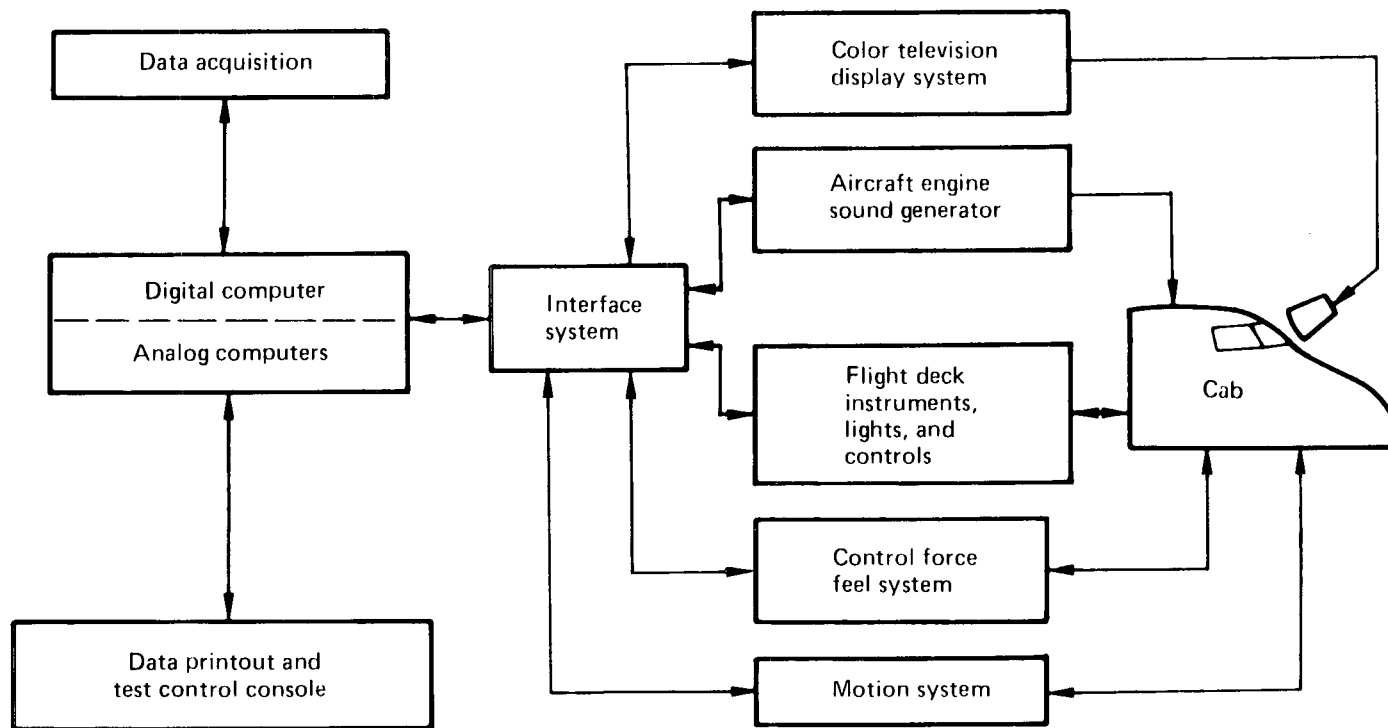
```
┌─────────────────────┐                                    ┌─────────────────────┐
│  Data acquisition   │                                    │  Color television   │
│                     │                                    │  display system     │
└─────────────────────┘                                    └─────────────────────┘
          ↕                                                 ┌─────────────────────┐
┌─────────────────────┐        ┌──────────────┐            │  Aircraft engine    │
│  Digital computer   │        │  Interface   │            │  sound generator    │
│  - - - - - - - - -  │ ←→     │  system      │            └─────────────────────┘
│  Analog computers   │        │              │            ┌─────────────────────┐    ┌─────┐
└─────────────────────┘        └──────────────┘            │  Flight deck        │    │ Cab │
          ↕                                                 │  instruments,       │    └─────┘
┌─────────────────────┐                                    │  lights, and        │
│  Data printout and  │                                    │  controls           │
│  test control       │                                    └─────────────────────┘
│  console            │                                    ┌─────────────────────┐
└─────────────────────┘                                    │  Control force      │
                                                           │  feel system        │
                                                           └─────────────────────┘
                                                           ┌─────────────────────┐
                                                           │  Motion system      │
                                                           └─────────────────────┘
```

FIGURE 23.—FSAA SIMULATION SYSTEM

Lateral Control System Design

Since the lateral control system was to be completely new, every attempt was made to produce a system with satisfactory flying qualities. Lateral control airworthiness criteria were established with considerable influence from reference 10. In summary, these criteria called for significant roll power, high roll sensitivity, low yawing moment, linearity, and one-hand control forces down to 60-kt STOL approach conditions. Lateral control surface gearing had been determined prior to the first simulator test. At landing approach the ailerons, spoilers, and augmentor chokes each contributed about one-third of the total roll power. A combination of surface mixing was found which produced linear rolling moment with control wheel inputs. Spoiler and choke favorable yawing moment offset the adverse effect of the ailerons to yield very little net yawing moment due to lateral control.

With the candidate lateral control system, pilots were asked to evaluate maximum roll power, system rate limits, roll sensitivity, wheel forces, lateral trim rate, hydraulic power failures, and control of an engine failure or a burst in body crossover air duct. Pilot evaluation centered on landing approach in the STOL configuration. Pilots were asked to make rapid turns, to capture and track the localizer starting from a 200-ft offset at 300-ft altitude. Tests were made with variations in dihedral effect, C_{ℓ_β}, roll inertia, I_{XX}, lateral control-to-wheel gearing, aileron droop angle, and feel-and-trim characteristics. Evaluations were made with SAS both on and off, with varying levels of turbulence and large discrete lateral gusts.

The simulator tests produced the following results:

- Roll power on approach should equal or exceed an instantaneous roll acceleration capability of $\ddot{\theta}_{max} = 0.4$ rad/sec^2 in order to control the airplane in heavy turbulence.

- The lateral control system should permit wheel inputs at a rate of $\dot{\delta}_w \geq 200$ deg/sec with full surface deflection within 1/2 sec.

- Lateral control sensitivity (roll acceleration produced per unit wheel) became very important at landing approach. Figure 24 shows the variation of pilot rating with control sensitivity, as judged by the three pilots who participated in the simulation. Roll sensitivity greater than $\ddot{\phi}/\delta_w \geq 0.07$ (rad/sec^2)/in. was required to obtain satisfactory ratings. The characteristics of the other airplanes shown for reference are taken from reference 10.

- Low wheel force of about $F_w = \pm 10$ lb maximum was found necessary to permit tighter control in turbulent or engine-out conditions. Positive system centering was considered a requirement by the pilots.

⊙ ▽ ◇ Modified C-8A
—— 60 kt
—— Flaps 65°
—— SAS on
—— Wheel control

Pilot
rating

Modified C-8A
current design

1
2
3   UF-XS ●   367-80 ●   ⊙   B-941 ●
                                                                                      Satisfactory
                                                                                      without
                                                                                      improvement
4   NC-130B ●
5   NC-130B ●
                         C-8
                                                                                      Deficiencies
6   warrant
                                                                                      improvement
7   ● C-8 ailerons
8   Deficiencies
                                                                                      require
9   improvement
10

                                                                                      Uncontrollable

0   .02   .04   .06   .08   .10   .12   .14   .16   .18   .20

Lateral control sensitivity, $\ddot{\phi}/\delta_W$, rad/sec²/in.
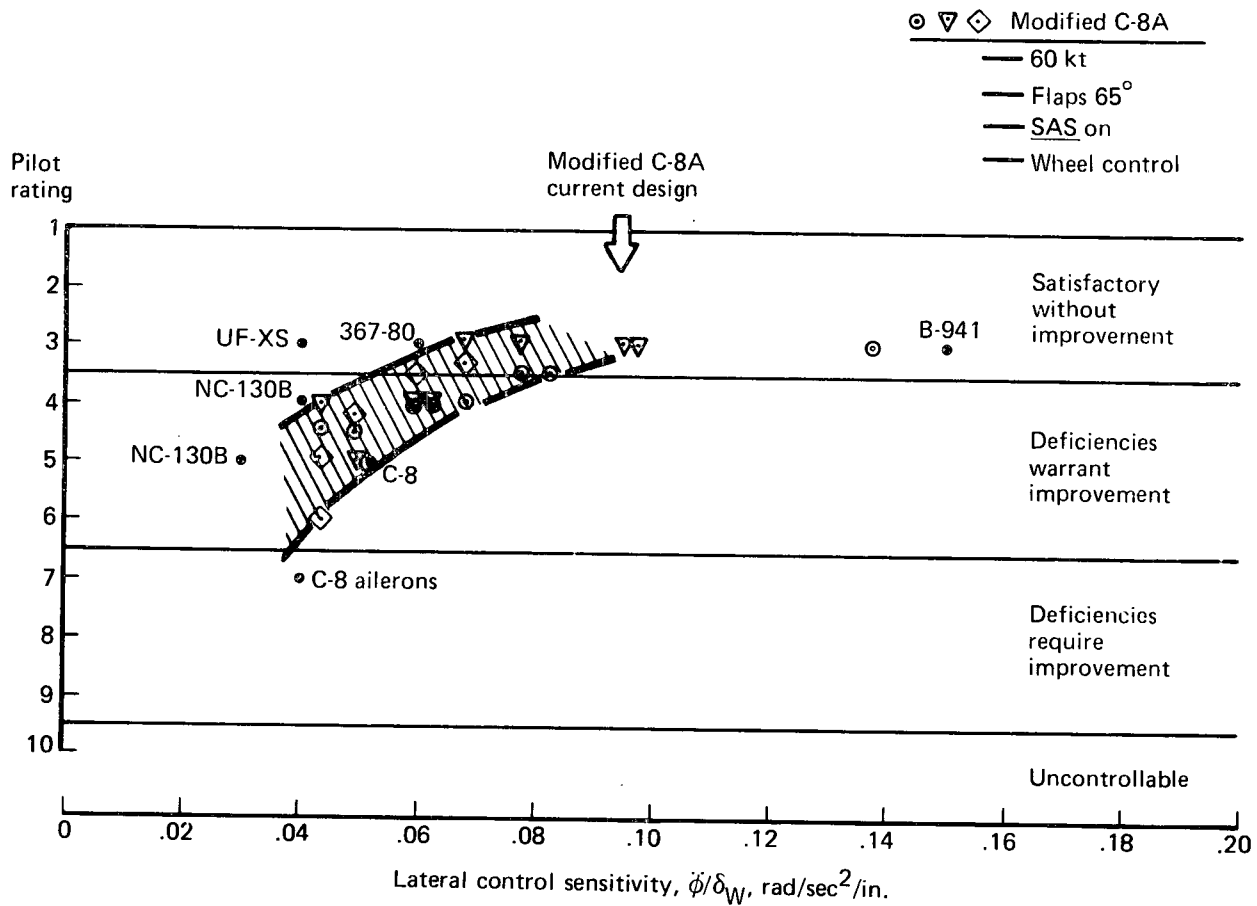
FIGURE 24.—PILOT RATING OF LATERAL CONTROL SENSITIVITY

- A single hydraulic system failure produced one-third loss in control power. The pilots found that they could continue the STOL approach to a safe landing with this level of degradation. Two hydraulic failures produced manual reversion conditions (aileron and elevator control only) with very high lateral forces. Pilot ratings of manual reversion at 60 kt were in the region of 8 to 9. At 90 kt and reduced flap setting, a conventional landing was deemed possible.

- A failure in the crossover duct produced large rolling and yawing moments due to asymmetric blowing. At STOL approach, where flap lift depended significantly on blowing level, the rolling moment was an appreciable fraction of the available lateral control power, which also changed due to duct burst. The pilots could not effectively counteract a failed blowing duct without diving for higher airspeed. Retarding the throttle on the engine connected to the failed duct permitted control of the airplane by using engine-out techniques.

The following actions were taken regarding design and operational features of the Modified C-8A based on results of the simulator tests:

- The Boeing 727 central power control unit was geared to the ailerons to achieve the very rapid wheel and surface rate requirements.

- The Boeing 747 lateral control feel, centering, and trim unit was used to produce low, one-hand control forces and positive centering.

- Optional control surface programming was incorporated to ensure nearly linear rolling moment with wheel deflection in flight test.

- The fuel system was modified to empty the outer tanks first to reduce rolling moment of inertia at the landing conditions. Figure 25 shows the one-third reduction in I_{XX} at the 40 000-lb landing condition.

- The lateral control surface programming was revised to produce full spoiler deflection at two-thirds wheel and added surface quickening about neutral wheel by signaling the central PCU through the series SAS servo. Figure 26 presents the final lateral control schematic and mechanical surface gearing at landing flaps. The improvements in lateral control power and sensitivity are presented in figure 27. The total roll power became $\ddot{\phi} = 0.5$ rad/sec^2 and sensitivity increased to $\ddot{\phi}/\delta_w \approx 0.1$ (rad/sec^2)/in.

- A conventional landing approach configuration was identified (flaps 30°, conical nozzles aft) for emergency landing at 90 kt from a 3° glide slope. After any system malfunction
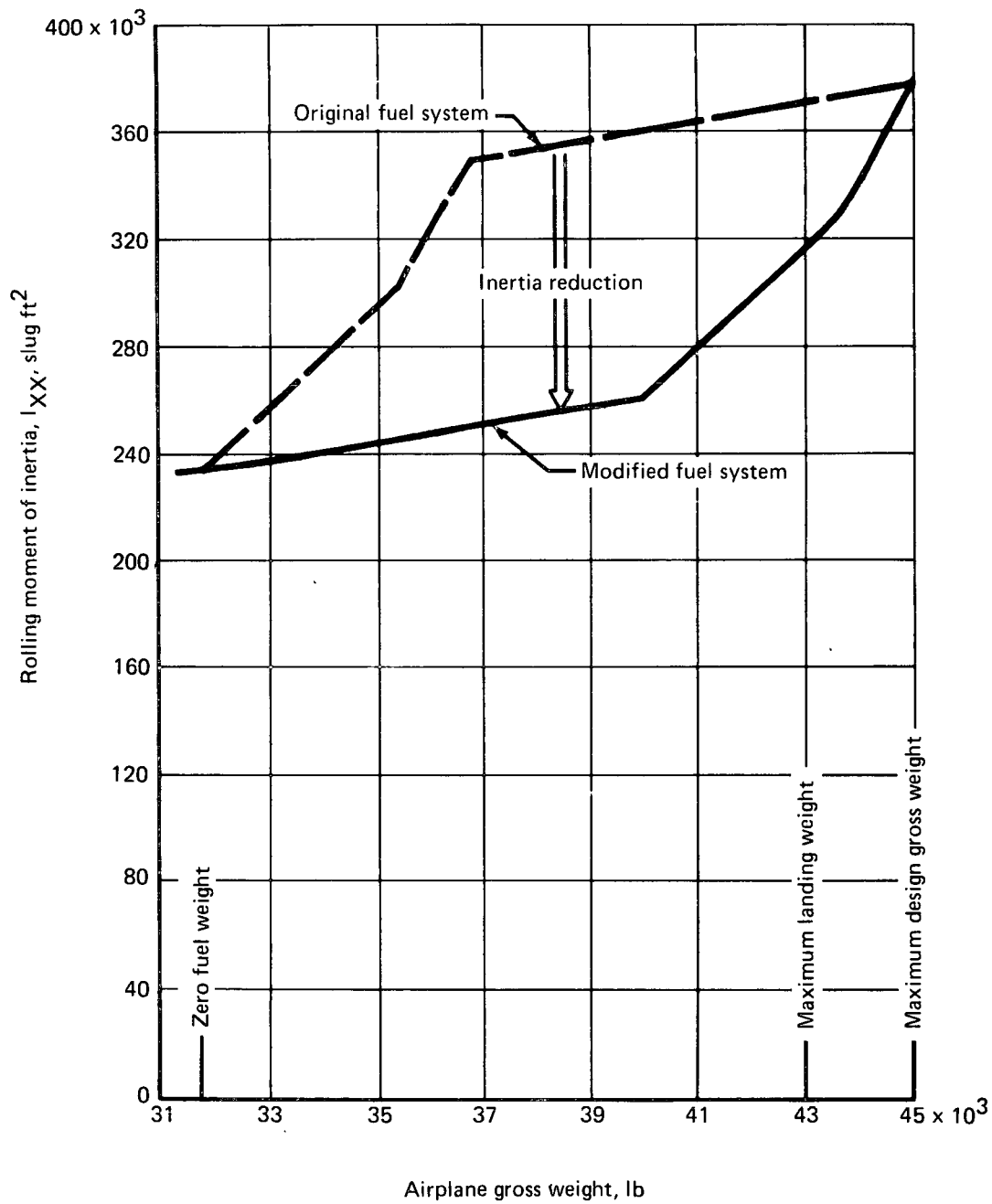
FIGURE 25.—REDUCED ROLL INERTIA
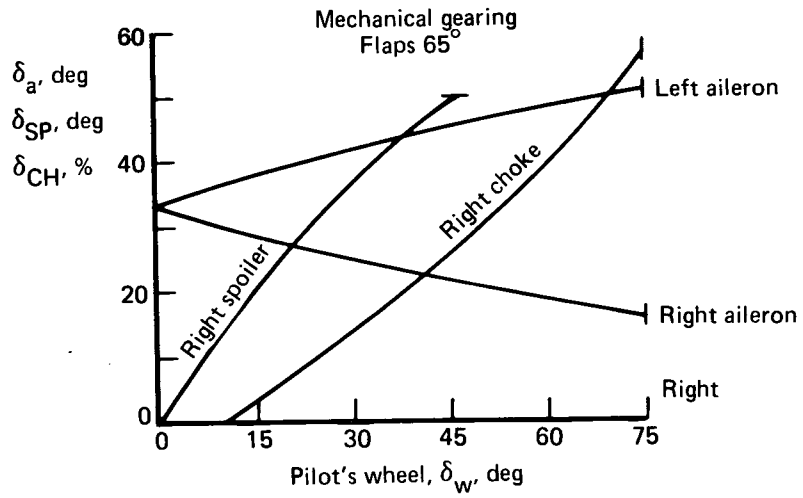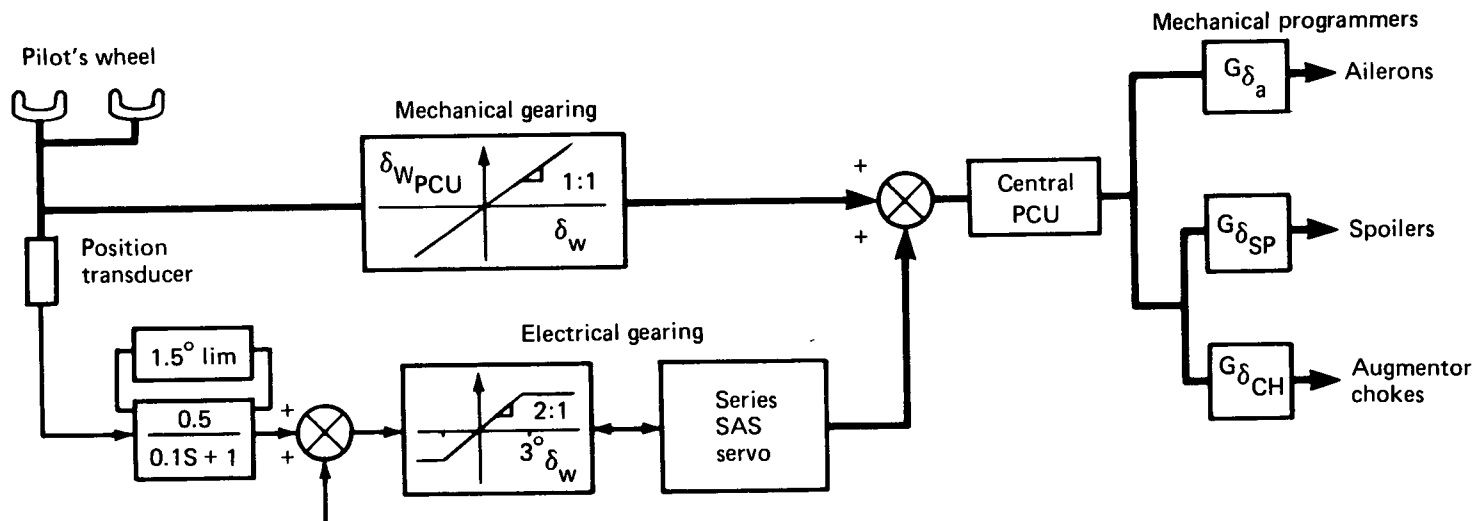
FIGURE 26.—LATERAL CONTROL PROGRAMMING
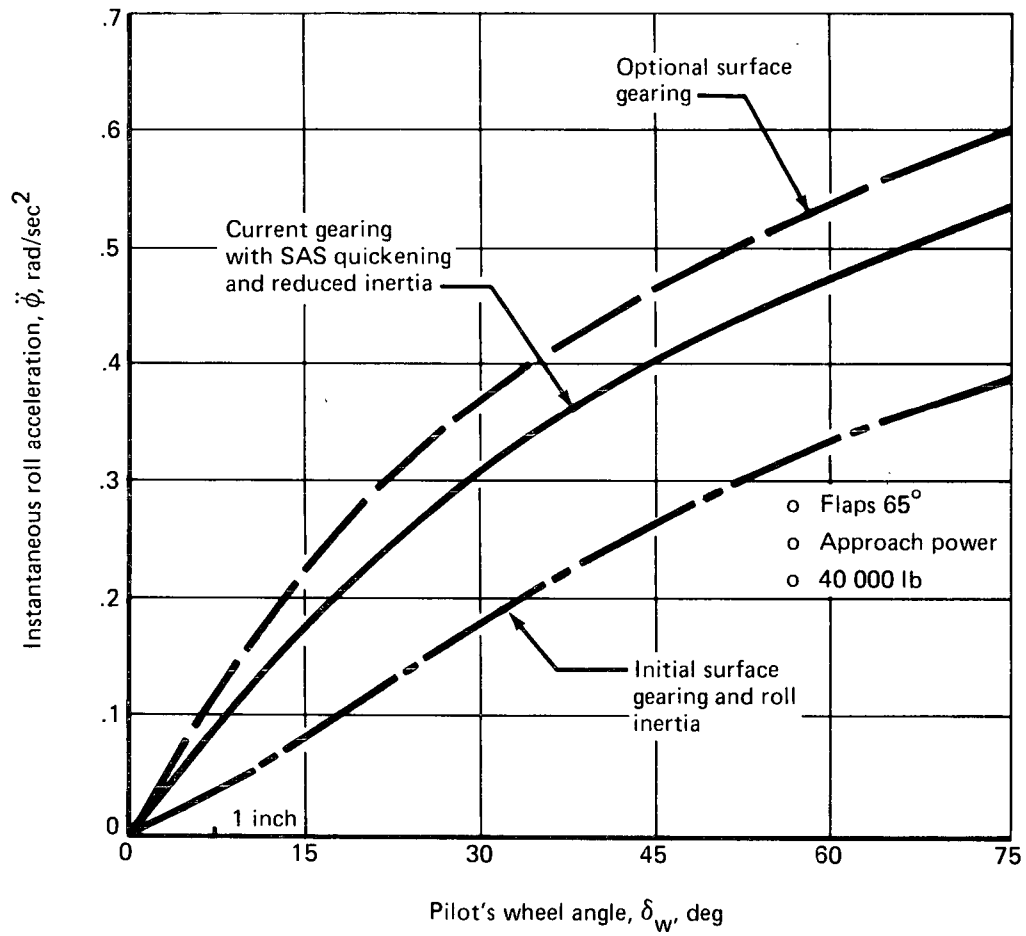
FIGURE 27.—LATERAL CONTROL EFFECTIVENESS AT 60-KT LANDING APPROACH

60

the pilot was instructed to achieve this configuration, which gave the best chance of surviving a second failure.

● The duct design was changed to safe-life stress levels to minimize the probability of duct burst. Ducting material was chosen specifically for good fatigue properties. In addition, a special system was installed in the airplane to sense differences in duct pressure and warn the pilot of possible leaking.

Longitudinal Control System

Longitudinal stability and control were evaluated in transitions from cruise, approach path control, and landing flare. The manual spring tab elevator system was also evaluated for stick force and dynamic characteristics. The simulated characteristics produced a requirement for longitudinal control system design for one-handed operation through transition, approach, and flare, as well as a likely requirement for longitudinal stability augmentation. In this area the simulator investigations resulted in changes to the existing elevator and spring tab mechanisms to lower stick forces to levels compatible with one-handed operation. The pitch trim system rate requirement was also set from the results of the simulator tests.

The system changes gave significant reductions in forces without any appreciable change in elevator to column ratio, i.e., at constant total elevator authority, see figure 28.

Flap System

In the initial design stages of the flap system it was thought that a fast flap retraction rate would be needed to allow quick cleanup from the high-drag approach flap angle to the single-engine go-around configuration. Wind tunnel data showed large drag changes with very little lift loss for flap angles between 50° and 75°. Fast flap retraction combined with control activity posed a hydraulic pump design problem when combined with an engine failure. It was also considered that flap actuation might possibly be used as a flightpath control device as suggested in reference 11, a feature which would require a fast flap rate.

Piloted simulations of single-engine go-arounds demonstrated the critical nature of the control problems associated with the engine failure, but, surprisingly enough, proved that flap retraction rates greater than 4 deg/sec gave no benefit in reducing the altitude loss in the go-around maneuver. Acceptable single-engine performance is not reached until the 30° flap position is reached. High flap retraction rates therefore led to lift losses which built up faster than the pilot was willing to compensate with increased angle of attack. With a 4 deg/sec rate the flap retraction is better matched to the single-engine airplane performance capability, and this rate was chosen for the design of the flap system.
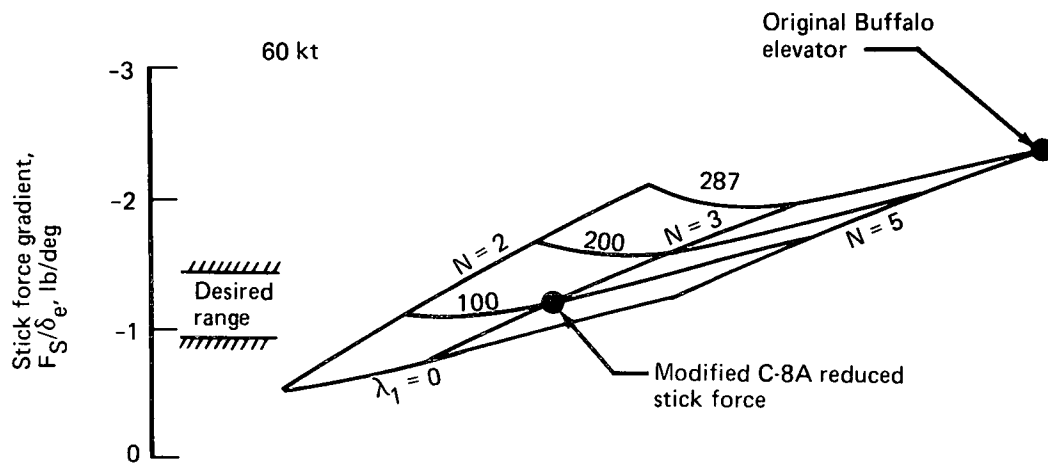
N = spring tab follow-up ratio
λ_1 = elevator spring constant, ft-lb/rad
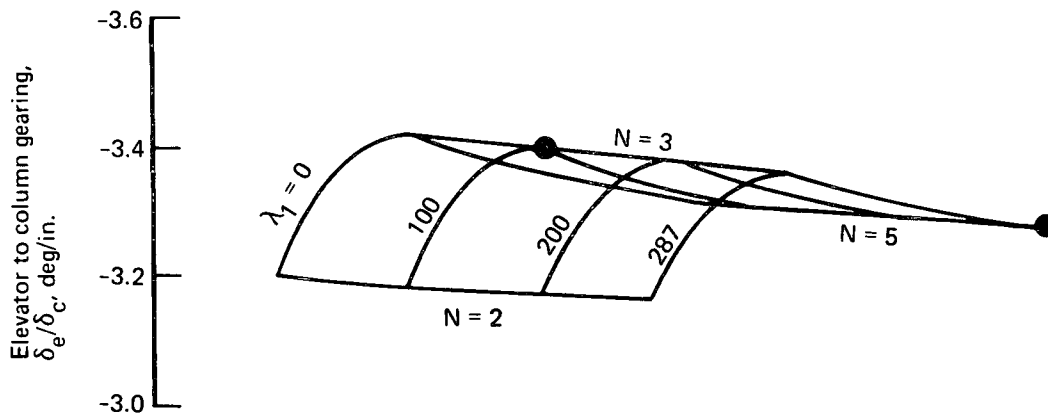
FIGURE 28.—MANUAL SPRING-TAB ELEVATOR CHARACTERISTICS

62

Lateral-Directional SAS

It was evident early in the simulator work conducted by NASA/DHC in the feasibility phase of the program that some lateral-directional stability augmentation would be necessary. The piloted simulator investigation determined a compromise set of SAS gains giving reasonable handling qualities for a range of dihedral effect. Authority limits were set, and it was determined that landings could be performed satisfactorily after SAS failure, thereby allowing a single-thread design to be used. Gain programming with flap angle was found to be necessary, and an SAS shutoff above 100 kt was incorporated since low-speed authority requirements were incompatible with structural limitations on rudder hardovers at high speed.

Engine Characteristics and Pegasus Nozzle Control System

The engines have good acceleration capability around the approach power setting. Full thrust can be reached within 2 seconds from this operating point, and this acceleration capability was considered adequate including use in the landing flare. However, the engine designers were anxious to extend the deceleration time to protect the engine against backpressures in the flap blowing ducts when the throttles were rapidly retarded. These sluggish characteristics were simulated and were found to be acceptable in all simulated maneuvers, thus clearing the way for design action on the engine. Another item investigated in the simulator was the effect of the thrust hysteresis loops induced by operation of the engine surge bleed valve. These small thrust changes were never noticeable to the pilots since their coarser movements of the throttle masked completely the operation of the valves.

The conical nozzle installation provided vectored thrust which gave considerable flexibility in controlling speed and flightpath angle. The engine and thrust vector controls were treated as primary flight controls by the pilots. The sensitivity of the nozzle vector levers and their physical location in the cockpit was the souce of a great deal of discussion prior to the November 1970 simulation period.

During the simulation, thrust vectoring was used by all the evaluation pilots as the standard method of controlling rate of descent. However, their use of the levers varied from large, coarse changes to smaller motions during each approach. The pilot's technique apparently required no more than fairly large open-loop movements of the nozzles, and so no sensitivity problems arose. Even the introduction of a $\pm3°$ deadspace in the nozzle controls went unnoticed during typical control tasks for the approach and landing. Further evaluations were made of lever handle shape and length. As a result, the final nozzle control levers are the same lengths as the adjoining stirrup-type throttle controls. The nozzle levers end in hemispherical handles which form a single ball when both levers are side by side. This arrangement allowed easy transfer of the hand from

throttles to vector levers and good judgment of the relative position of the nozzle levers without diverting the pilot's eyes from the instrument panel or the outside field of view. The go-around sequence could also be initiated with a single movement gathering throttles and vector levers together in one hand.

Structural Design

The piloted simulation of the Buffalo was also used to search for new airplane characteristics that could result in structural design requirements different from those used for conventional aircraft. In this investigation airplane handling qualities were evaluated at each structural placard, overspeeds and upsets were simulated, airplane behavior in step gusts and in evasive maneuvers was checked, and the conditions required for touchdown on the nose gear prior to the main wheels were determined.

These tests confirmed that a 20-kt increment in speed between V_{MO} and V_D was adequate and that load factor placards reduced from the usual transport design would be adequate. The handling tests at the flaps-down placard speeds had demonstrated the lively performance of the airplane. Acceleration capability was very good with the high installed T/W, even more so because of the almost instantaneous forward thrust response that was available by vectoring nozzles at high power settings. These characteristics led to increasing the flaps 30° placard from 105 to 120 kt, since vectoring thrust full aft at the approach configuration and retracting flaps allowed the airplane to exceed the 105 kt placard before reaching the 30° flap position.

Engine-Out Control

The Modified C-8A has engine-out characteristics typical of a powered-lift STOL transport. Engine-out climb performance is a significant problem, particularly at high-lift, high flap deflections. Loss of powered lift causes the airplane to sink at STOL flight conditions.

The most critical engine-out condition occurs at the low-speed, powered-lift STOL approach. Figure 29 shows the STOL approach trim condition with two engines. Single-engine trim at approach power (vertical hot thrust) is characterized by high descent rate and reduced stall margin compared to the design point. Increasing thrust setting and rotating nozzles aft achieves a 2° glide slope at 75 kt. Flap retraction to 30° takeoff setting is required to climb away. Engine-out go-around from STOL approach therefore requires four pilot actions:

● Advance power on remaining engine to emergency setting.

● Rotate the hot thrust nozzles fully aft.

64
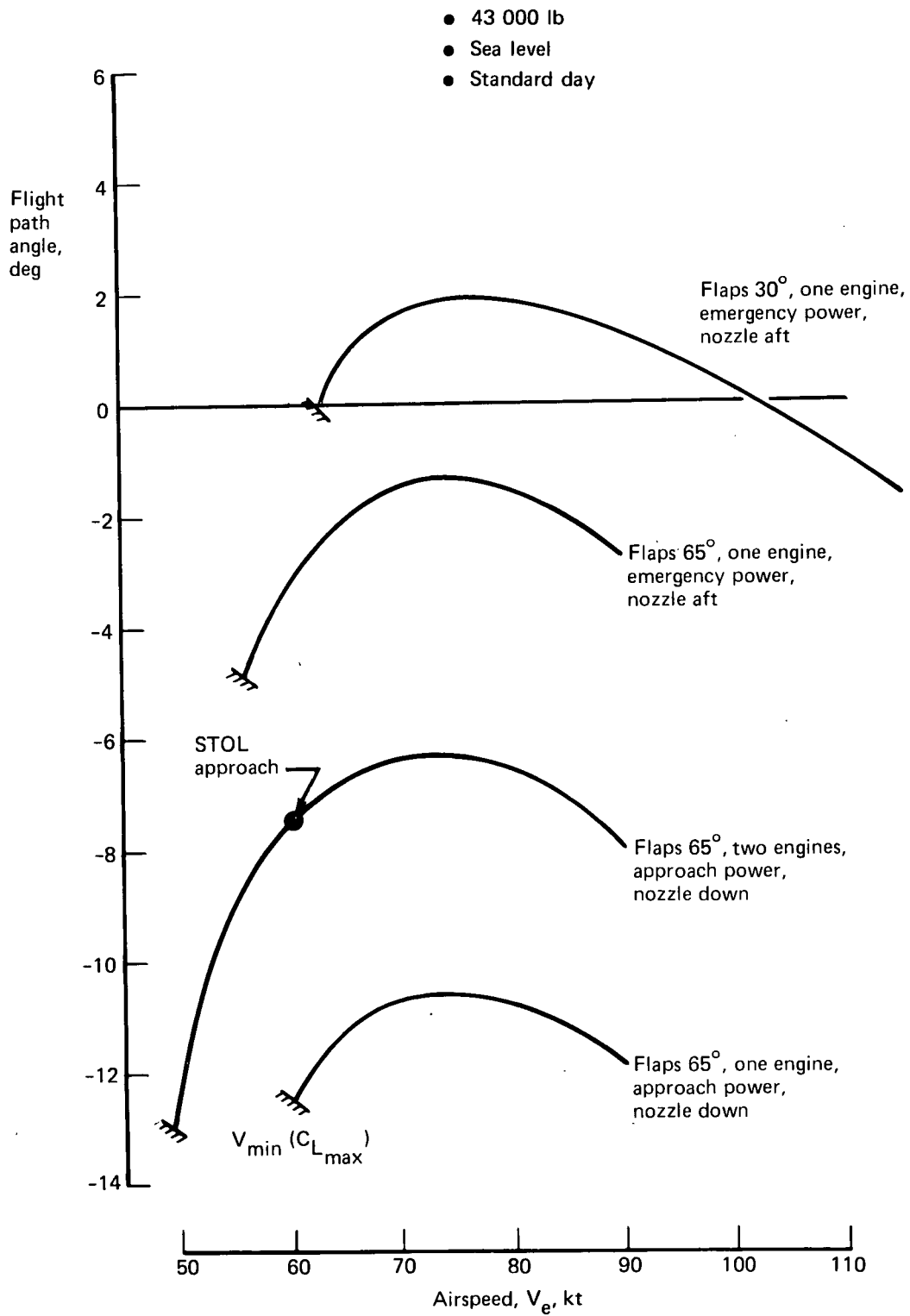
FIGURE 29.—ENGINE-OUT CLIMB CAPABILITY

● Retract flaps to the 30° position.

● Increase speed from 60 to 75 kt.

Vector hot thrust produces large rolling and/or yawing moment at engine failure depending on nozzle angle. At 60-kt STOL approach the vertical hot thrust rolling moment would exceed available lateral control capability if it were not for the compensating asymmetric blowing. The flap blowing distribution produces asymmetric lift distribution over the wing which, in turn, generates aerodynamic rolling moment to partially offset the hot thrust. Figure 30 shows the engine-out

● Flaps 65°
● Approach power
● Vertical hot thrust
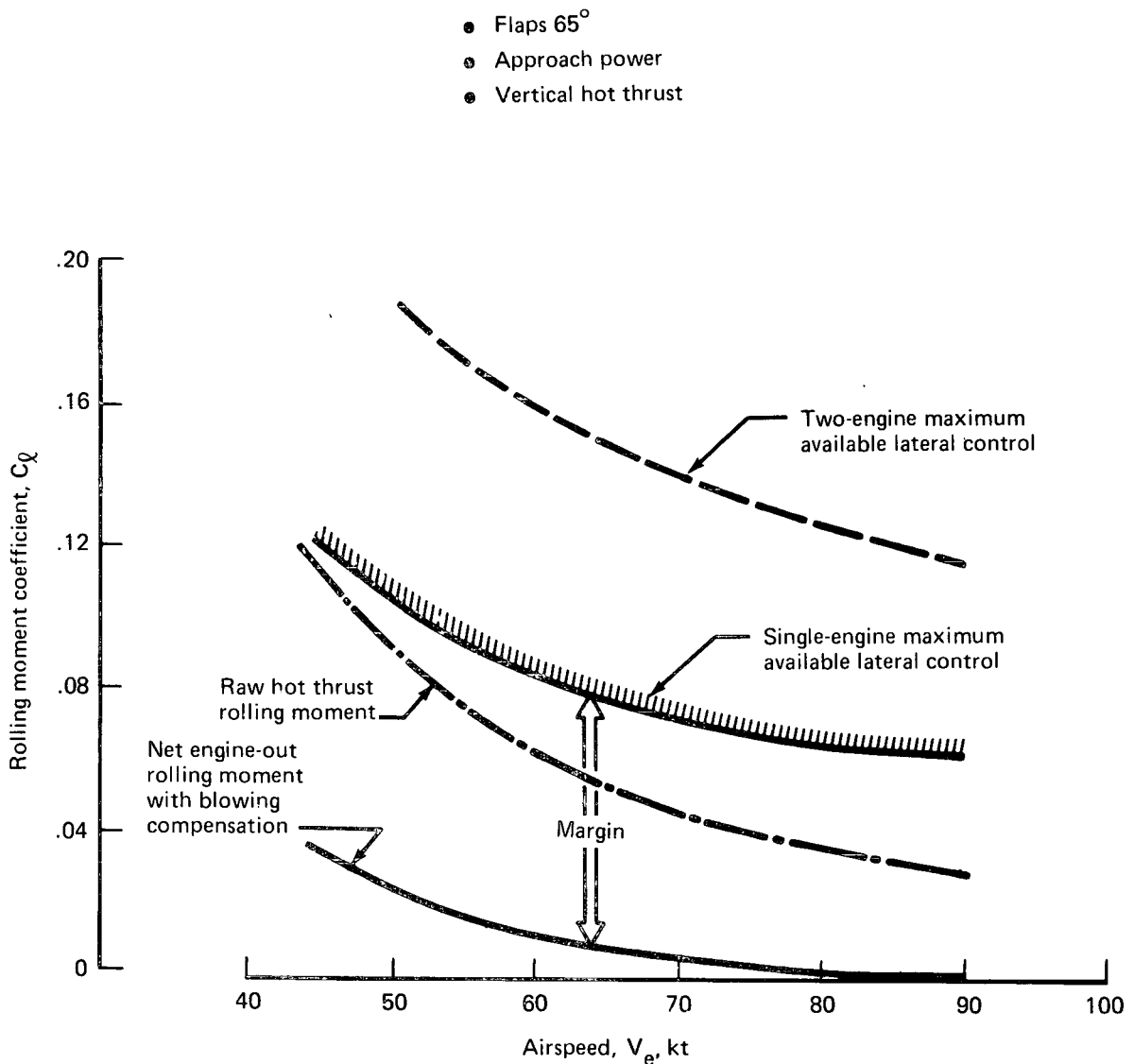
FIGURE 30.—ENGINE-OUT LATERAL CONTROL

rolling moment situation at approach power setting. Hot thrust rolling moment increases when power is advanced and then decreases as nozzles are rotated aft. Figure 31 illustrates the effect of thrust vector angle and blowing compensation on engine-out rolling and yawing moment at 60 kt, emergency power setting. About one-half of the available lateral control is required for engine-out control, nozzles down. Almost no rudder input is required nozzles down, but nearly full control must be used with nozzles aft. Nozzle rotation over the full deflection range produces reversals in lateral and directional control requirements.
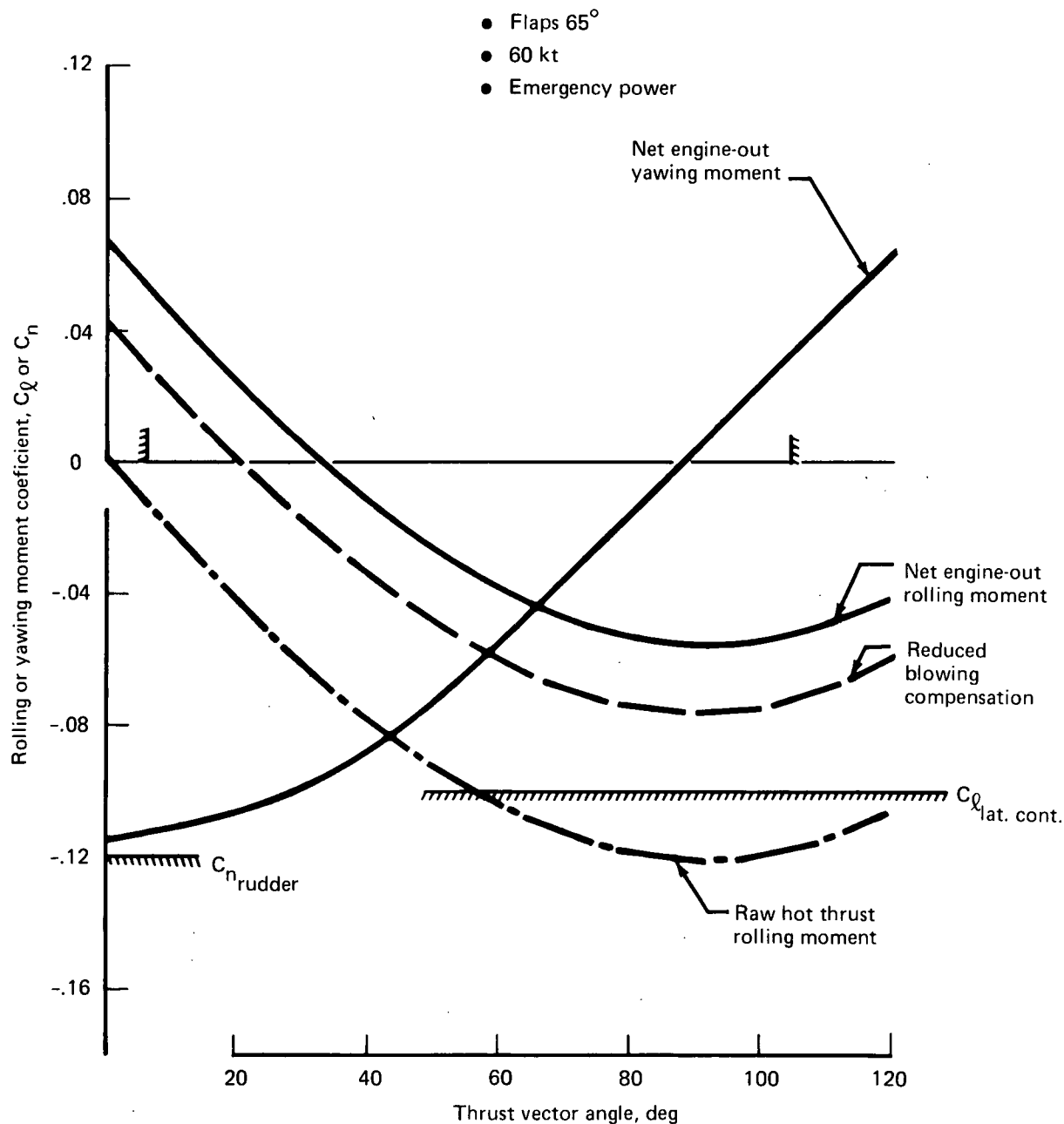
FIGURE 31.—EFFECT OF VECTORED THRUST ON ENGINE-OUT CONTROL

Faced with these characteristics, it became obvious that a pilot-in-the-loop simulation was necessary to appreciate transient characteristics, pilot time lags, and workload. The results follow.

While engine-out control at takeoff (nozzles aft, higher speeds) was no problem, engine failure on STOL approach presented a difficult situation. The first indication of engine failure was loss in lift and rapid buildup in sink rate. Airspeed and angle of attack inherently increased due to airplane settling. With nominal blowing asymmetry, initial rolling and yawing tendencies were small. Pilots almost immediately increased power on the remaining engine. Control response varied depending on subsequent action taken with the thrust nozzles and flap setting either to go-around or continue to a landing.

Go-Around

Out of a sampling of 70 engine failures by three pilots, about 60% of the conditions were go-arounds. If possible, a new approach at conventional conditions (30° flaps, 90 kt, nozzles aft) was deemed prudent. Figure 32 shows the control characteristics from the simulator for an engine-out go-around. Even though adequate control was available, the engine-out condition was rated as a very demanding task. Initial control was gained using 50% lateral and 20% directional control. With nozzles aft, rudder requirement increased to 50% rudder authority. The change in sign in rolling moment with nozzle angle coupled with lack of dihedral effect was very confusing. Yawing and pitching moment changes further complicated the problem. Rotating nozzles aft before or with power increase minimized control problems and reduced the confusing change in control direction.

The ducting system was designed to ensure adequate blowing asymmetry. Throttle and nozzle control levers were modified so that both could be advanced simultaneously using one hand. This resulted in full-power and vectors-aft conditions occurring at the same time, thereby speeding the recovery. Low wheel and reduced stick forces permitted easy control of the airplane using only one hand. Engine-out control was rated within the capability of the pilot and airplane.

The most pressing consideration lay in minimizing altitude loss in making the go-around. Steep approach, loss of lift, high drag flaps, etc., all added to the high sink rate encountered following engine failure. Figure 33 presents a selected example of a one-engine go-around. The rapid increase in sink rate (22 ft/sec) and loss in load factor had to be dealt with at the same time that roll, yaw, and pitch control were being maintained. Downward acceleration, increase in thrust, and thrust vectoring aft produced an increase in airspeed which helped to regain margin from stall and accelerate the airplane toward a positive climb gradient. Approximately constant pitch attitude was flown while flaps were retracted for go-around.
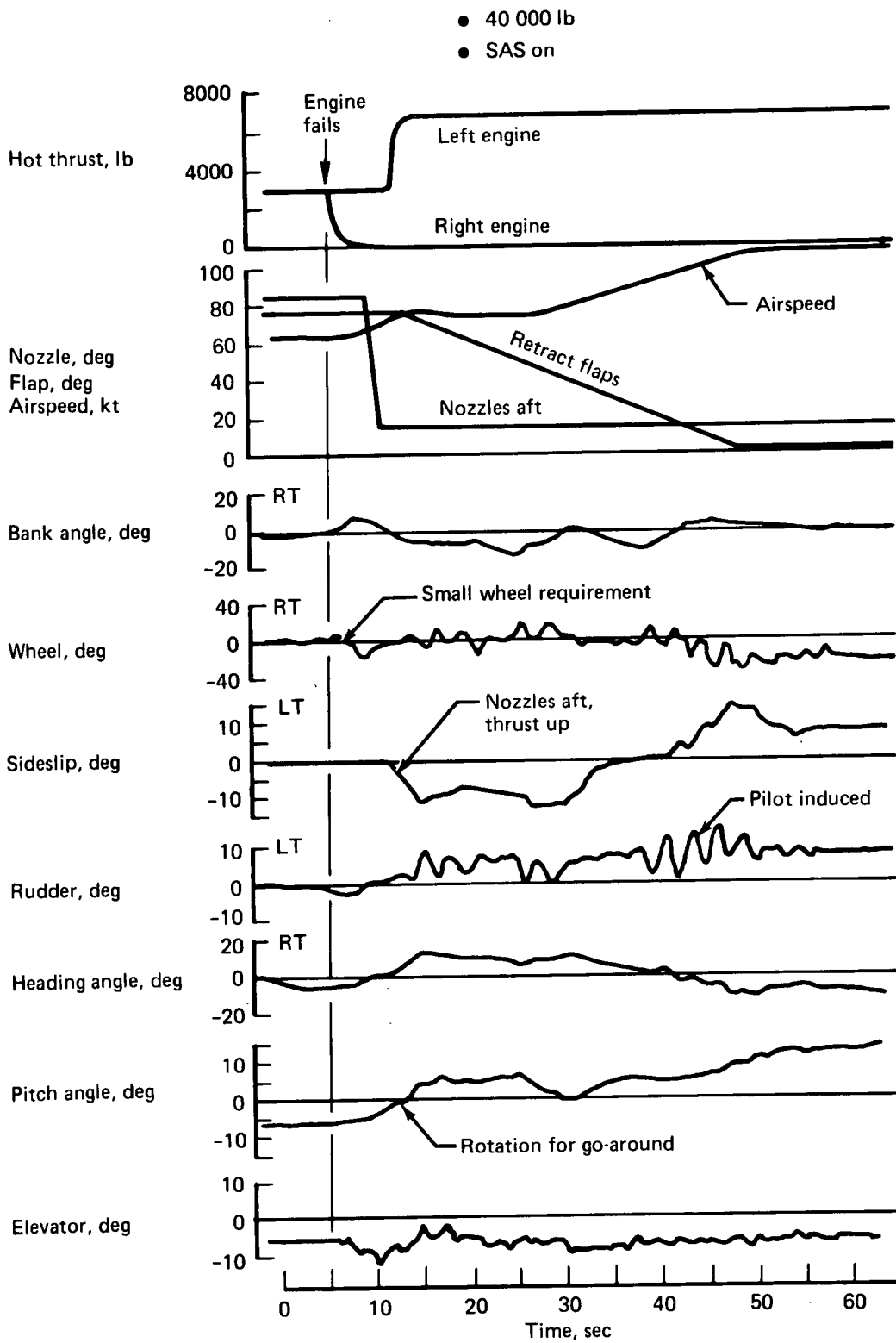
FIGURE 32.—CONTROL DURING ENGINE-OUT GO-AROUND
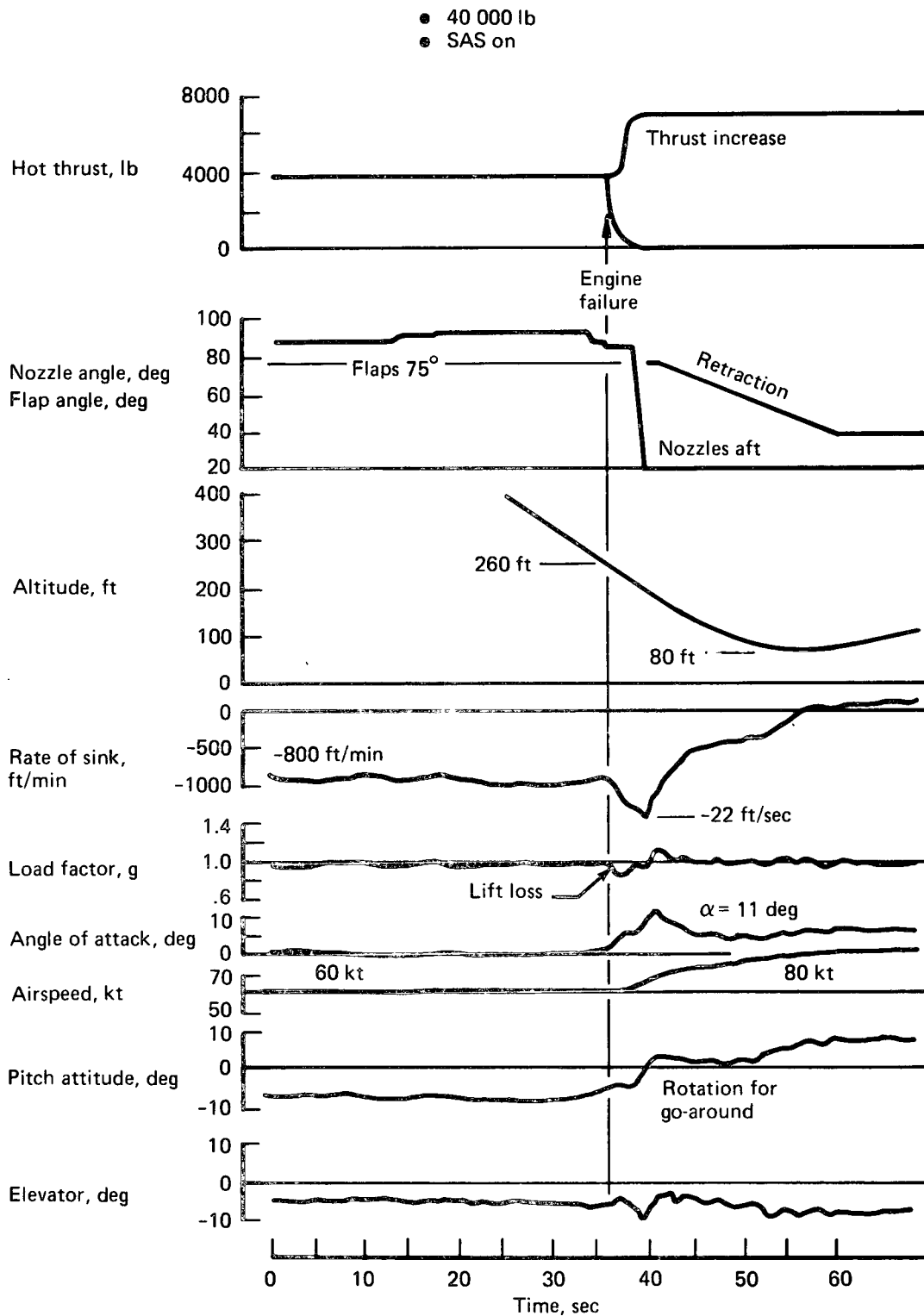
FIGURE 33.—ENGINE-OUT GO-AROUND

Fast reactions were needed to effect a go-around with minimum altitude loss. Early trials in the simulator saw an altitude loss from point of engine failure in excess of 350 ft. Mean levels from early piloted simulator work tended toward 250 ft altitude loss. Techniques for taking corrective action in minimum time were practiced in the second simulation period. Prior work using an "electronic" pilot showed the merits of moving quickly. The analysis showed that pull-up to moderate angle of attack ($\alpha_F = 12°$) followed by tracking on flaps 30° climb speed ($V_e \approx 75$ kt) results in minimum altitude loss in the go-around. This technique was followed by the pilots. Piloted recovery results are compared with the analysis in figure 34. Although go-arounds were accomplished from as low as 50 ft altitude in calm air, the minimum go-around altitude had to be increased in turbulent conditions. It appeared that minimum go-around altitude would be on the order of 150 ft.

Landings

The pilots elected to continue the approach to a landing in about 40% of the trials. Figure 35 shows a successful one-engine landing after engine failure at 150 ft altitude. In this case immediate reaction to an engine failure was to increase power, vector the thrust aft, and leave the flaps down for maximum lift capability. Again, note the reduction in load factor at engine failure and the large increase in sink rate of 23 ft/sec. Speed was allowed to build up only as necessary to retain stall margin and produce reasonable body attitude at an allowable rate of descent. As can be seen from this condition, there was plenty of flare capability; touchdown sink rate was held to only 3.5 ft/sec.

Engine-out landings occurred short of the original touchdown aiming point. Operational procedures were changed to move the aiming point well down a conventional runway.

There does exist a region near the ground where an engine failure would cause a very hard landing, beyond landing gear structural capability (12 ft/sec). This failure altitude roughly corresponds to that for flare initiation. Exposure to this critical condition lasts for about the last 4-5 seconds prior to touchdown. Special seats have been installed on the airplane to take high sink rate landings without injuring the pilot. New emergency egress doors have been added to the cockpit to facilitate getting out of the airplane. Since the exposure time is short, the risk of critical engine failure near the ground has been considered reasonable for a research airplane.

- Initially trimmed on 60 kt approach, flaps 65°, at 7.5° glide slope, approach power
- Engine out climb at flaps 30°, nozzles aft, emergency power
- 40 000 lb, sea level, standard day

Altitude loss, ft (from engine-out to zero sink rate)

280

240

200 — Piloted simulation

Pitch attitude over 15°

160

1.5/3/4.5

120

1/1/4

Analytical results with reaction time for thrust/nozzles/flaps

80

0/0/0

1 g stall
Flaps 30°

40

0

50   60   70   80   90   100

Stabilized climb-out speed, kt
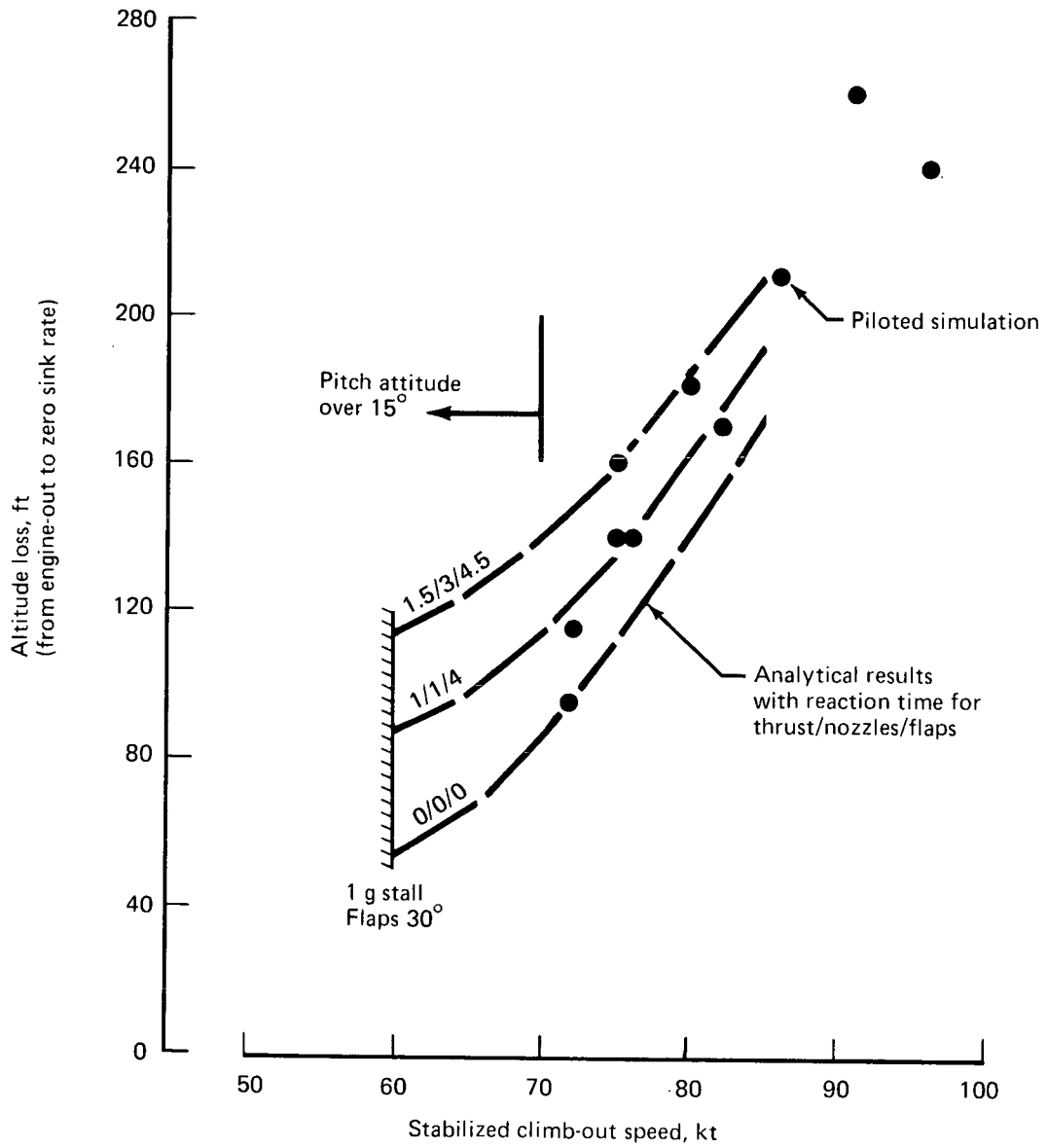
FIGURE 34.—ALTITUDE LOSS IN ENGINE-OUT GO-AROUND
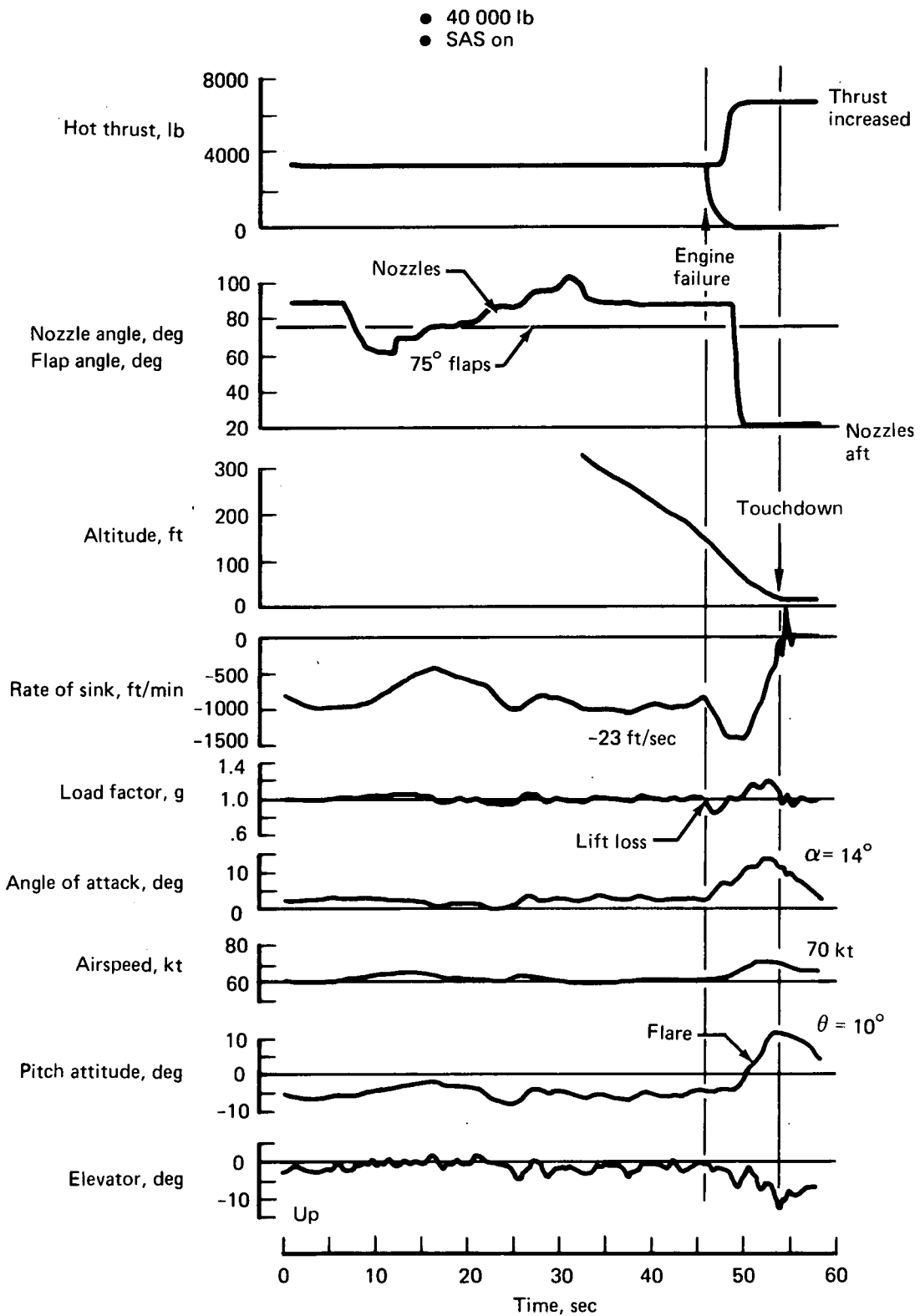
FIGURE 35.—LANDING AFTER ENGINE FAILURE AT 150 FT

STATIC MODEL TEST OF AUGMENTOR FLAP SYSTEM

To provide a high degree of confidence in the augmentor flap system proposal for the Modified C-8A, a 0.7-scale model of the flap system was built and tested. An end view of the model is shown in figure 36. The model configuration was essentially the same as the Ames wind tunnel model of reference 2 except for the differences required to adopt the augmentor flap to the full-scale airplane. These included a shorter flap chord and the addition of turning vanes within the nozzles.

The objectives of the test program were to determine the following:

● The thrust augmentation characteristics of the augmentor flap at large scale

● The sensitivity of augmentor performance to small changes in geometry such as might be caused by deflection under flight load conditions

● Augmentor choke effectiveness of thrust spoiling (This is used on the airplane for lateral control and lift dumping.)

● An understanding of the flow mechanism within the augmentor by surface pressure and rake total pressure measurements

● Nozzle flow angularity (turning vane effectiveness), discharge coefficient, and velocity coefficient along with momentum distribution characteristics of the augmentor.

● Augmentor noise characteristics

● Hinge-moment verification for design assumptions used for augmentor choke control surface

Based on the Boeing test facility maximum continuous airflow capacity and the tradeoff between model flap chord length and span section length, a 0.7-scale model of a complete duct-nozzle augmentor flap system was constructed and tested. The model simulated one-half of one side of the airplane augmentor flap system. The model had a span of 95 in. and a flap chord of 30 in. The model could be used to simulate the wing panel either inboard or outboard of the nacelle by rerouting the air supply system and changing the duct area distributions with duct liners. The model is shown mounted on the six-component balance in figure 37.

SHROUD

INTAKE

FLAP

COANDA

6A86926-3
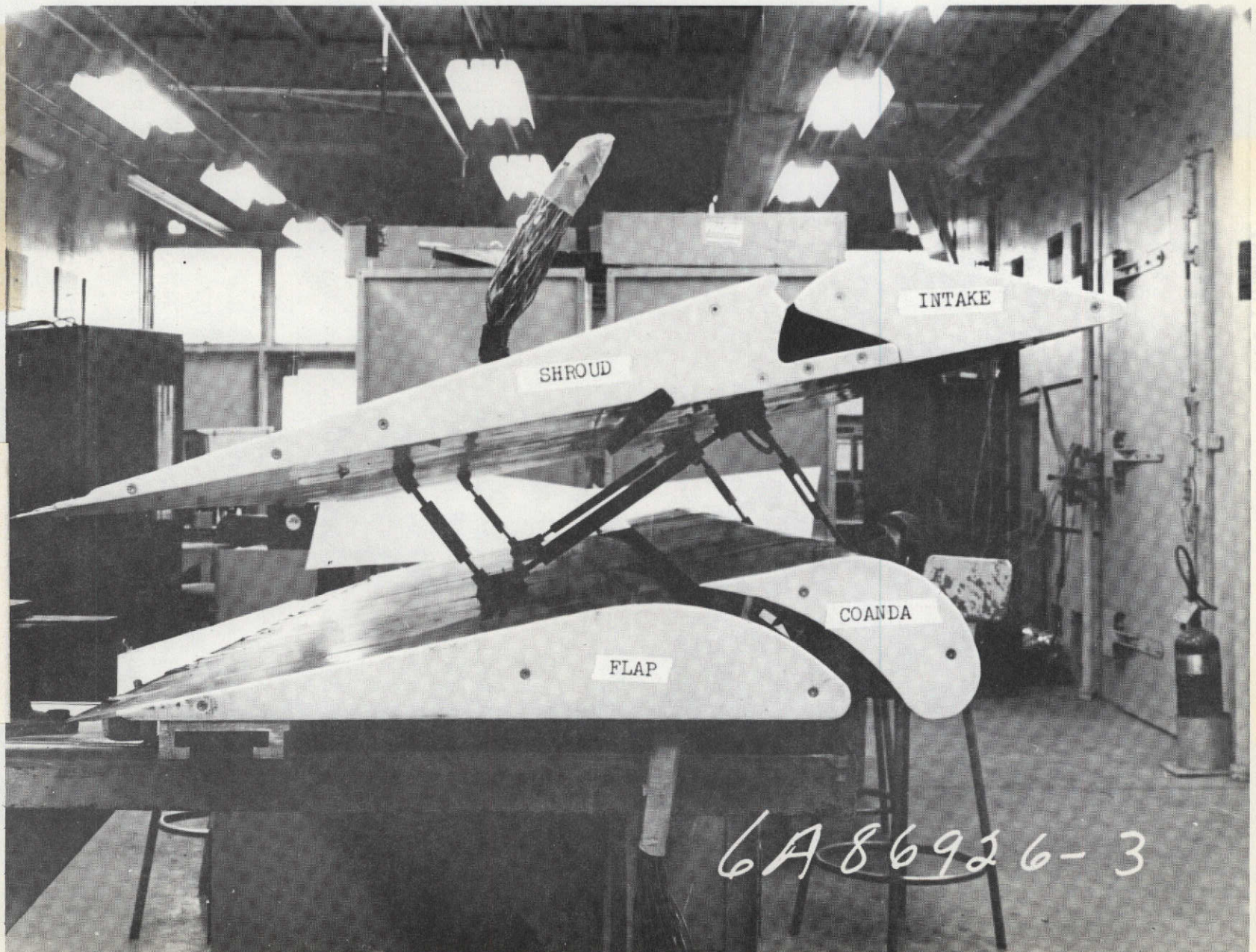
FIGURE 36.—END VIEW OF AUGMENTOR FLAP MODEL
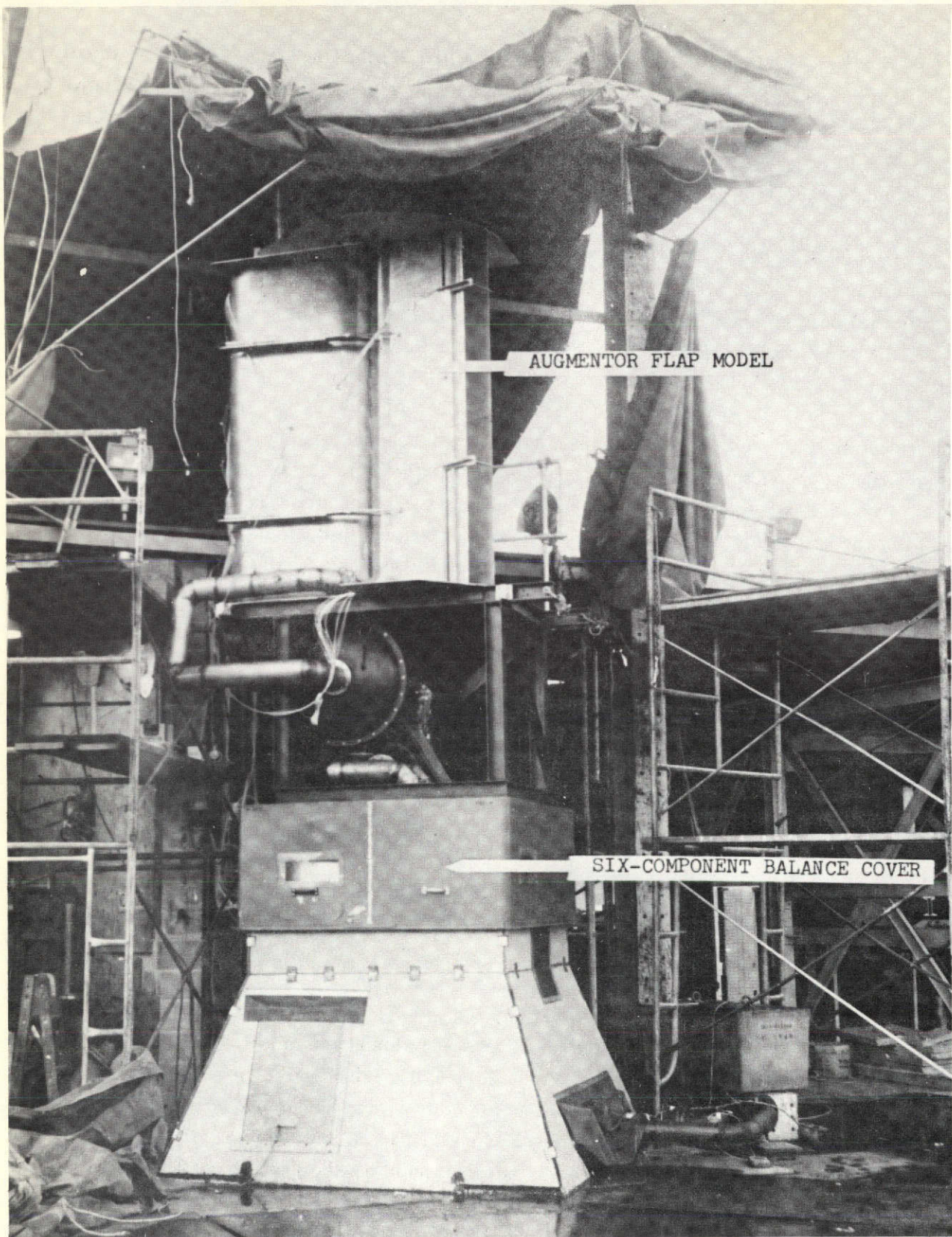
FIGURE 37.—AUGMENTOR FLAP MODEL INSTALLATION

The following geometric variations were investigated during the test: augmentor throat spacing, intake door opening, lift dump angle, diffuser exit angle, and Coanda flap positions relative to the slot nozzle exit at several flap deflection angles. In addition to testing these geometric variables for thrust performance, model acoustic levels, augmentor static pressures, and exit momentum data were recorded.

Augmentor performance may be presented in terms of the ratio of measured resultant thrust to the isentropic thrust at the augmentor nozzle entrance or as the ratio of measured resultant thrust to the measured nozzle thrust. Figure 38 presents the maximum levels of augmentation produced by the model for both definitions. The first definition, which includes the nozzle and nozzle duct plenum losses, has been used for the Modified C-8A program.

Test results indicated that the highest static thrust augmentation was obtained with the diffuser angle set between 4° and 5° using an augmentor throat to nozzle height ratio (ℓ_T/h_N) between 15 and 17. The static test results showed that the augmentor was fairly insensitive to movements in the Coanda flaps ℓ'_Z direction, but small changes in the Z direction could greatly affect performance. Thrust augmentation was determined for a large range of Coanda flap positions (ℓ'_Z and Z). A typical performance contour plot is shown in figure 39. The sensitivity to variations in the Coanda flap position relative to the nozzle exit is similar at $\delta_F = 30°$ to the sensitivity at other flap angles tested.

The test also showed that small local obstructions in the throat of the augmentor produced significant losses in augmentation, while large variations in the intake door opening produced little effect on performance. The "lift dump" tests showed that the augmentor thrust could be smoothly spoiled from maximum augmentation to slightly negative thrust values.

Flap static pressure data were used to determine airplane flap loads and hinge moments and also as an aid in understanding the augmentor flow characteristics. Total pressure surveys were taken at the augmentor exit to detect flow separation along the flap span and to evaluate the capability for determining airplane augmentor static performance.

The augmentor was tested with both nozzles operating (double nozzle), which is representative of two-engine operation, and with the nozzles operating individually (single nozzle) as for single-engine operation. The augmentation ratio for both double- and single-nozzle operation is shown in figure 40 for flaps deflected to 30° and 65°. There is considerable variation in the Z dimension for maximum performance. A single flap pivot point for the airplane augmentor flap was selected which was a compromise between single-nozzle (engine out) and double-nozzle (two engine) operation. Figure 41 presents the estimated airplane augmentor static performance versus

Double nozzle operation
Diffuser angle = 4.75°

$$\frac{\text{Augmentor throat height}}{\text{Nozzle exit height}} = 15$$

Nozzle pressure ratio = 2.25

Based on measured nozzle thrust (nozzle-duct losses not included)

Based on nozzle isentropic thrust
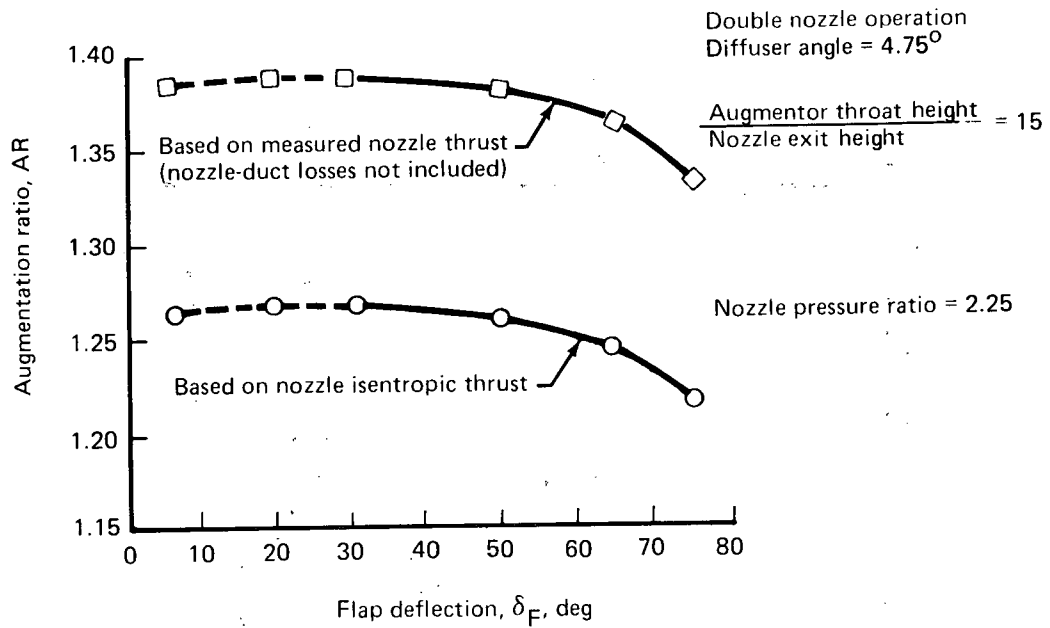
FIGURE 38.—MAXIMUM MEASURED AUGMENTATION RATIO

$\underline{\delta_F = 30°}$

*Model scale
PR = 1.80

- ● Optimum
- △ 2% loss
- ◇ 5% loss
- ▷ 8% loss
- X Final pivot
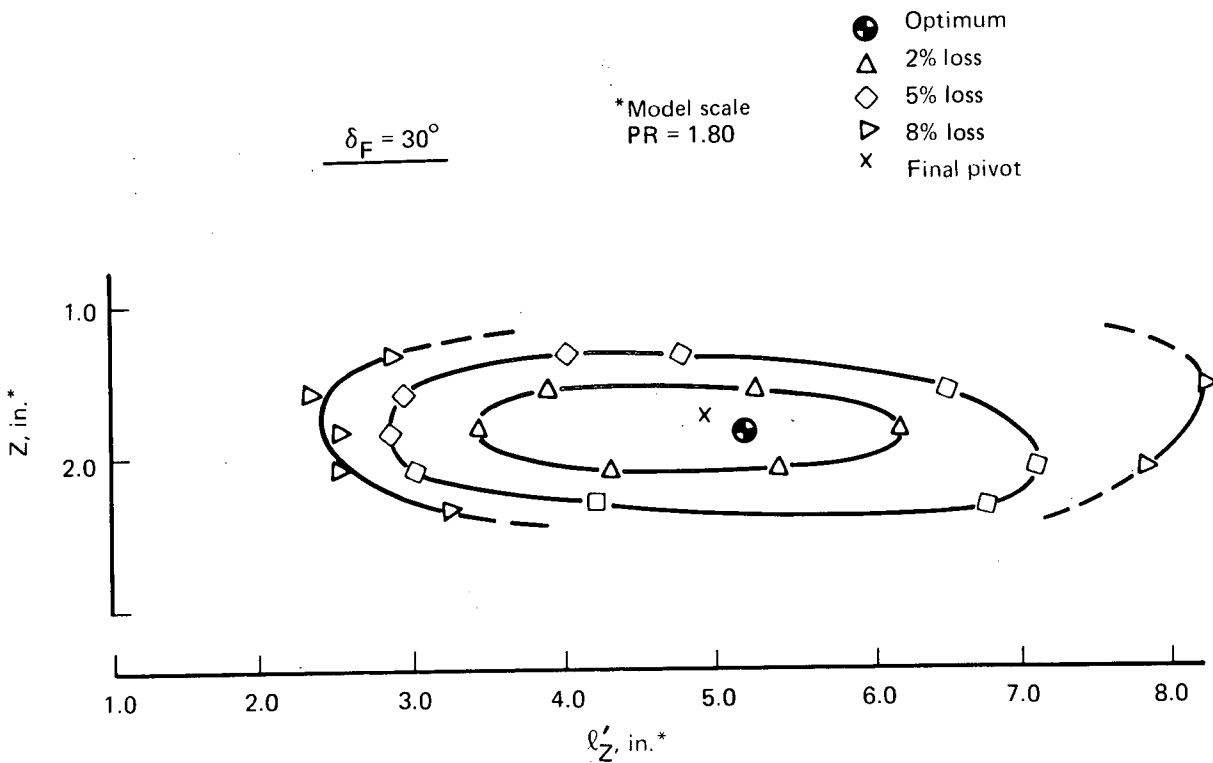
FIGURE 39.—AUGMENTOR-FLAP PERFORMANCE CONTOUR MAP AT 30° FLAP ANGLE
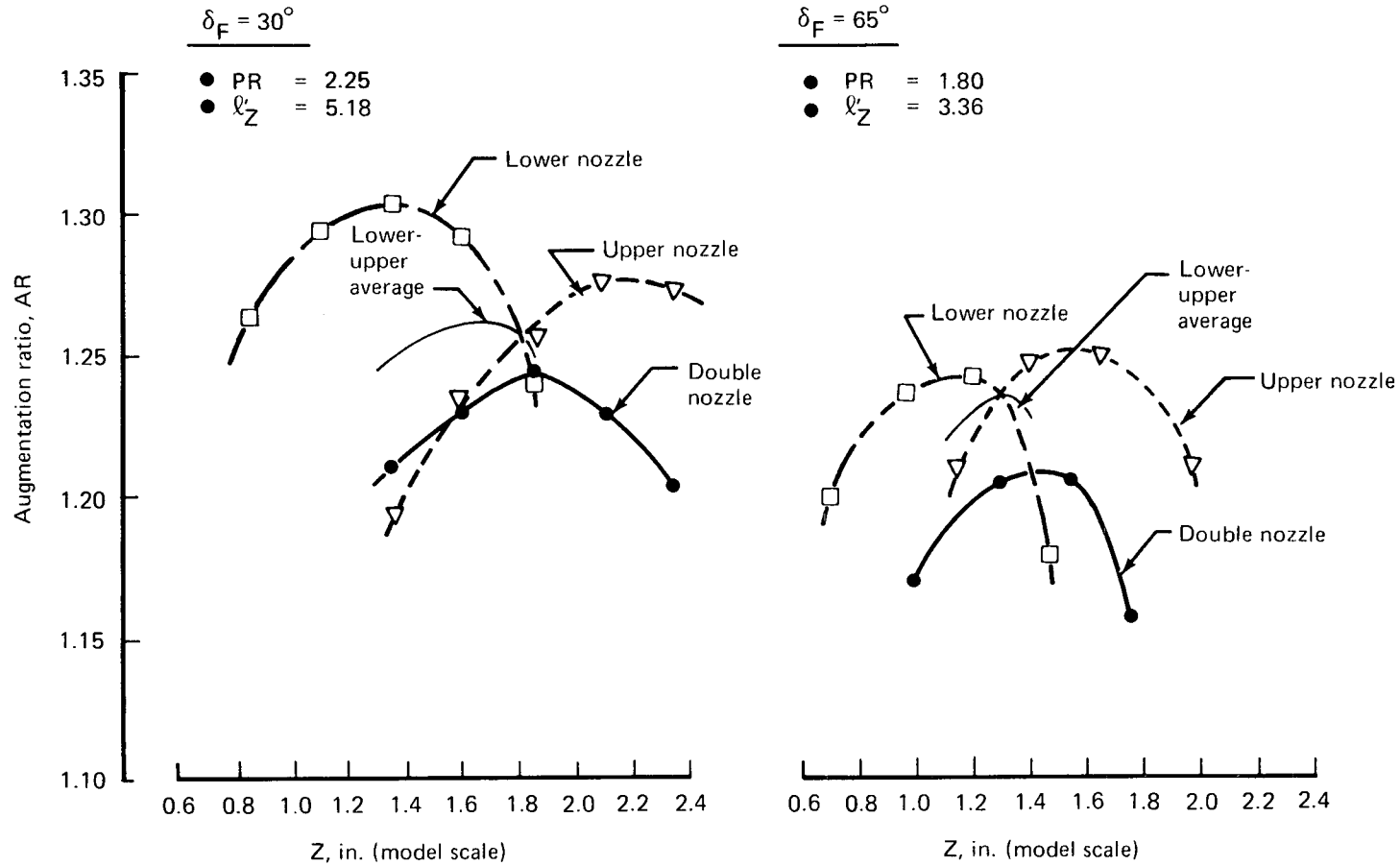
FIGURE 40.—AUGMENTATION RATIO VS Z FOR ALL NOZZLE COMBINATIONS—INBOARD SIMULATION
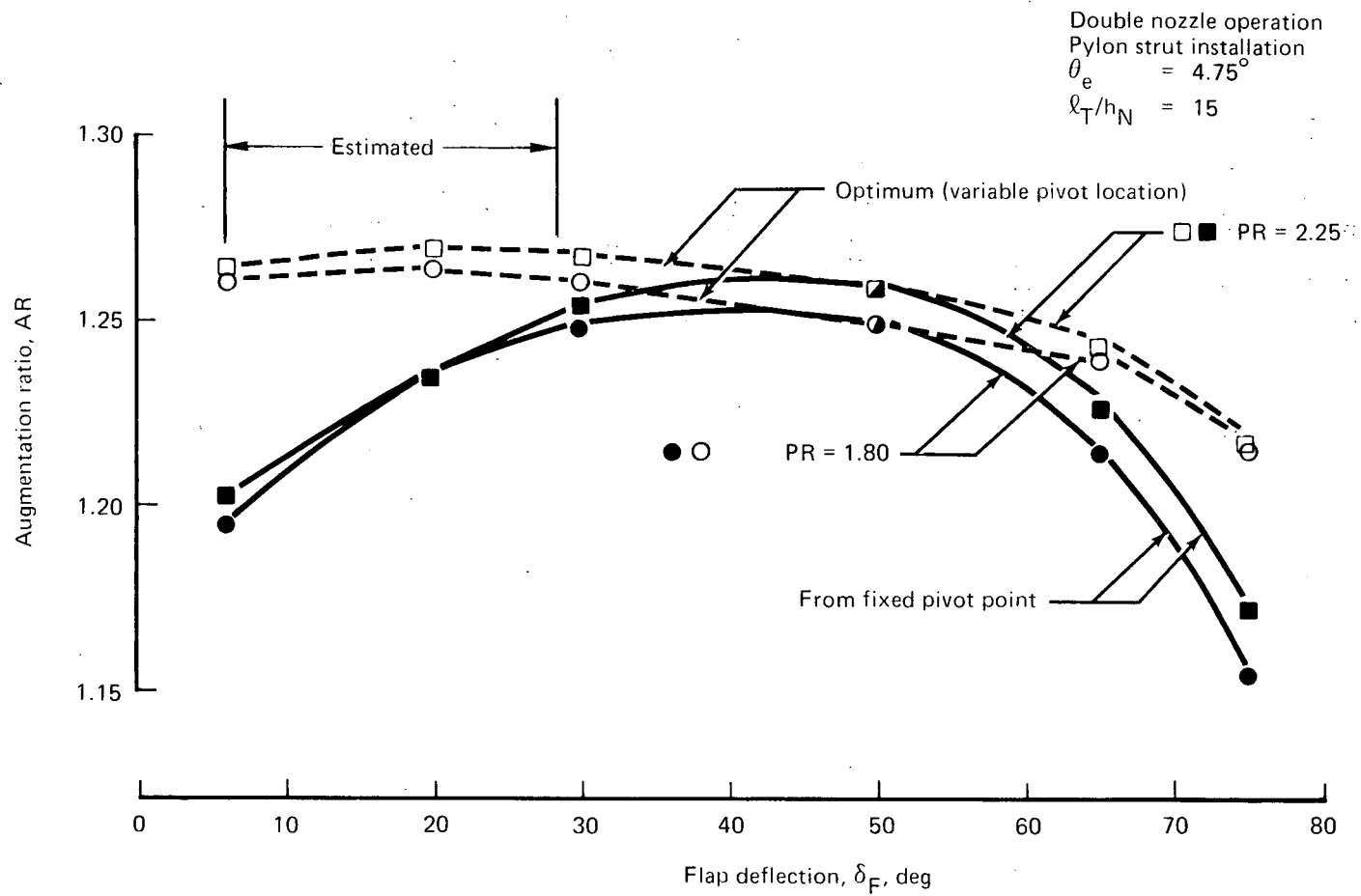
FIGURE 41.—ESTIMATED AIRPLANE AUGMENTOR STATIC PERFORMANCE VS FLAP DEFLECTION

flap deflection angle for the airplane flap pivot point selected. The maximum performance obtained, assuming infinite variation of the pivot point, is also shown. It is of interest to note that performance near the optimum obtained by the model can be achieved for the flap deflection angles of major interest (30° to 65°) by using a simple fixed pivot position in the airplane design.

In addition to the conclusions discussed above, the following observations were made:

- The 0.7-scale model developed approximately 4% higher thrust augmentation than the Ames phase IV wind tunnel model.

- Maximum nozzle velocity coefficient attained was 0.92, at a pressure ratio of 2.5.

- The model upper nozzle turning vanes overturned the flow 3.5°.

- The augmentor performance was not sensitive to upper and lower nozzles operating at moderately unequal pressure ratios.

- The passage between the intake door and the upper nozzle external surface should be convergent or parallel to provide vibration-free operation.

Acoustic measurements were recorded during the static test of the jet-augmentor flap system. The object of these recordings was to determine the basic noise characteristics and verify predicted noise levels of the augmentor system. The noise at the optimum performance configuration was a broadband distribution of energy between 800 and 8000 Hz. Small movements from the optimum position of the flap system relative to the axis of the slot nozzle caused discrete tones to be generated. The maximum perceived noise levels were observed to occur about 40° from the flap system centerline and were within 1 to 3.5 PNdB of estimates made prior to the test. At lower pressure ratios, the noise level of the 30° flap configuration is consistently higher than the levels for the higher flap angles.

Based on this test program, and the above conclusions, the following features were incorporated in the Modified C-8A airplane design:

- Flap diffuser angle was established at 4.75°.

- Flap pivot point was located to obtain the best augmentor performance compromise between engine-out operation (single nozzle) at 30° flap angle and two-engine operation (double nozzle) at 30° and 65° flap angles.

- Upper nozzle turning vane exit angle was adjusted to eliminate flow overturning and minimize double-nozzle crossflow losses.

- The flap internal support brackets and intake door arm were designed to eliminate obstructions in the augmentor throat.

- Intake door angle at the flaps up position was adjusted to eliminate possible vibration.

The estimated airplane augmentor performance based on static test data is approximately 3% higher than that produced by the full airplane model with similar flap geometry tested in the Ames 40- by 80-ft wind tunnel. Since the airplane performance was based on this wind tunnel data, the static test indicated that the augmentor flap system would perform satisfactorily and would not significantly contribute to the aircraft noise levels on the Modified C-8A airplane.

PREDICTED FLIGHT CHARACTERISTICS

Flight characteristics were predicted using adjusted wind tunnel data, theoretical techniques, and basic C-8A Buffalo data along with airplane and engine characteristics. Extensive use was made of digital computer programs to calculate trimmed flight conditions, dynamic characteristics, and performance. Considerable knowledge was gained about airplane handling qualities from the piloted simulator tests. Predicted flight characteristics have been published in reference 9, and are summarized in the following paragraphs.

LONGITUDINAL CHARACTERISTICS

The Modified C-8A has an installed thrust-to-weight ratio approaching $T/W = 0.5$. The very effective high-lift system generates a design approach lift coefficient of $W/qS = 4.0$, or roughly twice that of "conventional" high-lift systems. Maximum performance in terms of low operating speeds, short field length, and wide variation in flightpath angle is impressive. Typical flightpath capability for reasonable variation in power setting is shown in figure 42. Climb and descent angles are considerably steeper than for conventional transports. Body attitude also varies over a large range, as shown in figure 43. Takeoff attitude is quite high. Attitude changes significantly with speed in such a way that attitude becomes an indicator of flight condition.

Stall speed (1 g at $C_{L_{max}}$) varies over a considerable range as well. At 40 000 lb, stall speed is 90 kt at flaps up, idle power, and 37 kt at flaps 75°, takeoff power (nozzles down). Power effect is quite pronounced. At landing flaps ($\delta_F = 65°$), minimum airspeed varies more than 40 kt. Most operational flight speeds at takeoff and landing ($V_2 \approx 76$ kt, $V_{app} \approx 60$ kt) occur below power-off stall. The Modified C-8A truly operates in the "powered-lift" STOL regime.

The Modified C-8A has limited fore and aft center-of-gravity range. With fixed equipment installation (basically flight test instrumentation) and no provision for passengers, the need for loadability range is not great. Structural design CG limits have been further restricted by aerodynamic considerations resulting from fixed tail incidence. Nominal CG varies from 27% MAC at zero fuel weight to 30% MAC at maximum design gross weight (45 000 lb).

Elevator deflection is used for both 1 g trim and maneuvering. Elevator required to hold steady, 1 g flight has been computed for all combinations of weight, speed, flap deflection, power setting, and hot thrust nozzle angle at nominal CG locations along the fuel loading line. Figure 44 presents the envelope of these conditions for the existing stabilizer incidence setting of $i_T = +1°$.
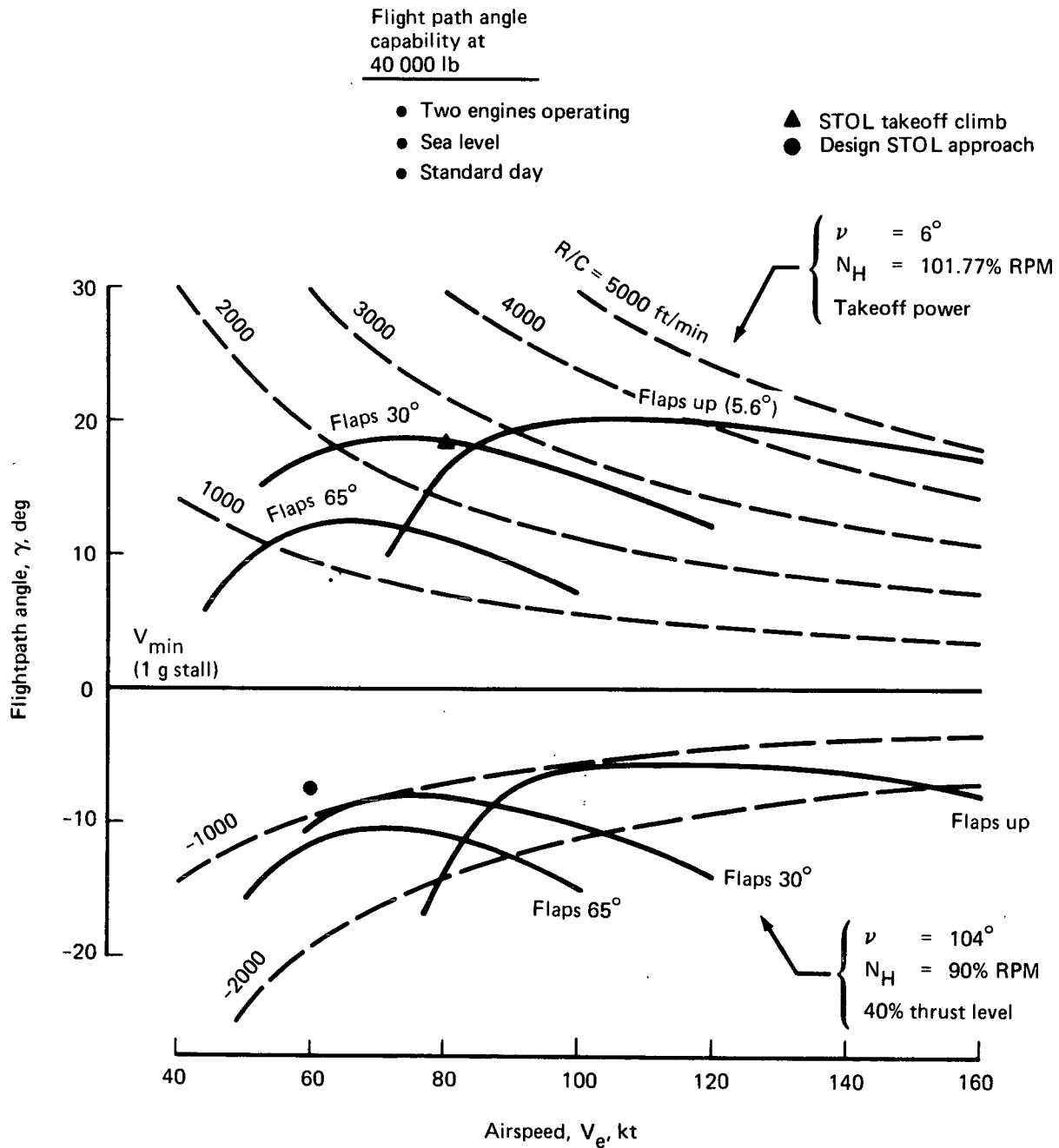
FIGURE 42.—TYPICAL FLIGHTPATH AND RATE OF CLIMB ENVELOPE
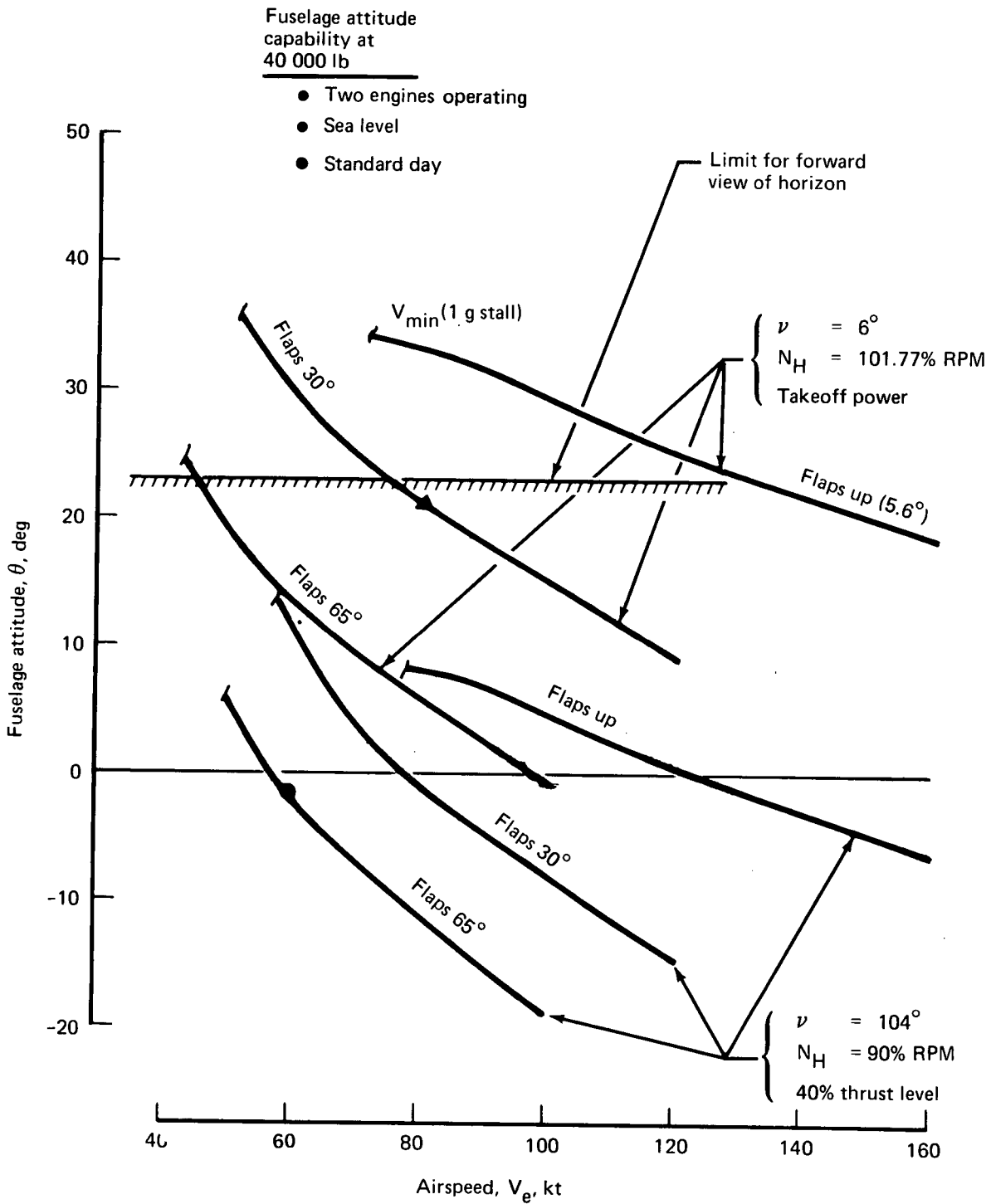
FIGURE 43.—TYPICAL BODY ATTITUDE ENVELOPE
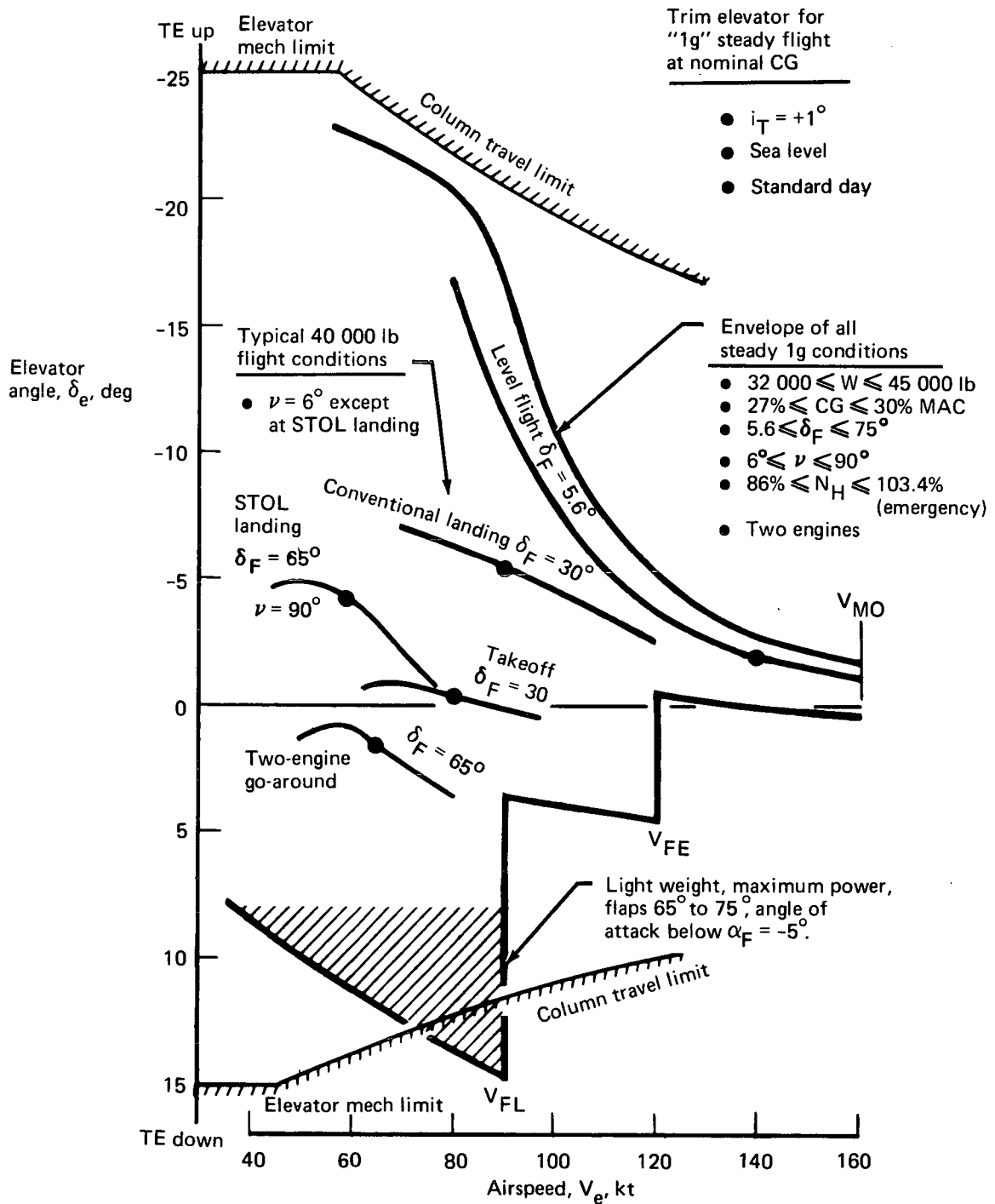
FIGURE 44.—ELEVATOR-TO-TRIM ENVELOPE

Typical trim requirements for normal operation at 40 000 lb are also shown in the figure. For most flight conditions, elevator deflections lie within a few degrees of neutral. This fortuitous situation occurs because pitching moment produced by flap deflection is almost entirely counteracted by tail lift induced by changes in downwash angle. Large elevator deflections are needed for stall maneuvers and full power application at landing flaps, vectors down.

The airplane longitudinal handling qualities in the approach and landing phase were characterized by four detrimental characteristics:

- Low static longitudinal stability, heightened in its effect by the fact that at low approach speeds the short period mode and the phugoid have frequencies much closer together than usual.

- Flight on the "back side" of the power-required curve, which increases pilot workload because of the need to constantly alter both pitch attitude and power setting to maintain speed and descent rate.

- Interaction of thrust and lift, giving uncoupled angle-of-attack and speed characteristics, and reversal of the pitch attitude-flightpath relationship at constant speed.

- Large elevator requirement for flare, due to the increased ground effects, the reduced aerodynamic control effectiveness at the low approach speed, and the sluggish flightpath response resulting from the low n_{z_α} at the approach lift coefficient.

Classical static longitudinal stability is characterized by the amount of stick force (elevator deflection) required to slow down (pull) or speed up (push) away from a trimmed flight condition. The airplane has adequate longitudinal stability at cruise conditions and on the "conventional" landing approach (flaps 30°, and 90 kt). Above 75 to 80 kt the airplane is generally on the "front side" of the power-required curve, thereby possessing "speed stability." Powered lift effects are also mild at conventional conditions.

Powered lift effects become very pronounced at the design STOL landing approach ($\gamma = -7.5°$ at 60 kt). The flightpath may be controlled in two ways: by power changes or by thrust vector (nozzle) modulation. Figure 45 illustrates the wide variation in glide slope attained by either method. The design approach condition ($\delta_F = 65°$, $\nu = 90°$, 92% RPM) was selected to ensure the following margins with hot thrust perpendicular to flightpath: $\Delta n_z \geqslant 0.35$ g, $V_{app} \geqslant 10$ kt from V_{min} and $\alpha_F \leqslant 5°$ (15° from stall). It can be seen that power changes vary the margins. At 80 kt, advancing throttles to takeoff setting produces $\Delta n_z \approx 0.65$ g and $\Delta V \approx 22$ kt. On the other hand, reducing power setting lowers margins. This characteristic is due to the "lift coupling" with the

FIGURE 45.—TWO FLIGHTPATH CONTROL TECHNIQUES AT STOL APPROACH

throttle. In fact, advancing throttles on approach generates a net instantaneous force on the airplane oriented almost directly perpendicular to the flightpath. Significant changes of nozzle angle on figure 45 show that margins and trim angle of attack remain relatively constant when hot thrust vectoring is used to set glide slope. Nozzle modulation about the $\nu = 90°$ trim point produces instantaneous axial forces on the airplane analogous to power setting on conventional airplanes.

Figure 46 illustrates the effect of the two control techniques on airplane attitude and trim. Extending the approach, i.e., raising the flightpath angle by rotating the nozzles aft, produces a conventional nose-up change in attitude. Increased power also reduces glide slope but the airplane pitches nose down, which is unconventional. Airplane attitude variation with change in airspeed at $\gamma = -7.5°$ is quite pronounced but conventional in direction. Trim elevator change is small in all cases. In the simulator studies, the pilots considered the reversed attitude change with power as "unstable." For STOL approach the pilots concluded that nozzle modulation provided the best means of flightpath control.

Figure 47 presents typical static longitudinal stability characteristics at STOL landing approach. The rate of change of glide slope with speed is $\partial\gamma/\partial V = 0.2$ deg/kt (unstable), which is over three times greater than that permitted by MIL-F-8785 for conventional airplane operation. Using thrust vector modulation, the pilots were able to track the approach path with acceptable results. Static stability exists for speed increase above 60 kt, but the slope and magnitude of pull force below 60 kt is very low. The pilots had to devote considerable attention to the task of maintaining control at STOL approach.

Reduced stability with lowering flight speed is brought on by several effects. First, reduced airspeed increases blowing coefficient, C_j, thereby producing an inherent degradation in aerodynamic stability. This degradation is caused primarily by change in wing lift curve slope and downwash flow field at the tail. The second contributor to reduced stability is the nose-up hot thrust moment. The hot thrust nozzles are located below and ahead of the center of gravity. Tail lift is required to trim the thrust moment. If, for example, speed is reduced, the hot thrust nose-up moment remains constant while the aerodynamic pitching moment is reduced (q effect). The net result is a virtual destabilizing pitch-up due to thrust as speed decreases.

Typical longitudinal flight maneuvers consist of takeoff rotation, in-flight maneuvering, minimum speed demonstration, and landing flare. The Modified C-8A was predicted to have adequate maneuvering control capability. Maneuvering stability exists at constant speeds. Large elevator deflection is required to flare at STOL conditions due to strong, adverse ground effect.

**Attitude and trim changes
away from STOL approach**

- Flaps 65°, 40 000 lb
- Sea level
- Standard day
- Nominal CG at 29% MAC
- Trim at 60 kt, γ = -7.5 deg
  ν = 90°, N_H = 92% RPM

**Vary glide slope
at 60 kt**

**Vary airspeed
at γ = -7.5°**

Pegasus nozzle
thrust vectoring
(power constant at 92% RPM)

Pitch
attitude,
θ, deg

6°

ν = 50°

Trim

90%   80°   70°

92%   90°

Conventional
$\dfrac{\Delta\theta}{\Delta\gamma}$ = +1   104°

94%   96% RPM

101.8%

Throttle setting,
thrust level change
(nozzles fixed at ν = 90°

ν = 60°

Pegasus nozzle
thrust vectoring

70°

80°

96%

94%

90°

92%

91% RPM

Throttle setting,
thrust level
change   95°   92%

90°

TE up

-5

Elevator
angle,
δ_e, deg

Trim

0

5

-12   -8   -4   0

Flightpath angle, γ, deg

50   60   70

Airspeed, V_e, kt

*FIGURE 46.—EFFECT OF TWO FLIGHTPATH CONTROL TECHNIQUES
ON PITCH ATTITUDE AND TRIM AT STOL APPROACH*
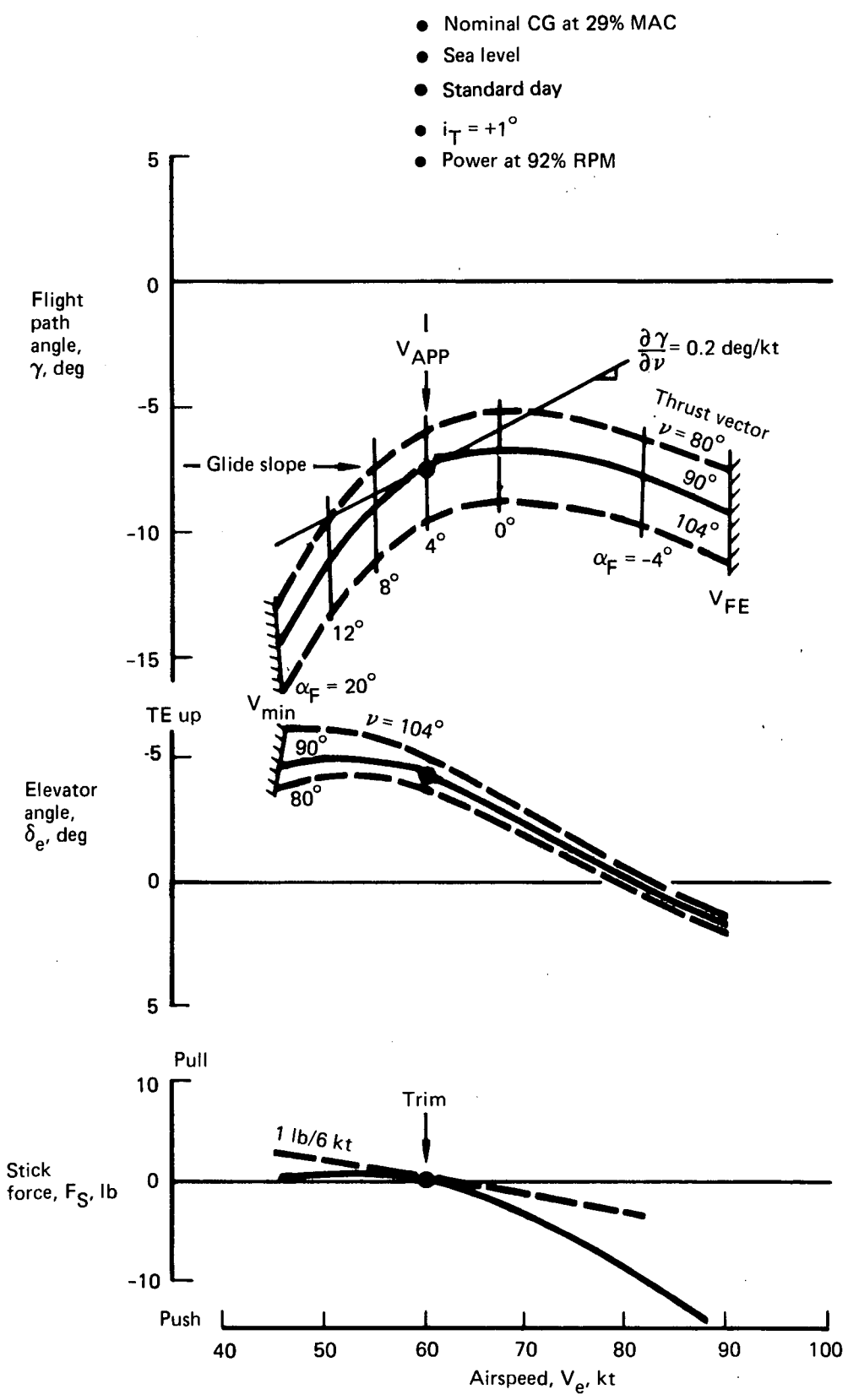
FIGURE 47.—STATIC LONGITUDINAL STABILITY AT
FLAPS 65°, STOL LANDING APPROACH

LATERAL-DIRECTIONAL CHARACTERISTICS

With its powerful rudder the Modified C-8A is capable of achieving large sideslip angles. Figure 48 presents sideslip-to-rudder characteristics at the critical STOL approach condition. Maximum rudder yields $\beta > 25°$ based on extrapolated data. Such angles appear feasible since U.S. Army flight tests on the original Buffalo showed capability at $\beta > 20°$ from 65 to 109 kt. The wheel deflection shown in figure 48 corresponds to two anticipated extremes in the value of C_{ℓ_β}. Wind tunnel data at landing flaps indicate that $C_{\ell_\beta} = 0$ while theoretical estimates would show $C_{\ell_\beta} = -0.004/\text{deg}$. A "statically stable" airplane requires right wheel for left pedal in a sideslip. With $C_{\ell_\beta} = 0$ an "unstable" left wheel input is required to offset rolling moment due to fin lift. In fact, the airplane will appear neutrally stable at $C_{\ell_\beta} = -0.0015/\text{deg}$. At 60 kt aerodynamic sideforce is relatively small compared to airplane weight; thus, only small bank angle is required to maintain straight flightpath.

The Modified C-8A has satisfactory lateral and directional control power for maneuvering on the critical STOL landing approach. Control power was evaluated on the simulator using "S-turns" on landing approach with moderate turbulence levels. Figure 49 presents maximum rolling moment capability ($C_{\ell_{max}}$) for variations in speed, flap angle, and power setting. Since surface effectiveness is related to blowing coefficient, $C_{\ell_{max}}$ changes significantly with speed and power. Superimposed on the figure are lines of constant roll acceleration. Time required to achieve a $\phi = 30°$ bank angle is less than 2.5 sec with SAS-improved roll time constant. Bank angle in the first second will exceed $\phi_1 = 6°$ with SAS. Steady-state roll rate is in excess of 20 deg/sec even with some control power used by the SAS for roll damping. The Modified C-8A meets its lateral control design criteria.

Rudder control power is high. Figure 50 presents instantaneous yawing acceleration due to full rudder and heading angle change in 2.2 sec. The heading change maneuver was calculated including the effect of yaw damping from the SAS. At 60-kt approach the Modified C-8A meets the design criteria and has more than adequate control power for decrab on the crosswind landing.

The unaugmented Modified C-8A suffers a deterioration in lateral-directional handling qualities in the STOL flight regime due to the increased importance of the aerodynamic cross coupling terms and the reduced importance of the aerodynamic static stability terms at low dynamic pressures relative to the inertia forces. These effects lead to:

- Low static directional stability, with long Dutch roll periods and a tendency towards "snaking"
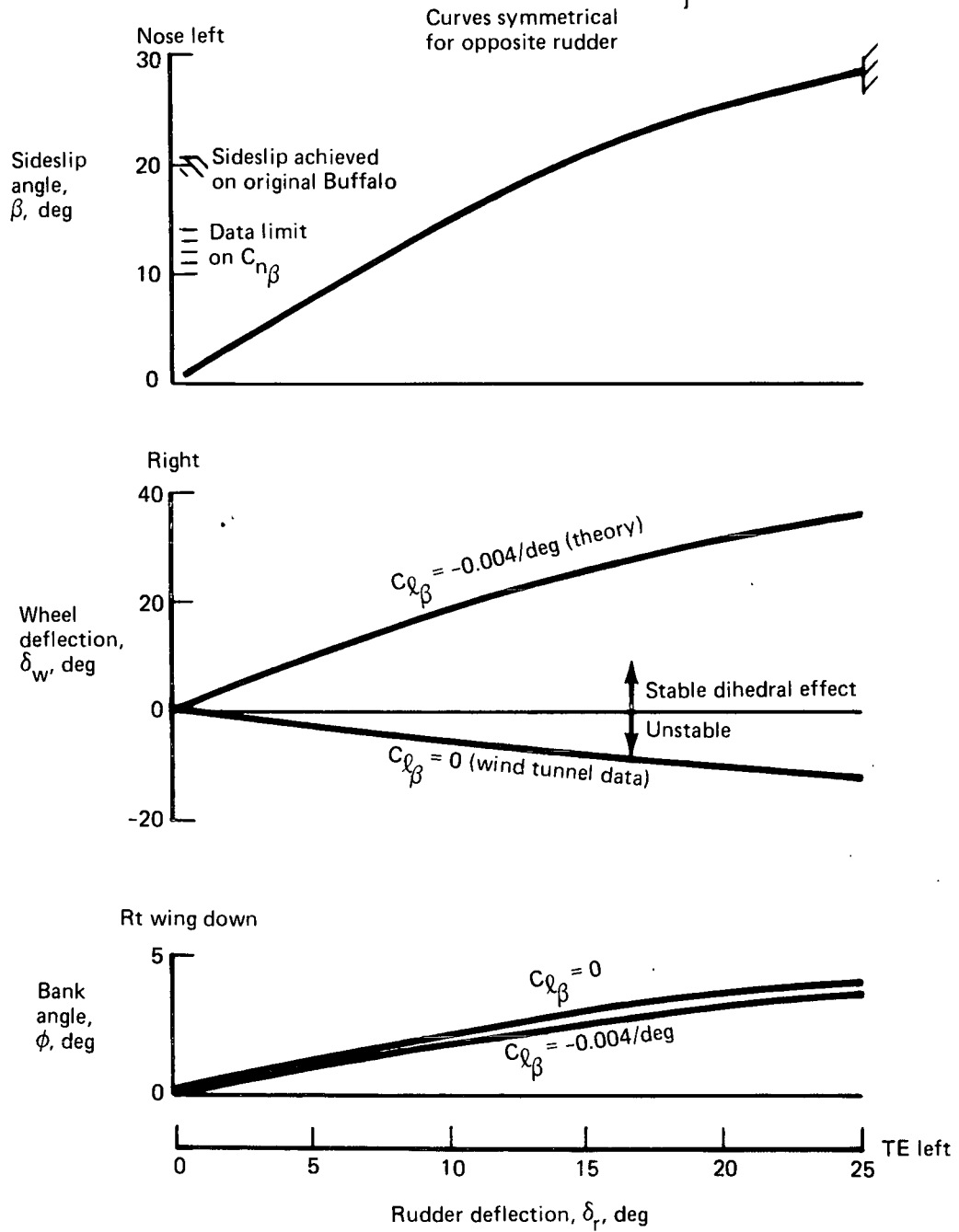
FIGURE 48.—STATIC LATERAL-DIRECTIONAL STABILITY AT LANDING APPROACH

Maximum wheel input at $\delta_w = 75°$

Both engines and hydraulic systems operating

$-5° < \alpha_F < 10°$

$\ddot{\phi}$ calc at $\dot{\phi} = 0$

$I_{xx} = 260\ 000$ slug-ft^2 (40 000 lb)
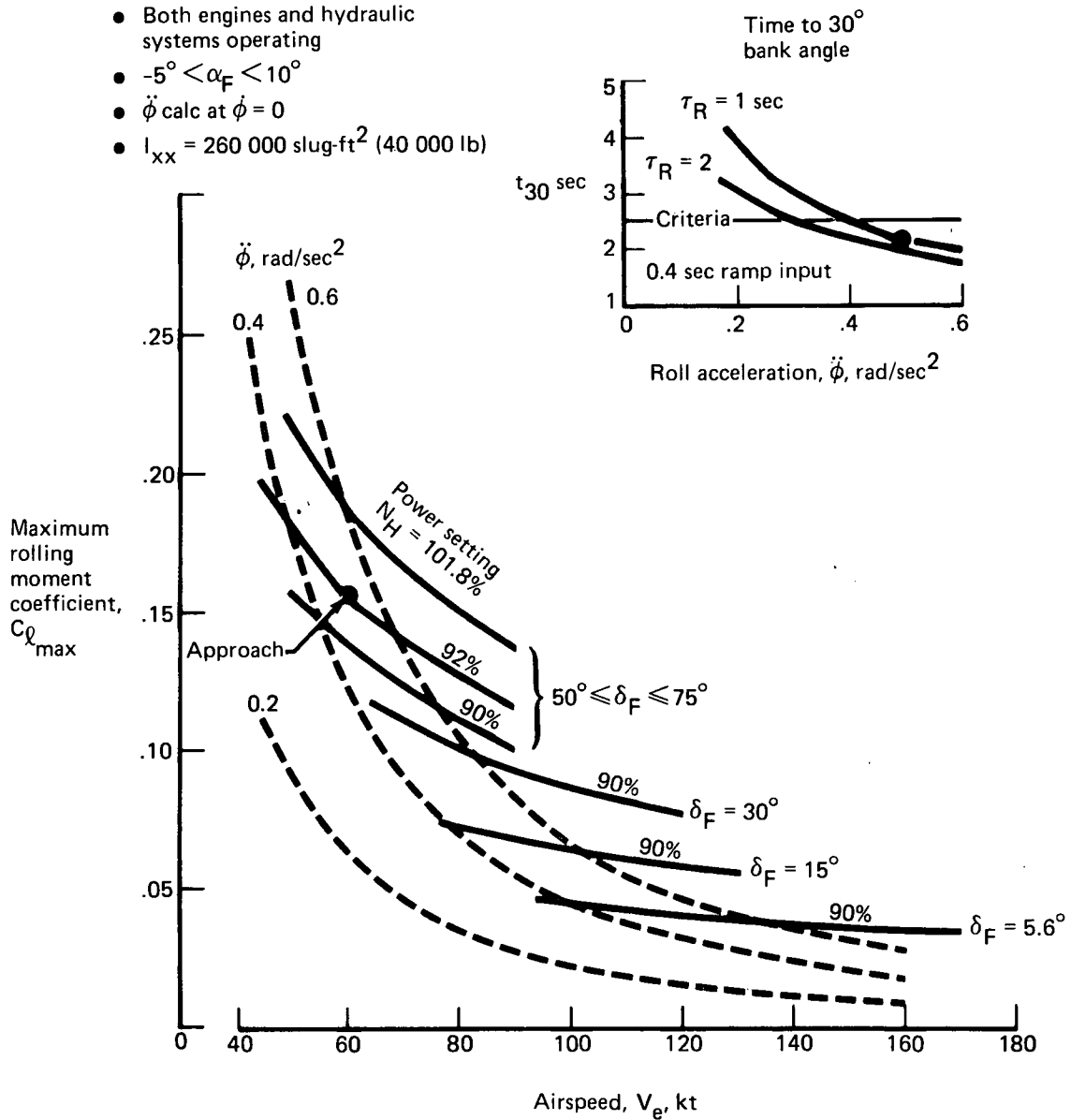
FIGURE 49.—MAXIMUM ROLLING MOMENT LATERAL MANEUVERING CAPABILITY
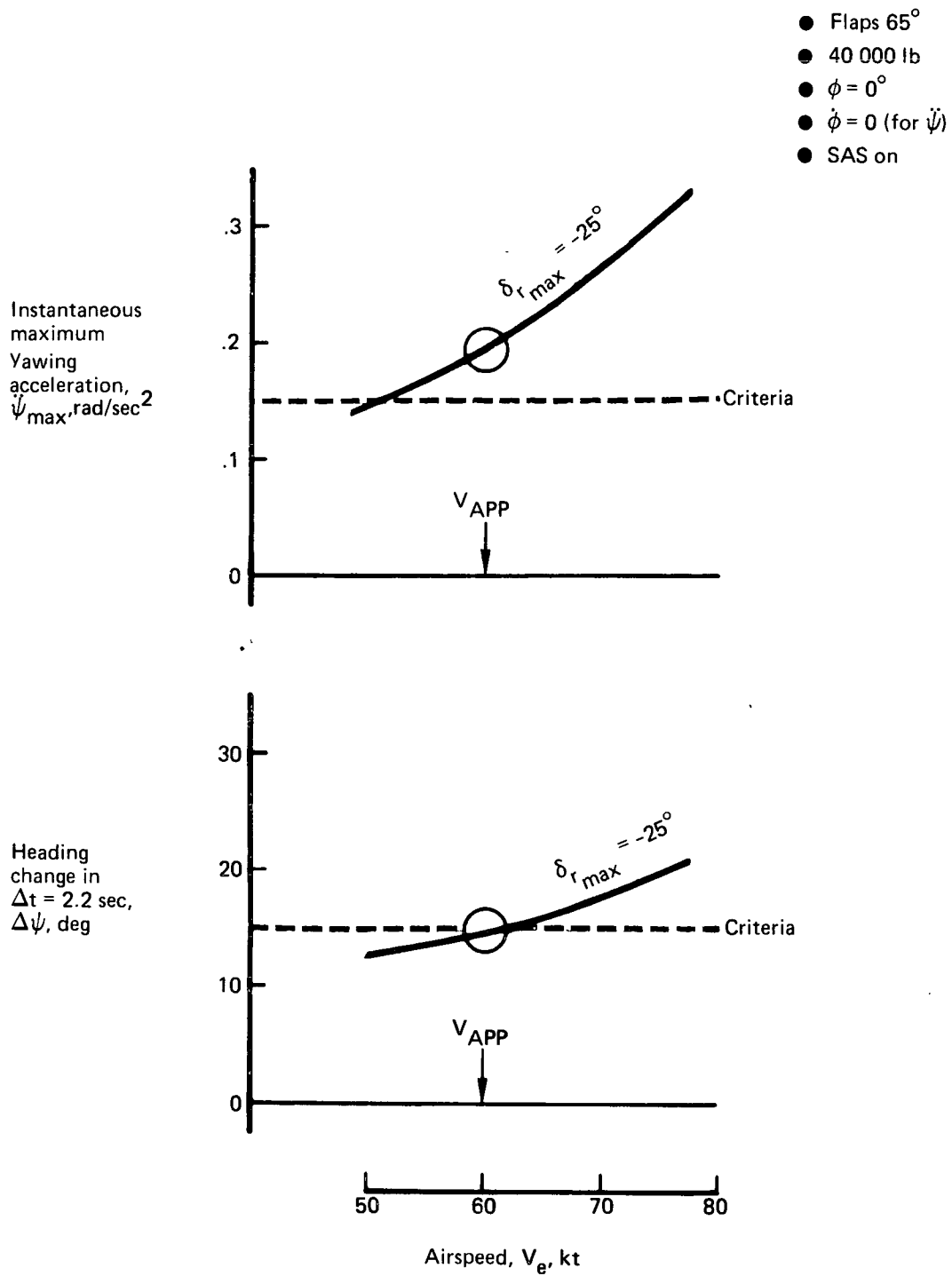
FIGURE 50.—YAWING MANEUVER CAPABILITY

- Large sideslip buildups during turn entry even when yawing moment from lateral control is small (Adverse sideslip-to-bank angle reaches $\Delta\beta/\Delta\phi = 0.65$ compared to an acceptable level at $\Delta\beta/\Delta\phi \leqslant 0.3$)

- Low Dutch roll damping or unstable spiral modes depending on the level of the lateral static stability (C_{ℓ_β})

Wind tunnel testing of the modified Buffalo airplane had not clearly defined the derivative C_{ℓ_β} for the approach and landing configuration except that it lay somewhere in the range $-0.004 < C_{\ell_\beta} < 0$ per degree. Over this range of values the lateral-directional dynamic characteristics varied from the extremes of 5% to 25% Dutch roll damping ratio, and 13 to 3.5 sec to double amplitude of the spiral mode. In the simulator the pilots were able to fly the airplane to a STOL landing without SAS. Pilot rating ranged from 6.0 to 9.0 on the Cooper-Harper scale. SAS-off flight in the STOL regime should not be attempted in normal circumstances.

Early in the program it was decided that a lateral-directional stability augmentation system was mandatory for good handling qualities. The two-mode SAS resulted: "normal mode" for handling qualities improvement and "variable stability mode" for research. The "normal mode" SAS schematics are shown in figures 51 and 52. This SAS configuration produced the following:

- Improved spiral stability to time to double or half amplitude greater than 20 sec.

- Maintained well-damped Dutch roll mode.

- Reduced the roll mode time constant to $\tau_R < 1.0$ sec.

- Provided turn coordination with ratio of peak sideslip to bank angle developed during rapid turn entry at $\Delta\beta/\Delta\phi < 0.3$ and heading delay less than 2 sec.

The augmented lateral-directional handling qualities were rated as satisfactory (pilot ratings of 3.5).

Flaps >40°

1.50

Flaps <40°

0.75

Roll rate, deg/sec

+ Roll mode augmentation

Yaw rate, deg/sec

1.75

Spiral stability augmentation

$V_e > 100$ kt

Equivalent wheel command, $\delta_{w_{SAS}}$, deg

Authority limited to $\delta_{w_{SAS}} = \pm 20$ deg
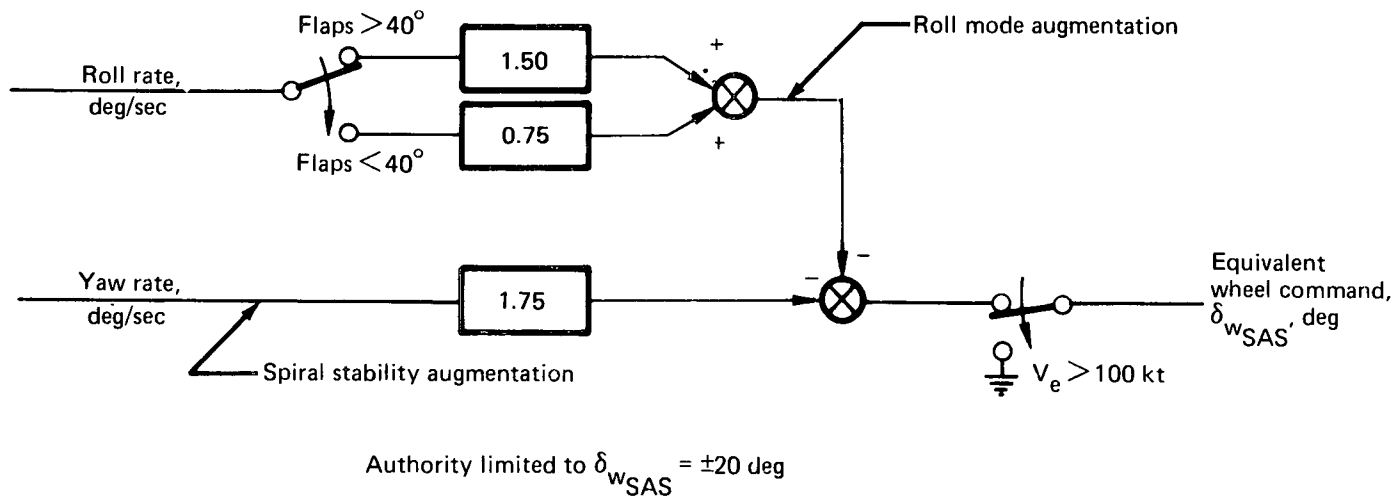
FIGURE 51.—LATERAL AXIS STABILITY AUGMENTATION (NORMAL MODE)

Roll rate (derived)
deg/sec

Flaps $>40°$

0.60

Flaps $<40°$

0.30

+
+

Turn coordination

Roll angle,
ϕ, deg

Flaps $>40°$

0.10

Flaps $<40°$

Steady-state turn
coordination

$\frac{g}{V}$ 0.29

−
−

Equivalent
rudder command,
$\delta_{r_{SAS}}$, deg

$V_e > 100$ kt

Yaw rate, −
deg/sec

−
+

$\frac{2.5S}{(2.5S + 1)(.25S + 1)}$

0.40

$\dot{\beta}$ yaw damping

Authority limited to $\delta_{r_{SAS}} = \pm 5$ deg
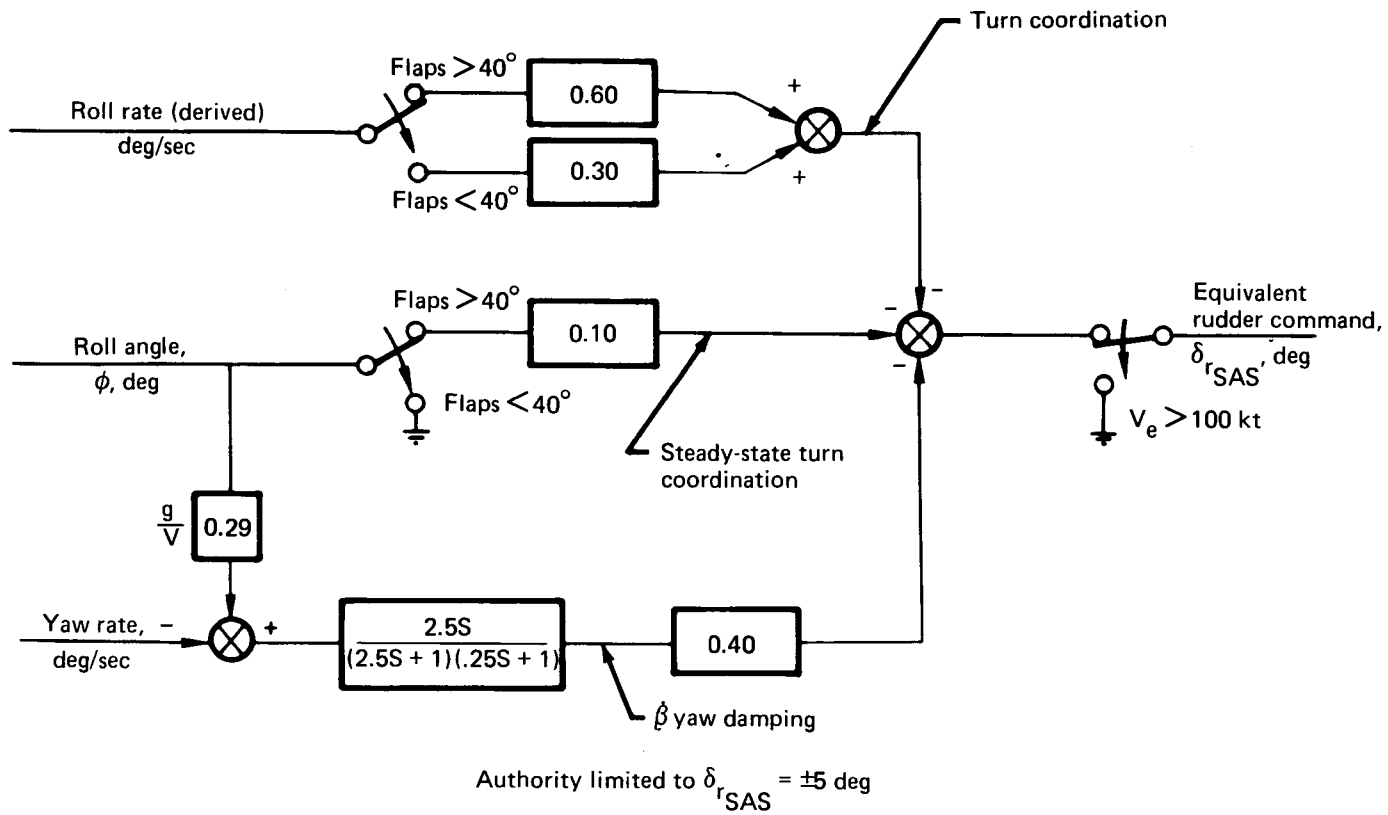
FIGURE 52.—DIRECTIONAL AXIS STABILITY AUGMENTATION (NORMAL MODE)

GROUND TESTS

Ground testing of the Modified C-8A airplane was conducted during the period January 25 to April 10, 1972. The objectives of the ground tests were to verify that the airplane and all associated systems were ready for flight and to determine the installed engine performance. Tests were conducted within the following categories:

- Structures

- Augmentor flap air supply system
-
- Propulsion system

- Airplane systems (hydraulic, control, and electrical)

The results are briefly summarized below.

STRUCTURES

Structural testing consisted of ground vibration testing, controls proof testing, and a ground loads survey.

Controls Proof Test

The purpose of the ground vibration test was to ensure that the airplane fundamental wing and T-tail modes are similar to those used in the flutter analyses. A comparison of the frequency values obtained during the test and those used in the analysis is shown in table IV for the various modes investigated.

The test and analytical results of the antisymmetric wing and T-tail modes are found to be in good agreement. The difference in the first symmetric wing mode is due to the fact that the test airplane was supported on its tires. This mode is 2.72 Hz for the basic C-8A airplane, with outboard wing tanks full and gears up. It is expected that the Modified C-8A airplane will have a free-free airplane, zero-fuel frequency somewhat higher than 2.72 Hz.

The 5.49- and 5.71-Hz modes are basically nacelle modes. The nacelle frequencies and mode shapes were estimated for analyses, and the variations of the nacelle vertical bending frequency were

TABLE IV.—COMPARISON OF FREQUENCY VALUES—GROUND VIBRATION TEST AND ANALYSIS

Modal frequency, Hz			Model description
Test (on tires)	Analyses (zero airspeed, gear off ground)		
	Symmetric	Antisymmetric	
2.27	3.15		Symmetric wing bending
2.94		2.89	T-tail mode
4.16		4.13	Antisymmetric bending wing
5.49	Parametric		Nacelle modes
5.71	variation		
6.98	6.8		Aft-body vertical bending
9.57		8.9	Aft-body side bending

made to evaluate its influence on wing flutter. The flutter results indicated satisfactory flutter margins for the nacelle frequency range from 4.5 to 7.5 Hz.

Based on the above testing and associated analyses, the airplane was given a flutter clearance for initial flight test.

Controls Proof Test

Structural tests were performed on the control systems, which were either modified or new to ensure structural integrity up to limit load of all levers, bearings, cables and cable pulleys, and supporting brackets and connections. Table V summarizes the design and test loads for the control systems tested and includes previous de Havilland data where relevant.

The torque required to shear out the fused connection between the lateral control actuator and the main aileron bus cable was verified by test and found to be within acceptable limits.

Ground Loads Survey

A survey of loads and stresses was conducted on the Modified C-8A in static ground conditions. Structural effects investigated were limited to those induced by running engines (and blowing over flaps and ailerons) at various power settings and cycling lateral controls and flaps through their full ranges of travel.

C-2

TABLE V.—MODIFIED C-8A CONTROL SYSTEM DESIGN AND TEST LOADS

Control system	de Havilland ultimate design load	de Havilland test load	Boeing ultimate design load	Boeing test load minimum
Throttle	150 lb	None	75 lb	50 lb
Fuel shutoff	137 lb	None	75 lb	50 lb
Pegasus nozzle control (formerly propeller control)	150 lb (propeller)	None	225 lb	75 lb
Rudder	337 lb x 2.0	225 lb x 2.0	337 lb x 2.0	225 lb x 2.0
Lateral controls (pilot's wheels to lateral actuator only)	1142 in.-lb x 2.0 'D' - 12.7 in.	761 in.-lb x 2.0 1020 in.-lb on each separately	LH 1260 in.-lb 'D' = 14.0 in. RH 1142 in.-lb 'D' = 12.7 in.	840 in.-lb x 2.0
Aileron bus (system—flaps zero, ailerons neutral)	N/A	N/A	Aileron HM = 40 000 in.-lb Cable load = 3010 lb	Aileron HM = 20 000 in.-lb Cable load = 1500 lb
Spoiler/choke bus system	N/A	N/A	450 lb cable load, which is 1.5 x load to fail fused link. Equivalent to 900 in.-lb on one pilot's wheel	2/3 x load required to fail fused link. 200 lb cable load obtained by applying $2/3 \times \frac{1.0}{1.5} \times 900$ = 400 in.-lb on one wheel
Elevator (included for completeness)	337 lb x 2.0	225 lb x 2.0 300 lb on each separately	337 lb x 2.0	None

The following measurements were analyzed:

- Aileron hinge moments versus total aileron angle (100% blowing)

- Total flap pivot moments (100% blowing)

- Augmentor duct stresses at WS 178

- Augmentor duct stresses at WS 193

A brief statement on all other quantities not analyzed in detail is given for completeness.

Slat loads.—No data were obtained on slat loads.

Flap loads.—Pivot moments were estimated from hydraulic system pressures, and are shown in figure 53. The magnitudes of the moments were small, with the largest occurring with choke operation and flaps down (14 000 in.-lb per flap). This is well within actuator capability to react, which is 146 000 in.-lb per flap (down) and 86 000 in.-lb (up).

Aileron hinge moments.—Aileron hinge moments are shown in figure 54. The magnitudes are small, the largest occurring with full-down aileron, flaps at 65°, 2000 in.-lb down. The limit design hinge moments of the aileron are 26 500 in.-lb up and 13 500 in.-lb down.

Lower wing surface, WS 165.—Stress level variations were low, as expected, and no analysis was done.

Front spar web, WS 220.—No analysis was performed.

Augmentor duct.—The duct support loads were lowere than estimated. The augmentor duct T-joint stresses are as expected except for those at gage D (see figs. 55 and 56). Because of the high stresses indicated at gage D additional strain gages were installed at the T-joint on the other side of the airplane. One was essentially a duplicate of gage D, one was in a location similar to gage B but oriented to measure hoop stress, and one was approximately 9 in. higher than D on the outer surface of the rib. Results from these gages verified that the stress at gage D was a localized effect, which is maximum for ground running and decreases in flight. Further discussion on this subject is given in reference 1. Gages B and C show maximum longitudinal stresses when one engine is run up to maximum power. These are temperature induced due to differential thermal expansions of the inner and out ducts.

Flap bus torque tube.—The highest torque measured was 5000 in.-lb compared to a design limit load value of 40 000 in.-lb. This torque occurred during maximum lateral control swings with flaps at 65°. During flap operation no significant torque was indicated except when flaps bottomed out, either full up or full down. In this case, the torque was due to minor rigging errors.

AUGMENTOR FLAP AIR SUPPLY SYSTEM

The augmentor flap air supply system was evaluated to determine duct loss characteristics, airflow and thrust distribution, and the recommended pressure differential setting for the
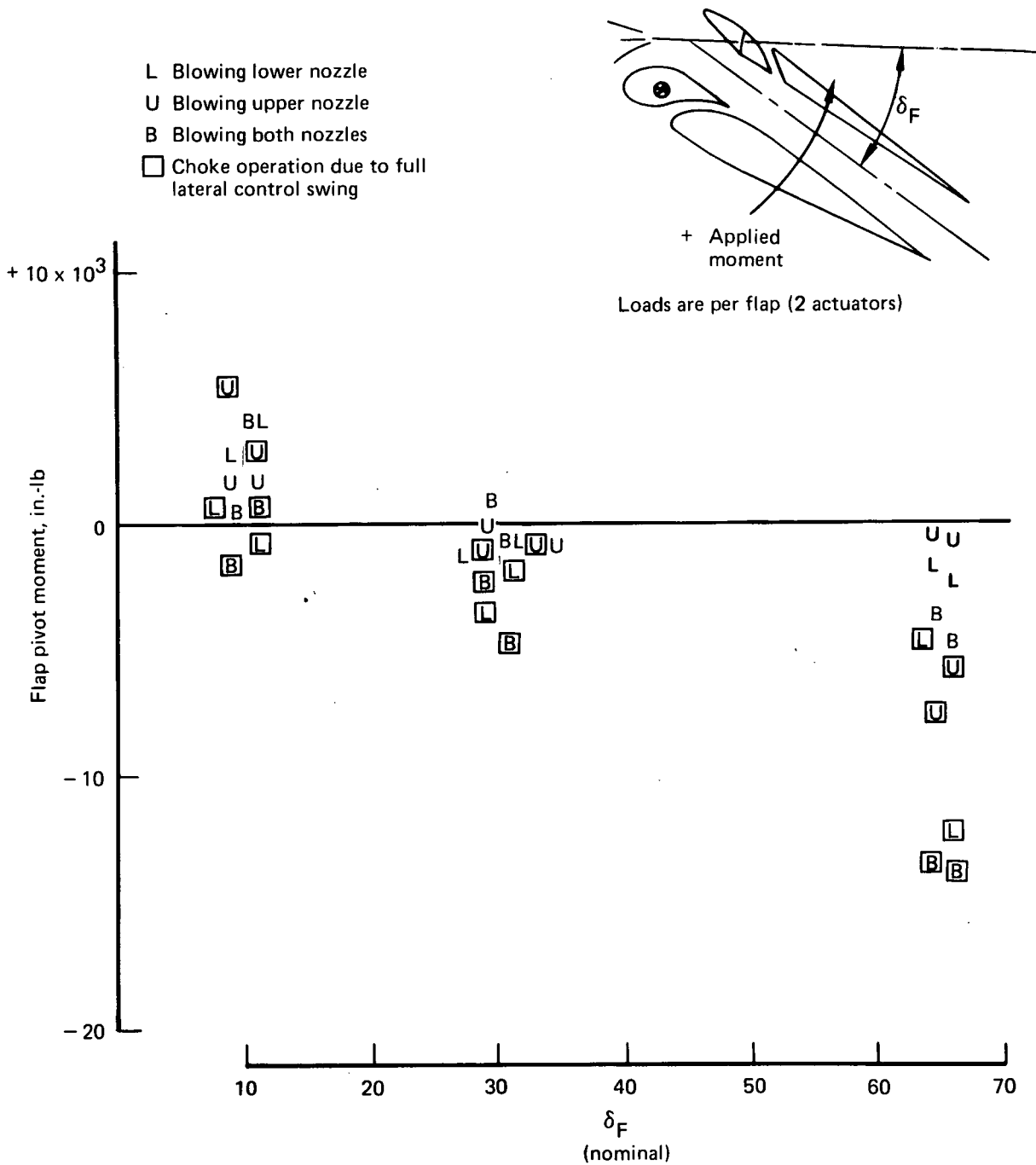
FIGURE 53.—GROUND LOAD SURVEY FLAP PIVOT MOMENTS
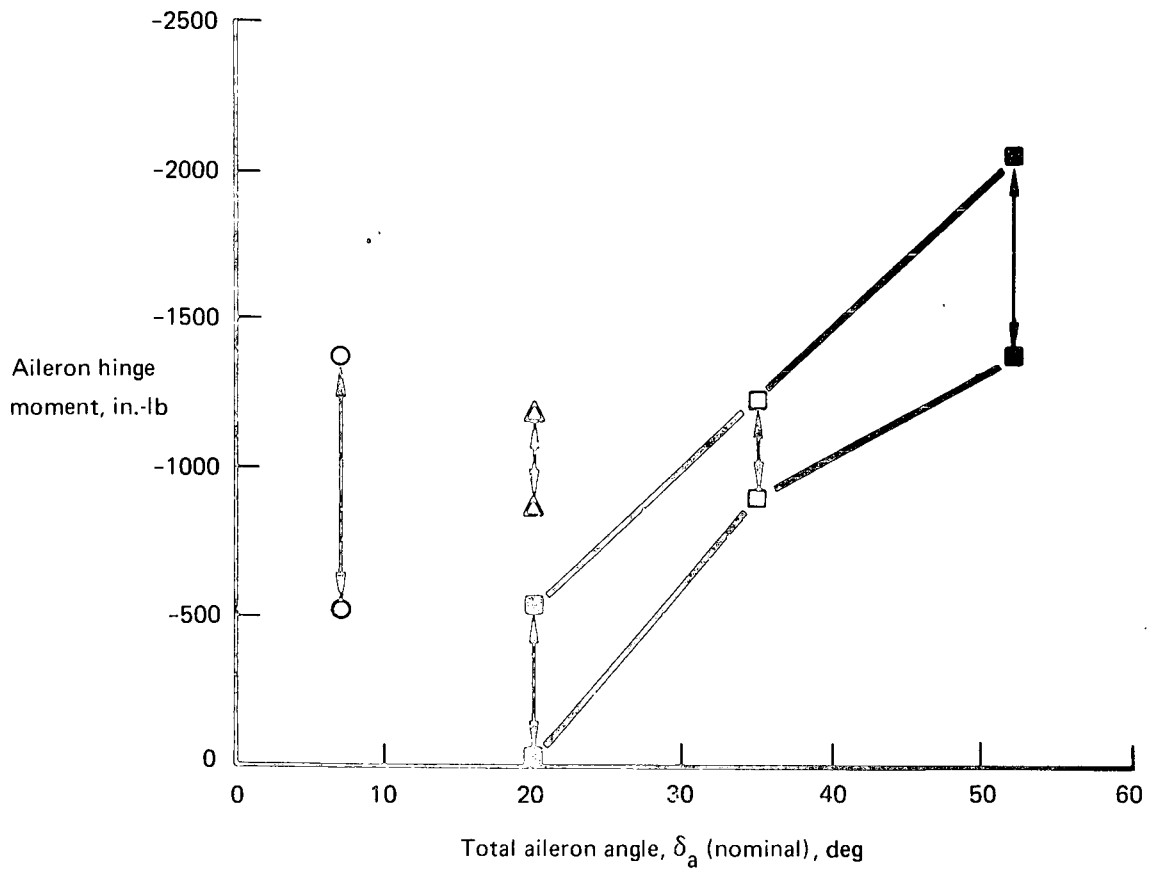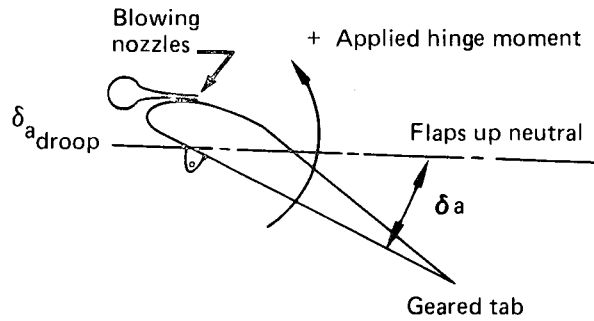
FIGURE 54.—GROUND LOAD SURVEY AILERON HINGE MOMENTS
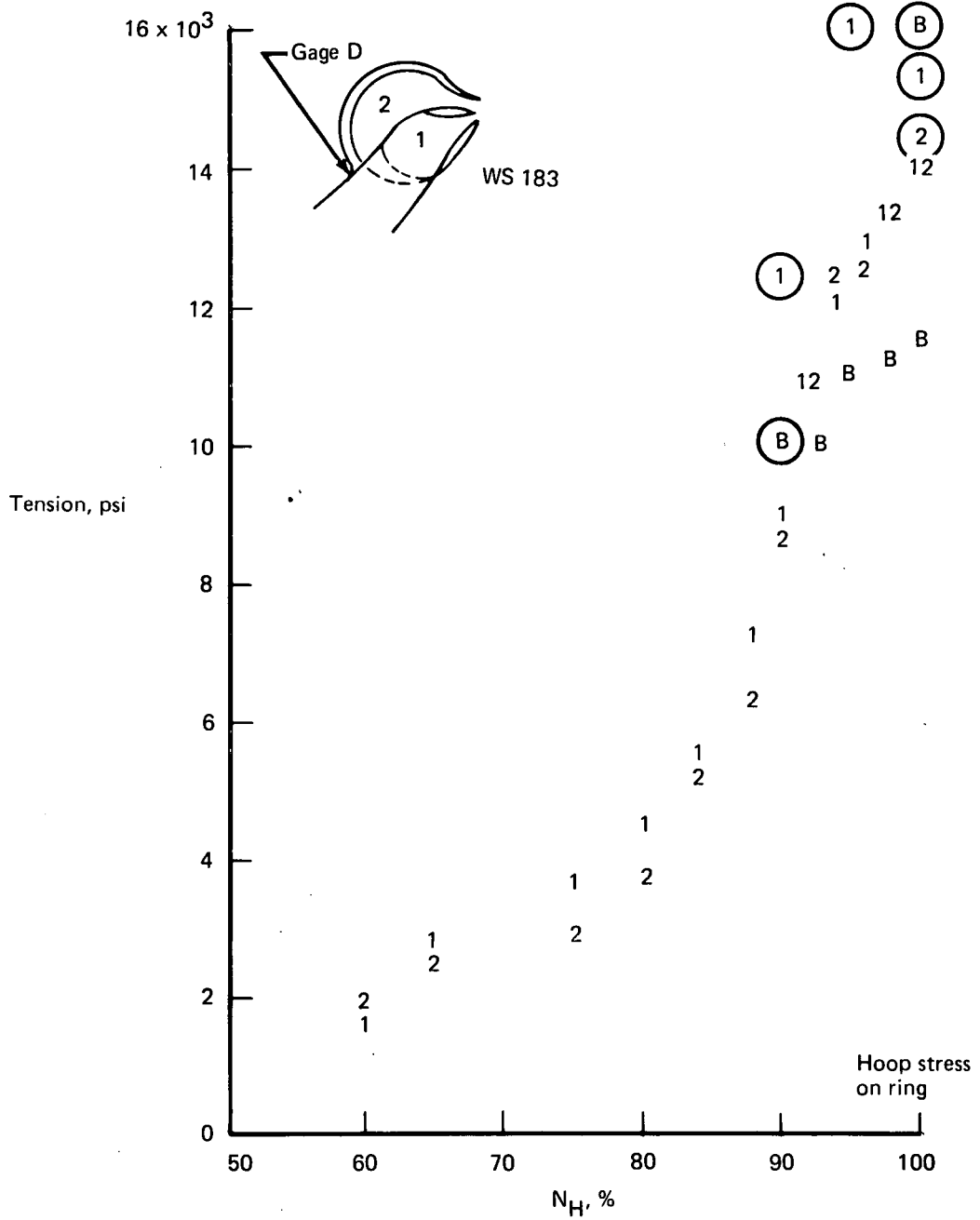
FIGURE 55.—GROUND LOAD SURVEY AUGMENTOR DUCT STRESS GAGE "D"
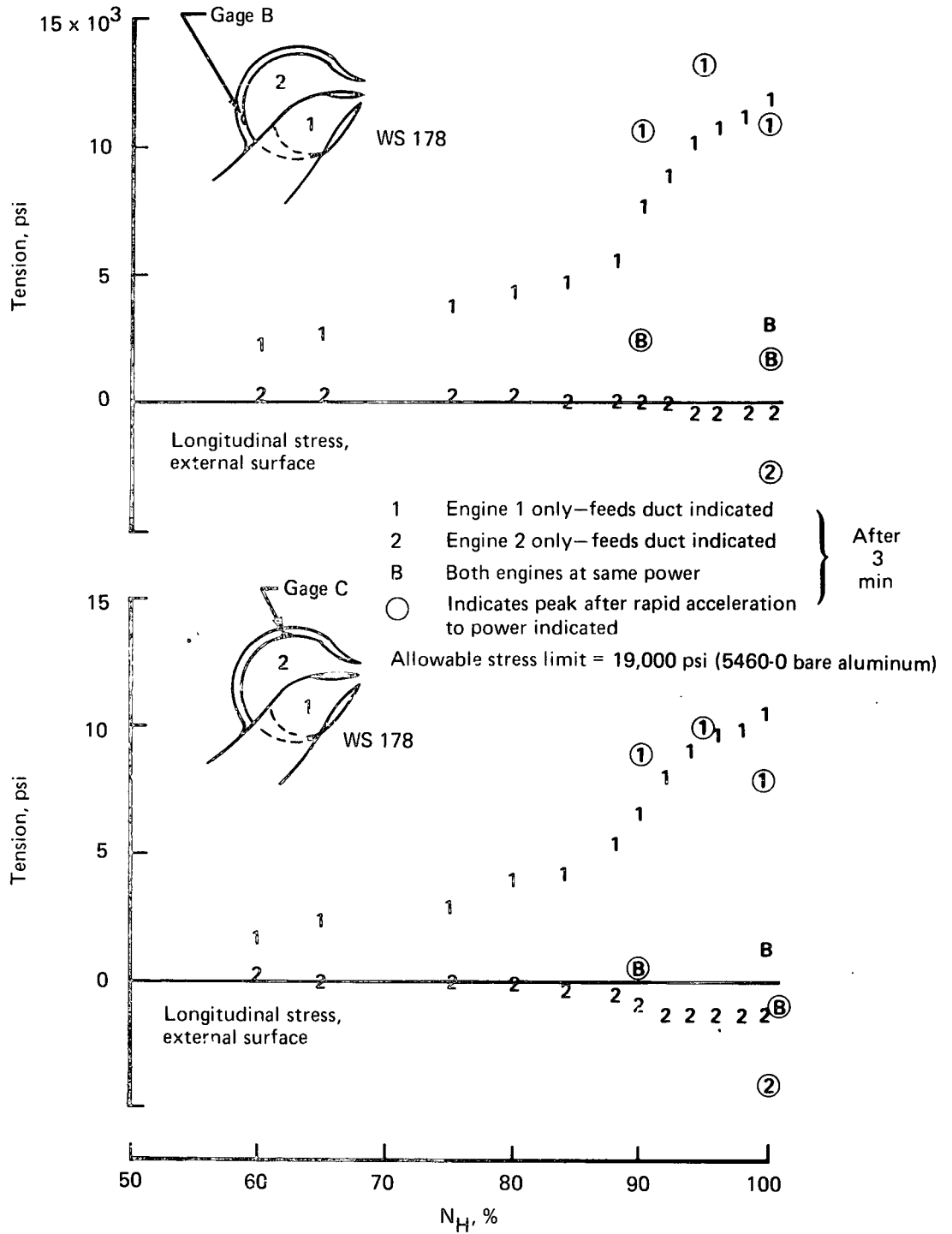
FIGURE 56.—GROUND LOAD SURVEY AUGMENTOR DUCT STRESSES GAGES "B" AND "C"

augmentor duct failure warning circuit. A preliminary evaluation of the system performance was made during the engine match tests. Final performance data were taken concurrently with the engine performance tests.

Fan Nozzle Area Adjustment

The initial engine match tests indicated that the nozzle for the bypass airflow was approximately 6% over area. This overarea was essentially equal to the overarea sizing that had been included in the body and aileron nozzle areas for engine matching adjustments. The body blowing nozzles were adjusted by blocking off the central nozzles located at the top of the body as illustrated in figure 57. The aileron nozzle area was reduced by squeezing the nozzles against 0.01-in. undersized sheet stock, as illustrated in figure 58.

It was necessary to make a second adjustment on the right engine nozzle area to complete engine match. This area reduction was beyond the built-in adjustment capability of the body and aileron nozzles. Therefore, the left wing upper and right wing lower augmentor nozzles were blocked over a 5-in. length at the inboard and outboard flap junctions, as illustrated in figure 59.

The actual nozzle area change is shown in figure 60. The resulting geometric nozzle areas are shown in figure 61.

Airflow Distribution

The targeted airflow split for each engine was 36% to the aft duct and 64% to the cross duct. The final resultant test flow split was 36.8 aft, 63.2 cross and 36.1 aft, 63.9 cross for the left and right engines, respectively. It is significant that the percentage remains relatively constant from approach to maximum engine power settings (fig. 62).

System Pressure Loss Comparison

The system pressure losses were essentially as predicted. The losses from the engine to the aft reference station were slightly higher than predicted, while the losses in the cross duct are slightly lower (fig. 63). The overall duct system losses are relatively low. Therefore, if relatively high percentage change in a particular pressure loss difference had occurred, it would have had little effect on the overall system losses.

Left hand engine supplied body duct (No. 1)

1/2   1/2

From LH
engine

Right hand engine supplied body duct (No. 2)

1/2   1/2

Side view

From RH
engine

Plan view

Nozzle area blocked

First adjustment

Second adjustment

Typical nozzle plug
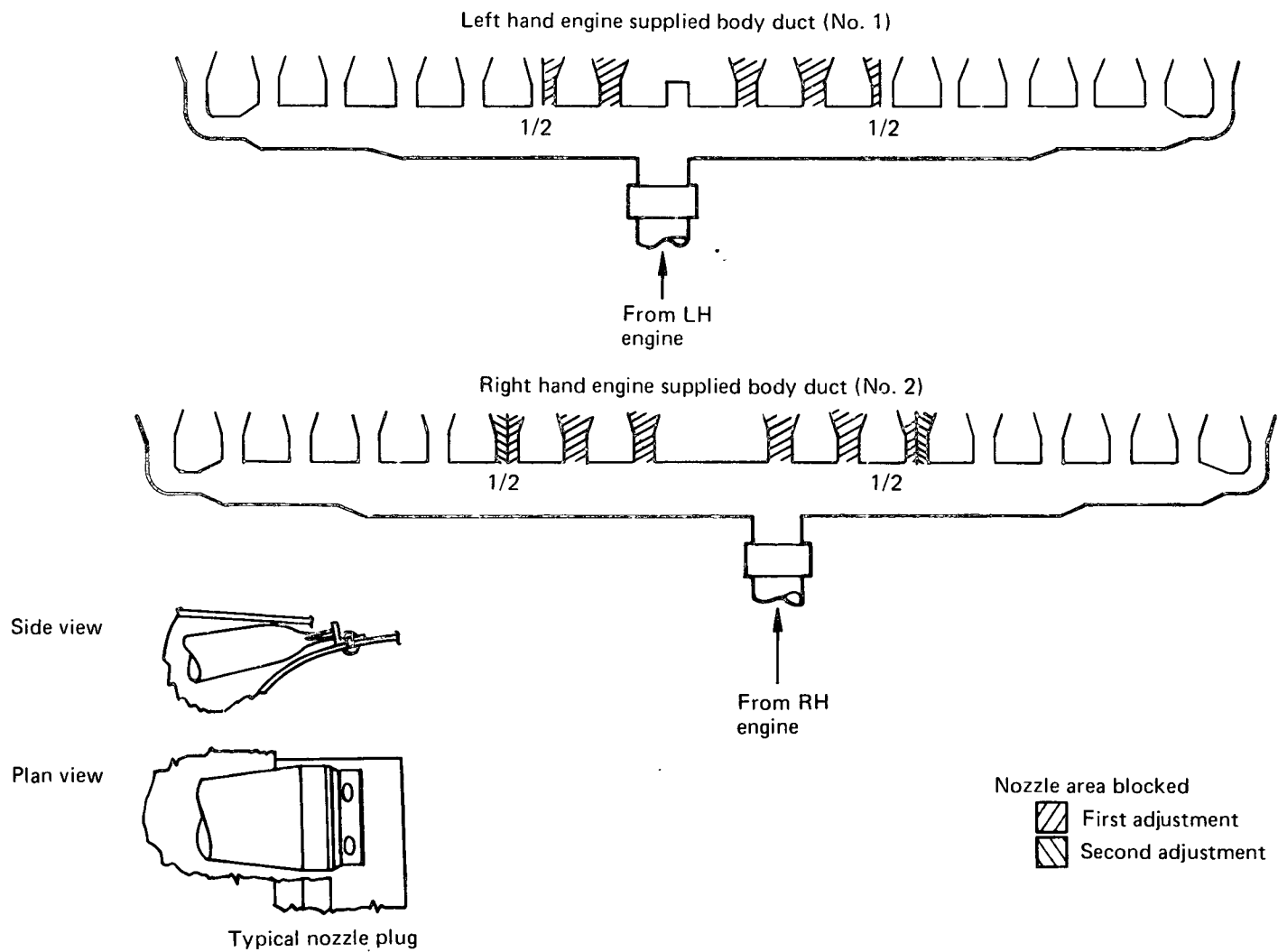
FIGURE 57.—BODY BLOWING NOZZLE AREA REDUCTION

TYPICAL NOZZLE SECTION

Nozzle

A

Supply duct
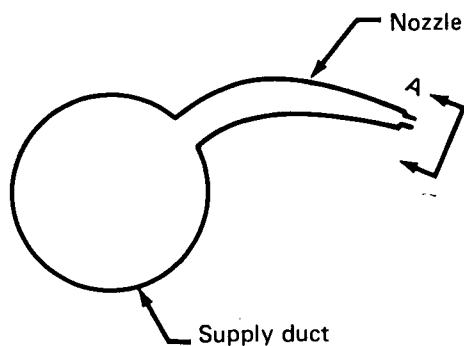
TYPICAL AILERON NOZZLE ADJUSTMENT*

Left wing (RH engine 2)

Right wing (LH engine 1)

0.14   0.11   0.10

0.105   0.14

Sec AA
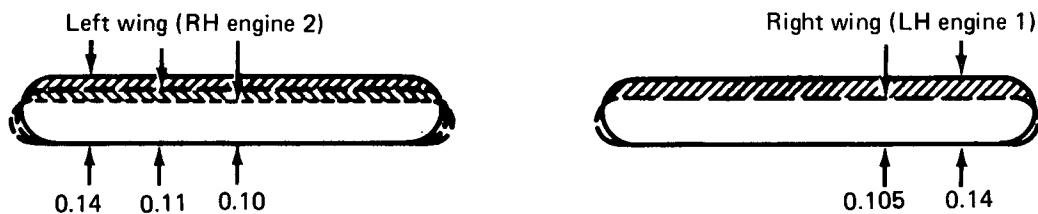
First area reduction

Second area reduction

*Dimensions are nominal ±0.05 in.
with composite as shown

NOZZLE ADJUSTMENT METHOD

Nozzle and tube

Sheet stock 0.01 to 0.015 in. thinner
than final setting

Supply duct

Tool bits
Silver soldered
to pliers
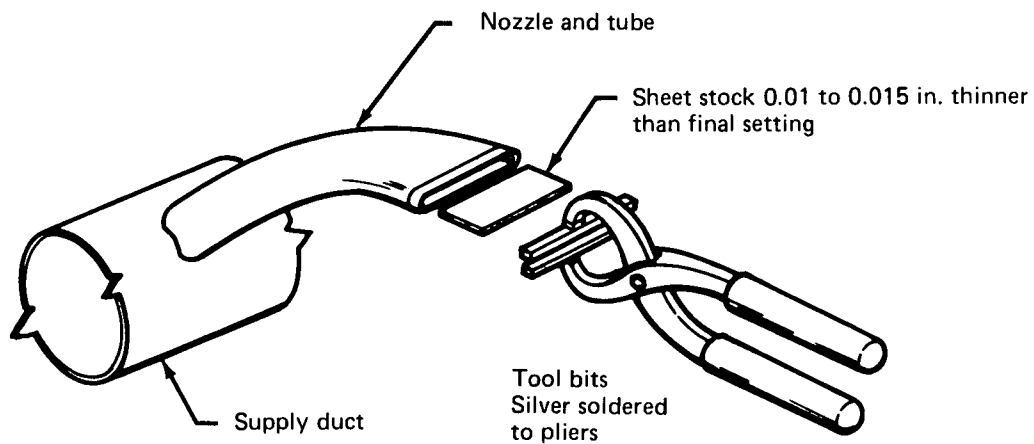
FIGURE 58.—AILERON NOZZLE ADJUSTMENT

113

PLAN VIEW

Augmentor duct,
right wing

Augmentor duct,
left wing

Upper
nozzle blocked

Lower
nozzle blocked

REAR VIEW

Upper
nozzle blocked

Lower
nozzle blocked

Upper nozzle
block

Lower nozzle
block

5 in.

5 in.

Gasket material

Sheet metal

Roll pin

Typical augmentor
nozzle plug
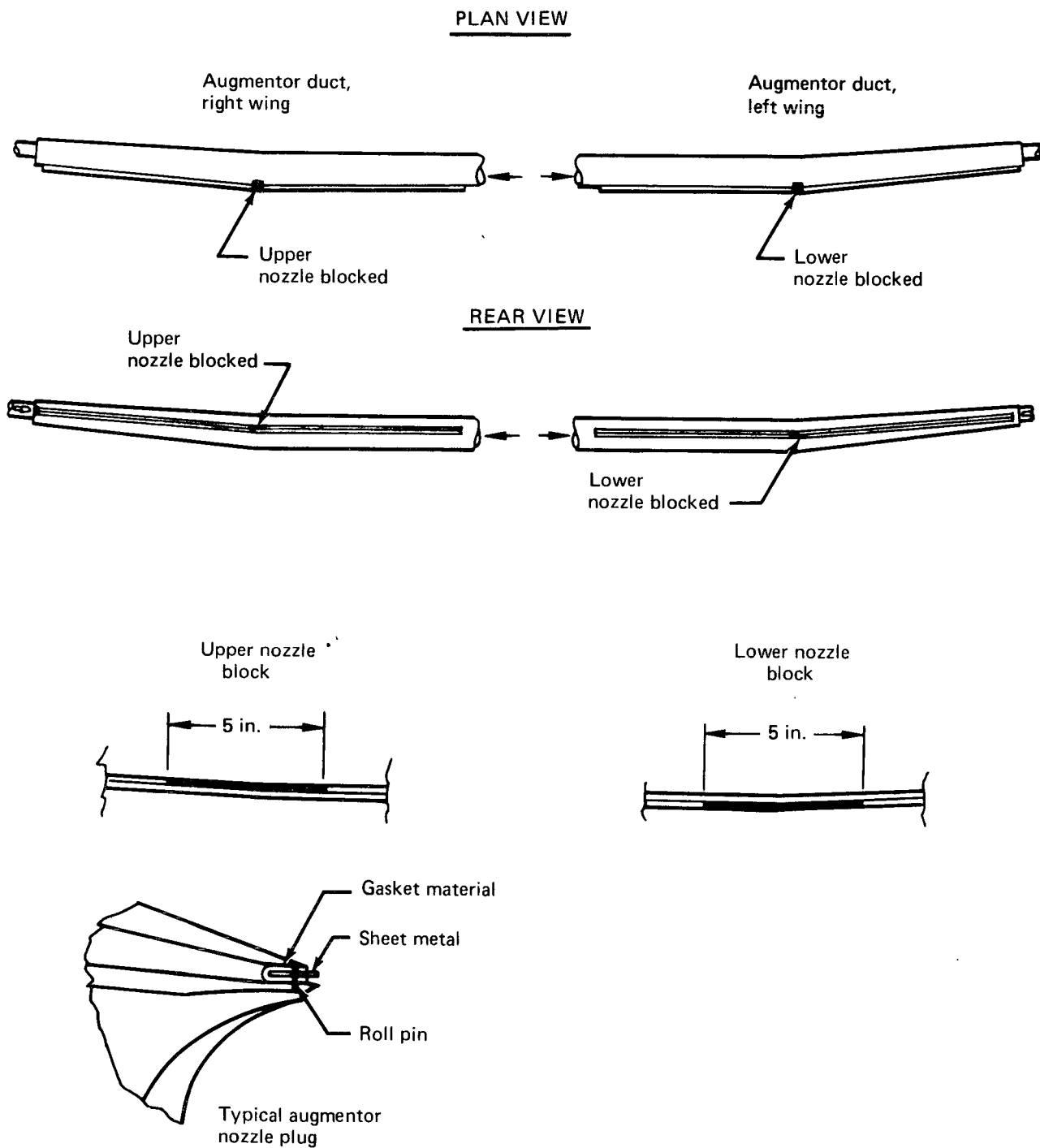
FIGURE 59.—AUGMENTOR NOZZLE AREA REDUCTION

114
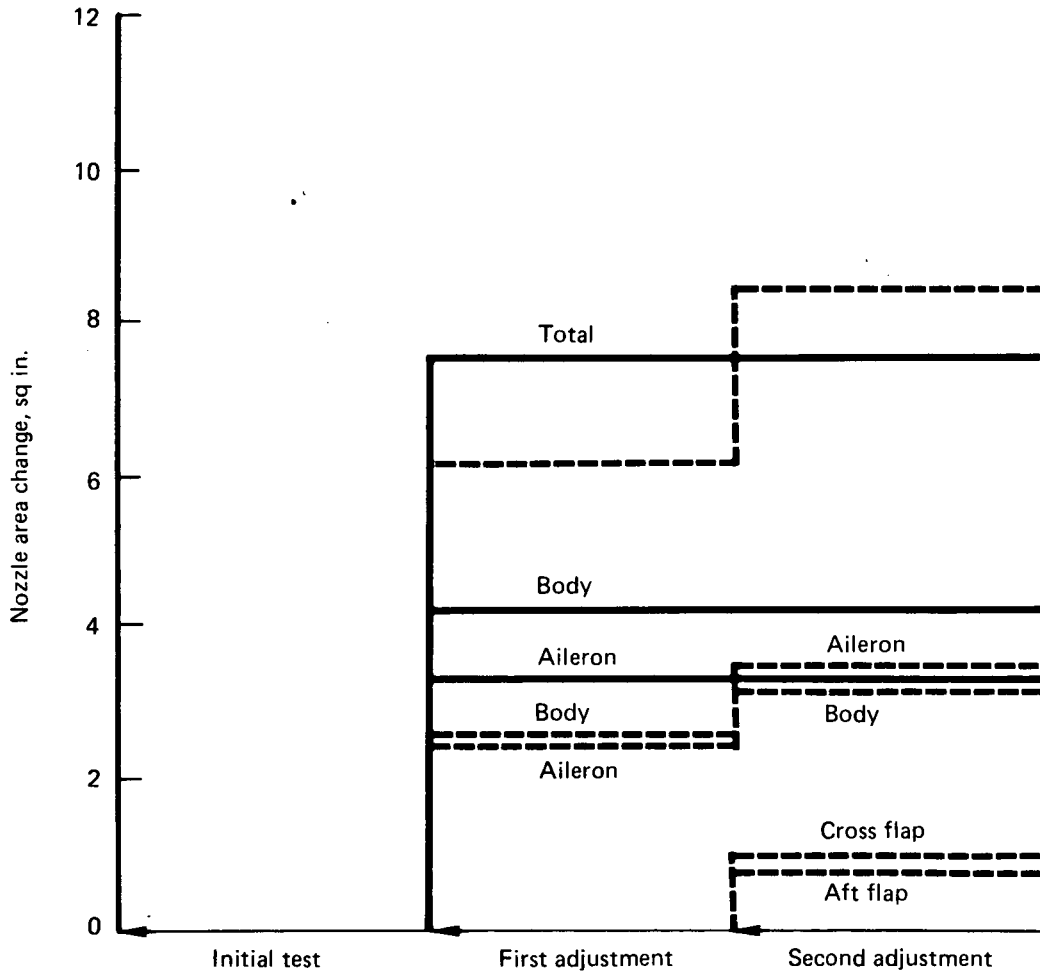
FIGURE 60.—BYPASS AIR GEOMETRIC NOZZLE AREA CHANGE

115
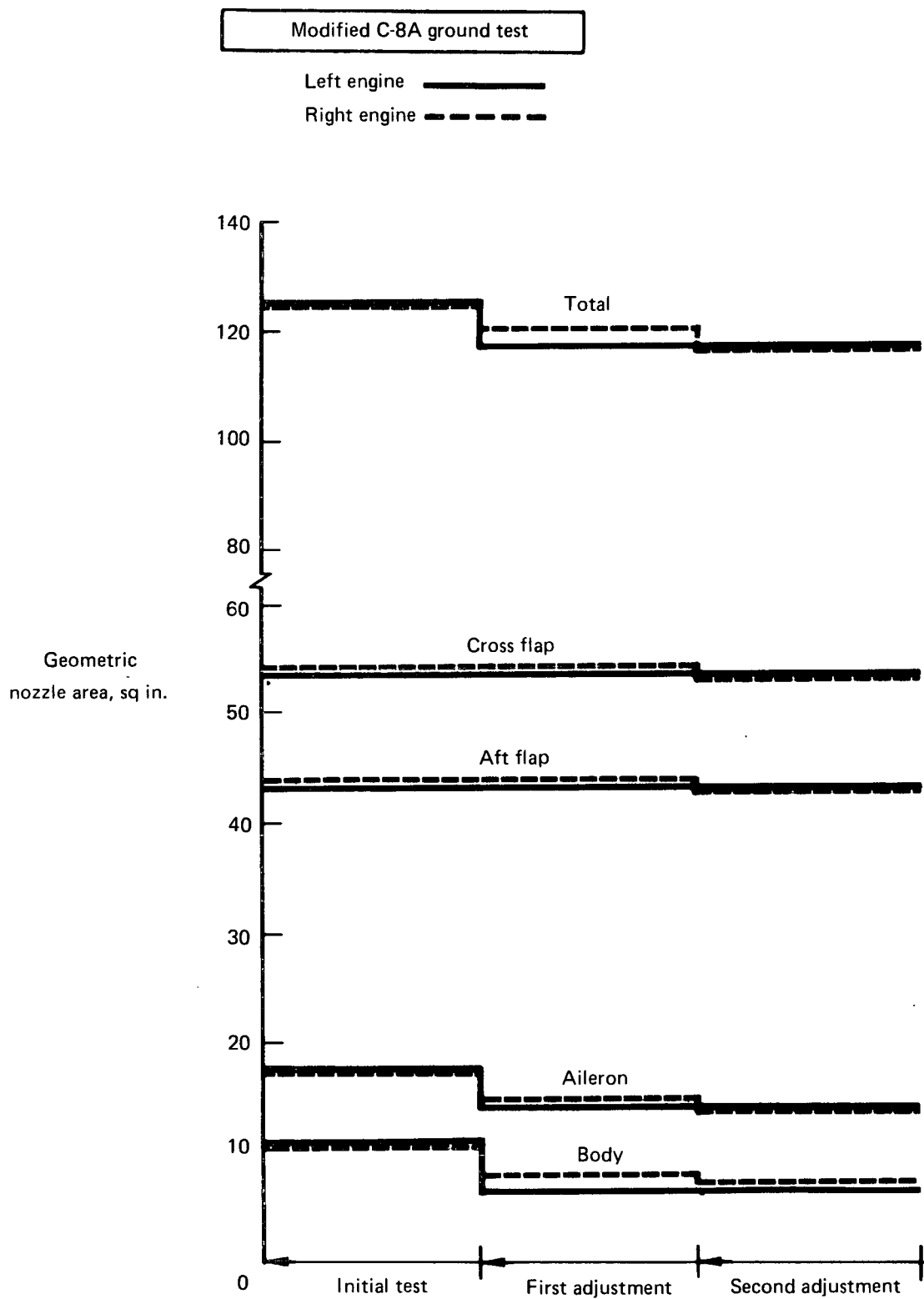
FIGURE 61.—BYPASS AIR GEOMETRIC NOZZLE AREA ADJUSTMENT
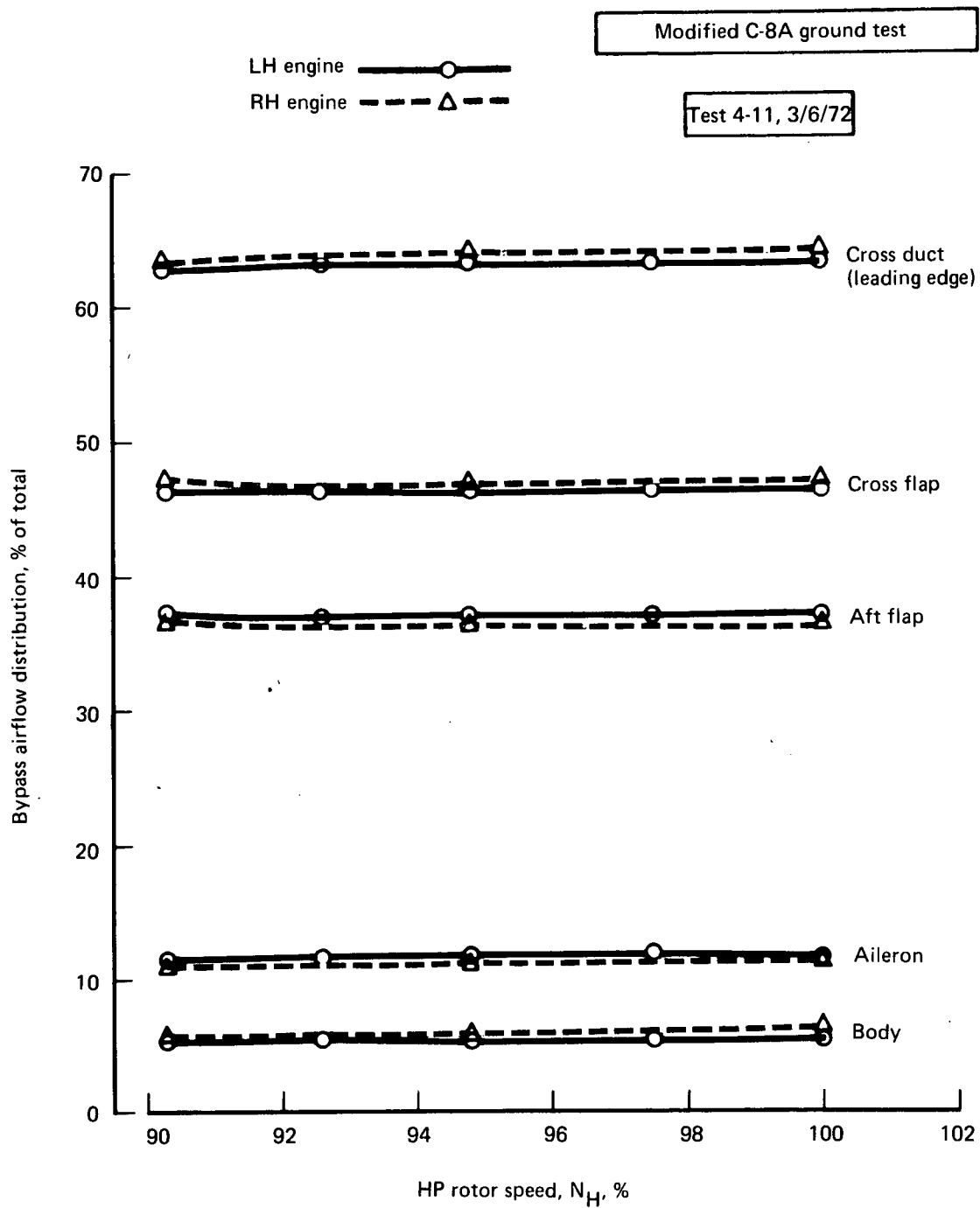
FIGURE 62.—ENGINE BYPASS AIRFLOW DISTRIBUTION

———————— Left engine

— — — — — Right engine
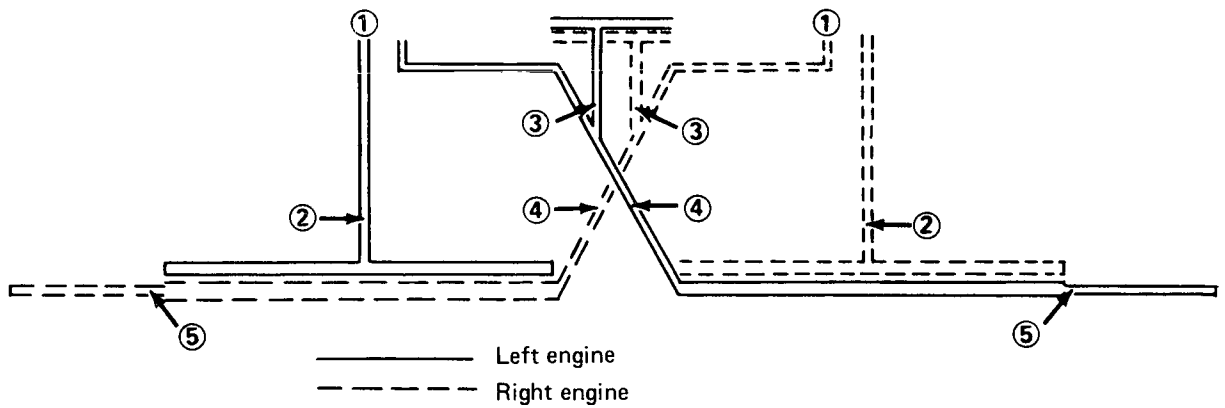
Test 4-11

Condition 3.18.003.077 65° flap 6° nozzle	Condition 2.04.002.024 6° flap 6° nozzle

Airflow, lb/sec
    Left engine   = 79.32
    Right engine* = 78.44
$P_{T2.5}$ ~in. Hg Ab
    Left engine   = 79.6
    Right engine = 79.2
	Airflow, lb/sec
	    Left engine = 81.19
	    Right engine = 80.15
	$P_{T2.5}$ ~in. Hg Ab
	    Left engine = 81.9
	    Right engine = 81.8

Location	Item	Pressure loss, in. Hg*			
		Left engine		Right engine	
		Estimated	Test	Estimated	Test
		Condition 3.18.003.077			
1	Port loss (aft)	–	2.40	–	2.40
	Port loss (cross)	–	2.80	–	2.80
1-2	To aft reference station	3.6	3.94	3.4	3.69
1-3	To body duct calibration station	10.9	9.43	9.9	9.27
1-4	To cross duct reference station	8.8	6.9	8.3	7.5
1-5	To aileron calibration station	11.3	10.12	11.0	10.2
		Condition 2.04.002.024			
1	Port loss (aft)	–	2.6	–	2.6
	Port loss (cross)	–	3.0	–	3.0
1-2	To aft reference station	3.5	4.2	3.5	4.0
1-3	To body duct calibration station	10.4	10.0	10.4	9.8
1-4	To cross duct reference station	9.0	7.5	9.0	7.8
1-5	To aileron duct calibration station	11.9	10.56	11.8	11.02

*Referenced to $P_{T2.5}$

FIGURE 63.—AIR DISTRIBUTION SYSTEM PRESSURE LOSSES

Thrust Loss and Distribution

The airflow distribution, duct pressure losses, and nozzle velocity coefficients have a direct effect on the resultant engine bypass airflow distribution. For instance, the engine offtake losses consume from 1.5% to 2.0% of the available thrust. The duct losses result in another 3.3% to 3.7% thrust loss, and the nozzle discharge characteristics extract 7.1% to 7.5%. The resulting bypass airflow thrust distribution for approach and medium engine power setting conditions are shown in figures 64 and 65, respectively. The nozzle velocity coefficients were based on the Boeing 0.7-scale static tests with adjustments to account for the increased internal augmentor duct roughness due to fasteners and the increased losses due to reference station change (fig. 66). The thrust distribution is differences are approximately -200 lb for each engine, which is the established requirement. The defferences are approximately -200 lb for each engine, which is the established requirement. The aileron thrusts are 275 and 294 lb for the left and right wings, respectively, which is slightly higher than the minimum 260 lb required. The body blowing airflow thrusts are 137 and 147 lb for the left and right engines, respectively, which is less than the required 150 lb. However, the blowing span has been reduced by approximately one-third, resulting in a higher local thrust at the wing body joints.

Duct Failure Warning Light Switch

The two-engine duct pressures are closely matched at the cross and aft duct reference stations. This is shown in figure 67. Examination of the duct pressure differentials shows that, for normal engine operation, the pressure difference from the aft duct of one engine to the cross duct of the other is from 3 to 4 in. Hg (1 to 2 psi). The engine power setting range included is from approach to maximum engine power.

An increase of 11 sq in. in geometric nozzle area on one engine (bypass valve opening on one engine) causes the pressure differential from the aft duct of the larger nozzle area engine to go negative with respect to the smaller nozzle area engine at an $N_H/\sqrt{T_1}$ = 660. Extending the engine characteristics to higher power settings indicates that the pressure differential characteristics remain similar. Therefore, setting the differential switch to indicate at pressure differences of zero and lower (measured from the lower augmentor nozzle to the upper nozzle for each wing) should provide adequate duct failure warning.

FIGURE 64.—AIR DISTRIBUTION SYSTEM THRUST LOSSES (APPROACH)

Left engine

100
(3540 lb)

Right engine

100
(3480 lb)
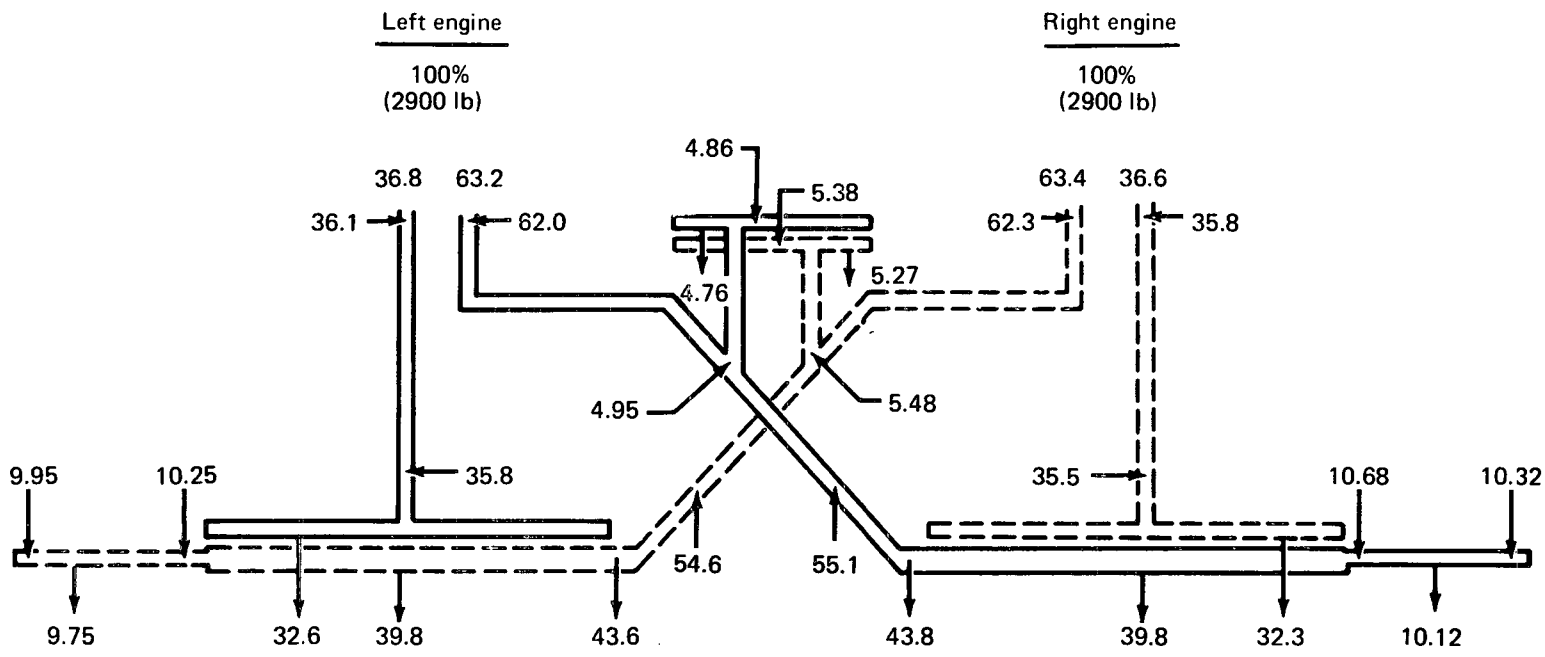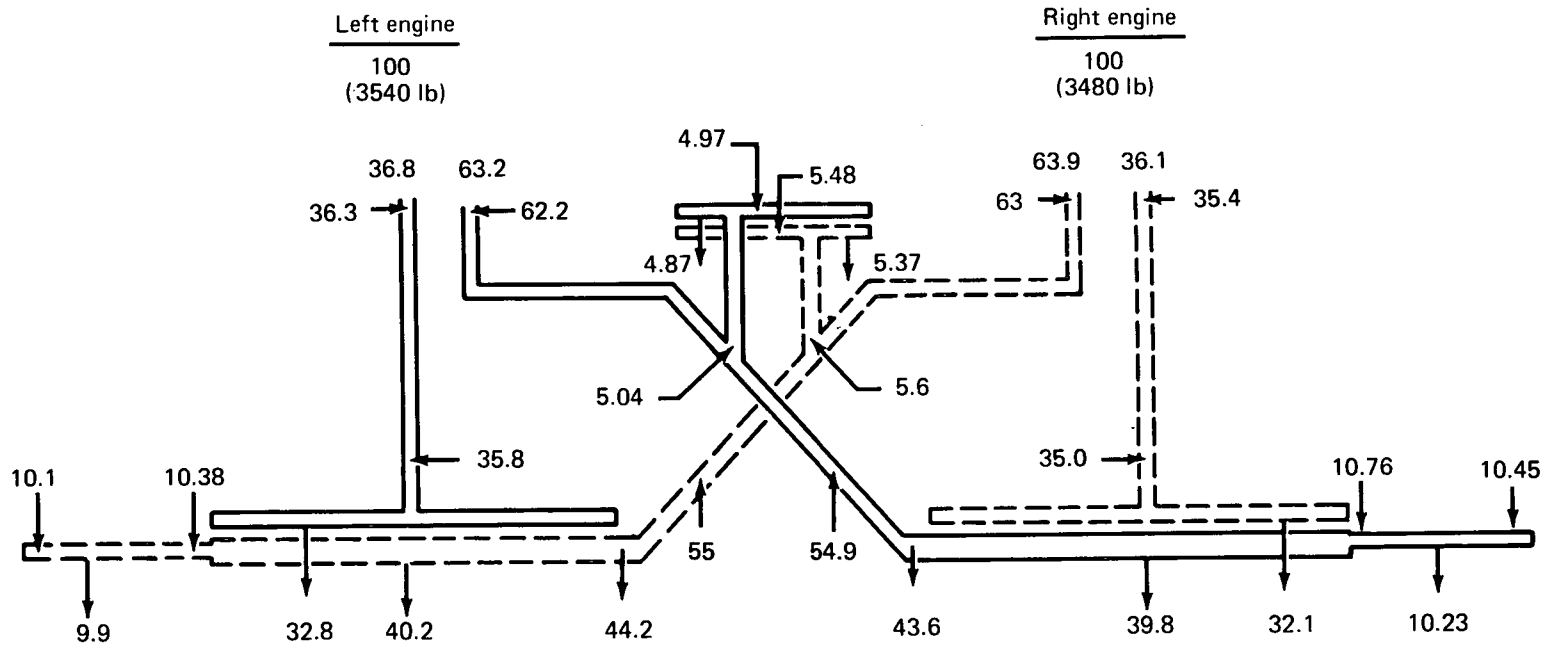
Loss summary, %*		
Item	Left engine	Right engine
Port	1.5	1.6
Duct	3.68	3.62
Nozzles	7.12	7.21
Total	12.3	12.43

Test 4-11 Condition 3.18.003.077

$N_H/\sqrt{T_1}$ = 706 left engine, 705 right engine
Augmentor flap 65°
Conical nozzle 6°

↓ % of engine thrust available

*Based on engine $P_{T2.5}$

FIGURE 65.—AIR DISTRIBUTION SYSTEM THRUST LOSSES (MEDIUM POWER SETTING)
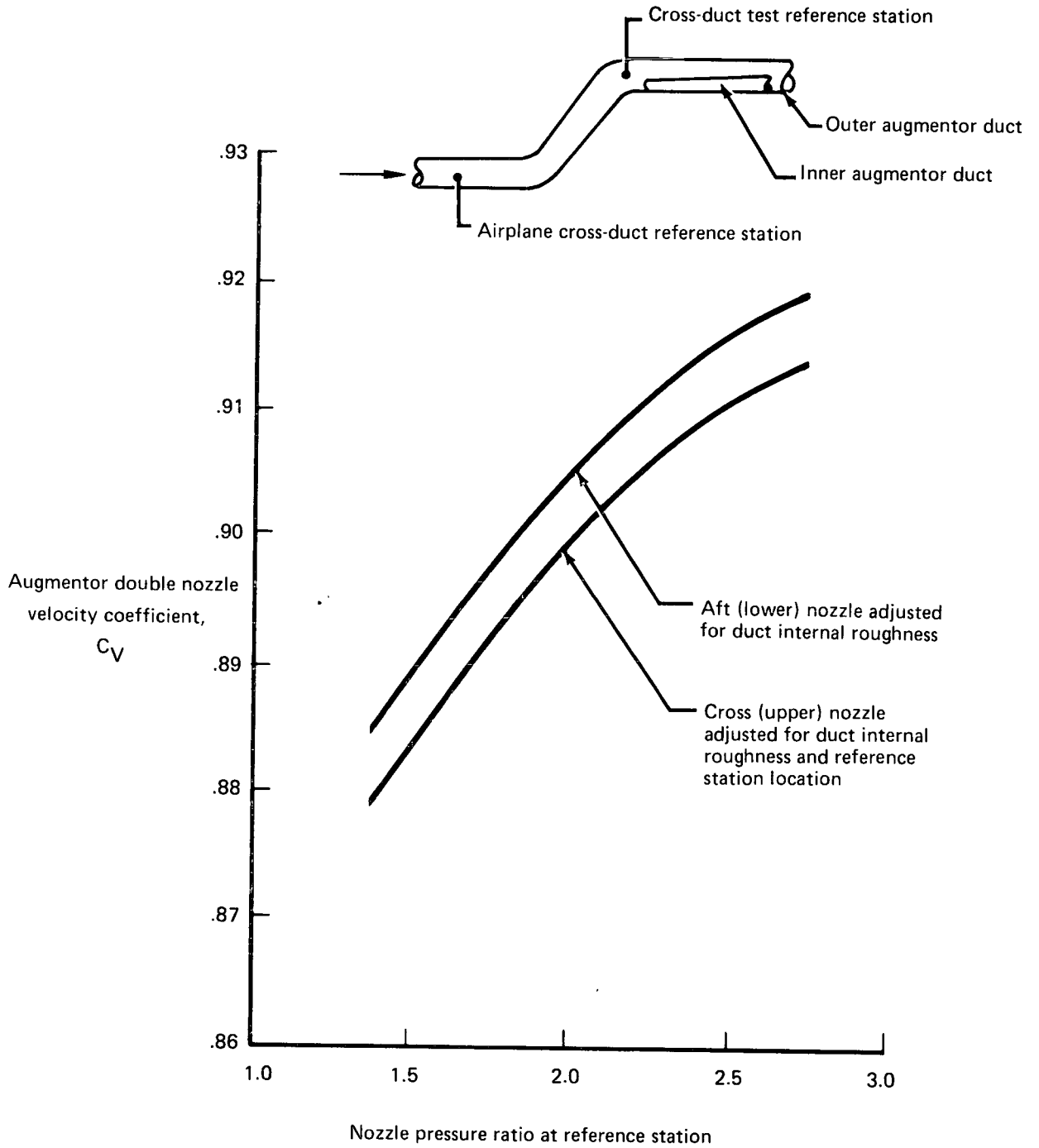
FIGURE 66.—AUGMENTOR NOZZLE DISCHARGE COEFFICIENT

Modified C-8A ground test
Test 4-11, 3/6/72

LH engine
RH engine } both operating
RH engine only

80

75

70

65

60

55

50

45

40

Pressure, in. HgAb

Aft duct, inner nozzle

Cross duct, outer nozzle

Bypass valve operation

P_{S_8}

600   620   640   660   680   700   720

Corrected high-pressure rotor speed, $N_H/\sqrt{T_1}$
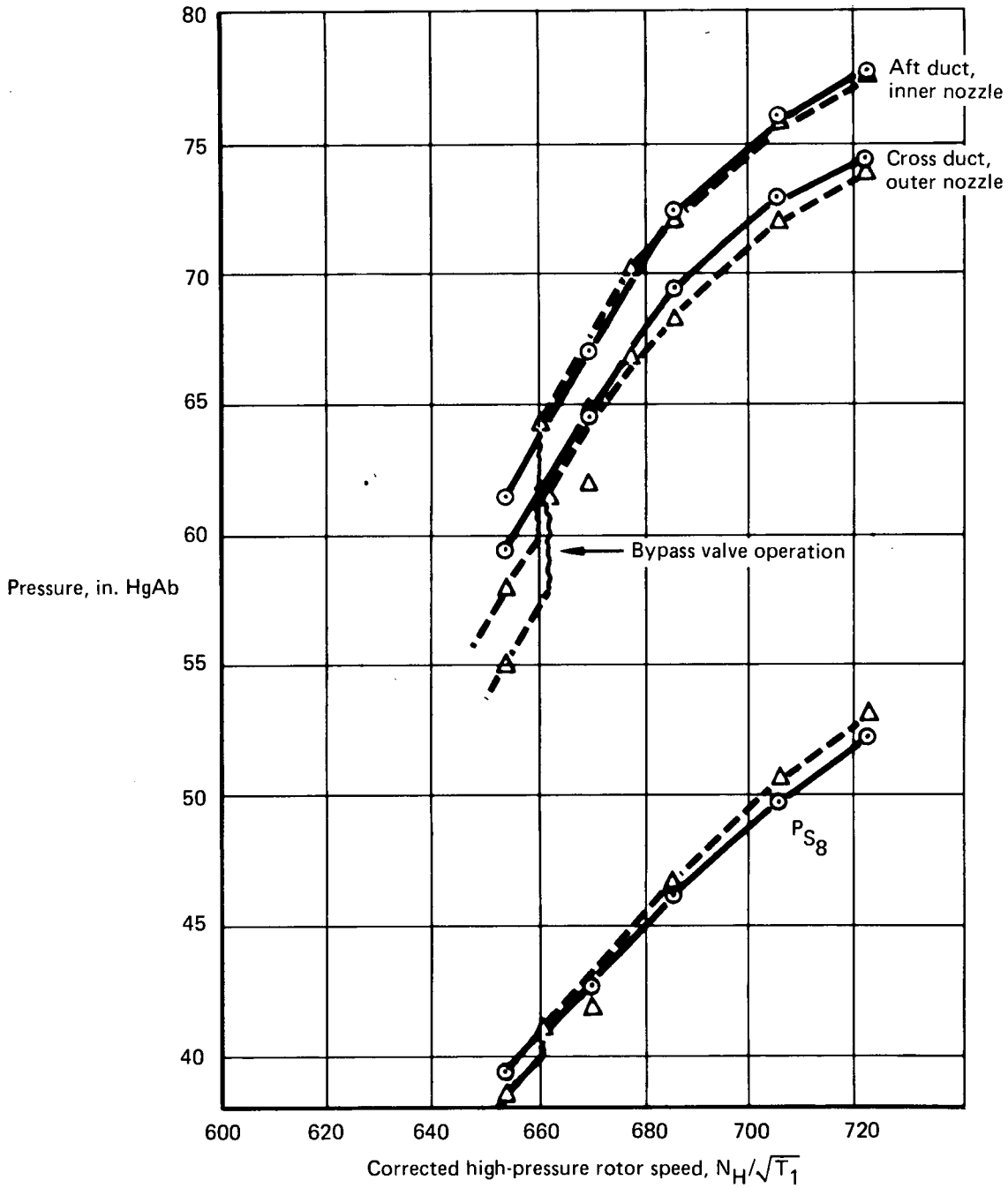
FIGURE 67.—ENGINE DUCT PRESSURES AT CROSS
AND AFT DUCT REFERENCE STATIONS

PROPULSION SYSTEM

The propulsion system testing included the necessary ground running to accomplish the following:

- Match the fan nozzle areas with engines installed

- Trim the throttles

- Perform functional checks on engine operation

- Determine the installed performance

- Perform functional check of fuel system operation

The results of this testing are summarized below.

Engine Match

Small adjustments were made (approximately 7% decreases in area) to the fan nozzle areas, including body, aileron, and augmentor nozzles. Upon completion of the nozzle adjustments, the low pressure (LP) compressor working lines were almost identical to the working lines obtained on the Rolls-Royce (Canada) test bed in Montreal. Comparisons of the LP compressor working lines and the surge lines are shown in figures 68 and 69 for the two engines. A significant surge margin is evident.

The HP and LP shaft speeds also matched, as was experienced on the Rolls-Royce (Canada) test bed.

Engine Trim

The throttle rigging was adjusted to essentially eliminate throttle stagger for the two engines when running at the same speed throughout the speed range.
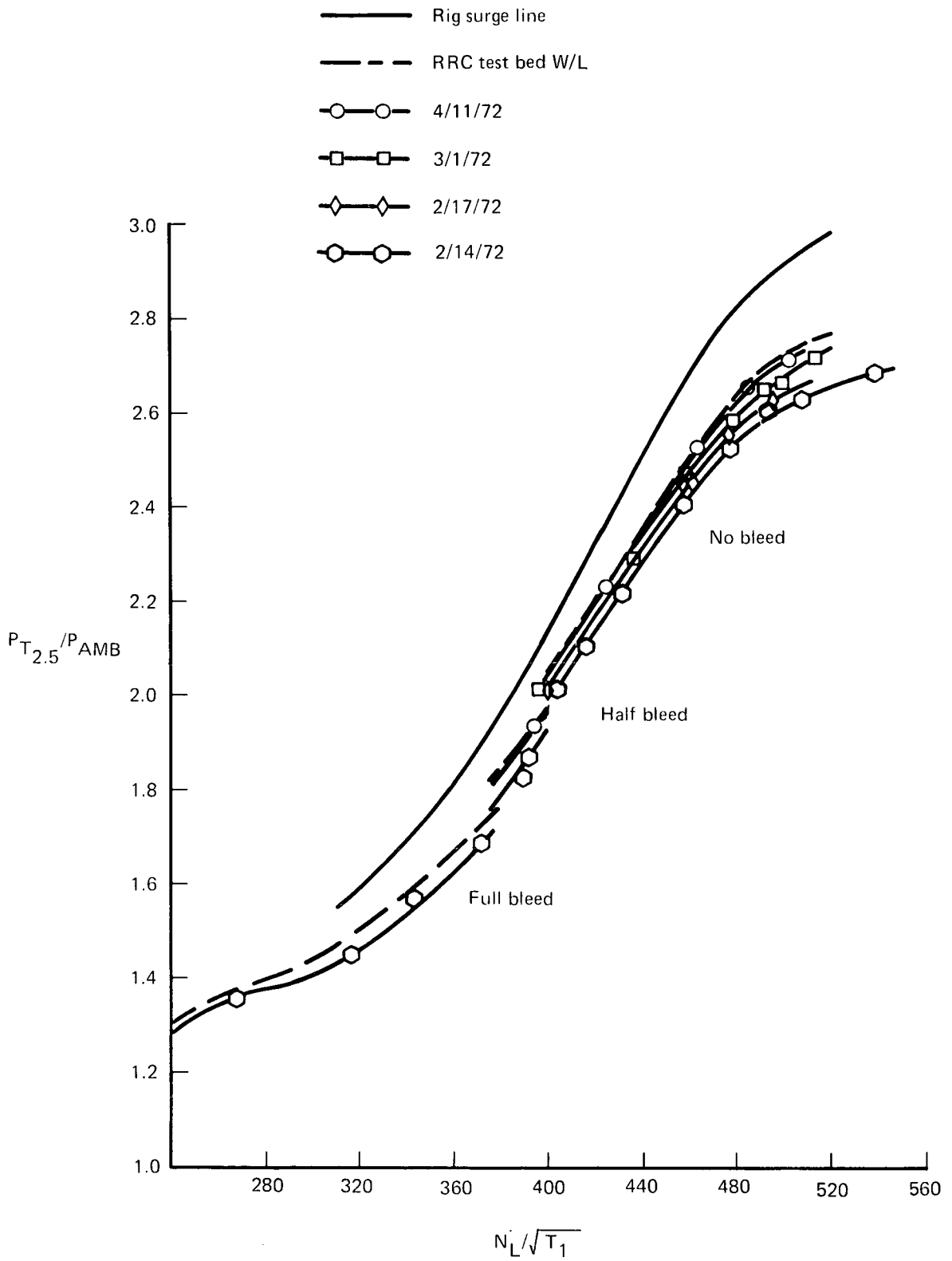
FIGURE 68.—LP COMPRESSOR WORKING LINES—ENGINE NO. 8745
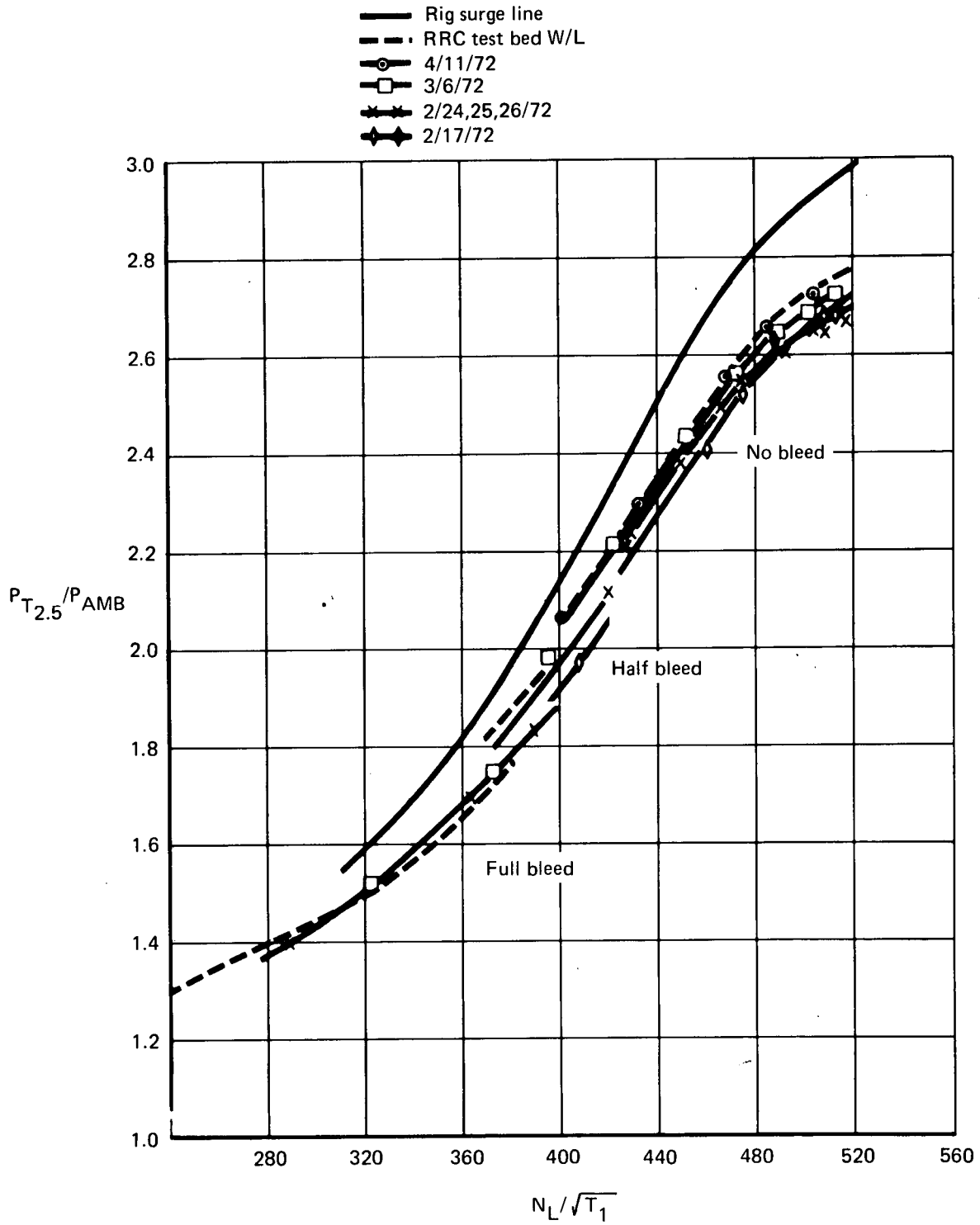
FIGURE 69.—LP COMPRESSOR WORKING LINES—ENGINE NO. 8746

Functional Checks

Accelerations and Decelerations

The acceleration/deceleration tests were carried out on both engines on March 15. The nominal requirements are:

● An acceleration time of 6 to 7 sec from idling speed to 95% of emergency power

● A deceleration time of 13 to 15 sec from emergency power to 8600 rpm—71% N_H

The equivalent top speed conditions used were 100% N_H at the end of the acceleration and 600° EGT at the start of the deceleration.

Several runs were made both ways, starting at various intermediate speed conditions and going to the same end point. The results are shown in table VI, with time recorded in seconds.

TABLE VI.—ACCELERATION/DECELERATION TIME IN SECONDS

Start speed	Accelerations to 100% N_H		Decelerations to 71% N_H	
	1-8745	2-8746	1-8745	2-8746
Idle	6.7	5.6	—	—
65% N_H	5.7	4.9	—	—
75	4.7	4.0	—	—
80	3.6	3.1	3.0	5.3
85	3.0	2.7	4.6	7.3
90	2.0	1.7	7.4	12.3
95	0.7	0.8	10.0	15.8
100% N_H	—	—	11.7	17.4
600° EGT	—	—	11.5	17.5

Only engine 1's acceleration time was initially within limits. The time had been set at Rolls-Royce (Canada) (RRC), but it is a very sensitive adjustment and normally needs resetting in the field. The fact that there was no surge during engine 1's fast deceleration demonstrates that there is considerable margin available. Both engines were finally set correctly.

The fuel flow regulators were reset on the final ground run, with a full acceleration and deceleration for each engine obtained within the nominal requirements.

Engine Vibration

Engine vibration was detected radially at the LP turbine bearing housing, and was measured as peak-to-peak displacement at frequencies between 40 and 300 Hz. The means of all vibration readings after February 24 were as shown in table VII, expressed in mils.

TABLE VII.—MEAN OF VIBRATION READINGS

	Engine vibration levels (mils—peak-to-peak)								
Speed N_L%	Idle	40	50	60	70	80	90	100	105
Approximate N_H%	Idle	73	80	84	87	90	94	100	102
Engine 1-8745	0.1	0.4	0.3	0.3	0.4	0.5	0.7	1.0	1.1
Engine 2-8746	0.1	0.1	0.3	0.4	0.5	0.6	0.8	1.1	1.2

These vibration levels form the data against which future vibration levels should be assessed. The figures show a trace of LP turbine critical at 40% N_L on engine 1, and a trace of the approaching LP compressor critical on both engines at top speed. The overall levels are similar to those measured at RRC. The nominal vibration limit is 3.0 mils, but a change of 1.0 mil from the datum level at any speed is also considered significant.

Additional Checks

Minor adjustments were made to the HP airflow regulator, the LP surge bleed valves, and the EGT top temperature controller to obtain satisfactory engine operation at all conditions.

Installed Engine Performance

One of the primary purposes of the ground testing was to determine that the engine was operating correctly installed and to determine the installed thrust. Two methods were used to determine the installed thrust: one was to calculate it from measurements of engine parameters, and the other was to measure the forces on the airplane directly. Results from both methods are discussed the following paragraphs.

Thrust Calculated from Engine Parameters

Ground testing included the measurement of the following engine parameters:

Fan total pressure, $P_{T_{2.5}}$

HP compressor delivery static pressure, P_{S_3}

LP turbine exit total pressure, P_{T_6}

Static pressure at exhaust nozzle hinge plane, P_{S_8}

High-pressure shaft speed, N_H

Fan pressure shaft speed, N_L

Exhaust gas temperature, EGT

Fuel flow, W_F

Engine inlet temperature, T_1

Engine inlet pressure, P_{T_1}

The above parameters, as well as some additional ones, were measured during the engine development testing by Rolls-Royce (Canada) in Montreal.

Several nozzle configurations were tested at that time. Reference data are presented in figures 70 through 73 for the nozzles and associated engine listed in table VIII.

No test bed curve for $P_{T_{2.5}}/P_{T_1}$ was available with conical nozzles for engine 1 (8745), but it is assumed that it would have the same relationship to Pegasus nozzles 3 and 8 as that of engine 2 (8746).

Data points from the March and April ground tests in Seattle are shown on the reference curves (figs. 70 through 73). Agreement of the test points for the engine installed with the reference data is good, although the pressure ratios are all a trace higher (N.B.: the Pegasus nozzle curve of P_{S_8}/P_{T_1} for engine 2 is believed to be too high because of a test bed instrumentation problem).
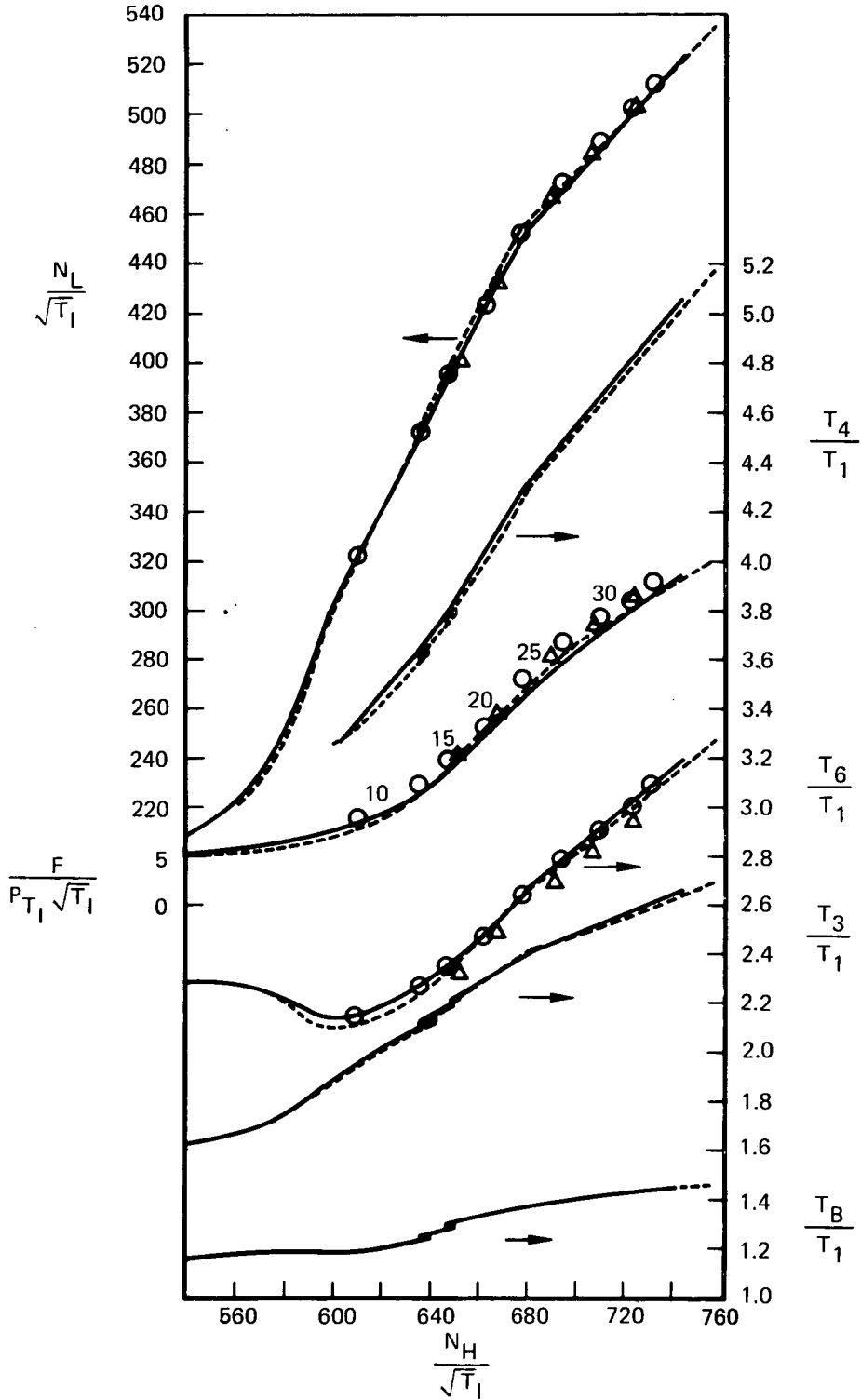
FIGURE 70.—TEMPERATURE RATIOS, ENGINE 2 (8746) TEST
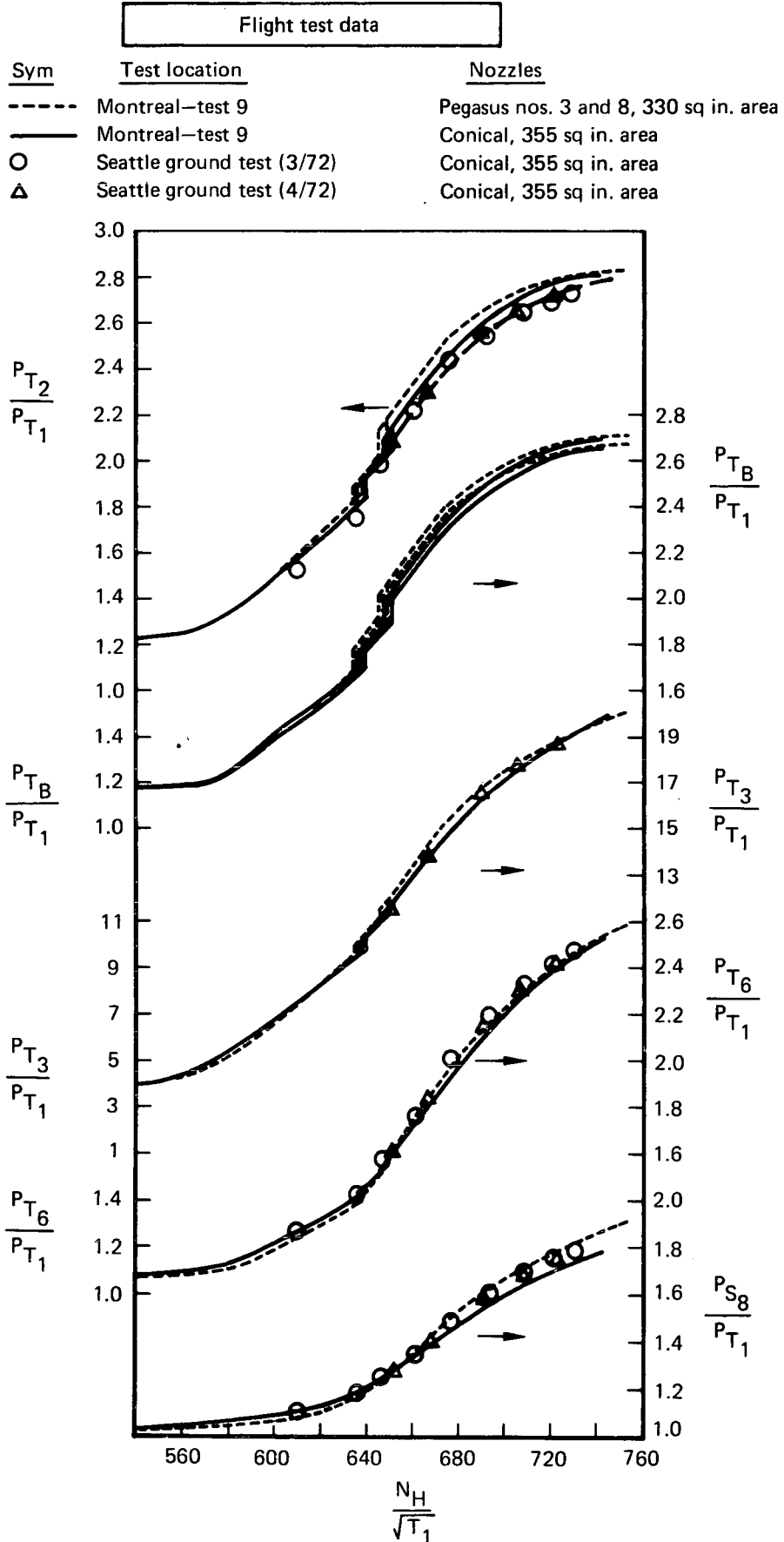
FIGURE 71.—PRESSURE RATIOS, ENGINE 2 (8746) TEST

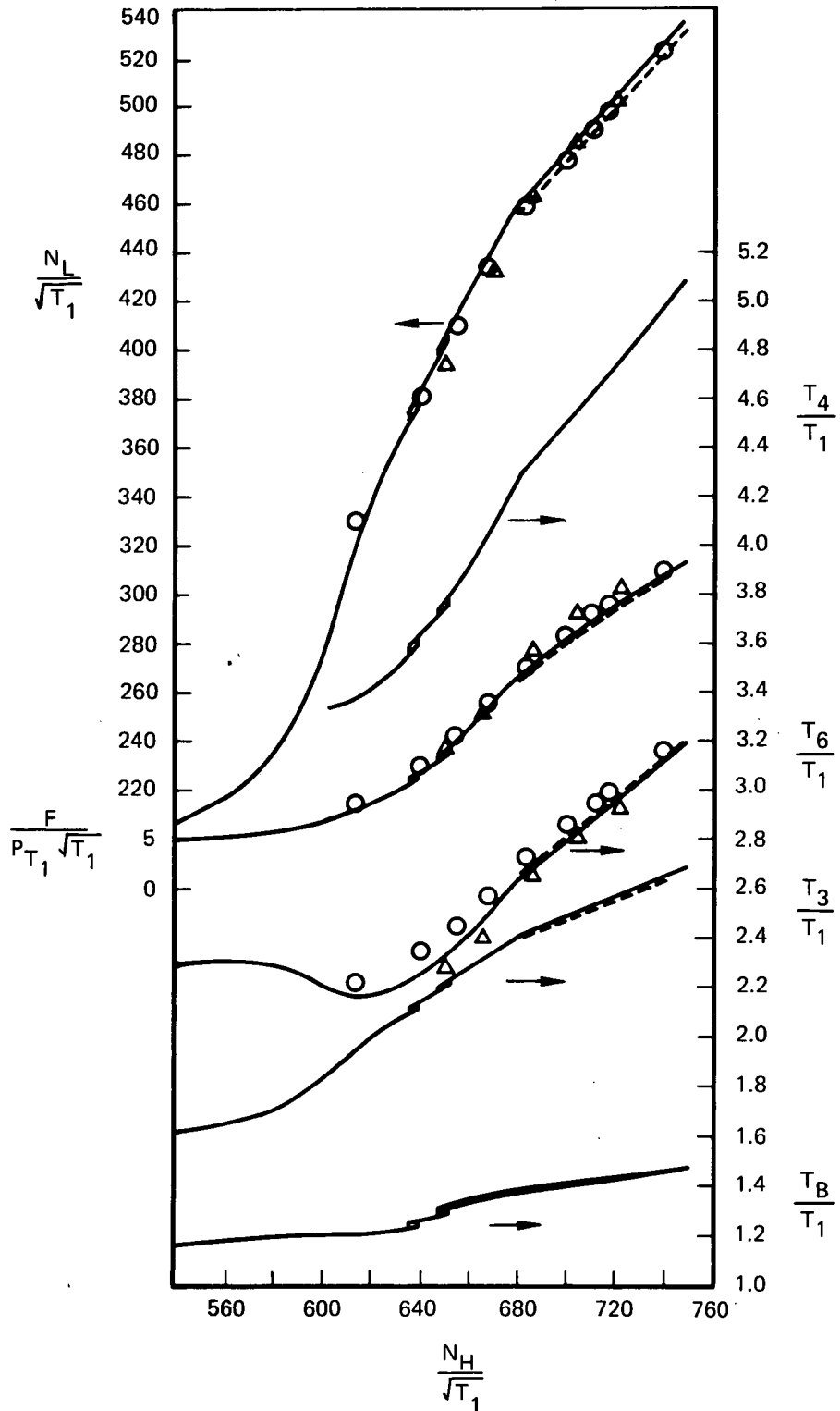| Sym	Test location	Nozzles
– – – – –	Montreal—Test 1	Pegasus, nos. 3 and 8, 330 sq in. area
———	Montreal—Test 1	Pegasus, nos. 9 and 10, 342 sq in. area
O	Seattle ground test (3/72)	Conical, 342 sq in. area
Δ	Seattle ground test (4/72)	Conical, 342 sq in. area

Flight test data

FIGURE 72.—TEMPERATURE RATIOS, ENGINE 1 (8745) TEST
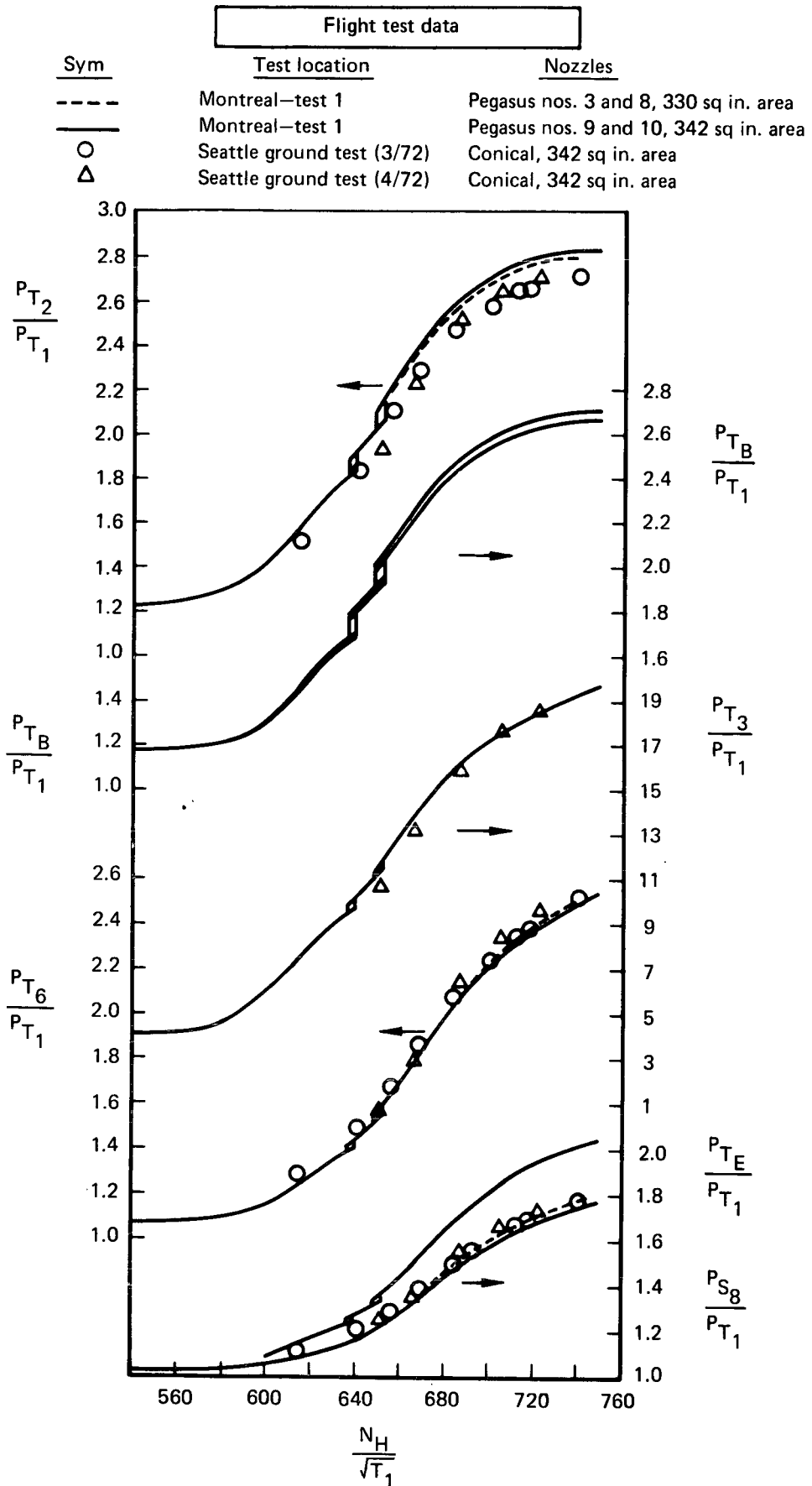
FIGURE 73.—PRESSURE RATIOS, ENGINE 1 (8745) TEST

TABLE VIII.—NOZZLE REFERENCE DATA

Nozzle	Reference area	Engine
Pegasus 3 and 8	330 (total)	1 & 2
Pegasus 9 and 10	342 (total)	1
Conical (2)	[a]355 (total)	2

[a]Conical nozzles with 355 square inches give equivalent top
speed engine matching to Pegasus nozzles 3 and 8.

Primary Exhaust Thrust

Some discrepancies have occurred concerning the true thrust levels. Their resolution was hindered by two aspects of the testing at RRC, the nonavailability of conical nozzles when engine 8745 was tested and the suspected P_{S_8} instrumentation error during the final test of engine 8746. Furthermore, engine 2 (8746) was fitted with a new exhaust trouser piece at Seattle, replacing the old unit which had been damaged by earlier testing at RRC and was not considered flightworthy. The new unit had not been available in time for the final test at RRC. The thrust versus pressure ratio curves were therefore derived and were not direct test results. Initial test stand data showed that engine 2 had less total thrust at a speed than engine 1; this was directly opposite to RRC experience. Testing in March showed that the two engines had the same thrust, however, and the P_{T_6} levels were also the same. Basic characteristics of $N_H/\sqrt{T_1}$ and F_{gp} were therefore drawn against P_{T_6}/P_{AMB} to apply to both engines with conical nozzles, and these were used to calculate the reference engine data used in the following section. They are shown in figure 74 and a matching curve of C_g vs P_{T_6}/P_{AMB} is shown as the solid line of figure 75; the dotted line for engine 2 (for reference only) is based on the more optimistic thrust vs P_{T_6} curve from the RRC test bed.

The primary thrust may also be obtained from P_{S_8} values, using the curve of P_{S_8}/P_{AMB} vs F_{gp} shown in figure 76. The primary thrust values for engines 1 and 2, based on both P_{S_8} and P_{T_6} values observed during the Seattle testing, are shown in figures 77 and 78, together with reference curves for the thrust measured in Montreal. Good correlation is shown for engine 2. The calculated thrust is somewhat higher for engine 1, due partially to the conical nozzle. The remaining difference may be due to the installation or instrumentation error as previously discussed. For convenient reference, the total thrust, as measured by RRC for engine 2 with conical nozzles, is shown in figure 79 vs HP rotor speed and $N_H/\sqrt{T_1}$. The thrust values from the primary and fan nozzles are also shown.
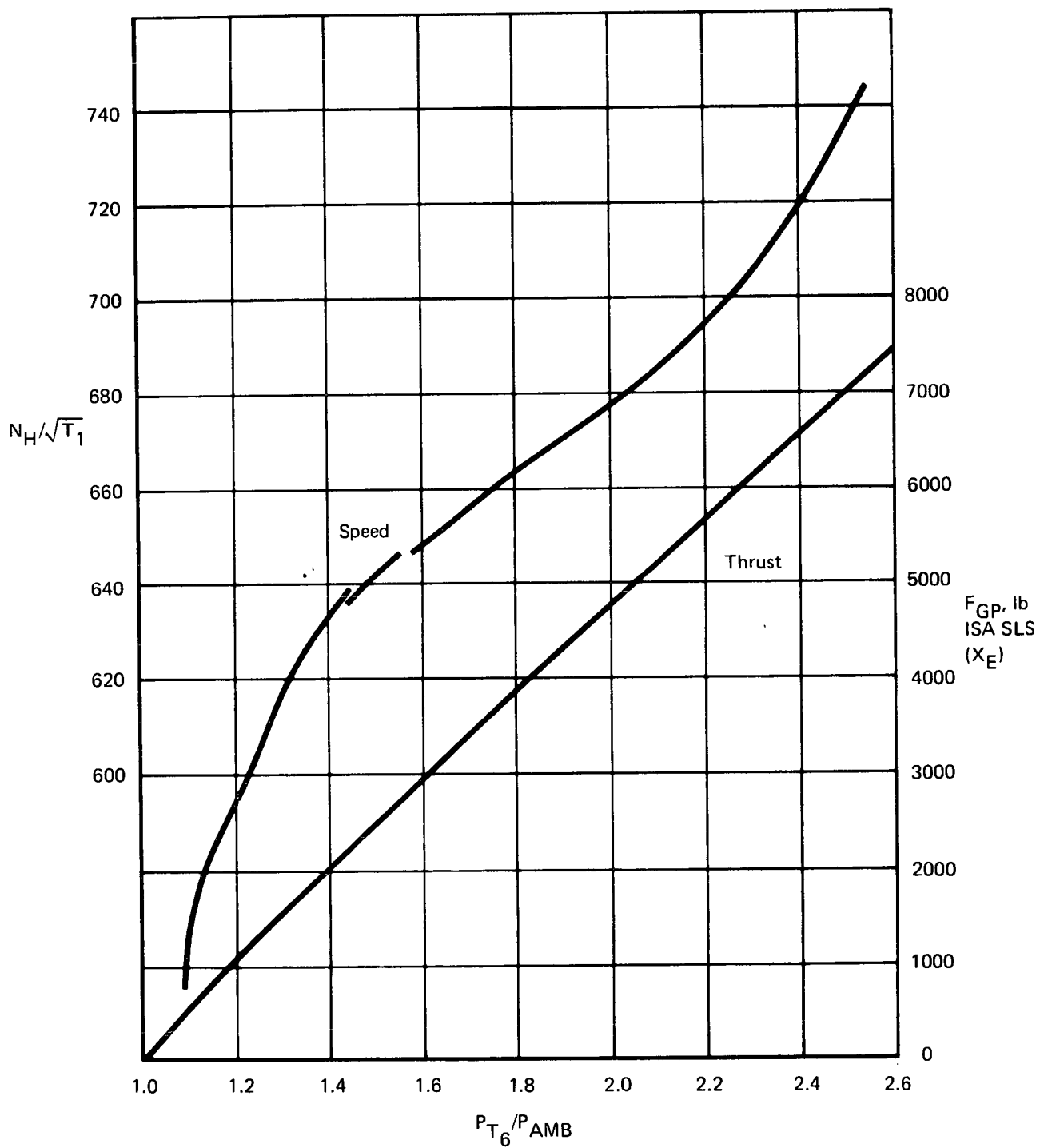
FIGURE 74.—PRIMARY THRUST AND $N_H/\sqrt{T_1}$ VS P_{T_6}/P_{AMB}

$$X_E = C_g \, P_{AMB} A_E \left(\frac{2\gamma}{\gamma-1}\right)\left[\left(\frac{P_{T_6}}{P_{AMB}}\right)^{(\gamma-1)/\gamma} - 1\right] \quad \text{unchoked}$$

$$X_E = C_g \, P_{AMB} A_E \left[2\left(\frac{2}{\gamma+1}\right)^{1/\gamma-1} \frac{P_{T_6}}{P_{AMB}} - 1\right] \quad \text{choked}$$
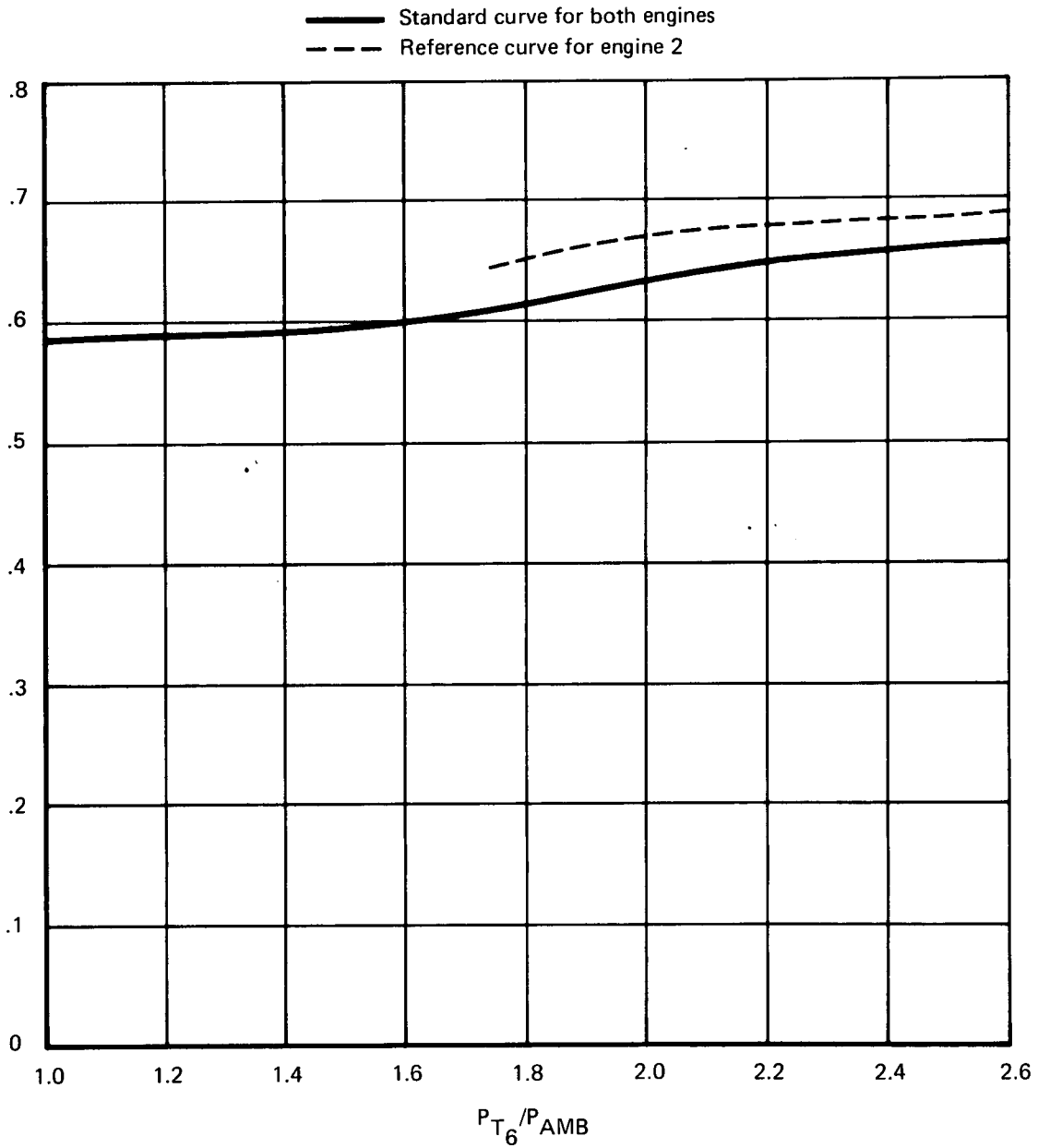
where P_{AMB} = 14.7 psi and A_E = 337 sq in.

—— Standard curve for both engines
– – – Reference curve for engine 2

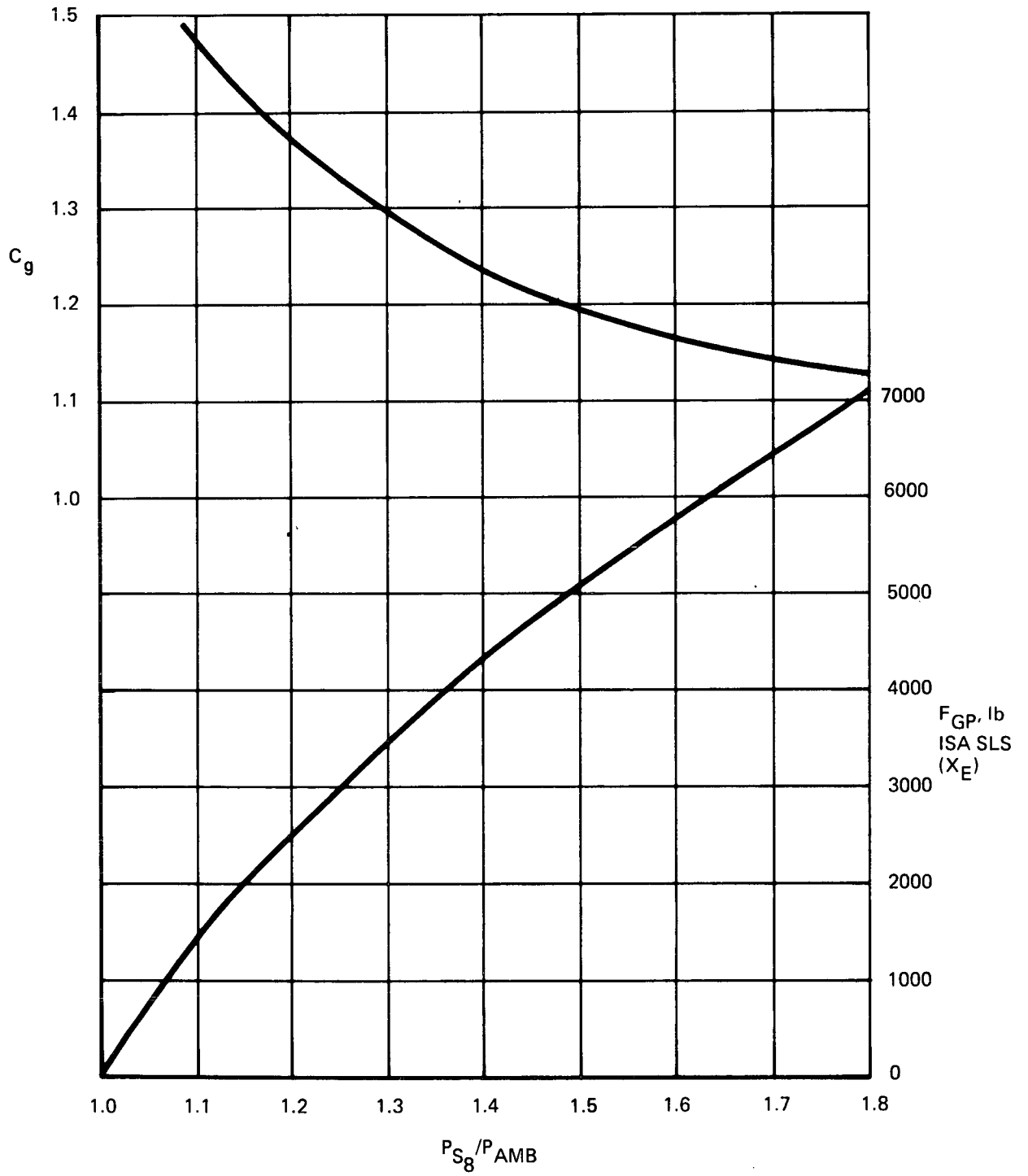FIGURE 75.—CURVE OF C_g VS P_{T_6}/P_{AMB}

137

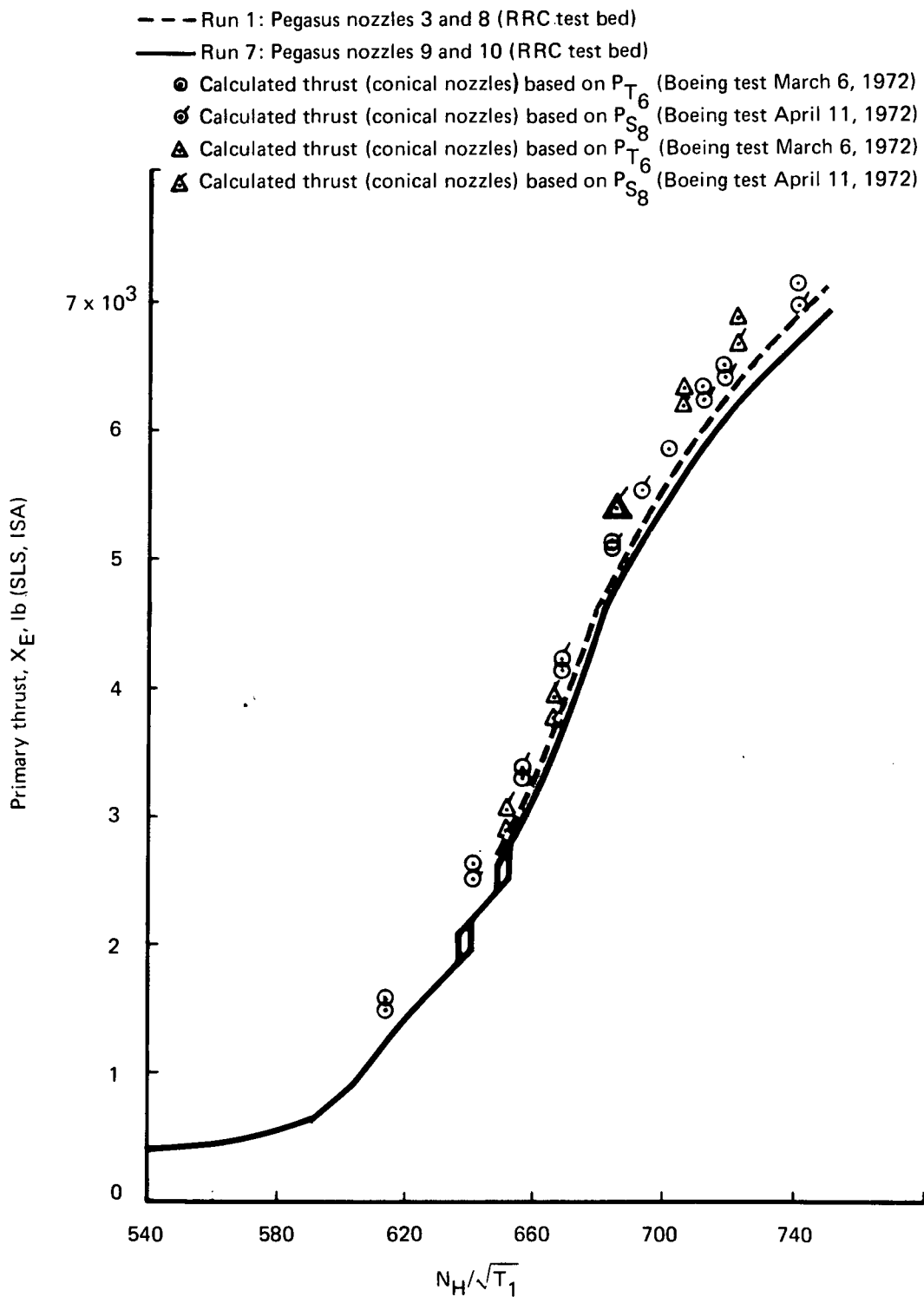FIGURE 76.—PRIMARY THRUST AND C_g CURVES VS P_{S_8}/P_{AMB}

FIGURE 77.–PRIMARY THRUST VS $N_H/\sqrt{T_1}$

(ENGINE 1)

---- Run 1: Pegasus nozzles (RRC test bed)

⊙ Run 7: Conical nozzles (RRC test bed)

♂ Calculated thrust (conical nozzles) based on P_{T_6} (Boeing test March 6, 1972)

Calculated thrust (conical nozzles) based on P_{S_8} (Boeing test April 11, 1972)

△ Calculated thrust (conical nozzles) based on P_{T_6} (Boeing test, March 6, 1972)

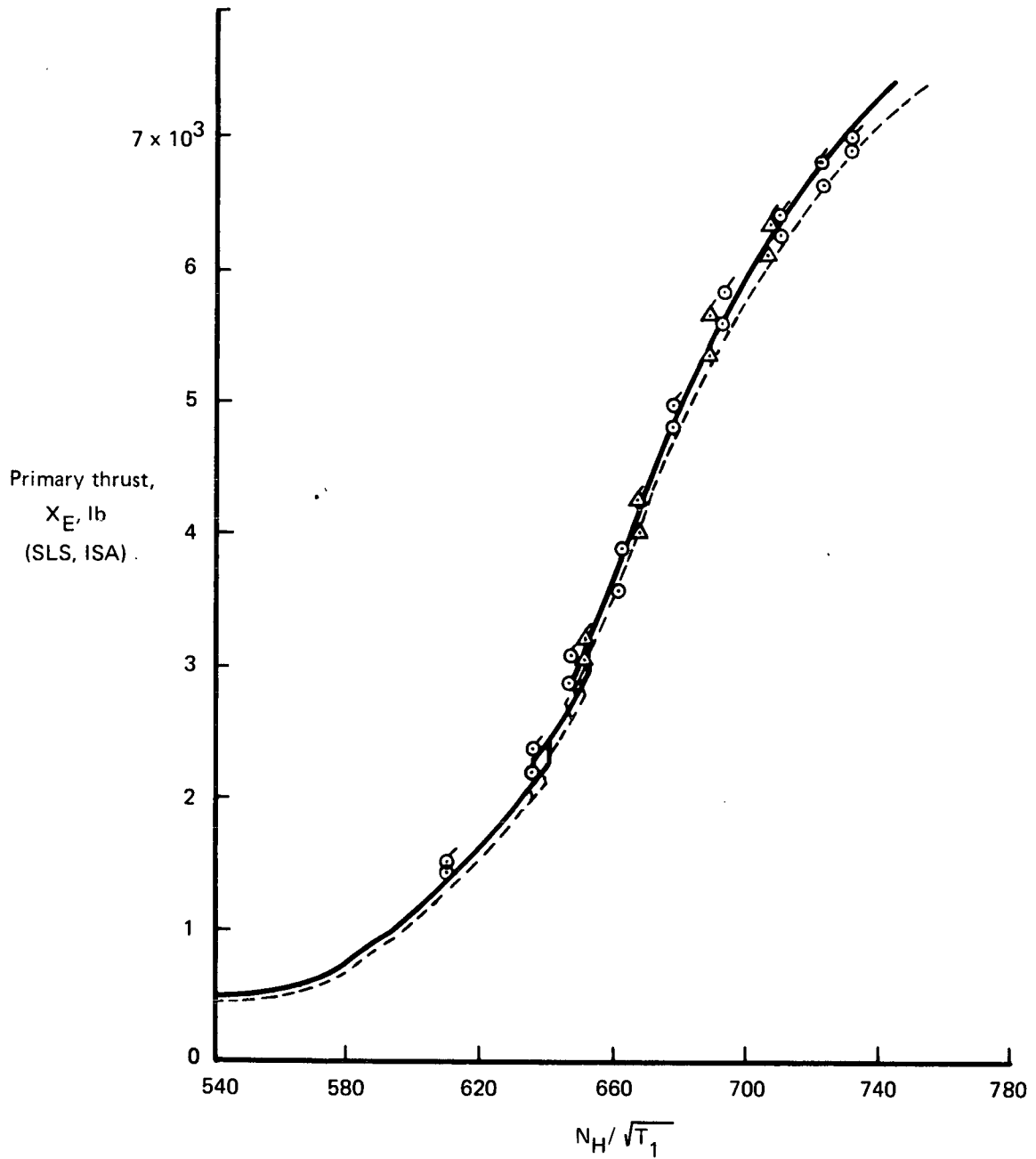⧊ Calculated thrust (conical nozzles) based on P_{S_8} (Boeing test, April 11, 1972)

Primary thrust,

X_E, lb

(SLS, ISA) .

$N_H / \sqrt{T_1}$

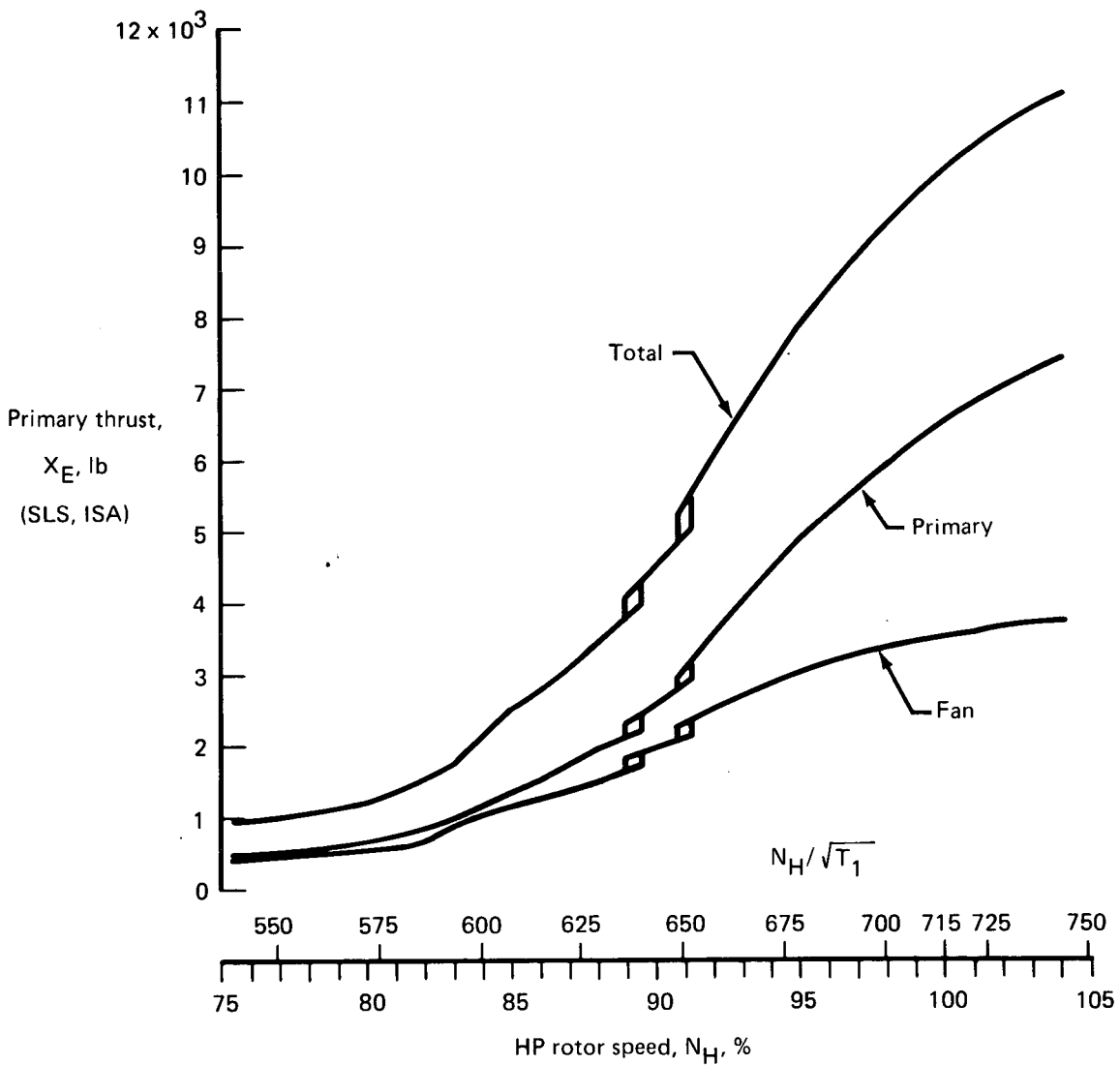FIGURE 78.—PRIMARY THRUST VS $N_H / \sqrt{T_1}$ (ENGINE 2)

FIGURE 79.—THRUST CHARACTERISTICS, SPEY MK 801-SF

141

Direct Thrust Measurement

Test hardware was designed and fabricated to determine the total static thrust of the airframe/propulsion system by direct measurement. The airplane was mounted on three thrust pads, one under the nose wheel and one under each of the main gear, as illustrated in figure 80. The three pads were identical and measured both vertical and horizontal force by strain gaged flectures.

The airplane as mounted on the thrust pads had to be located outdoors to permit unrestricted engine operation. Due to adverse weather conditions, difficulty was experienced with moisture getting inside the right-hand thrust pad even though measures had been taken to prevent it. The moisture affected the seating of the strain gage on the balance flectures, causing large zero shifts in the data such that it was unacceptable for accurate thrust measurements.

As an alternate to the direct thrust measurement, the hot and cold thrust were analyzed independently. The hot thrust was discussed in the preceding section, "Primary Exhaust Thrust." The cold thrust was obtained from internal duct measurements of pressure and temperature for each of its three components illustrated in figure 81, augmentor nozzles (upper and lower), aileron blowing, and body blowing. The location of the instrumentation is given in figure 82. The isentropic cold thrust for engine 1 in figure 83 is slightly higher (about 1%) than the cold thrust used to estimate the airplane performance, whereas in figure 84 for engine 2 the cold thrust is slightly lower than the reference cold thrust.
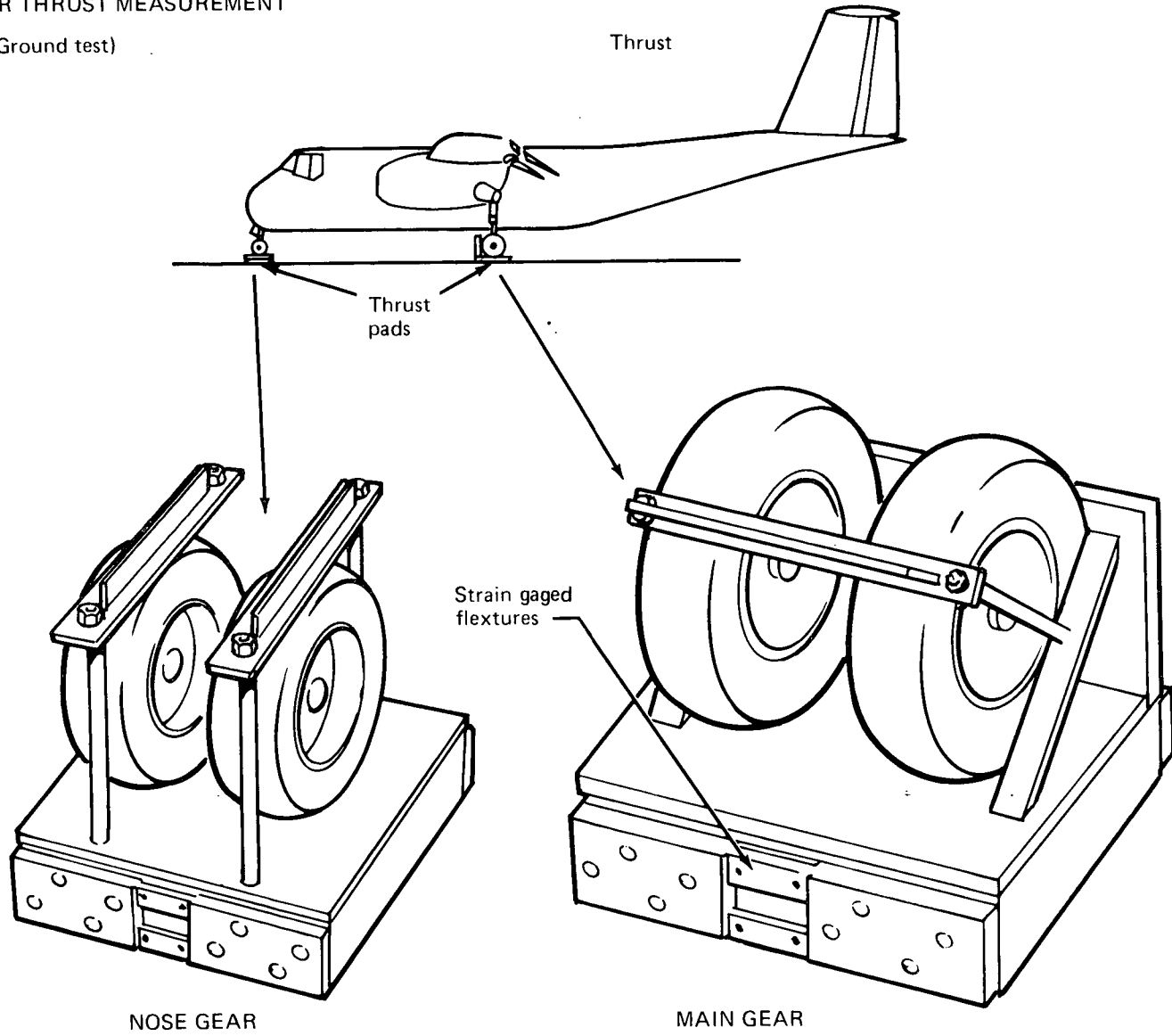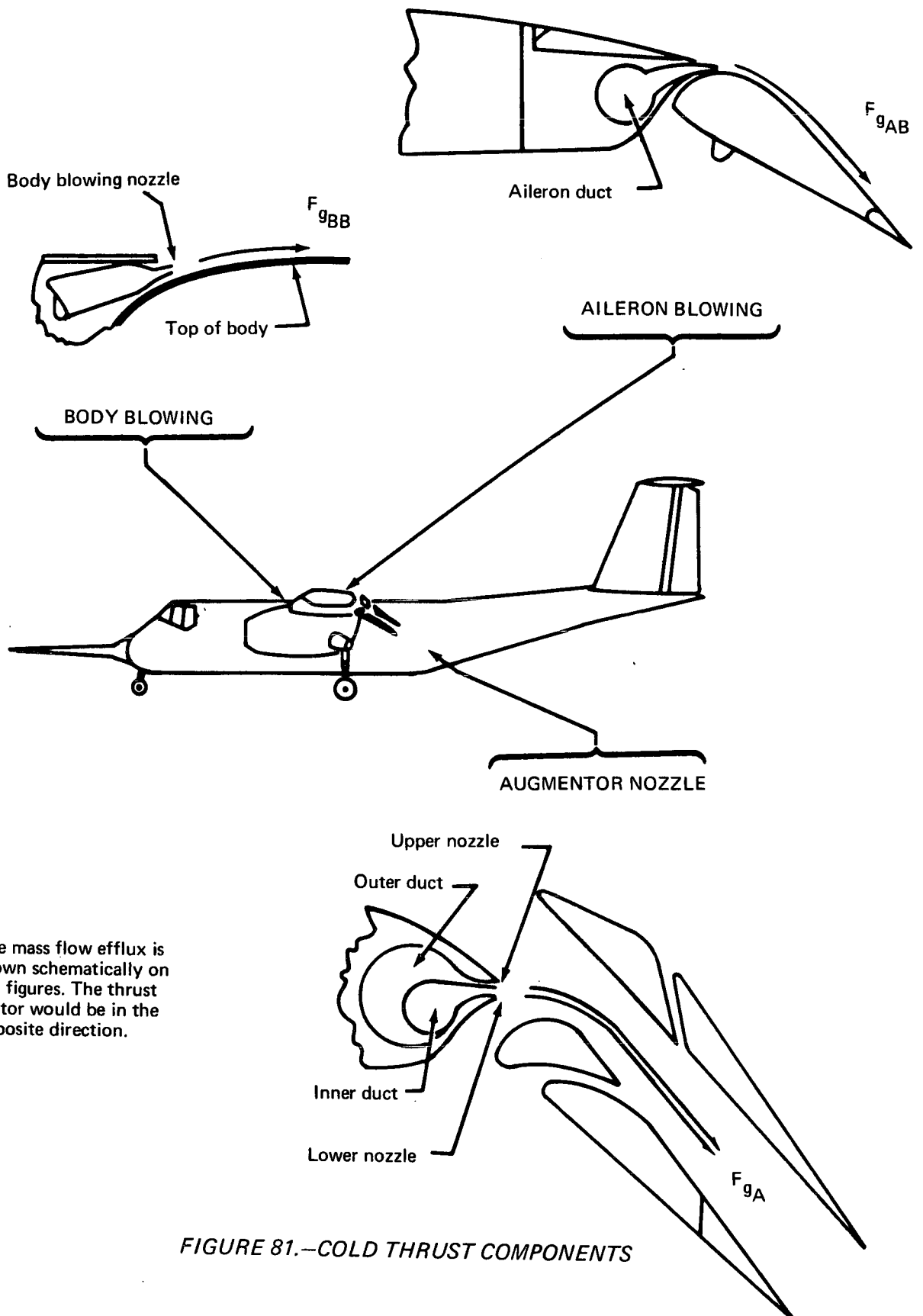
AUGMENTOR THRUST MEASUREMENT

(Ground test)

Thrust

Thrust pads

Strain gaged flextures

NOSE GEAR

MAIN GEAR

FIGURE 80.–THRUST PAD SCHEMATICS

Body blowing nozzle

$F_{g_{BB}}$

Top of body

BODY BLOWING

$F_{g_{AB}}$

Aileron duct

AILERON BLOWING

AUGMENTOR NOZZLE

Note:
The mass flow efflux is
shown schematically on
the figures. The thrust
vector would be in the
opposite direction.

Upper nozzle

Outer duct

Inner duct
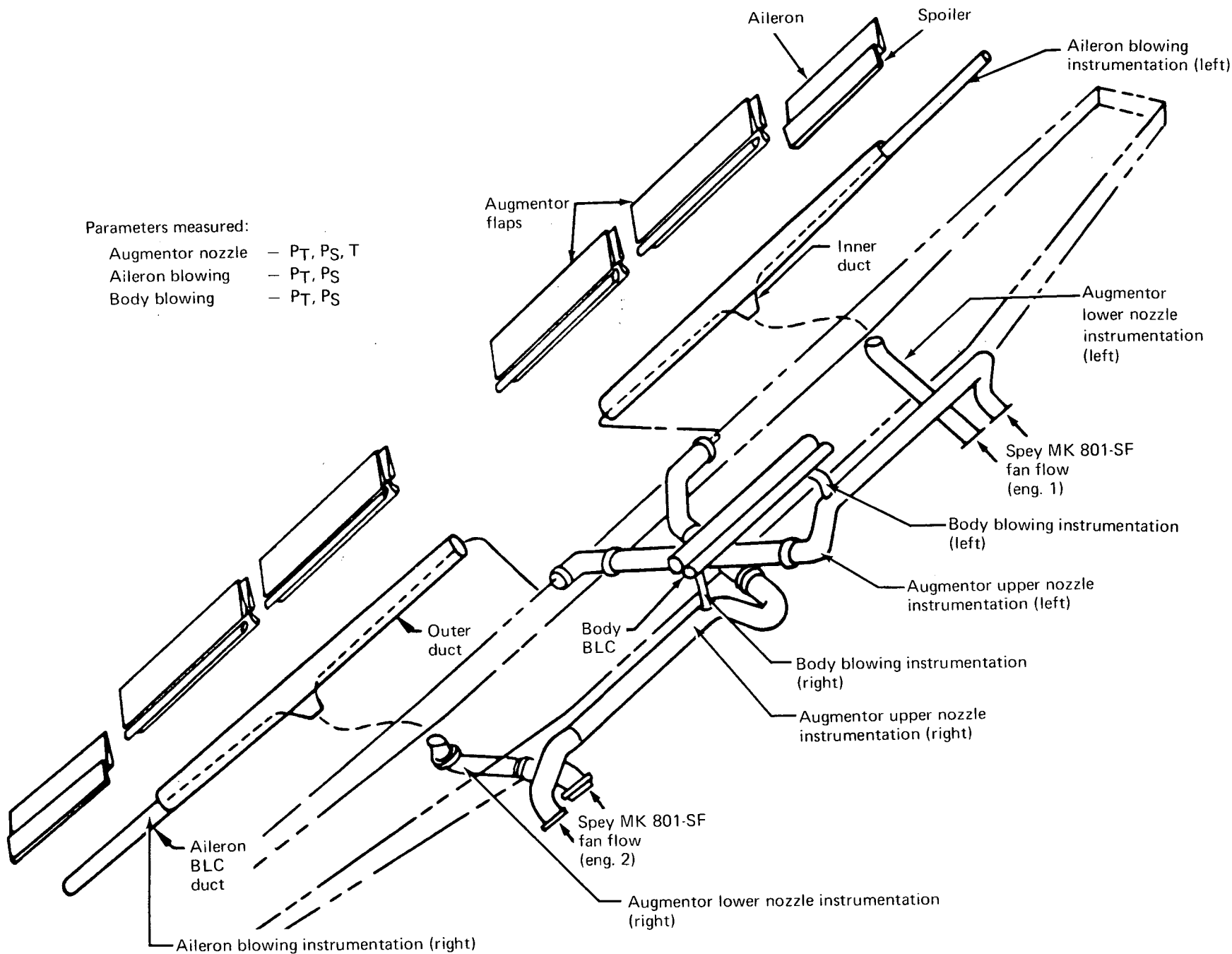
Lower nozzle

F_{g_A}

FIGURE 81.—COLD THRUST COMPONENTS

144

Parameters measured:

Augmentor nozzle — P_T, P_S, T
Aileron blowing — P_T, P_S
Body blowing — P_T, P_S

Aileron

Spoiler

Aileron blowing
instrumentation (left)

Augmentor
flaps

Inner
duct

Augmentor
lower nozzle
instrumentation
(left)

Spey MK 801-SF
fan flow
(eng. 1)

Body blowing instrumentation
(left)

Augmentor upper nozzle
instrumentation (left)

Outer
duct

Body
BLC

Body blowing instrumentation
(right)

Augmentor upper nozzle
instrumentation (right)

Aileron
BLC
duct

Spey MK 801-SF
fan flow
(eng. 2)

Augmentor lower nozzle instrumentation
(right)

Aileron blowing instrumentation (right)

FIGURE 82.—INSTRUMENTATION FOR OBTAINING COLD THRUST
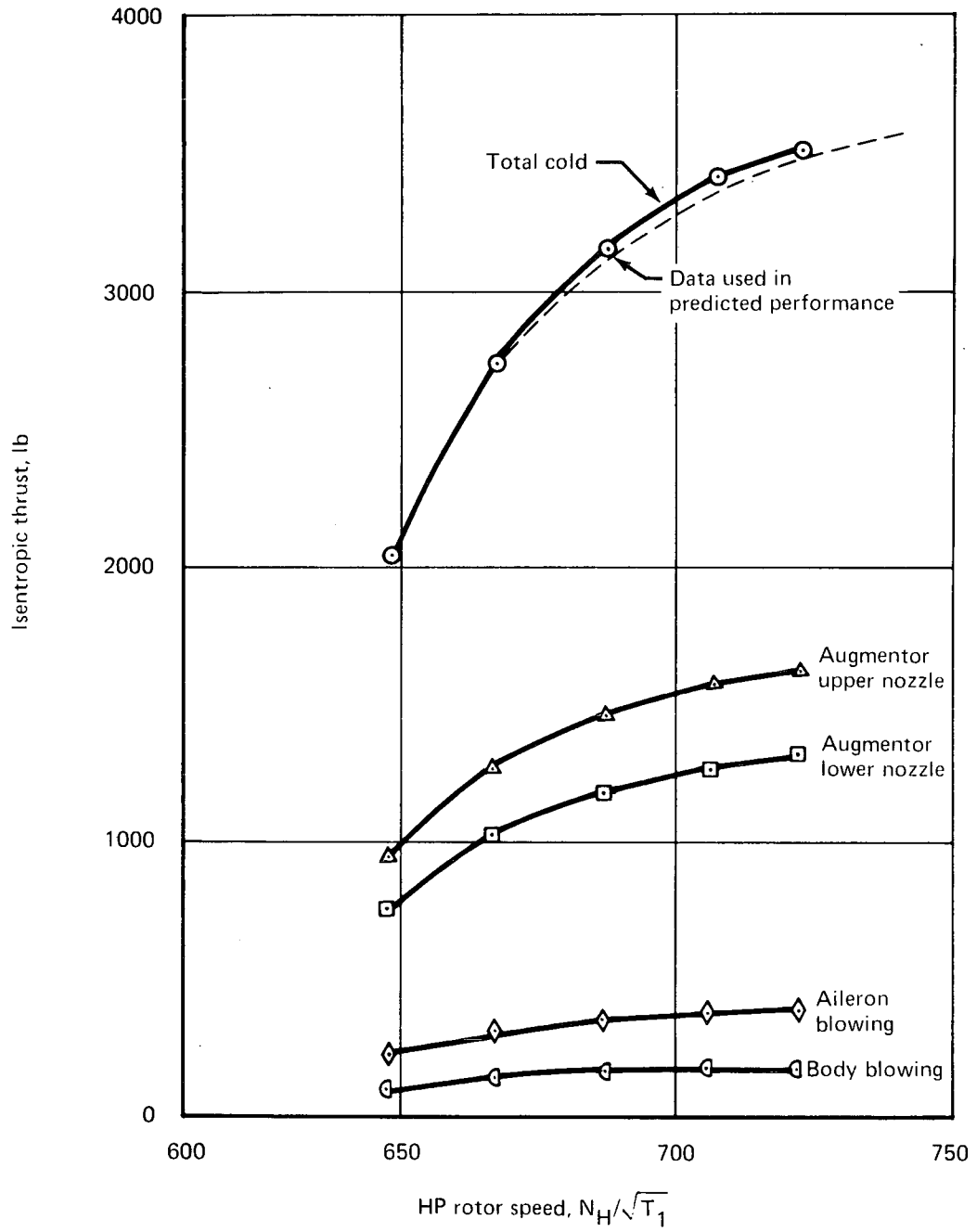
FIGURE 83.—COLD THRUST PERFORMANCE, ENGINE 1

Isentropic thrust, lb

Data used in
predicted performance

Total cold

Augmentor
upper nozzle

Augmentor
lower nozzle

Aileron
blowing

Body blowing

3000

2000

1000

650   700   750
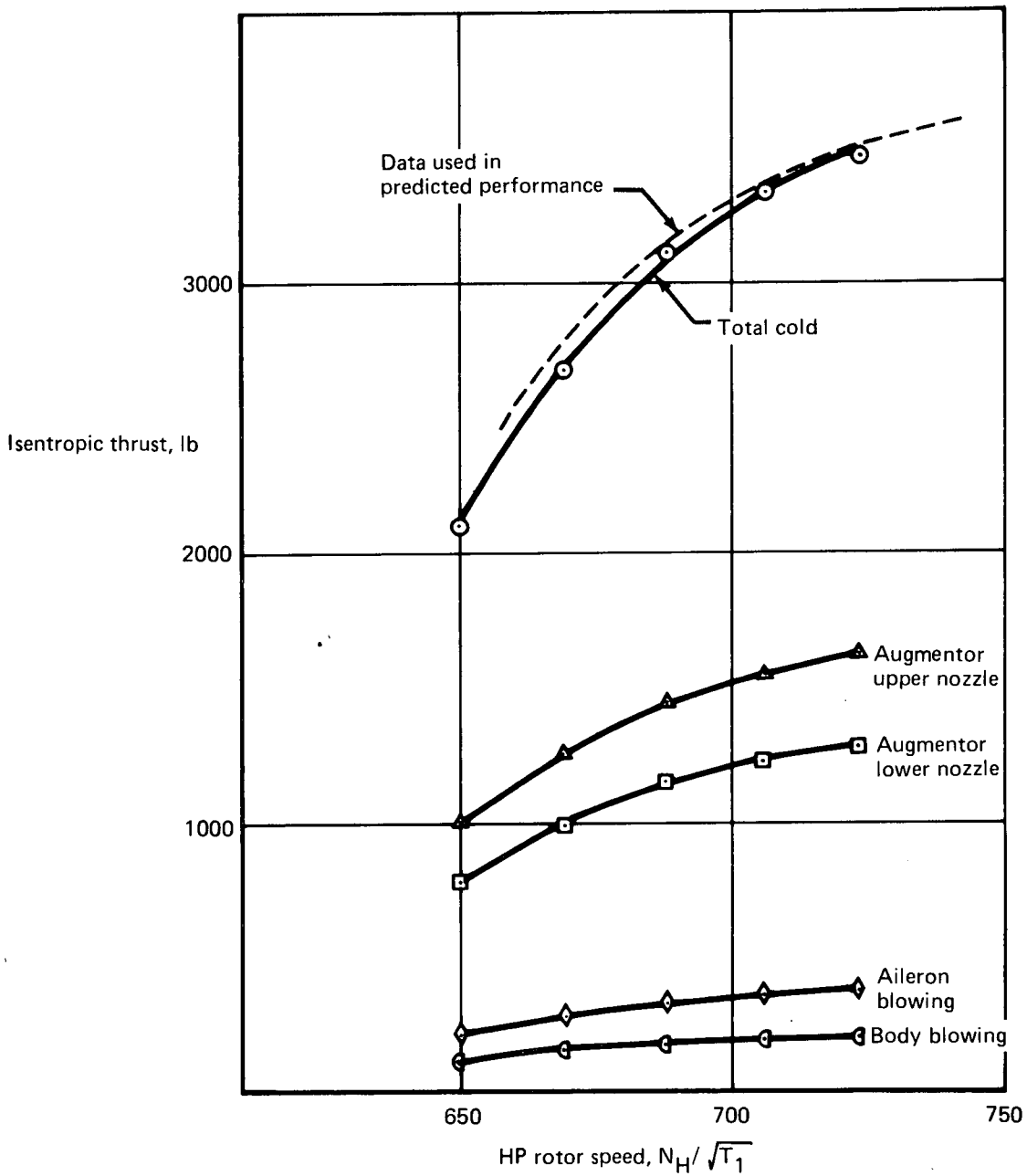
HP rotor speed, $N_H / \sqrt{T_1}$

FIGURE 84.—COLD THRUST PERFORMANCE, ENGINE 2

147

Fuel System

Tests were conducted on the fuel system to establish the fuel feed and transfer capabilities for both normal and abnormal conditions and to determine the unusable fuel quantity. The results are summarized below.

For the tank-to-engine fuel feed mode, engine-driven pump inlet pressure requirements are met with a margin of about 20 psi in a 0° pitch attitude. This margin would decrease to 18.2 psi in a 25° nose-up pitch attitude.

With one inner tank feeding both engines, engine-driven pump inlet pressure requirements are met with a margin of at least 12 psi in a 0° pitch attitude. This margin would decrease to 10.2 psi in a 25° nose-up pitch attitude.

The minimum unusable fuel quantity from the boost pump outlet was measured to be 251 lb per tank at 0° pitch attitude. This increases to 563 lb at 10° pitch down and 476 lb at 10° pitch up.

The engine-driven pump inlet pressure of -1.27 psig during suction feed at sea level under the most adverse conditions (takeoff power, 25° nose up) is 1.4 psi above the Rolls-Royce requirement of 12.0 psia. The requirement would still be met at approximately 30 000 ft without any reduction in flow or nose-up attitude.

AIRPLANE SYSTEMS (HYDRAULIC, CONTROL, AND ELECTRICAL)

General

The specific purpose of the systems ground testing was to verify and evaluate the design and performance of the flight controls, hydraulics, and electrical systems. Characteristics throughout most of the systems' operating ranges were demonstrated during the test program. A sufficient amount of data was derived from the relatively short test time to give a good indication of the performance and expected in-flight characteristics of the subject systems.

In general, the systems performed satisfactorily, subsequent to any required modifications. However, it was felt that certain areas could be further modified or adjusted to provide improved performance, e.g., control asymmetries and offsets, control response, and system rigging. Although improvements can be identified, it was felt that the systems operation is completely satisfactory for the Buffalo research airplane, and any further effort to make improvements was beyond the scope of the basic program.

Specific

Hydraulic systems tests were run concurrently with other ground tests and consisted of a continuous time survey of system parameters. The tests performed verified the required design pressures and confirmed that fluid operating temperatures are within the limits of the design requirements.

Initial lateral control system ground testing indicated that the spoiler and augmentor choke hydraulic control valves needed modification to overcome inadequate response characteristics. Subsequent to valve modification and reinstallation, correcting and repairing certain electrical control discrepancies, modifying the control wheel breakout force detent, rerigging the control system, and noting instrumentation transducer locations relative to actual control parameters, surface gearing versus pilot wheel inputs with SAS on and off were determined. The resulting surface programming to wheel was essentially as expected. The lateral SAS feed-forward input command is slightly offset, but acceptable. Aileron droop programming is very close to the prediction. The pilot's wheel force hysteresis is within the force detent, and the control system exhibits good centering characteristics.

Frequency response testing of the lateral control system was conducted by inputting signals to the roll SAS servo actuator. Although data were obtained over a limited frequency range due to SAS servo actuator rate saturation, good correlation was obtained between theoretical and test data.

Lateral control system resolution was determined by sinusoidally driving the SAS servo actuator and by manually cycling the pilot's control wheel. The performance is considered satisfactory, with a surface resolution capability of less than $\pm 0.2°$ aileron for both the electrical and manual inputs.

The lateral-directional stability augmentation system was tested extensively in the laboratory and on the airplane. Static and dynamic characteristics for the roll axis SAS yaw rate, roll rate, lateral control wheel, and variable stability input signals were determined. Steady-state gains and frequency response characteristics of the yaw axis SAS yaw rate signal path, roll attitude to rudder command, and the derived roll rate signal were determined. Static and dynamic characteristics of the variable stability system were determined both in the laboratory and on the airplane. Ground testing showed that control surface transients can occur when the gain setting on the variable stability control panel is changed. Therefore, discretion should be exercised in setting variable stability gains. The static gains, frequency response, and resolution characteristics of control surface position versus SAS servo actuator commands were determined for both the lateral and the directional axes.

The lateral-directional SAS system was found to operate satisfactorily in the airplane with no electromagnetic interference or engine-induced vibration problems. The test data compared satisfactorily with theoretical predictions.

Flap control system tests were conducted to verify the stability and response characteristics of the powered control system. The system was operated with one and two hydraulic systems operative and with both engines operating at two power settings. The test data indicate maximum surface rates between 3.2 and 3.7 deg/sec. The system is completely stable with no indications of oscillations or overshoots. Comparison of test data and analytical characteristics shows a good correlation.

Lift dump control system tests were conducted to verify the required response characteristics in the airplane. The system was operated with both hydraulic systems pressurized, with both engines operating at idle power, and with varying flap settings. Lift dump surface response was determined as well as lift dump schedule with flap position. The static gain and response characteristics are in agreement with predictions, and system operation is completely satisfactory.

Tests of the electrical power generation system, including the constant speed drive and generator cooling provisions, were conducted to verify satisfactory operation within acceptable limits. Power quality as measured at the primary ac and dc busses during normal operation was satisfactory. Power quality on the sub-busses should be equally satisfactory since wire run distances

150

are short and wiring continuity was verified. Power quality during engine shutdown with the associated generator switch in the ON position was found to be abnormal for a few seconds prior to automatic trip of the generator. This condition is probably not detrimental to aircraft equipment or flight test equipment. However, as a precaution, an operational procedure of shutting the generator off prior to engine shutdown has been incorporated. Data from a simplified cooling test at one outside ambient temperature verified that cooling provisions are adequate for the CSD generator.

TAXI TESTS

Taxi tests were conducted during the period April 18 to 27, 1972 to further verify that all systems were operational prior to flight. Operational tests were conducted to provide a qualitative evaluation of the fuel vent system, braking system, flight control systems, hydraulic systems, engine operation characteristics at high rotation angles, conical nozzle operation, and structural dynamic damping characteristics at the higher taxi speeds (100 to 110 kt). Two brief liftoffs were also accomplished.

Results of the taxi tests are summarized briefly in the following paragraphs. Additional analyses are presented in reference 1 (volume II).

FUEL VENT SYSTEM

The vent system was evaluated for possible spillage by making two figure eight turns on the taxi strip with outboard tanks full. Washable white paint had been applied at the vent locations. No fuel spillage was observed during the figure eight turns and no indication of spillage was evident on the painted surface.

BRAKING SYSTEM

The brake system tests consisted of evaluating brake operating characteristics during low-speed taxi operations and progressively increasing to approximately 100 kt. Braking temperatures were monitored during all braking tests.

A functional check of the system using brake accumulator pressure only (i.e., hydraulic system A selected off) was conducted. Similarly, a check of the system using the emergency braking system (air bottle) was conducted. All systems performed satisfactorily.

FLIGHT CONTROL SYSTEMS

Flight control systems were evaluated during the taxi tests preceding first flight. The pilot found the rudder effective for directional control almost immediately after brake release, before the airspeed indicator showed 30 kt. The airplane exhibited symmetrical lateral control characteristics

during short airborne hops at flaps 30° and 65°. These tests provided confidence that the spanwise flap and aileron blowing was symmetrical.

The lateral-directional stability augmentation system was checked for proper operation during the taxi tests in both the "normal" mode and the "variable stability" mode. Small-amplitude oscillations were detected in the rudder and ailerons during taxi. These oscillations stopped when the airplane was standing still. An investigation showed that structural vibrations were being passed by the "shock mounts" on the SAS computer boxes to the rate gyros contained in the computer boxes. The SAS computer mountings were modified to solve the problem.

During the initial taxi tests the airplane failed to achieve maximum trailing-edge-up elevator without extremely high stick forces. After a thorough inspection and the extension of the spring tab and control column deflection limits, a special taxi test was conducted to determine elevator characteristics. The testing revealed that significant elevator upfloat occurs at low airspeeds, that stick force characteristics were near prediction for low elevator deflection, that the tab stalled prematurely at higher elevator deflection, and that 75 lb of pull force produced only 16° elevator deflection at 60 kt. Conventional flight characteristics were judged acceptable, thus permitting the flight test program to continue. STOL takeoff rotation, landing flare, and stall recovery capabilities were reduced by the lack of elevator and were not attempted during the flight test program, based on the taxi test findings.

HYDRAULIC SYSTEMS

No specific taxi tests were conducted for the hydraulic systems. Hydraulic fluid temperatures were monitored concurrently with the taxi testing. All temperatures were below the design values, and the systems operated satisfactorily throughout the test.

ENGINE OPERATION

The airplane was rotated approximately 15° while taxiing at relatively low speeds with nozzles aft to explore any possibility of engine surge at high angles of attack. No surging occurred and engine operation was normal in all other respects with nozzles rotated aft. As indicated in table IX, surging did occur at low airspeeds with nozzles rotated forward (108°). Extensive investigation after these occurrences revealed no internal damage and only a very slight FOD mark on one stage 2 compressor blade on engine 2, which was polished in place.

TABLE IX.—SURGE TESTING RESULTS

Engine	N_H, %	IAS, kt	Nozzle angle, deg	Type of surge
Both	96	43	108	Bang
1	92	47	108	Rumble
1	92	50	108	Rumble
Both	92	53	108	None

Forward thrust or idle power should be selected when the airplane speed is below 60 kt to prevent reingestion.

CONICAL NOZZLE OPERATION

During taxi runs, the conical nozzles were operated at various rates and with the engines at several power settings. Operation of the nozzles was quite smooth although "bounceback" of a few degrees occurred following rapid movement of the nozzle control levers. No dynamic instability occurred. With the nozzles set during low power, application of high power caused some nozzle position drift before stabilizing. However, this was not considered to be detrimental to the flight test program.

STRUCTURAL DYNAMIC DAMPING

Although the true in-flight damping characteristics cannot be obtained from taxi testing, it does provide a reasonably good indication of any potential instability. Taxi speeds were progressively increased up to 120 KIAS. No structural dynamic instability occurred during the taxi tests, and all surfaces appeared to be adequately damped.

FLIGHT TESTS

The contractor's flight testing of the Modified C-8A airplane was conducted during May 1972. The primary objective of the testing was to establish the basic airworthiness of the research vehicle. This included verification of the structural design and evaluation of the aircraft's systems. The Modified C-8A research aircraft was demonstrated to be airworthy.

The first flight was made on May 1, 1972. The flight program was completed in eight flights, with a total flight time of 9 hours and 8 minutes. The testing was conducted from Boeing Field International and Snohomish County Airport (Paine Field). During the last flight, the starter on the left-hand engine malfunctioned during an in-flight start, which resulted in the loss of the lower cowling of engine 1 and subsequent damage to the airplane. Repairs were made, a functional check flight was conducted, and the airplane was delivered on July 31, 1972.

The flight envelope was investigated from a minimum airspeed of 50 KEAS to the design dive speed (V_D) of 180 KEAS. Flap placards were reached at flaps 65° (90 KEAS) and flaps 30° (120 KEAS). Approaches to stall were made at three primary flap settings: up, 30°, and 65°. The full ranges of flap setting, conical nozzle deflection, and power setting were evaluated.

The angle of attack and load factor range achieved during the test program is summarized in figure 85. Angles of attack greater than 22° were attained. Variations in load factor from 0.3 to 1.8 g were obtained during pushover/pull-up maneuvers. Sideslip angles of 15° were tested and bank angles exceeding 45° were reached. The flight envelope was sufficiently explored to clear the airplane for the augmentor wing research flight test program.

STRUCTURAL TESTING

A major objective of the contractor's flight test program was to aid in validation of the airworthiness of the aircraft structure. Three topics were investigated: flutter, loads on the modified components, and stresses on the modified components. The velocity-load factor envelope tested is shown in figure 85.

Flutter

The flight flutter checks demonstrate that the Modified C-8A airplane is free from flutter and has adequate damping for all normal operating conditions within the aircraft design speed envelope, 180 KEAS.
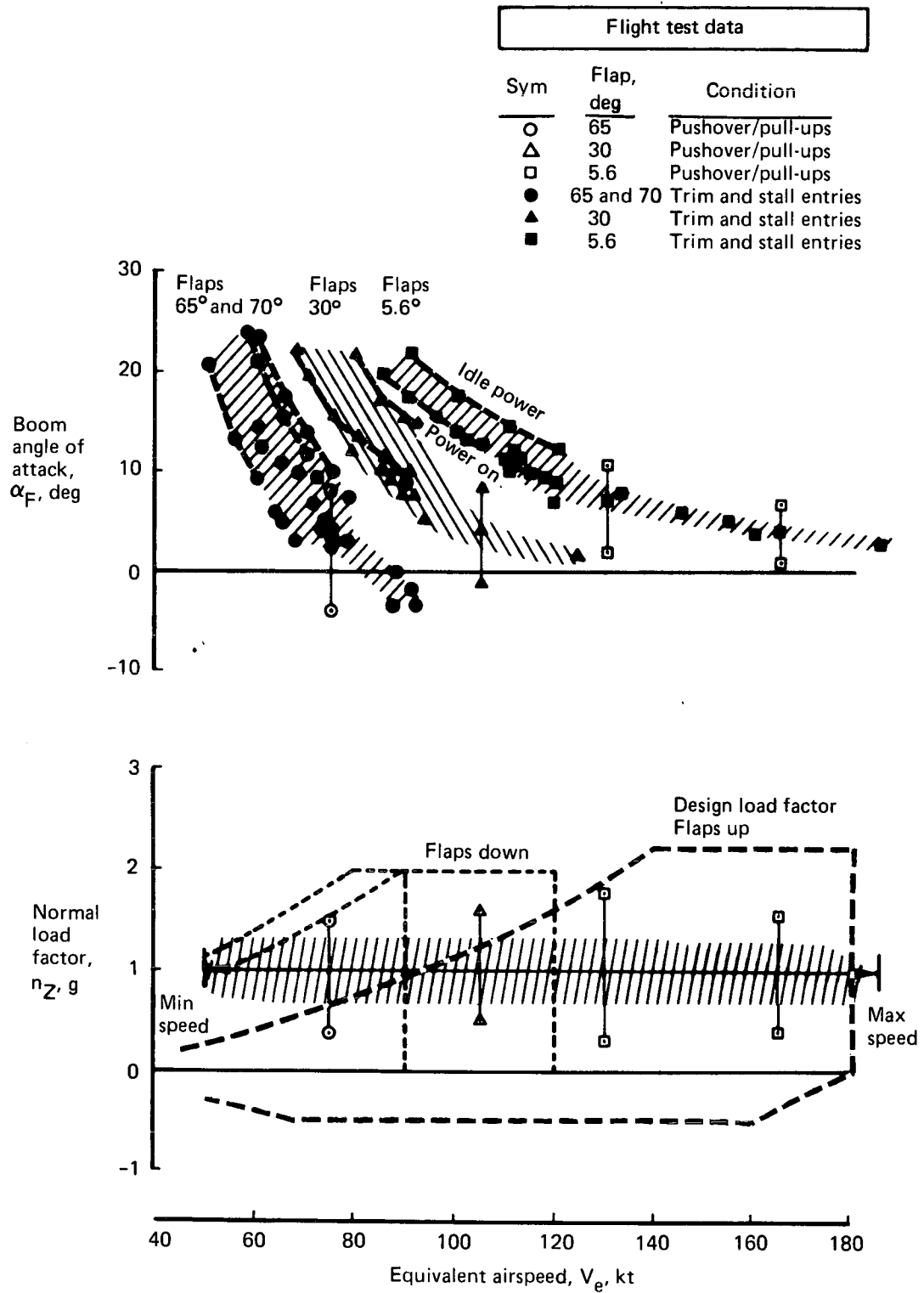
FIGURE 85.—FLIGHT TEST DEMONSTRATED ANGLE OF ATTACK,
LOAD FACTOR, AND AIRSPEED ENVELOPE

Loads

Loads were calculated from flight test measurements on the leading edge slat, aileron, empennage, and main landing gear. All loads were within design levels.

Stresses

Stresses were measured in the augmentor duct system, on the wing, aileron flap relief link, aileron outboard hinge support, main flap torque tube, flap intake door link, and flap support beam. With the exception of two places within the augmentor duct system, all stresses measured indicate adequate strength. The critical stress condition observed in the augmentor duct is caused by the transient loading during engine start. The resulting stresses approach limit design stress. This was discussed in greater detail in the "Ground Tests" section. Figures 55 and 56 show the results of strain gage measurements.

The hinge moments on the flaps were measured by measuring the actuator pressure. These results are also described in "Ground Tests".

PERFORMANCE

Although the specific purpose of the contractor's flight test was to verify the structural design and evaluate the aircraft's systems, a significant amount of performance information was also extracted from the relatively short airworthiness testing to give a preliminary indication of the aircraft's performance and flight characteristics. These performance data provide a basis for future flight test planning and investigations. It should be noted that position errors for airspeed or angle of attack have not been used in any of the data.

Minimum Test Speeds

The minimum test speeds attained during the program are compared to the predicted 1 g stall speeds in figures 86 and 87 for two-engine and single-engine operation, respectively. The approach-to-stall conditions were stopped at a predetermined angle of attack and not continued into full stall. However, no significant increase in buffet was noted during the stall approach to indicate pending stall. The demonstrated speeds were within 0 to 7 kt of the predicted 1 g stall speeds. Fuselage angle of attack, as measured by the nose boom (uncalibrated) exceeded 20° for all flap settings, and alphas up to 25° were attained for specific cases. For all conditions, the minimum test speeds are limited by angle of attack and the aircraft does not appear to have any minimum control speed restrictions.

FIGURE 86.—MINIMUM TEST SPEEDS, TWO ENGINES

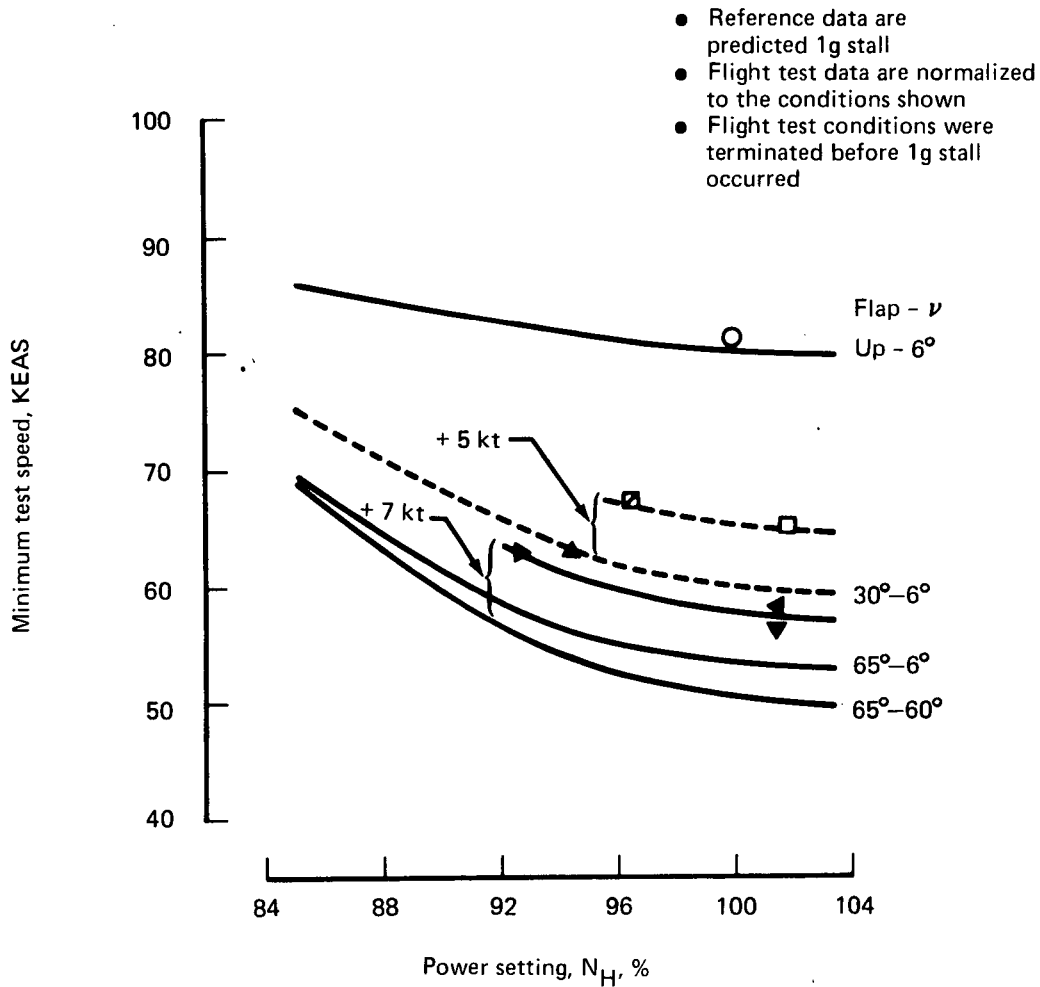|	Flight test data			
Sym	Flap, deg	Test	ν, deg	$\%N_H/\%N_H$
O	Up	9-5	7	60.9/99.9
□	30	9-5	9	60.6/101.7
▨	30	9-5	8	60.7/96.5
▲	65	10-1	57	60.4/94.3
▶	65	10-1	57	60.6/92.6
▼	65	10-1	57	60.5/101.4
◀	65	10-1	56	60.6/101.4

- 40,000 lb
- Sea level
- Standard day

- Reference data are predicted 1g stall
- Flight test data are normalized to the conditions shown
- Flight test conditions were terminated before 1g stall occurred

Flap – ν
Up – 6°

+ 5 kt

+ 7 kt

30°–6°

65°–6°

65°–60°

Minimum test speed, KEAS

Power setting, N_H, %

FIGURE 87.—MINIMUM TEST SPEEDS, ONE ENGINE

161

The lowest speed attained during the test program was 50 KEAS, corresponding to an equivalent lift coefficient (W/qS) of 5.4. The configuration was representative of a STOL approach with the flaps at 65° and the conical nozzles deflected down to 58°.

Takeoff Performance

Takeoff distances less than 2000 ft were demonstrated although high power STOL takeoffs were not conducted. The takeoff power setting used during the contractor's test program ranged from 95% to 97% N_H, which corresponds to 75% to 85% of the maximum takeoff thrust available. The nominal takeoff gross weight was 46 600 lb, which exceeded the design maximum weight of 45 000 lb. The high takeoff gross weights were used to extend the testing time for each flight.

Several single-engine climb checks were made to verify the takeoff flap settings being used. Figure 88 indicates that the flight test data are nominally as predicted. Sufficient emergency climb capability exists to permit takeoffs over a reasonable range of gross weights and ambient conditions.

Climb/Cruise/Descent

Descent and climb capability from -2000 to +3000 ft/min were demonstrated during the flight test program. Flap setting was varied from up (5.6°) to full down (73°). The climb performance for the conical nozzles aft is compared with that predicted in figures 89, 90, and 91 for the primary flap settings: cruise (5.6°), takeoff (30°), and landing (65°). The measured flight test data are shown relative to the power setting required in flight. As noted by the figures, a higher power setting is required to maintain a given rate of climb than was predicted. The higher thrust required corresponds to a 10%-20% drag increase over that predicted after corrections are made to account for configuration changes and excrescences not included in the original prediction. It was not possible to determine the reasons for the higher drag because of the limited amount of performance testing. Possible explanations include local separated regions as indicated by a buffet level noted in flight, a lower augmentation ratio, and the inability to resolve drag and thrust to the necessary accuracies. The measured angle of attack at a given flight condition was 1° to 2° higher than predicted for all flap settings. The measured data do not include position error corrections.

The power required for level flight is given in figure 92 for flaps up. As noted, the aircraft can easily attain the maximum operating speed of 160 KEAS with a power setting of 92% (approximately 75% of the maximum thrust available). Specific range at the 5000-ft altitude shown will be 0.023 to 0.025 nautical air miles per pound. The maximum range shown in figure 93 is expected to be approximately 235 nmi at the fuel capacity of 13 500 lb with fuel reserves of 2000 lb.
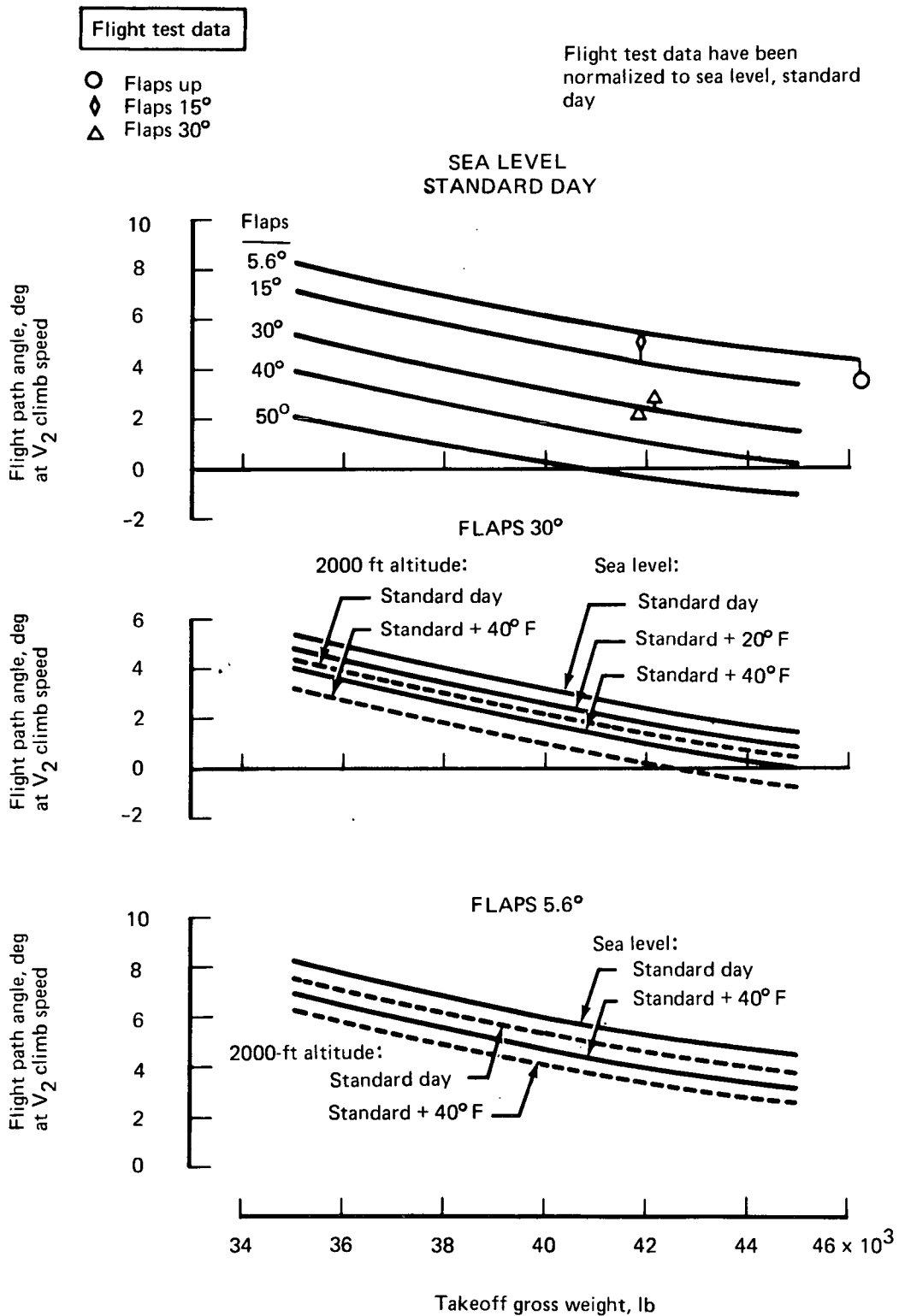
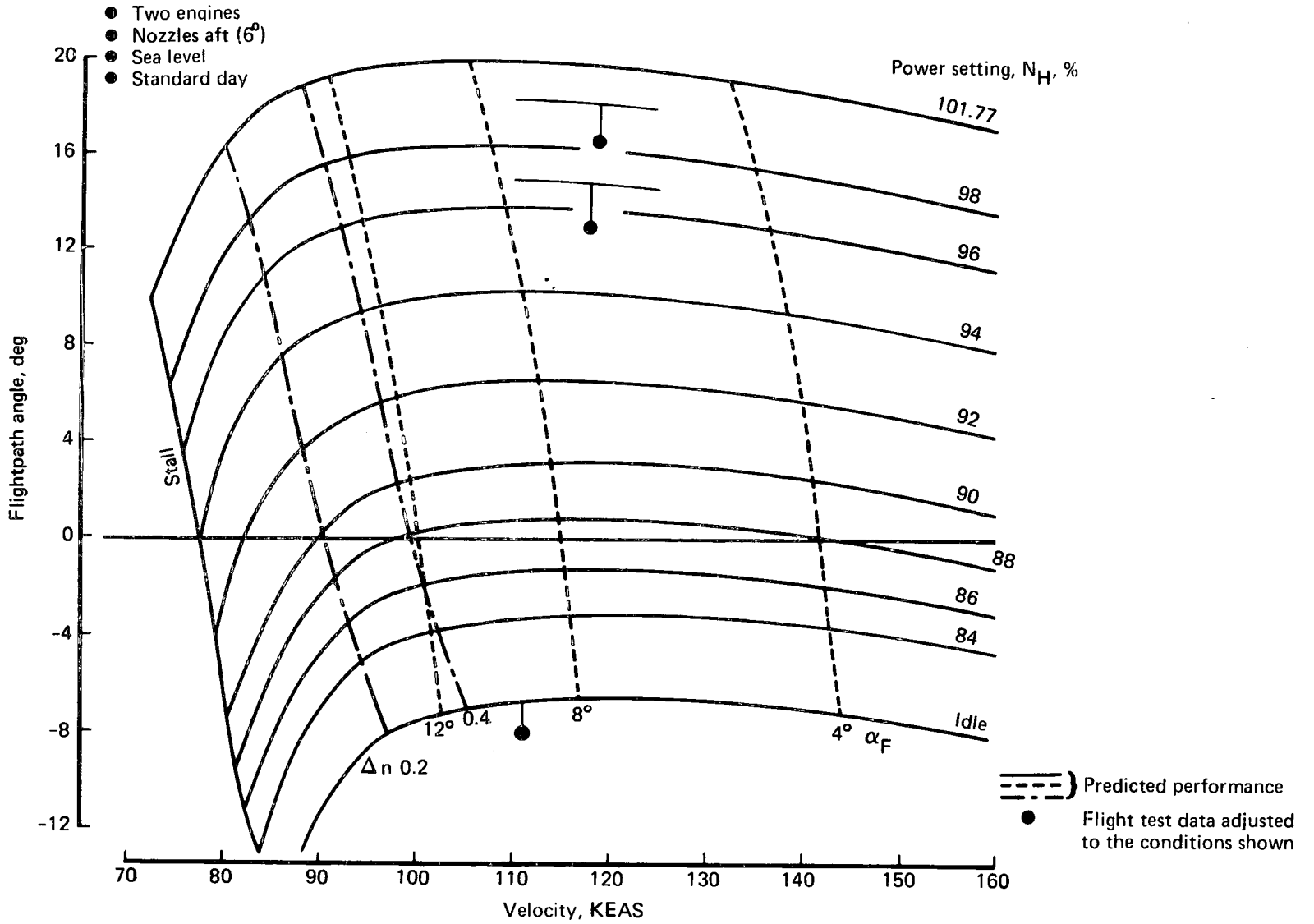FIGURE 88.—SECOND SEGMENT CLIMB, ONE ENGINE AT
EMERGENCY POWER, 6°NOZZLE ANGLE
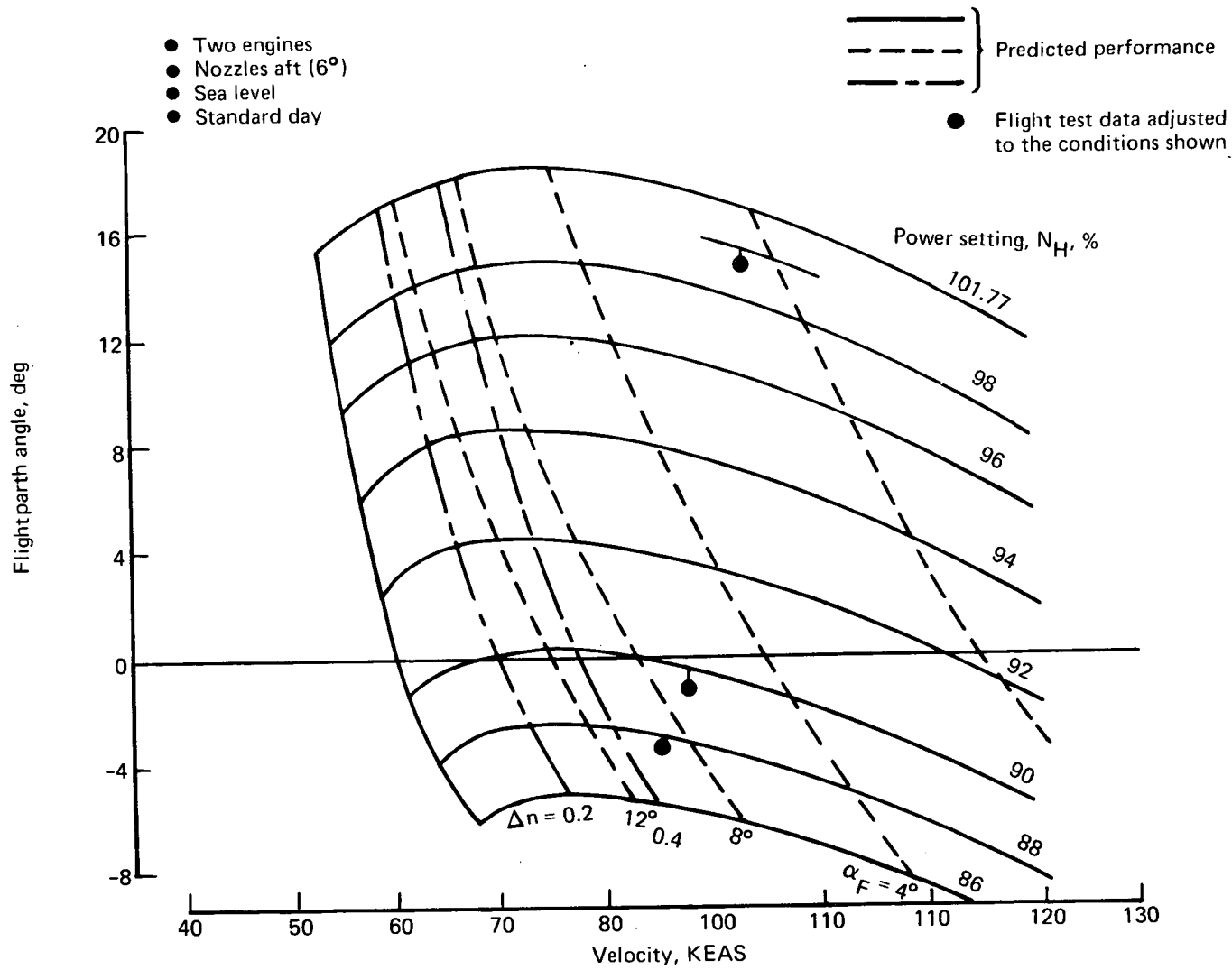
FIGURE 89.—FLAPS UP CLIMB, GROSS WEIGHT = 40 000 LB

FIGURE 90.—FLAPS 30° CLIMB, GROSS WEIGHT = 40 000 LB
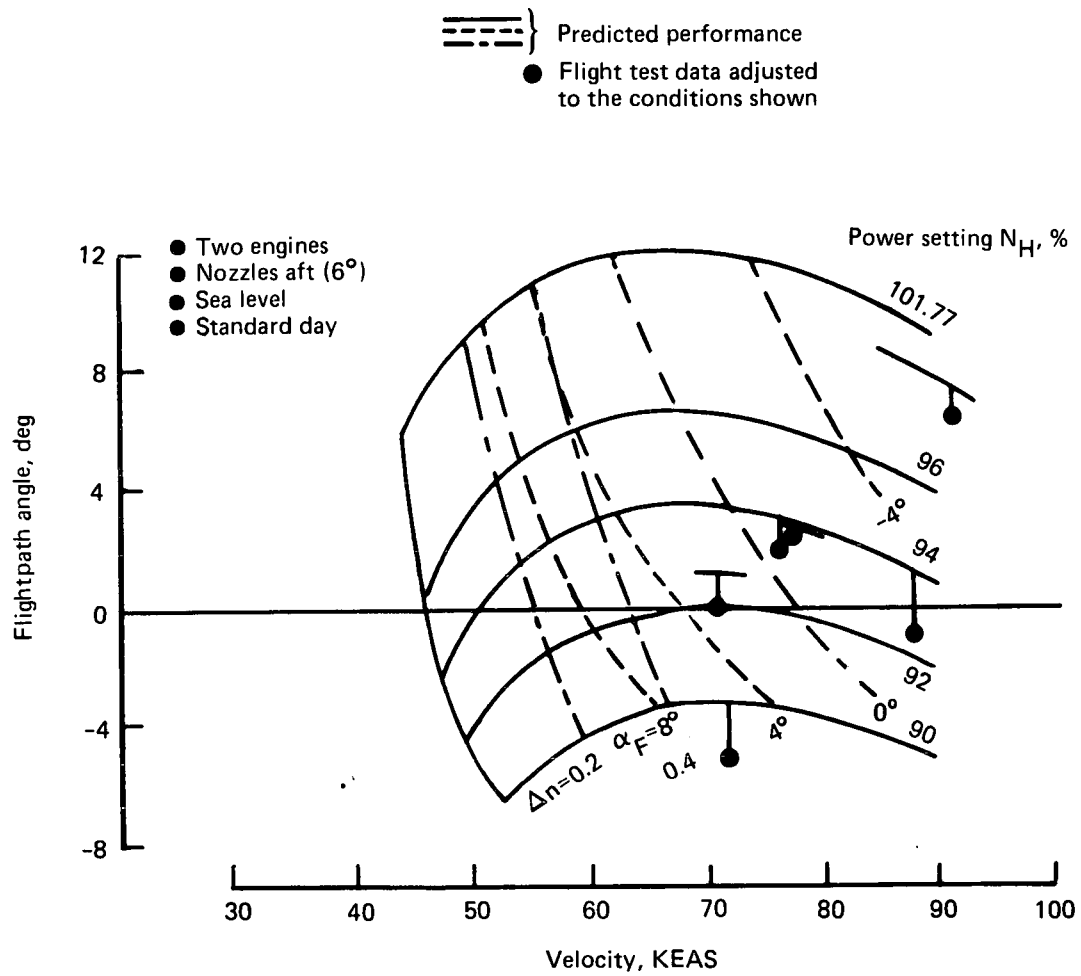
FIGURE 91.—FLAPS 65°CLIMB, GROSS WEIGHT = 40 000 LB

- Level flight
- 40 000 lb
- 5000 ft altitude
- Standard day
- Nozzles aft
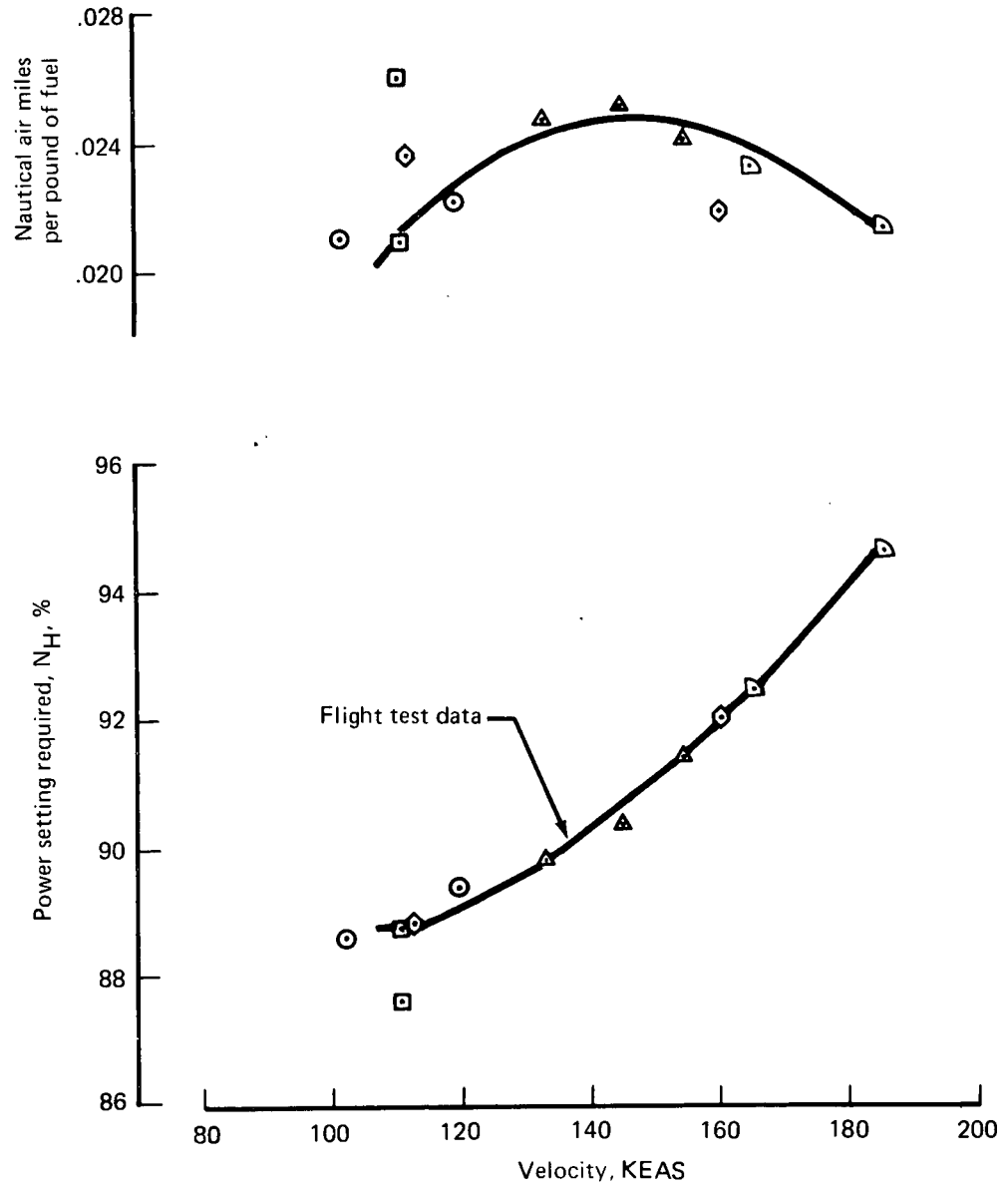- Flight test data normalized to the conditions shown

FIGURE 92.—LEVEL FLIGHT PERFORMANCE, FLAPS UP

- OEW = 32 600 lb
- Reserves = 2000 lb
- Unusable fuel = 740 lb at θ = 5°
- Fuel capacity = 13 500 lb
- Standard day
- Sea level airport
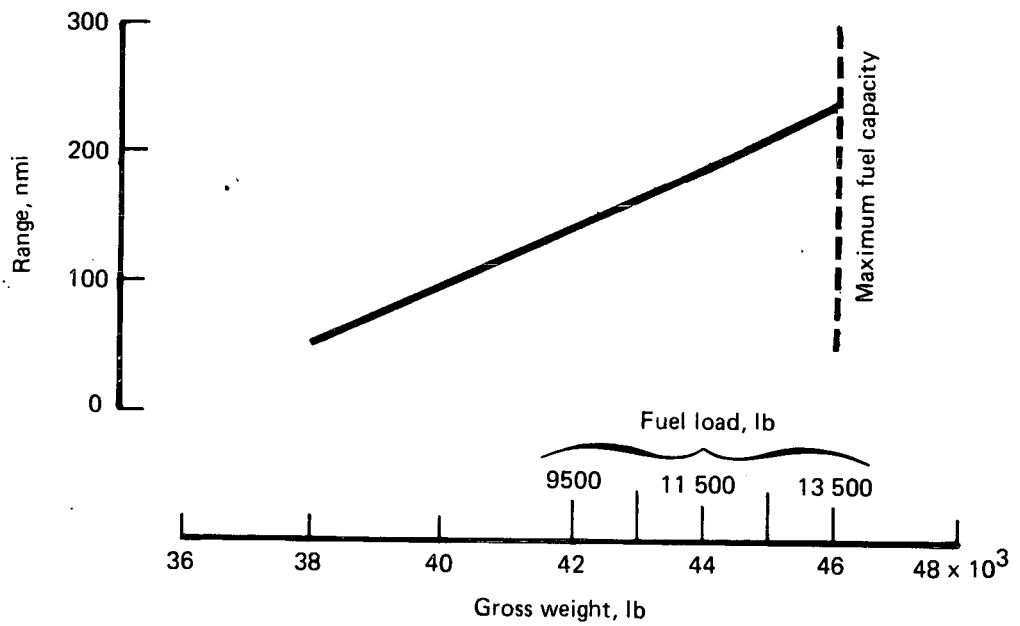- Zero winds
- Cruise: 160 KEAS at 10 000 ft altitude

FIGURE 93.—RANGE

Approach and Landing

All the landings during the test program were conducted with conventional approaches; 3° glide slope and the conical nozzles aft at 6°. The landing flap setting varied from 25° to 54°. Single-engine landings were made with flaps 30° without difficulty.

No landings from a STOL approach were scheduled. A trim condition closely representing the design approach of 60 KEAS, 800 ft/min rate of descent, and 40 000 lb gross weight was tested at an altitude of 7670 ft. Extrapolating the test data to represent a standard day landing at sea level, the STOL approach characteristics would be 11° to 12° fuselage angle of attack and 93% N_H with the conical nozzles at 58°. Rotating the conical nozzles to 90° would decrease the angle of attack to 3° and increase the power to 96% or 97% N_H.

Full elevator deflections could not be obtained due to an apparent stalling of the elevator spring tab.

LONGITUDINAL STABILITY AND CONTROL

The elevator required for all of the steady '1 g' trim points conducted during the flight test program is presented in figure 94. The airplane maintained trim within ±5° of elevator from neutral for all takeoff, climb, cruise, descent, and landing conditions.

The CG for the test flights varied between 29% and 31% MAC. No attempt was made to examine forward or aft CG characteristics, and aerodynamic limitations were not established. For the CG range tested, it appears that the stabilizer incidence setting, trim tab authority, and tail lift capability are adequate for all normal flight conditions. However, the premature elevator tab stall noted during the taxi test has a detrimental effect on the low-speed control capability required for STOL takeoff rotations, landing flares from steep approaches, and stall recovery. The extent to which the elevator control system will limit STOL performance was not determined during the test program.

The static longitudinal stability levels demonstrated in flight were low, with flaps up being positive and flaps down stability virtually nonexistent. The stick force required to change airspeed was zero for flaps 65° and, as a result, very close attention was required to maintain a trim condition. The low static stability produced constant wandering in airspeed and altitude below 75 kt.
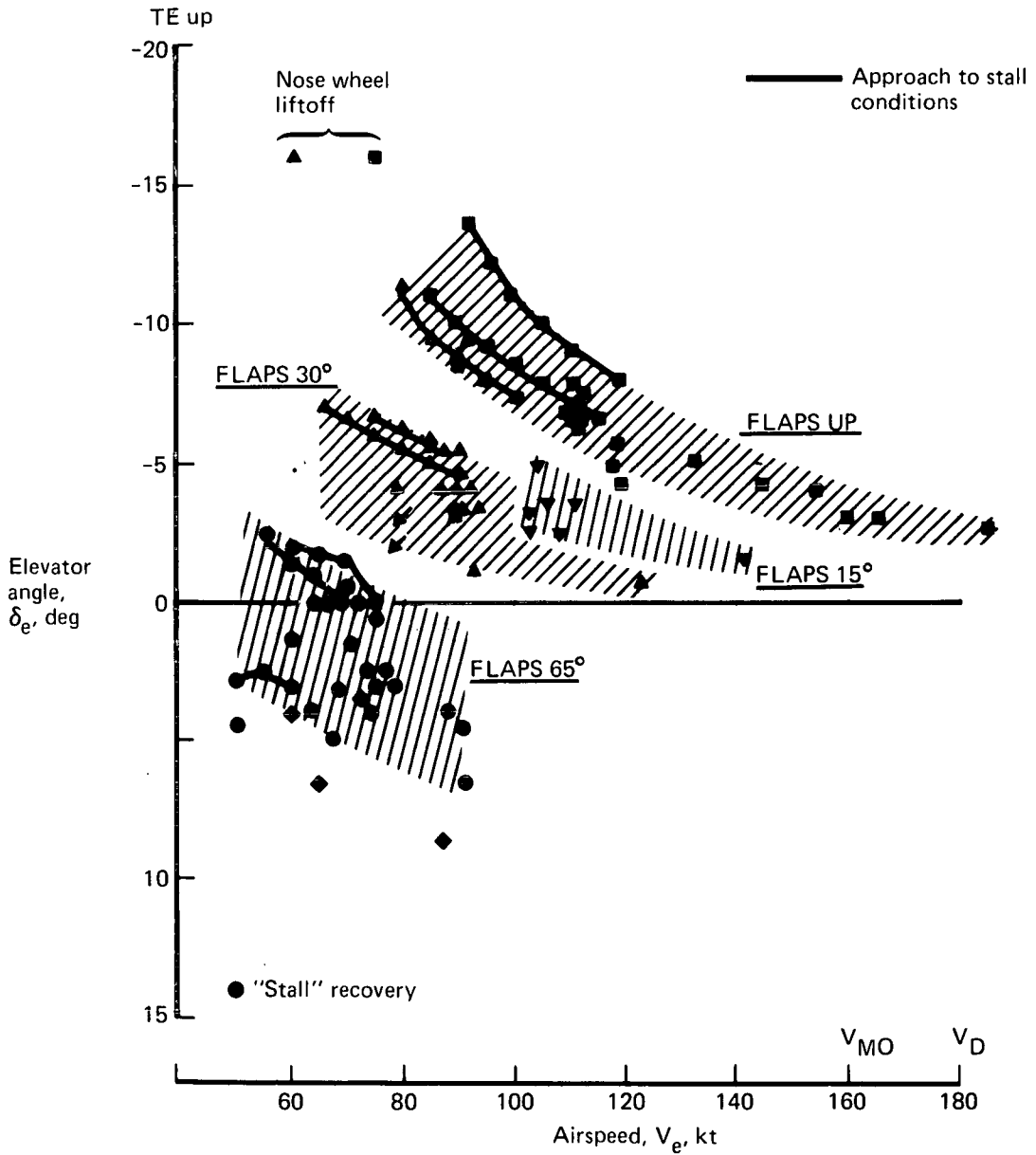
FIGURE 94.—FLIGHT TEST TRIM ELEVATOR SUMMARY

The maneuvering characteristics are summarized in figure 95. The increments in elevator and wing angle of attack required per unit load factor are as predicted or better. Acceptable one-hand maneuvering capability was demonstrated as a result of the spring tab modification to the elevator.

The estimated maneuvering capability for the airplane is presented in figure 96 based on flight test data. Load factor will be limited both by wing lift and the elevator control system. The maneuver margin of 0.3 g at 60 kt should be adequate for trim alphas of 10° or less.

Airplane response to elevator was good down to 50 kt, the minimum airspeed tested. Elevator authority was adequate, and trim changes were reasonable during flap extensions and retractions, thrust changes from takeoff to idle, and conical nozzle vectoring.

LATERAL-DIRECTIONAL STABILITY AND CONTROL

The static lateral-directional stability characteristics were evaluated by performing steady sideslip maneuvers. The research vehicle was statically stable about both the lateral and directional axes. Lateral stability (dihedral effect) existed at the STOL conditions.

The airplane should be capable of reaching high sideslip angles, since the 15° sideslip demonstrated in flight required only about half the total rudder power. To prevent large sideslips and resulting high empennage loads from occurring at high speeds, one of the two rudder hydraulic systems is disengaged at speeds greater than 100 kt. The sideslip is then limited by rudder blowdown at 160 kt, as predicted.

The one undesirable lateral-directional characteristic found during the flight test program was a low-amplitude directional "snaking" tendency below 90 kt. At 60 kt, the aircraft was described as "snaking" ±3° in sideslip and "wallowing" ±2° in bank angle.

Directional control power was found to be adequate for engine-out control and large sideslip conditions. The airplane will not be limited by a lack of directional control capability at any flap setting.

Lateral control system characteristics were found to be satisfactory. Wheel forces were light and centering was positive. Lateral control power was demonstrated by conducting full wheel roll reversal maneuvers. The airplane has considerable roll power and exceeds the design criteria of 0.4 rad/sec² roll acceleration at 60 kt.
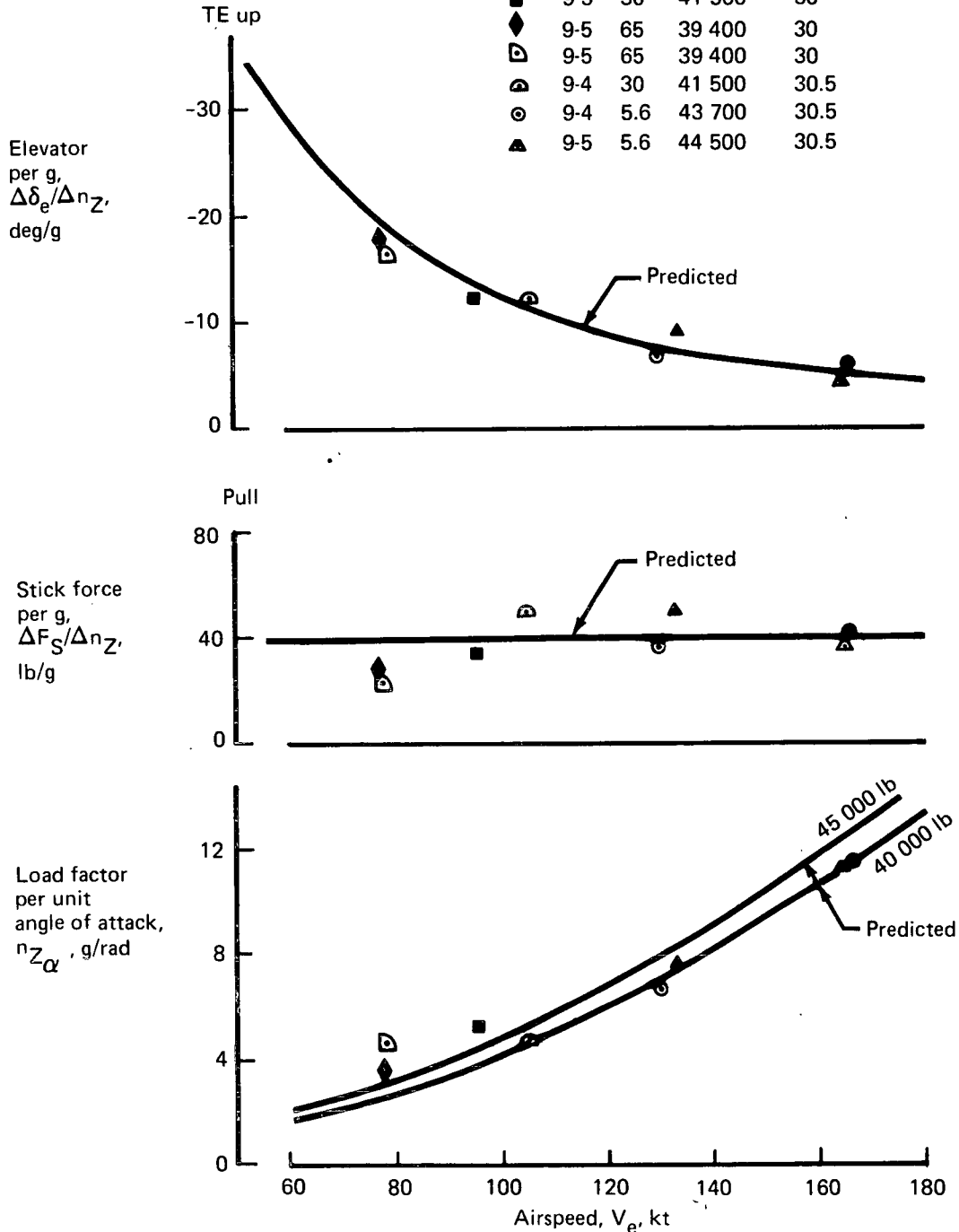
FIGURE 95.—MANEUVERING STABILITY SUMMARY

- $W \approx 40\ 000$ lb
- Based on flight test n_{z_α} and $\Delta\delta_e/\Delta g$
- θ_1 stops based on taxi test data
- Free air
- Flaps 30° and up, α_{trim} at level flight (test data)
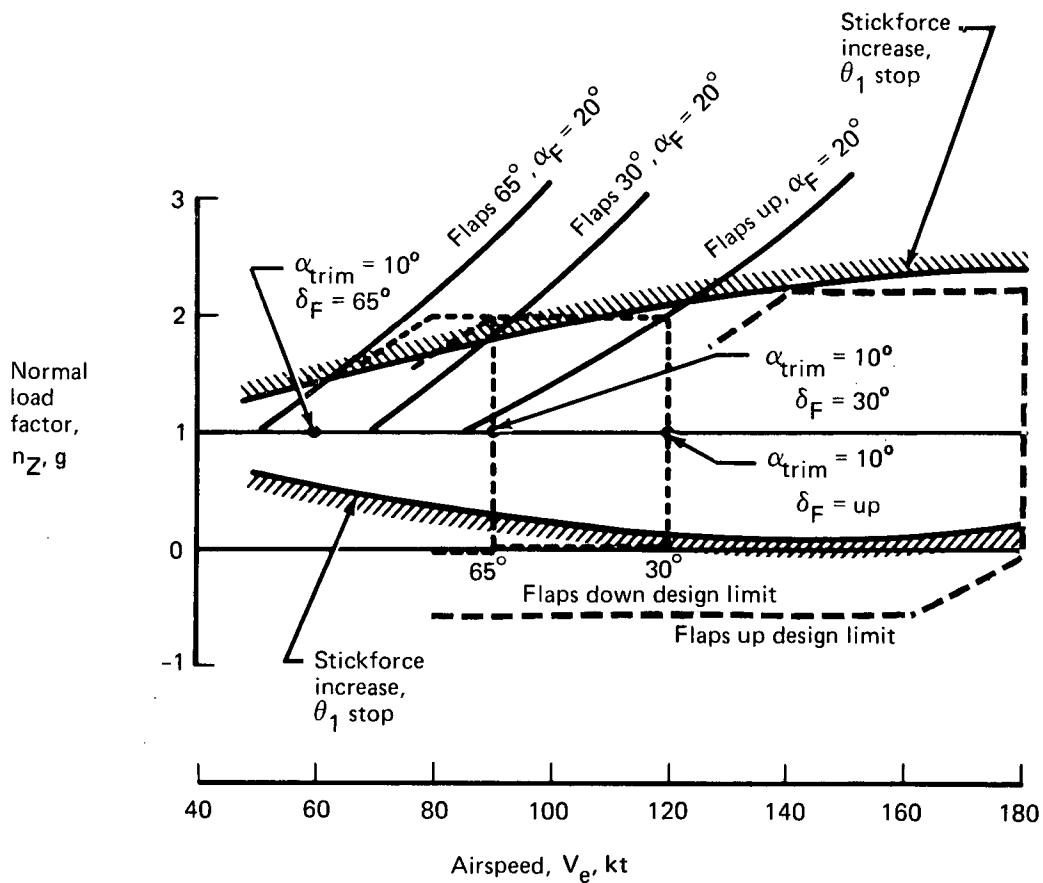- Flaps 65°, α_{trim} at nozzles down approach (test data)

FIGURE 96.—ESTIMATED MANEUVERING CAPABILITY BASED ON
FLIGHT TEST DATA

Manual reversion was not explicitly tested. However, based on flutter testing where the hydraulic power to the aileron and augmentor choke was turned off, it appears that a manual reversion landing may not be possible because of high friction in the system in addition to the aerodynamic forces present. Application of up to 50 lb of wheel force generated only $1°$ of aileron deflection and $5°$ of spoiler deflection, which produced a roll rate of about 1 deg/sec.

With the lateral-directional stability augmentation system (SAS) the aircraft exhibited acceptable turn entry characteristics, positive spiral stability, and adequate Dutch roll damping. With the SAS off, the airplane was judged controllable to a landing. SAS failures were evaluated and the resulting hardovers could be overridden or disconnected.

CONCLUDING REMARKS AND RECOMMENDATIONS

The necessary modifications to convert a de Havilland C-8A airplane to an augmentor wing jet STOL research aircraft have been designed, fabricated, and installed. These modifications included the following items:

- New Rolls-Royce Spey MK 801-SF split-flow fan engines, which replace the T-64 turbo-prop engines

- Vectorable primary nozzles, installed on the engines by installing conical nozzles on the Pegasus nozzle system which was adapted to the Spey MK 801-SF engine

- An augmentor flap system, blown ailerons, and spoilers, which replace all original structure aft of the rear spar

- Fixed leading edge slats attached forward of the existing wing contour

- Wing span reduced from 96 to 78.75 ft

- A low-pressure air distribution system, which distributes all the fan air to the augmentor flaps, aileron, and body blowing nozzles

- Lateral and directional stability augmentation system

- Pulse code modulation data system

- An increase in the maximum gross weight to 45 000 lb

- Pilot escape provisions

- Improved braking system

- Fuel system modification

- Longitudinal control system modification

Development testing was accomplished which included a static test of a 0.7-scale model of the augmentor flap system, simulator tests using the ARC Flight Simulator for Advanced Aircraft, ground tests, taxi tests and, finally, airworthiness flight tests.

The flight envelope was investigated from a minimum airspeed of 50 KEAS to the design dive speed (V_D) of 180 KEAS. Flap placards were reached at flaps 65° (90 KEAS) and flaps 30° (120 KEAS). Approaches to stall were made at three primary flap settings: up, 30°, and 65°. The full ranges of flap setting, conical nozzle deflection, and power setting were evaluated.

Angles of attack from -3° to 24° were investigated. Variations in load from 0.3 to 1.8 g were obtained during pushover/pull-up maneuvers. Sideslip angles of 15° were tested and bank angles exceeding 45° were flown. The flight envelope was sufficiently explored to clear the airplane for the augmentor wing research flight test program.

Since the original objectives of the Modified C-8A program were to prove the augmentor wing concept with respect to aerodynamics, performance, and handling qualities and to contribute to the development of jet STOL transport design and operating criteria, it is recommended that NASA extend the flight test program into the following areas:

- Conduct a test program exploring the STOL flight regime in further depth. Particular emphasis should be placed on landing maneuvers, including the following specific items:

    - Steep approach flare techniques related to simulator findings

    - Evaluation and, possibly, measurement of ground effects

    - Simulation of engine failure at critical conditions

    Caution is urged in approaching flight conditions having low margins. Give particular attention to the type of longitudinal stability augmentation needed on the airplane.

- Conduct a flight test investigation to determine accurate performance characteristics, including a ground test to measure static thrust. With accurate data in hand, conduct an analysis of airplane performance. Static thrust data, flaps on and off, will allow investigation of static augmentation. Tuft studies of suspected areas of poor flow during both flight and static tests will allow qualitative assessment of drag sources and will guide corrective action to improve performance. This work is recommended as essential to the proof of the augmentor wing concept.

- Install a powered elevator system on the airplane to permit full and safe exploration of the airplane's high-lift and STOL operation capabilities.

- Use the variable-gain SAS to find the optimum lateral-directional handling qualities and reduce the "snaking" tendency, then modify the fixed-gain SAS to this configuration.

REFERENCES

1. Skavdahl, H.; and Patterson, D. H.: The Development of an Augmentor Wing Jet STOL Research Aircraft (Modified C-8A), Volume II—Analysis of Contractor's Flight Test. NASA CR-114504, NASA contract NAS2-6025, Boeing Commercial Airplane Company, Seattle, Washington, August 1972.

2. Cook, Anthony M.; and Aiken, Thomas N.: Low Speed Aerodynamic Characteristics of a Large Scale STOL Transport with an Augmented Jet Flap. NASA TMX-62017, March 1971.

3. Joseph J. Zuccaro: The Flight Simulator for Advanced Aircraft—A New Aeronautical Research Tool. AIAA Visual and Motion Simulation Technology Conference, March 1970.

4. Cleveland, W. B.: Augmentor Wing Jet STOL Research Aircraft Digital Simulation. NASA TMX-62139, March 1972.

5. Rumsey, P. C.; and Spitzer, R. E.: Simulator Model Specification for the Augmentor Wing Jet STOL Research Aircraft. NASA CR-114434, December 1971.

6. Quigley, H. C.; Sinclair, S. R. M.; Nark, T. C.; and O'Keefe, J. V.: A Progress Report on the Development of an Augmentor Wing Jet STOL Research Aircraft. SAE Paper 710757, National Aeronautic and Space Engineering and Manufacturing Meeting, Los Angeles, California, September 1971.

7. Rumsey, P. C.; Spitzer, R. E.; and Glende, W. L. B.: A Design Support Simulation of the Augmentor Wing Jet STOL Research Aircraft. NASA CR-114435, January 1972.

8. Franklin, J. A.; and Innis, R. C.: Longitudinal Handling Qualities During Approach and Landing of a Powered Lift STOL Aircraft. NASA TMX-62144 March 1972.

9. Spitzer, R. E.: Predicted Flight Characteristics of the Augmentor Wing Jet STOL Aircraft. NASA CR-114463, July 1972.

10. Innis, R. C.; Holzhauser, C. A.; and Quigley, H. C.: Airworthiness Considerations for STOL Aircraft. NASA TND-5594, January 1970.

11. Innis, R. C.; Holzhauser, C. A.; and Gallant, R. P.: Flight Tests Under IFR With a STOL Transport Aircraft. NASA TND-4939, December 1968.

THE FOLLOWING PAGES ARE DUPLICATES OF

ILLUSTRATIONS APPEARING ELSEWHERE IN THIS

REPORT. THEY HAVE BEEN REPRODUCED HERE BY

A DIFFERENT METHOD TO PROVIDE BETTER DETAIL